FLUE GAS DESULPHURISATION UNDER SOUTH AFRICAN CONDITIONS

By

Siagi Otara Zachary

Submitted in partial fulfillment of the requirements for the degree

DOCTOR TECHNOLOGIAE

in the

Department of Mechanical Engineering

FACULTY OF ENGINEERING AND THE BUILT ENVIRONMENT

TSHWANE UNIVERSITY OF TECHNOLOGY

Supervisor: Prof Makame Mbarawa

Co-Supervisor: Dr Av Kolesnikov

Co-Supervisor: Dr Mark Van Der Riet

July 2010

DECLARATION BY CANDIDATE

"I hereby declare that the thesis submitted for the degree D. Tech: Mechanical Engineering, at Tshwane University of Technology, is my own original work and has not previously been submitted to any other institution of higher education. I further declare that all sources cited or quoted are indicated and acknowledged by means of a comprehensive list of references".

Siagi Otara Zachary

This research is dedicated to:

My parents

And

My son Richard

Whose love and support has seen me this far.

ACKNOWLEDGEMENT

Many individuals and institutions have contributed either directly or indirectly to the accomplishment of this study. Due to constraints of space, I will only mention a few by name.

To my supervisor, Prof. Makame Mbarawa, thank you for the assistance, support, and guidance during the entire study period. Thank you for believing in me and for encouraging me to be all that I am.

Dr Mark Van Der Riet deserves credit for his idea for the ranking of South African sorbents, which is the core of the thesis. To Dr. AV Kolesnikov for accepting to be my co-supervisor. Special thanks to Naushaad of eskom for his tireless efforts in acquiring and characterizing the study materials.

Thanks to Prof Rahman, Dr Lee, and Irvan Dahlan of the Universiti Sains Malaysia for their assistance during the laboratory tests and for making my stay in Malaysia a memorable one.

My gratitude to all my friends and colleagues at the Department of Mechanical Engineering of the Tswane University of Technology for creating an inspiring atmosphere in which the current work was carried out.

I acknowledge the financial support of the Tswane University of Technology, the German Academic Exchange Program (DAAD), Technology Services International – eskom, and NRF/THRIP funding. I also thank Moi University for granting me a study leave.

To my host country, South Africa, the Rainbow Nation for providing the opportunity.

Last but not least to my parents and my son, Richard, for their support and patience.

ABSTRACT

Coal is the primary energy source in South Africa and accounts for about 75% of the total energy consumption in the country and 90 per cent of the total electricity capacity of 43 142 MW is coal-derived. Upon combustion, the sulphur contained in the fuel is oxidized to sulphur dioxide (SO_2). Emissions of SO_2 lead to the formation of acid rain which is harmful to the environment. Besides this environmental problem, SO_2 is a health hazard causing problems to the respiratory and cardio-vascular system.

The objective of this investigation was to study and/or rank the performance of locally available materials (i.e. limestone, dolomite, or calcrete) as sorbents in the capture of SO_2 emissions from coal-fired power plants. Two experimental procedures were adopted in this work: the pH-stat method was used to simulate conditions encountered in wet flue gas desulphurisation (WFGD); and the fixed-bed reactor was used to simulate conditions encountered in the dry in-duct flue gas desulphurisation (DFGD) process.

The dissolution rate in the pH-stat apparatus was observed to be a strong function of the particle size; the finer the particles the higher the conversion within the same time period. The dissolution rate decreased with an increase in the pH for the range tested ($4 \leq pH \leq 6$). This result indicated that the dissolution of calcium – based materials is controlled by the mass transfer of the hydrogen ions accompanied by chemical reactions in the mass transfer boundary layer. The origin of the sorbent material and its chemical composition had an influence on the dissolution process; calcitic limestones generally displayed a higher rate than their dolomitic counterparts. The reaction rate was observed to increase with an increase in the reaction temperature for the range tested ($30 \leq T \leq 70$ºC).

Kinetic analysis of the results indicated that the dissolution process takes place according to the shrinking core model with surface control. The reaction rate constant obtained varied from low values for dolomite to high values for the limestone samples ($0.00415 \leq k \leq 0.0190$ min^{-1}). Thus the performance of the limestone samples is expected to be better than that of the dolomite samples in full-scale operation. The activation energy also showed a similar trend with that of limestone samples being higher than that for the dolomite samples ($14.7 \leq E_a \leq 27.5$ kJ/mol). Thus a ranking of the sorbents can be obtained either by using the reaction rate constant or the amount of acid consumed over a specified period during the pH-stat reactivity experiments.

Experiments of the desulphurisation activity in the fixed-bed reactor showed that the capture capacity depends on the sorbent type as well as its chemical composition. It was observed that an approximation of the reactivity of the sorbent can be obtained by observing the relative rise in temperature (ΔT) during the hydration of the calcined sorbent to produce the relevant slaked lime. Sorbents with a higher reactivity were exhibited a higher temperature rise than those with a lower capture capacity. This is thought to be due to a more porous structure that results with a higher temperature rise. Variation of relative humidity ($0 \leq RH \leq 40\%$) indicated that the relative humidity is the single most influential parameter on the capture capacity in conditions similar to those encountered in dry FGD. An increase in the relative humidity resulted in an increase in the capture capacity. The influence of the SO_2 concentration ($1000 \leq C_0 \leq 2500$ ppm) was studied at a reactor temperature of 80°C and 0% RH. Although the initial sorbent activity increases as the concentration of SO_2 increases, the maximum conversion of the sorbent is independent of the SO_2 concentration. The reaction temperature on the other hand was seen to have a minimal effect on the sorbent activity.

The desulphurisation activity in the fixed-bed can be satisfactorily modeled using the surface coverage model. The hypothesis of this model is that the sorbent is made up of plate grains and that the reaction is controlled by chemical reaction on the surface of a grain and the reacting surface area of the grain decreases with the deposition of solid product. A comparison of the model and experimental results showed a close agreement between the two.

A comparison between the pH-stat and the fixed bed results showed that the pH-stat process can be used to reliably rank the performance of the different sorbent materials as sorbents in the flue gas desulphurisation process. The materials that had a higher dissolution rate also showed a higher sulphur capture capacity in the fixed-bed reactor.

CONTENTS

LIST OF FIGURES

LIST OF TABLES

PUBLICATIONS EMANATING FROM THE RESEARCH

1. **Siagi Z.O**., Mbarawa M., Mohamed A.R., Lee K.T., & Dahlan I. 2007. The effects of limestone type on the sulphur capture capacity of slaked lime. Fuel 86: 2660-2666.

2. **Siagi Z.O**. & Mbarawa M. 2008. An overview of SO_2 emission reduction techniques. R&D Journal. Volume 24, No. 1. 26-33.

3. **Siagi Z.O**. & Mbarawa M. Dissolution rate of South African Calcium Based materials. Journal of Hazardous Materials. Article in Press, 2008.

4. **Z.O. Siagi**, M. Mbarawa, A.R. Mohammed, K.T. Lee, and I. Dahlan: Removal of sulphur dioxide by calcium-based materials from different sources in South Africa. *8th International Symposium on Combustion and Energy Utilization*. October 10-12 2006, Sochi, Russian Federation.

5. **Z.O. Siagi**, and M. Mbarawa. Experimental investigation of the SO_2 abatement capacity of south african calcium – based materials. *ASME Energy Sustainability 2007*. June 27-30, 2007, Hilton Long Beach, California.

6. **Z.O. Siagi**, and M. Mbarawa. Reactivity of South African Calcium-Based sorbents. *5th International Conference on Heat Transfer, Fluid Mechanics and Thermodynamics (HEFAT) 2007*. June 27-30, Sun City.

CHAPTER 1

1 INTRODUCTION

1.1. GLOBAL INTRODUCTION

Coal is the main source of energy in South Africa. Coal, being the most abundant energy resource will have an important role to meet the increasing demand of electricity in the South Africa. For example the demand for electricity in South Africa is expected to double by 2020. Although coal has an important role as a source of energy in South Africa, its utilization in producing electricity gives rise to a number of ecological problems, such as ash waste, air pollution from particulate and acid gas pollutants.

The strict legislation on the acid gas pollutants introduced internationally has forced the power stations manufacturers and operators world wide to seek means of reducing these pollutants. This has resulted in much research being done internationally in an attempt to learn more about the mechanisms of the acid gas pollutants formation, pollutant control techniques and the factors that influence them. The majority of this research has been done in those countries where stringent emission legislations are enforced. Much of the undertaken research was based on the local conditions of the research country of origin.

In South Africa, there is still no strict legislation on acid gas pollutants emission from power stations. Furthermore, in order to reduce the plant operating costs, all South African coal-fired power stations were designed to burn low-grade coals allowing high grade coal to be available for the export market. In addition, these coal-fired stations were designed to remove

dust and other particles from the waste gases but none were fitted with acid gas pollutants control equipment. This is because the use of these equipment would increase the cost of electricity substantially. Due to these conditions the coal-fired power stations are the primary source of acid gas pollutants.

All of the above factors imply that results achieved internationally may not be directly translatable to the local conditions. Therefore, there is a need to understand the best way to reduce these emissions efficiently and cost effective under South Africa conditions.

1.2. ENERGY SCENARIO IN THE REPUBLIC OF SOUTH AFRICA

The bulk of South Africa's energy consumption is comprised of coal, which the country primarily uses to generate electricity and produce synthetic fuels. South Africa also consumes a substantial amount of oil. Only a small percentage of the energy consumption mix is comprised of natural gas and nuclear. South Africa's coal reserves are mainly bituminous, with a relatively high ash content (about 45%) and a low sulfur content (about 1%). In 2005, South Africa's recoverable coal reserves were estimated to be 28.6 billion tons. In the same year, South Africa produced 245 million tons of coal of which 174 million tons were used locally. The vast majority of the consumed coal is used in electricity generation and the synthetic fuel industry (South Africa Year book, 2007).

South Africa annually consumes 23 million tons of liquid fuel products, of which 45% is gasoline and 26% diesel. The country's petroleum reserves are currently estimated to be 29.4 million barrels. Domestic oil production is 25,000 barrels per day (b/d), which comes from offshore oil fields. Because of the abundant supplies of cheap coal, liquid fuels only

provide 21% of the energy requirements of the country. A significant portion of liquid fuel needs are met through production of synthetic fuels from coal, natural gas, and condensate. Sasol currently has the capacity to produce 150,000 b/d of liquid fuels. The country's natural gas reserves are currently estimated at 780 billion cubic feet (bcf) but the gas fields off of South Africa's West Coast and neighboring Namibia may contain as much as 15 trillion cubic feet (tcf) of natural gas. South Africa's production of natural gas now accounts for only about 2% of the country's total energy needs.

Including hydroelectric power, close to 10% of South Africa's primary energy supply is listed as renewable. These sources include biomass, wind energy, solar energy, and hydroelectric power. One-third of the population depends on firewood for their household heating and cooking needs. Firewood collected from forests as well as waste from sugar and lumber processing are the main supplies. There are five relatively small power stations in South Africa that use process waste (bagasse) mixed with coal as fuel. These are all cogeneration facilities located at the sugar mills, and produce steam and electricity for captive use by those sugar mills; they produce about 0.2% of the electricity consumed in South Africa. The country does not yet commercially generate electricity from wind power. About 400 kilowatts (kWe) of small wind turbines for power generation have been installed, but are not yet connected to the power grid. Current uses of wind power include about 300,000 wind pumps for livestock and community water use. A solar equipment industry has begun to take root in South Africa; annual photovoltaic panel assembly capacity totals 6 MWe and a number of companies manufacture solar water-heaters. South Africa is a relatively arid country, and it has a large number of dams in its river systems to conserve water for use in agriculture and for urban areas. Relatively few of them, however, generate hydroelectric

power. The largest hydroelectric power plant in South Africa is the 1,000 MWe Drakensberg Pumped-Storage Facility, which is actually part of a larger scheme of water management that brings water into the Vaal watershed from the Tugela River.

South Africa is presently the only country in Africa that has a commercial nuclear power plant. The Koeberg Nuclear Power Plant, operated by Eskom, is located near Cape Town and was commissioned in 1984. Koeberg accounts for about 7 % of South Africa's electricity generation. The plant utilizes pressurized-water reactor (PWR) technology and has a licensed generating capacity of 1,840 MWe. A breakdown of the energy supply in South Africa in 2004 is shown in Figure 1.1.

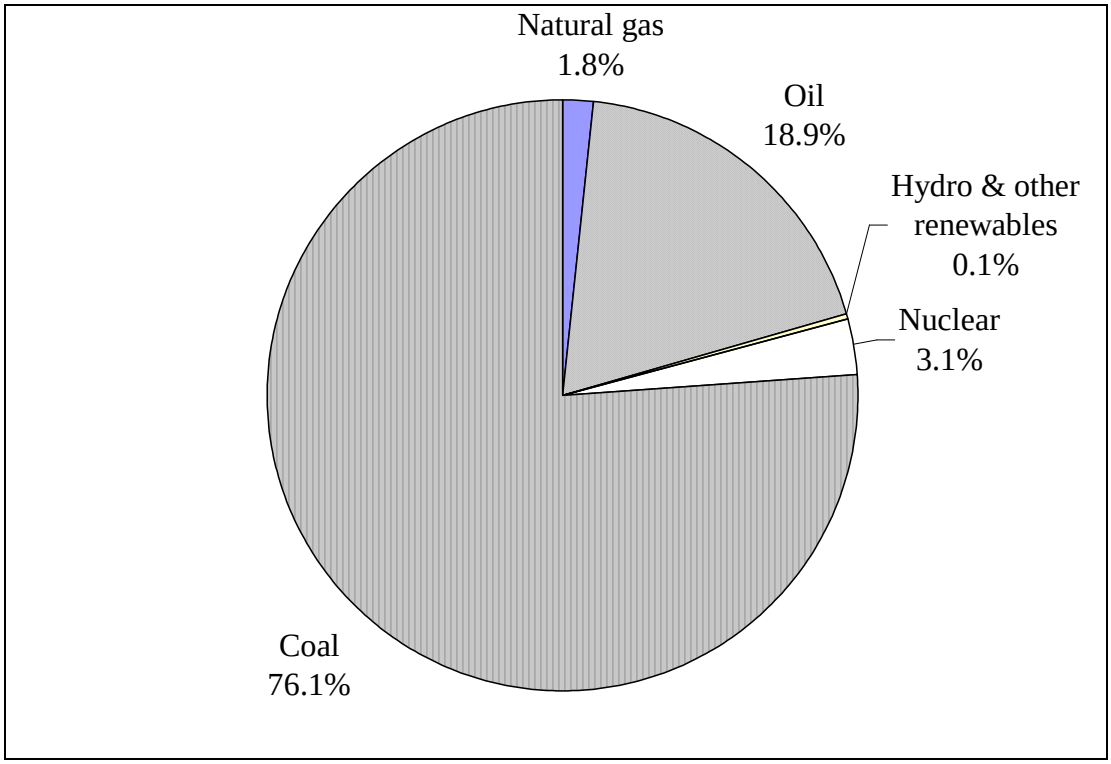

FIGURE 1.1: Total energy consumption in South Africa by Type (EIA, 2004)

A large share of the final energy in the country is consumed by industry, transport and mining (Figure 1.2). Energy consumption levels in South Africa are significantly higher than many other developing countries, particularly consumption of electricity where South Africa consumes half of Africa's electricity with only 5 % of her population (EIA, 2001). Energy intensity – how much energy is required to generate a unit of economic output – is 18 % higher than for OECD countries' average.

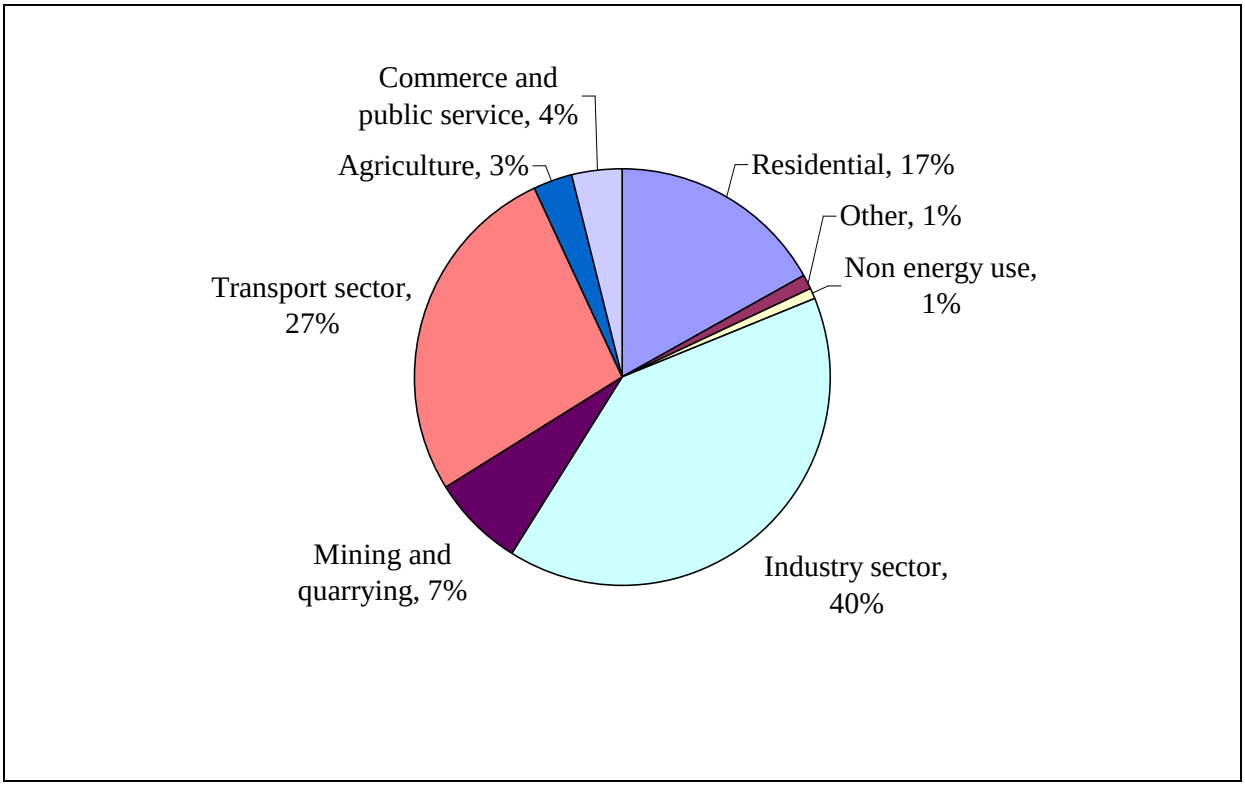

FIGURE 1.2: Share of the final energy consumption in South Africa in 1999 (Randall & Matibe, 2003)

1.3. SULPHUR OXIDES (SO_X)

Elemental sulphur is relatively inert and harmless to human beings and in fact is needed in some quantity for life. It occurs naturally in the environment, mostly in the form of sulphates

like $CaSO_4$. However, sulphur oxides (SO_x) are recognized as pollutants that are harmful to the environment. Sulphur dioxide (SO_2) is the most predominant form of SO_x emitted from systems containing sulphur. It is a colourless nonflammable acidic gas with a pungent odor that is detected by the human nose and is used in a variety of chemical processes. SO_2 can be very corrosive in the presence of water and is highly soluble in water. Some of its important physical properties are reported in Table 1.1.

TABLE 1.1**:** Physical properties of SO_2 (Lee, 2004).

Property	**Value**
Molecular mass	64.06
Melting point (101.3 kPa)	-75.5ºC
Latent heat of fusion	115.6 kJ/kg
Dynamic viscosity at 0ºC	368 Pa.s
Density at -10ºC	1.46 g/cm^3
Critical density	0.525 g/cm^3
Critical pressure	78.8 bar
Critical temperature	157.5ºC
Boiling point (101.3 kPa)	-10.0ºC
Latent heat of vaporization	402 kJ/kg
Standard density at 0ºC (101.3 kPa)	2.93 kg/m^3
Density relative to air (0ºC, 101.3 kPa)	2.263
Molar volume (0ºC, 101.3 kPa)	21.9 L/mol
Specific heat capacity, C_p (0ºC, 101.3 kPa)	586 J/kg K
C_p/C_v (0ºC, 101.3 kPa)	1.29

1.3.1. Sulphur dioxide Emissions

All raw materials, including coal, crude oil, and ore that contain common metals like aluminum, copper, zinc, lead, and iron have sulfur in them. SO_2 is formed as a result of combustion of fuel containing sulfur, such as coal and oil, during distillation of crude oil, or metal during extraction.

Currently, global SO_2 emissions arising from human activity amount to approximately 140 million tones (Mt) (Department of Trade and Industry, 2000). Emissions are highly site specific depending upon the fuel being burnt and the combustion system, and the evolution of SO_2 emissions varies from region to region in the world (Figure 1.3). SO_2 emissions have been reduced in the USA and Europe in the last decades (by 45 % from 1975 to 2002 and 60 % from 1980 to 1997, respectively) and are tending to a level value at present, while those in developing countries are steadily going up. According to World Bank projections, SO_2 emissions in Asia will be greater than those of North America and Europe combined by the first decade of the 21st century, unless substantial investments in pollution control equipment are made (Downing, Ramankutty, & Shah, 1997).

Globally, coal combustion accounts for more than half of the SO_2 and some 30 % of the NO_x released into the atmosphere by human activities. SO_2 is evolved from coal combustion through oxidation of the sulphur (S), typically resulting in flue gas SO_2 concentrations of 500 – 2000 ppmv (Kiil, Nygaard, & Johnson, 2002). Figure 1.4 shows the variation of the SO_2 emitted from South African coal-fired power stations between 1996 and 2000.

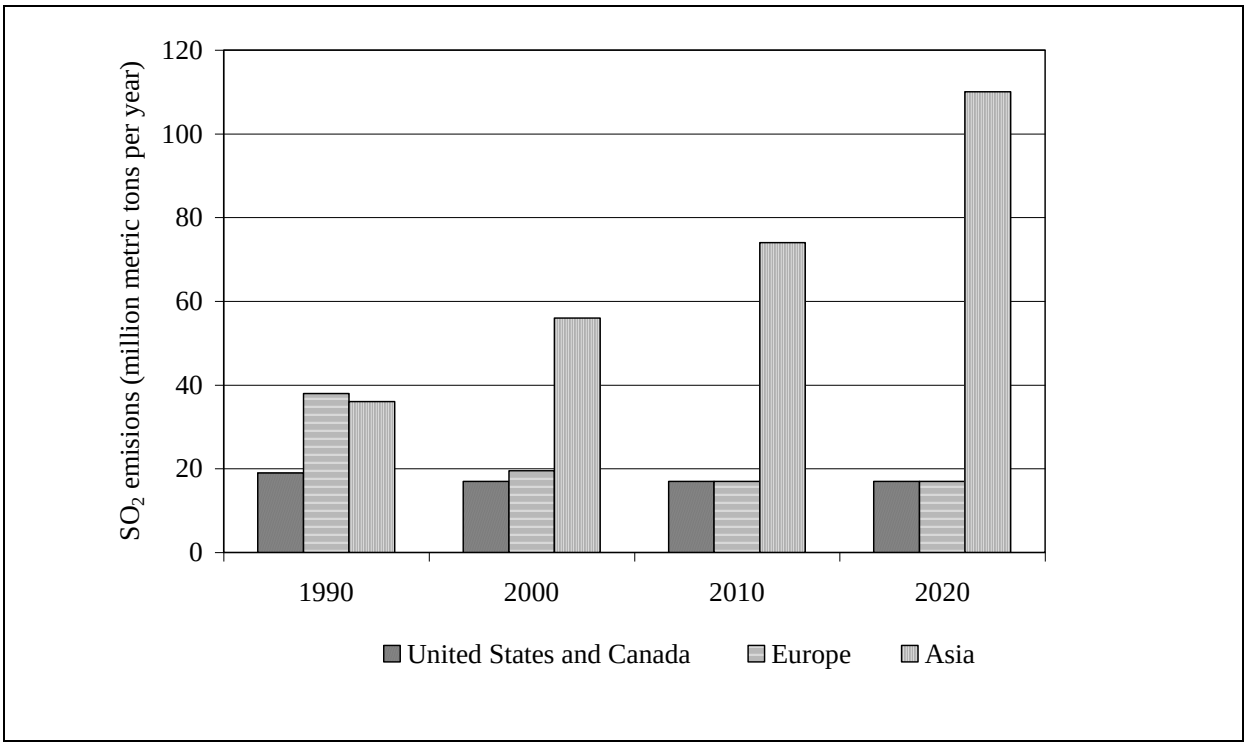

FIGURE 1.3: SO_2 emissions in Europe, United States/Canada, and Asia. (www.wri.org)

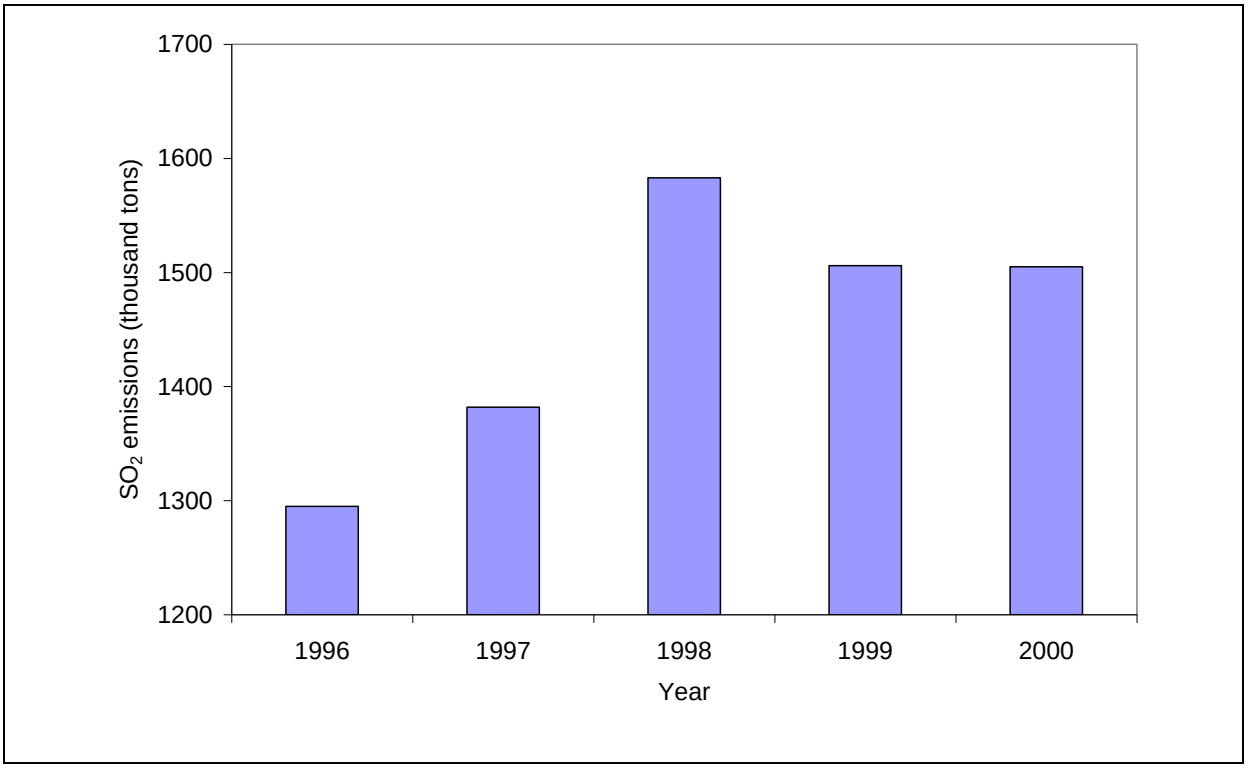

FIGURE 1.4: SO_2 emitted from South African coal-fired power stations (Nkomo, 2005)

In general, there was a general increase except for the year 1998 to 1999. The general increase in emissions between 1996 and 2000 is primarily due to an increase in the amount of coal burnt at the power stations. Currently, electric utilities in South Africa, especially the ones using coal for combustion, are the primary sources of SO_2 releasing as much as 2.19 million tons every year, which is about 66 % of the total SO_2 released into the air (South Africa Year Book, 2007).

1.3.2. SO_2 formation mechanisms

One of the most common sources of sulphur in industrial combustion processes is in the fuel. Solid fuels like coal and coke may contain 1% or more sulphur by weight. In a high temperature combustion process, the sulphur is oxidized by oxygen from the combustion air to form SO_x. The first oxidation step is:

$$S_{(s)} + O_{2(g)} \rightarrow SO_{2(g)} \quad (1.1)$$

This step takes place in the high temperature combustor. The second oxidation step is:

$$SO_{2(g)} + \tfrac{1}{2} O_{2(g)} \rightarrow SO_{3(g)} \quad (1.2)$$

This step can occur in the combustion system but the ratio of SO_2/SO_3 is typically on the order of 40-80:1 (Baukal, 2004). Most of the SO_x in the flue gas is in the form of SO_2. The problem in the atmosphere is that SO_3 reacts with water (e.g., rain) to form sulphuric acid:

$$SO_{3(g)} + H_2O_{(l)} \rightarrow H_2SO_{4(aq)} \quad (1.3)$$

1.3.3. Environmental and Health Concerns

SO_2 concentrations below 0.6 ppm (parts per million) produce no ill effects in human beings. Most people, however, become cognizant of sulphur at about 5 ppm and become irritated at about 10 ppm. A one-hour exposure to a SO_2 concentration of 10 ppm can cause breathing problems (El-Wakil, 1984). Effects range from temporary breathing difficulties to severe heart and lung problems. The effects become much more serious when SO_2 is combined with particulates and enters the digestive system, a phenomenon known as the "cocktail effect". Research has shown that exposure for asthmatics is significantly more damaging than for normal subjects and even moderate concentrations may result in a fall in lung function in these cases. According to a 1999 World Bank study in India, air pollution was responsible for 40,000 premature deaths, 17 million respiratory hospital admissions and 1.2 billion restricted activity days (Mitra & Sharma, 2002). In addition to the health effects, moderate to high levels of SO_2 contributes to acid rain. Acid rain causes decimation or deformation of aquatic life in streams and lakes. Additionally, it leads to damage of trees and agricultural crops and degradation or destruction of bridges, buildings, and monuments. Airborne SO_2 and its derivatives can also contribute to degradation of visibility due to formation of a haze.

1.3.4. Regulations

Considering these health and environmental impacts, most countries now place some limits on the allowable levels of SO_2 emissions originating from power plants. The earliest introduction of emission standards was made on a national basis in the 1970s in Japan and the United States (Plant & Mathay, 1999). As awareness of the environmental impact increased in the 1980s, regulations became more stringent and widely applicable. This trend continued in the

1990s as greater understanding was gained on the detrimental effects of atmospheric pollution and the knowledge of what is technically and economically feasible for control of emissions. On the global front, there are several emission Legislation currently in place including: the Large Combustion Plant Directive (LCPD) adopted by the European Union in 1988 which define emission limits for solid, liquid, and gaseous fuels for units exceeding 50 MW (Plant and Mathay, 1999); the Clean Air Act Amendment (CAAA) of the United States passed in late 1990 and targets emission limits of 0.5 kg per 10^9 J of heat input. Currently there are in excess of 15,000 MW of electricity in Japan equipped with air pollution installations. Table 1.2 shows the SO_2 emissions limits that have been adopted by the European Union.

TABLE 1.2: SO_2 limit emissions for large combustion plants (European Directive 2001/80/EC)

Type of plant	**Limit**
Existing solid/liquid-fuel burning plant > 500 MWth	142 ppm
Existing solid-fuel burning plant 50 – 700 MWth	710-142 ppm*
Existing liquid-fuel burning plant 50 – 500 MWth	603-142 ppm*
New solid-fuel burning plant (excepting biomass) > 100 MWth	71 ppm
New solid-fuel burning plant (excepting biomass) 50-100 MWth	301 ppm
New biomass burning plant	71 ppm
New liquid-fuel burning plant > 300 MWth	71 ppm
New liquid-fuel burning plant 100-300 MWth	142-71 ppm*
New liquid-fuel burning plant 50-100 MWth	302 ppm

*Linear decrease

From a South African perspective, present local power plant has particulate but no gaseous emission control requirements, due mainly to the relatively low sulphur content of local coals (Van Der Riet & Begg, 2003). However, the South African Government is committed to providing reasonable measures for the prevention of pollution and ecological degradation. According to an environmental act (SA, 2005) signed into law in 2005, ambient concentrations of sulphur dioxide (SO_2) may not exceed:

- A ten-minute average instant peak of 0.191 ppm measured at S.T.P.
- An instant peak of 500 $\mu g/m^3$ measured at STP.
- A 24-hour average of 0.048 ppm or 125 $\mu g/m^3$ measured at S.T.P.
- An annual average of 0.019 ppm or 50 $\mu g/m^3$ measured at S.T.P.

Furthermore, South Africa has a nascent, but growing, environmental protest movement. In recent years, environmental groups have challenged: strip mining operations in a sensitive wetland area, drawn world attention to pollution and conditions at the country's refineries, and legally challenged the establishment of South Africa's Pebble-Bed Modular Reactor (PBMR) program (Department of Energy: 2005). These indicate a growing awareness of environmental concerns in the country and point to a far stricter scrutiny for South African plants from both the local and international communities.

1.4 OPTIONS FOR SO_2 EMISSION CONTROL

Sulphur dioxide emissions reduction techniques can be categorized into three groups: 1) pre-combustion techniques, 2) combustion techniques, and 3) post-combustion techniques.

1.4.1 Pre-combustion Techniques

Fuel switching and coal cleaning are two pre-combustion techniques. Some power plant designs allow for fuel switching; for example, a natural gas-fired power plant may utilize oil as an auxiliary fuel. Similarly plants which burn wood waste may use coal to ensure base load operations. Table 1.3 shows typical emissions from different technologies using different fuels (Chaaban, Mezher, & Ouwayjan, 2004).

TABLE 1.3: Typical emissions from power plants (g/kWh)

Fuel Type	CO_2	SO_2	NO_x
Natural Gas	490	0.004	1.5
Fuel Oil	781	5.1	1.5
Coal	1060	5.5	2.4

Switching from a high sulphur coal to a low sulphur coal or blending a low sulphur coal with a coal of inferior quality may result in a fuel whose emissions could be within allowable limits. The appropriate coal quality, however, has to be considered with regard to other

pollutants because a decrease in SO_2 emissions may cause an increase in NO_x or fly ash (Kaminski, 2003).

Coal may be cleaned by physical, chemical or biological means. Sulphur is present in coal in two inorganic forms, these being pyritic sulphur (FeS_2) and sulphates (Na_2SO_4, $CaSO_4$, $FeSO_4$) and as organic sulphur (Cooper & Alley, 1994). Unless the chemical bonds that hold the sulphur are broken or the organic sulphur compound is extracted, organic sulphur cannot be removed from the coal. Therefore, the amount of organic sulphur present defines the lowest level to which a coal may be cleaned using physical methods. Biological processes theoretically offer the potential of totally removing sulphur near ambient conditions and with low energy requirements. Additionally, biological cleaning is attractive because it involves no associated loss of coal carbon (Rubiera et al., 1997).

1.4.2 Combustion Techniques

There are several technologies which results in improved thermal efficiency and reduced sulphur emissions. These include: bubbling fluidized bed combustion (BFBC), circulating fluidized bed combustion (CFBC), and pressurized fluidized bed combustion (PFBC); Integrated gasification combined cycle (IGCC) and Combined cycle gas turbine (CCGT). Fluidized bed combustion (FBC) is a technology for burning hard and brown coal, but it can also burn other solid fuels such as petroleum coke, and low grade fuels such as waste, peat and wood. The use of calcium-based sorbents, such as limestone or dolomite, in fluidized bed combustion of coal to reduce sulphur dioxide emissions is a well established technique (Xie et al., 1999). Limestone is introduced into the fluidized bed combustor within the temperature range 750-900ºC, the limestone is rapidly calcined to the porous calcium oxide, which can

subsequently react with SO_2 to form calcium sulphite and calcium sulphate. Emissions can be further reduced by integrated combustion control in the system due to the addition of lime/limestone to the bed material. The IGCC is based on the transformation of coal into synthetic gas. After the gasification stage, the gas is cleaned by means of water and absorption dissolvers. Thus an IGCC plant has significantly lower emissions of SO_2, NO_x, and particles than standard coal-fired power plants. However, the units for gasification, purification, and other auxiliary systems raise the initial capital outlay and imply higher operational costs (Abadie & Chamorro, 2006). The IGCC technology can reach SO_2 emissions limit values of 200 mg/m^3 or 1.7 g/kWh_e with coal of 1% sulphur.

1.4.3 Post-combustion Technologies

Flue gas desulphurization is one of the post combustion techniques used in reducing SO_2 emissions. Almost all commercial FGD processes are based on the fact that SO_2 is acidic in nature, and remove the SO_2 from flue gases by reaction with a suitable alkaline substance. The most commonly used alkaline materials are limestone (calcium carbonate), quicklime (calcium oxide) and hydrated lime (calcium hydroxide). Limestone is an abundant and therefore relatively cheap material and both quicklime and hydrated lime are produced from limestone by calcination. As the flue gas contacts with the slurry of calcium salts, SO_2 reacts with the calcium to form hydrous calcium sulphate/gypsum. Other alkalis sometimes used include sodium carbonate, magnesium carbonate and ammonia.

When the Phase I of the Clean Air Act was introduced in the United States, an overwhelming number of utilities chose to switch to low-sulphur fuels rather than install FGD (DePriest, & Gaikwad 2003). With impending bills set to recommend substantial reductions in SO_2

emissions, the units that had already fuel switched will need further reductions, which will not be possible by further fuel switching. The same argument applies to physical pretreatment and/or blending and boiler modernization i.e. their capacity to keep up with the changing emission reduction requirements is limited. Therefore, flue gas desulphurisation (FGD) technology offers the best option for meeting current and future SO_2 emission reduction requirements.

1.5. FLUE GAS DESULPHURISATION

The notion of scrubbing SO_2 from coal derived flue gas dates back to the 1920s and 30s when the first scrubbers were built in Great Britain. Flue gas desulphurization (FGD) was already applied in the Battersea power plant in London in 1926, where it consisted of scrubbing the flue gas with water from the station condensers together with alkali dosing (Heelen 2002). It was fitted to a 228 MW_e coal-fired boiler system and was commissioned in 1933. A further unit was commissioned in 1949 and both plants operated through the early 1970s (Department of Trade and Industry, 2003). This approach was similar to a modern sea-water washing (SWW) FGD process but with alkali dosing.

Almost all commercial FGD processes are based on the fact that SO_2 is acidic in nature, and remove the SO_2 from flue gases by reaction with a suitable alkaline substance. The most commonly used alkaline materials are limestone (calcium carbonate), quicklime (calcium oxide) and hydrated lime (calcium hydroxide). Limestone is an abundant and therefore relatively cheap material and both quicklime and hydrated lime are produced from limestone by calcination. Other alkalis sometimes used include sodium carbonate, magnesium carbonate and ammonia.

The major FGD processes are:

- Wet Processes: included here are the limestone gypsum, seawater washing, ammonia scrubbing, and the Wellman-Lord processes.

- Semi-dry Processes: Includes the circulating fluidized bed, and sorbent spray dry.

- Dry Processes: includes furnace sorbent injection, induct sorbent injection, and sodium bicarbonate injection.

The difference between the different classifications lies in the state of the reactants and the products. In the wet type FGD process, the reagent is introduced as a slurry and the reaction products are in a slurry form while in the semi-dry process, the reagent is introduced as a slurry and the reaction product is a dry solid. In the dry process, the reagent is introduced as a dry solid and the product is a dry solid.

Worldwide, by 2000, there were 678 FGD systems operating on a total capacity of 229 GW_e (Nolan, 2000). Approximately 79 % of the units, representing 199 GW_e of capacity, are based on lime or limestone wet scrubbing and 18 % of the units, or about 25 GW_e, utilize either sodium based or lime slurry (spray) dry scrubbing.

1.6. PROBLEM STATEMENT

It is important to note that most studies of using calcium-based materials as sorbents for SO_2 removal have been carried out in overseas countries. These studies were carried out using materials and research conditions prevailing in the particular countries. Furthermore, all South

African coal-fired power stations burn low grade coal allowing the high grade coal to be exported. As a result, coal-fired power stations in South Africa emit higher emissions than the overseas power stations which are operated on high grade coals. Thus the results achieved internationally may not be directly translated to the South African conditions. To the best of the author's knowledge, there has been no study reported in literature on the removal of SO_2 from flue gas by FGD using South African calcium-based materials under South African conditions. Therefore, in order to determine whether the South African calcium-based materials are technically feasible as sorbents for the removal of SO_2 and to bridge an existing gap in literature, it is the aim of this investigation is to study and/or rank the performance of locally available materials (i.e. limestone, dolomite, or calcrete) as sorbents in the capture of sulphur dioxide emissions from power plants.

1.7. OBJECTIVES OF THE CURRENT RESEARCH

The objectives of the current work in characterizing different calcium – based materials available in South Africa and estimating their SO_2 binding properties can be summarized as follows:

a) To develop an extensive literature database on SO_2 - reduction technologies

b) To characterize South African limestone and dolomite deposits as possible sorbents for SO_2 removal from power plant flue gasses.

c) To carry out a physico-chemical analysis of samples of limestone and dolomite of different geological age obtained from the most important deposits and mines and determine their chemical composition and physical properties.

d) To carry out experiments on the dissolution process of selected limestone and dolomite samples by means of the pH-stat method, estimate the change in structural properties of the samples during dissolution, describe the dissolution process mathematically, and determine the kinetic parameters of the process.

e) To carry out experiments of the sulphation process of selected limestone and dolomite samples at low temperatures, and determine the parameters describing the kinetics and diffusion in SO_2 binding.

f) To compare the SO_2 binding properties of the different limestone and dolomite samples.

g) To qualitatively rank the performance of the South African calcium-based materials as SO_2 sorbents

1.8 DELIMITATIONS

The current research will not involve the design and/or fabrication of an FGD system. Instead it will be limited to the investigation of performance of the local sorbents in a laboratory scale FGD test unit whose conditions approximate those found in full scale commercial FGD systems.

1.9 THESIS LAYOUT

Chapter 1 of this thesis presents an introduction to the problem under study and also presents the options which are currently available for the SO_2 control.

Chapter 2 gives an overview of the existing flue gas desulphurization (FGD) technologies, their application, and performance. A review of the available reactivity measurement techniques are also included in this chapter.

Chapter 3 gives a review of the theoretical models that have been used in the modeling of the desulphurisation process. Rate expressions for the dissolution process are also presented.

Chapter 4 describes the experimental equipment, procedures, and materials used in this study.

Chapter 5 presents the results obtained from the experiments and their analysis. The mathematical models discussed in Chapter 3 are used to obtain the corresponding rate constants by fitting to the experimental data.

Chapter 6 gives the a summary of the major findings of the research, the conclusions reached and recommendations for further work.

CHAPTER 2

2. LITERATURE SURVEY[1]

2.0 INTRODUCTION

This chapter gives an overview of the existing flue gas desulphurization (FGD) technologies, their application and performance. A review of the factors that influence the desulphurization process are also included.

The major FGD processes can be classified as:

- Wet Processes: includes the limestone gypsum, seawater washing, ammonia scrubbing, the Wellman-Lord processes, biological desulphurization, and magnesium enhanced lime,
- Semi-dry Processes: Includes the circulating fluidized bed, and sorbent spray dry; and
- Dry Processes: includes furnace sorbent injection, induct sorbent injection, and sodium bicarbonate injection.
- Combined SO_x/NO_x removal processes

Figure 2.1 shows the location of the FGD techniques in the overall power plant scheme.

2.1 WET FGD PROCESSES

Wet FGD scrubbers are the most widely used FGD technology for SO_2 control in the world accounting for about 84% of the total capacity of all desulphurisation methods (Kaminski,

[1] Based on: Siagi Z.O. & Mbarawa M. 2008. An overview of SO_2 emission reduction techniques. R&D Journal. Volume 24, No. 1. 26-33.

2003). Many FGD systems are operating successfully at many coal-fired power facilities ranging in size from less than 100 MW to 1000MW. They can achieve SO_2 removal efficiencies as high as 99 %. Calcium-, sodium-, and ammonia-based sorbents have been used in a slurry form, which is injected into a specially designed vessel to react with the SO_2 in the flue gas.

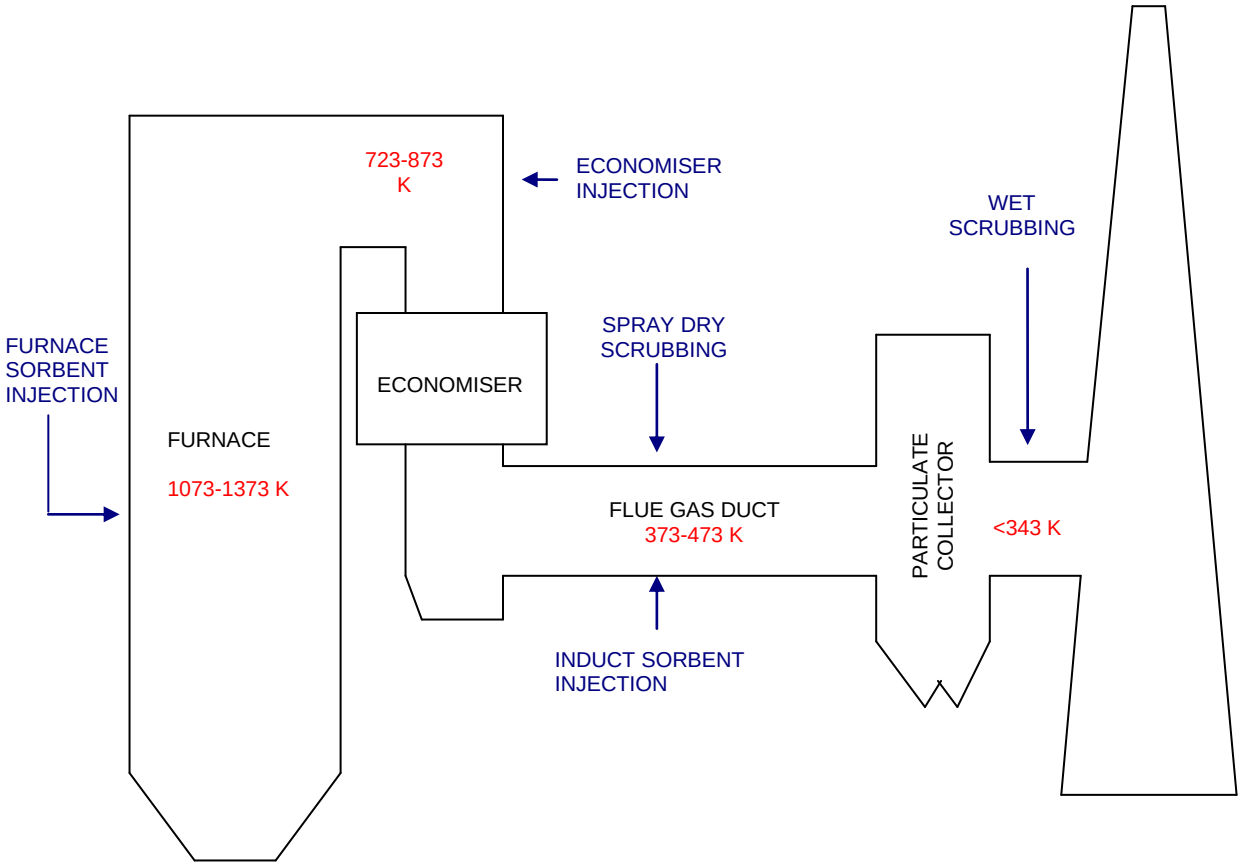

FIGURE 2.1**:** Principal flue gas scrubbing (Golesworthy, 1999)

The preferred sorbent in operating wet scrubbers is limestone followed by lime. The chemical reaction which occurs with a limestone sorbent can be expressed in a simple form as:

$$CaCO_{3(s)} + SO_{2(g)} \rightarrow CaSO_{4(s)} + CO_{2(g)} \qquad (2.1)$$

In practice, air in the flue gas causes some oxidation and the final product is a wet mixture of calcium sulphate and calcium sulphite. In a wet FGD employing forced oxidation, in situ or ex situ (in the scrubber or in a separate reaction chamber), the overall reaction is given by:

$$CaCO_{3(s)} + SO_{2(g)} + 1/2\,O_{2(g)} \rightarrow CaSO_4.2H_2O_{(s)} + CO_{2(g)} \qquad (2.2)$$

resulting in solid gypsum which has found commercial use in wallboards, cement, and plaster (Zheng et al., 2002). According to Danish and other European standards, gypsum should have less than 3-4 wt% residual limestone to be marketable (Kiil, Nygaard, & Johnson, 2002). A variety of scrubber designs have been developed depending on how the gas and sorbent slurry are brought into contact. Four main types of wet scrubbers are available: the spray scrubber, the packed tower, the jet bubbling reactor, and the double loop reactor (Zheng et al., 2002). Breakdown capacity in service with wet FGD technology is given in Table 2.1 (Maller & Holliden, 2003).

TABLE 2.1: MW capacity in service with wet FGD in 1998

Technology	**Capacity (MW)**
Limestone	163,330
Lime	21,172
Dolomitic Lime	10,342
Sodium Carbonate	2,831
Seawater	1,125
Other	433
Total wet FGD	199,233

2.1.1 Limestone Gypsum Process

In the limestone gypsum wet scrubbing process, the flue gas is treated with limestone slurry in order to remove the SO_2 and neutralize it. The final product is calcium sulphate dihydrate (gypsum). This is the most common FGD process now being installed worldwide, and has evolved over the last 30 years. Nowadays, a plant would normally be designed to achieve a high quality gypsum product, which is suitable for wallboard manufacture. As mentioned earlier there are a number of process variants and equipment arrangements which can be adopted. An advanced flue gas desulphurisation demonstration unit at the Bailly Generating station of Northern Indiana Public Service Company (NIPSCO) achieved a maximum removal efficiency of 98 % using coals having sulphur contents between 2.25 % and 4.5 % (Department of Energy, 1999). The availability of the system was high at 99.5 % over a three year period thereby eliminating the need of a spare module. The limestone gypsum process is the most well-developed and widely adopted FGD process worldwide, and is normally adopted for large power stations. The total worldwide installed capacity is approximately 149,000 MWe for coal-fired plant alone (Department of Trade and Industry, 2000).

The SO_2 removal efficiency of FGD plants using $CaCO_3$ as sorbent can be improved by the addition of various organic acids (Frandsen et al., 2001). These include adipic acid, dibasic acid (DBA), formic acid, glutaric acid and succinic acid. In a wet limestone scrubber demonstration project at the Milliken Power Station, Lansing New York, the SO_2 removal efficiency increased from 83 % without formic acid to 95 % with formic acid. At the same removal efficiency, using formic acid results in a 75 % reduction in energy required for circulating the sorbent slurry (Department of Energy, 1999). A jet bubbling reactor has also

been successfully demonstrated at Georgia Power Company's Plant Yates. This plant, rated at 100 MWe, burns coal with a sulphur content ranging from 1.2 % to 4.3 %. It had a limestone utilization greater than 97 % and achieved a SO_2 removal efficiency of 98 % when burning 2.2 % sulphur coal and about 95 % with 3.5 % sulphur coal (Department of Energy, 1999).

2.1.2 Sea Water Scrubbing (SWW) FGD Process

Sea-water washing is an economical alternative for plants located near the coast. The sea-water washing (SWW) process uses untreated sea water to scrub the flue gas, taking advantage of sea water's natural alkalinity in order to neutralize the SO_2. When SO_2 comes in contact with seawater, there is a fast and efficient reaction between the SO_2 and calcium carbonate in the sea water to form calcium sulphate and CO_2. The reaction neutralizes the acidity of SO_2 and consumes some of the buffering capacity of the seawater. The reaction is complete in a very short time, so the equipment to bring the flue gas and the seawater in contact can be compact. As a final product, dissolved sulphate ions are obtained, which are already contained in the sea water as a natural constituent. After scrubbing, the water used is treated with air to reduce its chemical oxygen demand and its acidity, and is then discharged back to the sea (Skaninavisk Miljo Service, 2007). In all applications of the SWW process on power plant, raw seawater is obtained from the steam turbine condenser outlet. SWW is a rapidly expanding Technology, particularly in tropical countries. There are two major suppliers of SWW units; Lurgi Lentjes Bischoff (LLB) and Asea Brown Boveri (ABB). ABB has built 21 plants with a total installed capacity equivalent to 2470 MW_e. LLB is currently commissioning two 660 MW_e plants in Indonesia (Department of Trade and Industry, 2000). Its main advantage is that it requires no solid sorbent as a reagent, unlike nearly all other FGD

processes. The plant design is relatively simple and the only obvious disadvantage is that it is limited to use at coastal sites. The process is capable of very high SO_2 removal (up to ~97 – 98 %) (Department of Trade and Industry, 2000), but only if the fuel sulphur content is below 2.5 - 3.0 wt.%. After an evaluation of various FGD technologies, the Scottish Power Company selected SWW as the most appropriate option for its large coal-fired power station at Longannet (Balint, 1995).

2.1.3 Ammonia Scrubbing FGD Process

The ammonia/ammonium sulphate scrubbing process works in a similar way to the limestone gypsum process except that aqueous ammonia is used as the scrubbing agent. SO_2 is removed from the flue gas by reaction with ammonia and the final product is ammonium sulphate. Ammonia scrubbing has been used intermittently since the 1950s. The only plant currently operational is installed on a 350 MW_e oil-fired boiler system at Dakota Gas company's Great Plains plant. This has been designed for 93 % SO_2 removal, treating gas from high-sulphur oil (Department of Trade and Industry, 2000). A potential risk arises from the need to store ammonia on site, either in anhydrous form or as a concentrated aqueous solution. The process has the advantage that there is no waste water discharge and there are unlikely to be problems of scaling and blockage. This process is very attractive for plants burning high sulphur fuels. However, it is unlikely to achieve widespread use because very few plants are needed to satisfy the market for ammonium sulphate fertilizer in a particular region or country.

2.1.4 The Wellman-Lord process

A well-developed sodium scrubber is the Wellman-Lord SO_2 recovery process, which has found use in power plants, refineries, sulphuric acid plants, and other industrial installations in the USA, Japan and Germany. The process utilizes a water solution of sodium sulphite for scrubbing and generates concentrated SO_2 (about 90 %), in effect removing the SO_2 gas from other flue gases. The Wellman-Lord process is regenerative, i.e. the active reagent used for SO_2 removal from the flue gas is regenerated in a second process stage, and returned to the first stage for re-use. This process has the advantage that it does not require the consumption of large quantities of sorbent and consequently does not produce large quantities of solid waste.

The flue gas from coal-fired power plants is first pretreated by cooling and removal of particulate matter, i.e. by electrostatic precipitators (ESP), prior to being sent to the absorber. In the absorber, the water solution of sodium sulphite absorbs the SO_2 in the pretreated flue gas to produce sodium bisulphite according to:

$$SO_{2(g)} + Na_2SO_{3(s)} + H_2O_{(l)} \rightarrow 2NaHSO_{3(s)} \qquad (2.3)$$

The desulphurized gas is reheated before going to the stack in order to improve atmospheric dispersion. The sodium bisulphite is sent to a forced-circulation evaporator-crystallizer via a surge tank. The surge tank allows steady flow rates into it despite gas flow and concentration fluctuations. Through the application of low pressure steam, such as from a turbine exhaust, the sulphite is regenerated in the form of a slurry according to:

$$2NaHSO_{3(aq)} \rightarrow SO_{2(g)} + Na_2SO_{3(aq)} + H_2O_{(l)} \quad (2.4)$$

The H_2O is separated from the SO_2 in a condenser and recycled to a dissolving tank where the sulphite slurry is redissolved and sent back to the absorber via a solution surge tank that has the same function as the one mentioned above. A small amount of circulating solution oxidizes to non-regenerable sodium sulphate crystals that must be disposed of. This necessitates purging a small stream of solution and adding fresh sulphite. The product SO_2 may be utilized to produce liquid SO_2 or sulphuric acid, on site or in a satellite plant, or to produce elemental sulphur. A well-known process for doing this is called the Claus process, which is based on the addition of H_2S according to:

$$SO_{2(g)} + 2H_2S_{(g)} \rightarrow 3S_{(s)} + H_2O_{(l)} \quad (2.5)$$

The San Juan generating station, located approximately five miles west of Farmington, New Mexico, is one of the power plants in the world that have been operating using a Wellman-Lord process to clean its flue gas. The plant consists of coal-fired pressurized units with a total generating capacity of 1614 MW. The plant meets or exceeds all state and federal standards using its Wellman-Lord FGD process. However, in 1998, Public Service of New Mexico elected to convert the Wellman-Lord system to a limestone forced oxidation system which is both environmentally sound and cost-effective to operate (Comstock, 1998; Taylor & Nischt, 1998).

2.1.5 Biological desulphurisation

Biotechnological flue gas desulphurisation makes use of the following conversions of the sulphur cycle:

$$SO_{2(g)} + H_2O_{(l)} \rightarrow HSO_{3(aq)}^{-} + H_{(aq)}^{+} \quad (2.6)$$

$$HSO_{3(aq)}^{-} + 1/2\,O_{2(g)} \rightarrow SO_{4(aq)}^{2-} + H_{(aq)}^{+} \quad (2.7)$$

$$HSO_{3(aq)}^{-} + 6\,\{H\}_{(aq)} \rightarrow HS_{(aq)}^{-} + 3H_2O_{(l)} \quad (2.8)$$

$$SO_{4(aq)}^{2-} + 8\,\{H\}_{(aq)} \rightarrow HS_{(aq)}^{-} + 3H_2O_{(l)} + OH_{(aq)}^{-} \quad (2.9)$$

In the first step of a biological FGD process, sulphur dioxide is scrubbed from the flue gas using a biocarbonate solution (Equation 2.6). The presence of oxygen in the flue gas results in oxidation of part of the sulphite into sulphate (Equation 2.7). In the subsequent step, sulphite and sulphate are reduced under anaerobic conditions with an added electron donor {H} to sulphide by sulphate-reducing bacteria (Equations 2.8 & 2.9). In a micro-aerobic reactor, the sulphide produced is partially oxidized by autotrophic sulphur bacteria with concomitant production of hydroxide. Separation of the solid sulphur from the medium enables the recovery of elemental sulphur as a valuable product. The remaining alkaline solution, with a pH of about 9, can be re-used for the scrubbing of SO_2. Because – along with SO_2 – heat is also transferred from the flue gas to the scrubbing solution, it is economically attractive to

operate the desulphurisation process at thermophilic conditions (50 – 65 ^{o}C) (Goorissen, 2000).

2.1.6 Magnesium enhanced lime (MEL) process

In the MEL process, slaked lime containing calcium hydroxide [$Ca(OH)_2$] and a portion of magnesium hydroxide [$Mg(OH)_2$], is used to react with SO_2. Calcium hydroxide in a slurry form, reacts with SO_2 to form solid calcium sulphite ($CaSO_3$. ½ H_2O). Magnesium hydroxide reacts with the remainder of the SO_2 to form soluble magnesium salts, magnesium sulphite and magnesium bisulphite [$MgSO_3$, $Mg(HSO_3)_2$]. These soluble magnesium salts greatly increase SO_2 capture and allow reduction in power consumption and equipment costs. When the magnesium sulphite is present in the slurry in contact with flue gas, it buffers (prevents from falling sharply) pH of the slurry as it absorbs acidic SO_2 (DePriest & Gaikwad, 2002). This improves absorber performance by increasing solubility of SO_2 in the slurry, which allows operation at a lower liquid/gas (L/G) ratio. MEL is able to achieve high SO_2 removal efficiencies in significantly smaller absorber towers than the limestone scrubbers. It also allows operation at a lower slurry pH, near 6.0, which improves reagent utilization to near 100% (Srivastava, 2000).

2.2 SEMI-DRY FGD PROCESSES

In this type of technology, the reactive reagent is introduced into the system as a fine suspension and results in a dry solid product.

2.2.1 Circulating Fluidized Bed (CFB) FGD Process

Circulating fluid bed (CFB) and moving bed technologies, which utilize a dry sorbent to reduce SO_2 emissions in a flue gas stream in a dedicated reaction chamber are categorized as dry scrubbers. The CFB principle for absorbing acid gases was developed in Germany in the 1970s (Ortiz & Ollelo, 2001). In the mid-1980s, this process was used for FGD in coal-fired power stations in Germany. Since 1984, only a few installations have been built in Germany and some neighbouring countries. Besides these plants, two North American units have been operational since 1995. There is also an operating CFB FGD plant at CINERGETICA (Czech Republic). Handling a flow volume of 400,000 m^3/h, it achieves a SO_2 removal efficiency of 93 % at a Ca/S ratio of 1.4 and 70 % for Ca/S ratio of 1.3 (Dipez, 2007) .

In the circulating fluid bed (CFB) scrubber process, hydrated lime is injected directly into the CFB reactor. Water is also injected into the bed to obtain an operation close to the adiabatic saturation temperature. Flue gas enters the CFB reactor at the bottom, flows vertically upwards through a venturi section and enters the upper cylindrical vessel (Figure 2.2). The height of the bed is designed to accommodate the mass of bed material required to achieve a residence time of about 3 seconds.

The process is easy to maintain and operate since it does not require high maintenance mechanical equipment such as abrasion resistant slurry pumps, water atomizers or sludge dewatering devices. The process can achieve >95 % SO_2 removal efficiencies. The CFB process, like any other dry post-furnace FGD process, has some generic advantages with respect to the widely used wet FGD technology: capital costs and energy consumption are

low, installation is simple, construction time is short, little space is needed, and no wastewater treatment is required.

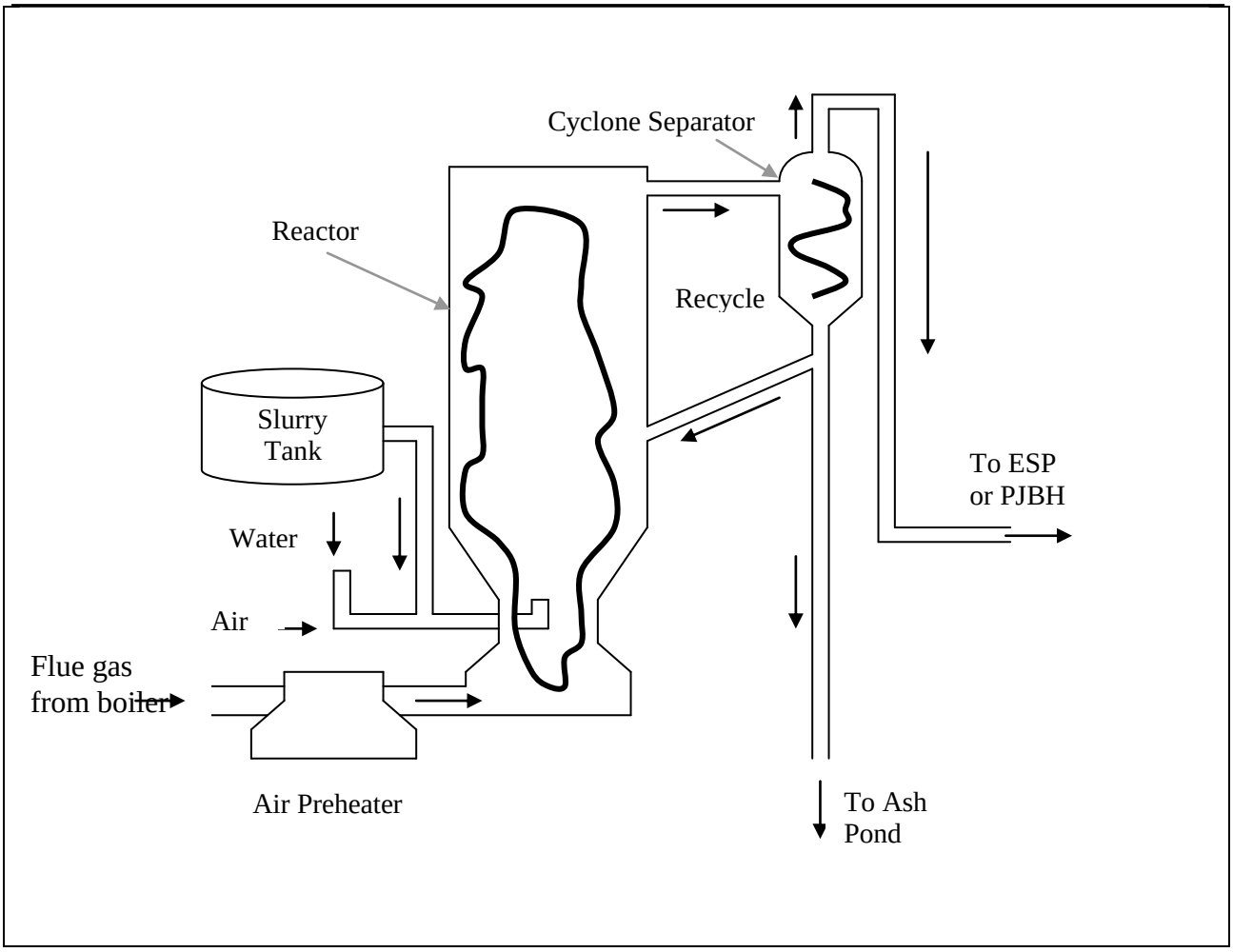

FIGURE 2.2: Circulating Fluid Bed (CFB) FGD process

However, the CFB process also shares some drawbacks with the other dry technologies: extremely high removal efficiencies are difficult to reach, the utilization of the expensive slaked lime is low to medium, the total amount of solid waste to be disposed of is great, and the risk of solid deposition inside the absorption unit is high, and, finally, the dust emissions from the ESP may increase due to the higher concentration of the particulate matter entering the collector (Ortiz & Ollelo, 2001).

The Tennessee Valley Authority has tested the gas suspension absorption (GSA) concept at a 10 MW_e demonstration project (Department of Energy, 2003). Results of the test program indicated that the calcium/sulphur (Ca/S) molar ratio had the greatest effect on SO_2 removal, with approach-to-saturation temperature next, followed closely by chloride content. At a Ca/S molar ratio of 1.4 with 18 ^oF approach-to-saturation and 0.12 % chloride, the GSA/ESP achieved 90 % sulphur capture while the GSA/ pulse jet baghouse (PJBH) achieved 96 % sulphur capture. In all the tests, a coal of sulphur content between 2.6 % and 3.5 % was used. On the operational, the GSA/ESP lime utilization averaged 66.1% and GSA/PJBH averaged 70.5 %. The reactor achieved the same performance as a conventional spray dryer, but at one-quarter to one-third the size. Additionally, the GSA generated lower particle loading than a conventional spray dryer, special steels were not required in construction, and only a single spray nozzle is needed. High reliability and availability similar to other commercial applications were also demonstrated.

2.2.2 Spray-Dry FGD Process

The flue gas from the air heater is carried into the spray-dryer vessel, where it comes into contact with a finely atomized spray of lime and by-product slurry, delivered from a high-speed atomizer. This removes up to 95 % of the SO_2 and most if not all SO_3 and HCl (Department of Trade and Industry, 2000). The normal sorbent fed to this process is quicklime. This is slaked on site, with excess water, to produce a calcium hydroxide slurry (slaked lime). This is mixed with recycled by-product before being pumped to the rotary atomizer. Water is evaporated by the heat of the flue gas. The residence time (about 10 seconds) in the reactor is sufficient to allow for the SO_2 and other acid gases, such as SO_3 and

HCL, to react simultaneously with the hydrated lime to form a dry mixture of calcium sulphate/sulphite. Waste water treatment is not required in spray dry scrubbers because the water is completely evaporated in the absorber. The flue gas, along with dried reaction products and solid particulate, is then passed through a fabric filter or an electrostatic precipitator. If a fabric filter is used, additional SO_2 and acid gas removal occurs as the flue gas passes the built up filter cake on the bag.

As with other semi-dry systems producing a throw-away by-product, the spray-dry process is relatively cheap to install, typically being ~70 % of the cost of the equivalent limestone gypsum system. However, the variable operating costs are among the highest of the major FGD processes, due to both the high lime usage and the costs of by-product disposal. Spray dry scrubbers are the second most widely used FGD technology. In commercial use, they have been known to achieve removal efficiency in excess of 90% with some suppliers giving >95 %. The total installed capacity worldwide is in excess of 15,000 MW_e. The technology is well understood and offered by a number of contractors (Srivastava, 2000).

2.3 DRY FGD PROCESSES

2.3.1 The Duct Sorbent Injection Process (DSI)

In-duct desulphurisation process involves the injection of a dry sorbent, typically hydrated lime, in conjunction with flue gas humidification achieved by spraying water into the ductwork downstream from the air preheater but upstream from the particulate collection equipment. The main reaction binding the SO_2 is a simple acid-base reaction:

$$SO_{2(g)} + Ca(OH)_{2(s)} \rightarrow CaSO_3 \cdot \tfrac{1}{2} H_2O_{(s)} + \tfrac{1}{2} H_2O_{(g)} \qquad (2.10)$$

The operating parameters of this DSI process are the Calcium/Sulphur (Ca/S) ratio and the approach to the adiabatic saturation temperature. Increasing the Ca/S ratio leads to higher SO_2 removal yields but at the expense of lower sorbent utilization (Ortiz & Ollelo, 2001). On the other hand, decreasing the approach to saturation temperature has a strong positive effect on the SO_2 removal efficiency and sorbent utilization. However, there is a minimum practical approach to saturation of around 8 – 10 ^oC due to the growing risk of solid deposits on the duct walls and on the internal parts of the process equipment and also due to corrosion of material. There are different DSI technologies based on three basic process alternatives – slurry injection and dry sorbent injection upstream/downstream from the spray humidification. The final product is a powdered mixture of calcium compounds. It is one of a number of FGD processes developed or being developed primarily for those instances in which a moderate degree of desulphurisation (50 – 75 %) is required on plant with limited operating hours and remaining lifetime (Department of Trade and Industry, 2000). So far, in-duct sorbent injection technology has been actively developed, mainly in the USA, since the 1980s. A 73.5 MW_e demonstration was conducted in a US coal-fired boiler, achieving 50% sulphur removal efficiency at flue gas temperatures of 149 – 154 ^oC and Ca/S ratios 2 - 2.5 (Ortiz & Ollelo, 2001). According to these data, sorbent utilization was less than 25 %. In this process, the lime was injected into the ductwork as a slurry.

2.3.2 Furnace Sorbent Injection

This is another process developed for moderate degrees of desulphurisation with low capital costs. The process involves the injection of hydrated lime into the furnace cavity of the boiler to absorb SO_2. Spent sorbent is extracted with the fly ash in an ESP or fabric filter (FF). The final product is a mixture of fly ash and calcium compounds. There are very few plants now in commercial use, most being in Poland. It is one of the cheapest FGD processes to install but can be expensive to operate because it is inefficient in its use of sorbent. Because of this, sorbent injection is most suitable for retrofit situations. It is well suited to a situation where only low SO_2 removal efficiency is required, and where there is little space available in the plant unit area (Golesworthy, 1999; Maller & Holliden, 2003).

2.3.3 The Sodium Bicarbonate Injection Process

This process involves the direct injection of sodium bicarbonate into the flue gas duct downstream of the air heater, to react with and remove acidic compounds such as SO_2, SO_3 and HCl. The final product is a dry powdered mixture of sodium compounds and fly ash. It is suitable primarily for those applications where a moderate degree of desulphurisation is required at low capital cost, although it should be noted that the reagent itself is relatively expensive. Sodium bicarbonate is pneumatically injected into the fly ash as a fine dry powder. This removes up to ~70 % of the SO_2 from the flue gas. From here, the gas is carried through the dust arrestor and the induced draft (ID) fan before discharge through the stack. All the particulate matter from the process are carried with the flue gas into the dust arrestor – an ESP or fabric filter (FF).

Sodium scrubbing has been successfully employed at the Jim Bridger Power station in Wyoming (Mortson & Telesz, 2001). The Electric Power Research Institute (EPRI) carried out the initial work on sodium scrubbing in 1978 and the Jim Bridger plant opened in the early 1980s. The Bridger plant is rated at 2200 MW (4 units). This installation clearly demonstrated the efficiency of sodium based FGD. However, the costs of the sodium absorbents for the system and waste stream management have prevented widespread use of sodium based scrubbing. There is ongoing research for the transformation of the sodium sulphate waste stream from the absorption step back into sodium bicarbonate sorbent and ammonium sulphate fertilizer. This would greatly improve the commercial viability of the process. The process can achieve SO_2 removal efficiencies of up to 95 % and up to 98 % using dry sodium bicarbonate and a wet sodium carbonate solution respectively. The extent of the NO_x reduction is 40 – 95 % depending on conditions (Mortson & Telesz, 2001).

2.3.4 Activated Carbon

The activated carbon process is a regenerable process that adsorbs SO_2 on a moving bed of granular activated carbon. After the adsorption, the activated carbon is thermally regenerated to produce a concentrated SO_2 stream. SO_2 may then be treated by conventional technologies to produce sulphuric acid (Srivastava, 2000). The activated carbon adsorption process is known to have high adsorption capacities for diverse toxic gases because of the high surface area and microporous structure of activated carbon (Lee et al., 2003). Advances in activated carbon FGD research have indicated that activated carbon fibers (ACF) have better performance characteristics than the carbon granules used in the early process (Boudon, 2003). Treatment with ammonia has been shown to enhance both the adsorption and oxidation

capacity of ACF. However, beyond the laboratory scale, activated carbon FGD has not found widespread application in the industrial market (Boudon, 2003; Boudon et al., 2003).

2.3.5 Copper oxide desulphurization

This is a regenerative process. The flue gas is brought in contact with CuO (Figure 2.3) whereupon SO_2 reacts with CuO and O_2 to form copper sulphate in the temperature range 350 – 500 ºC (Lin & Deng, 1998). The sorption of SO_2 may be represented by the following reactions (Piotrowski et al., 2005):

$$SO_{2(g)} + \tfrac{1}{2} O_{2(g)} \rightarrow SO_{3(g)} \quad (2.11)$$

$$CuO_{(s)} + SO_{3(g)} \rightarrow CuSO_{4(s)} \quad (2.12)$$

The copper, as copper oxide, acts both as a catalyst for the oxidation of SO_2 and as a sorbent of the SO_3 formed. Figure2.3 shows a schematic of the process. Recent research has been focused on fixing copper into a porous, strong support that optimizes the reaction of SO_2 with CuO. Good results have been obtained using γ-alumina in terms of mechanical strength, sorbent reactivity, and regenerability (Buelna & Lin, 2004). Granular sorbents can be prepared by wet-impregnation method, immersing the γ-alumina granules in a copper solution followed by drying and calcinations, or by solution-sol mixing method, which allows in-situ coating of active species in the granulation step. Other metal oxides which have been investigated for SO_2 capture include; CrO_2, BeO, ZrO_2, ZnO, MoO_2, WO_2, NiO, SnO_2, MnO_2, TiO_2, Al_2O_3, and MgO (Elseviers & Verelst, 1999).

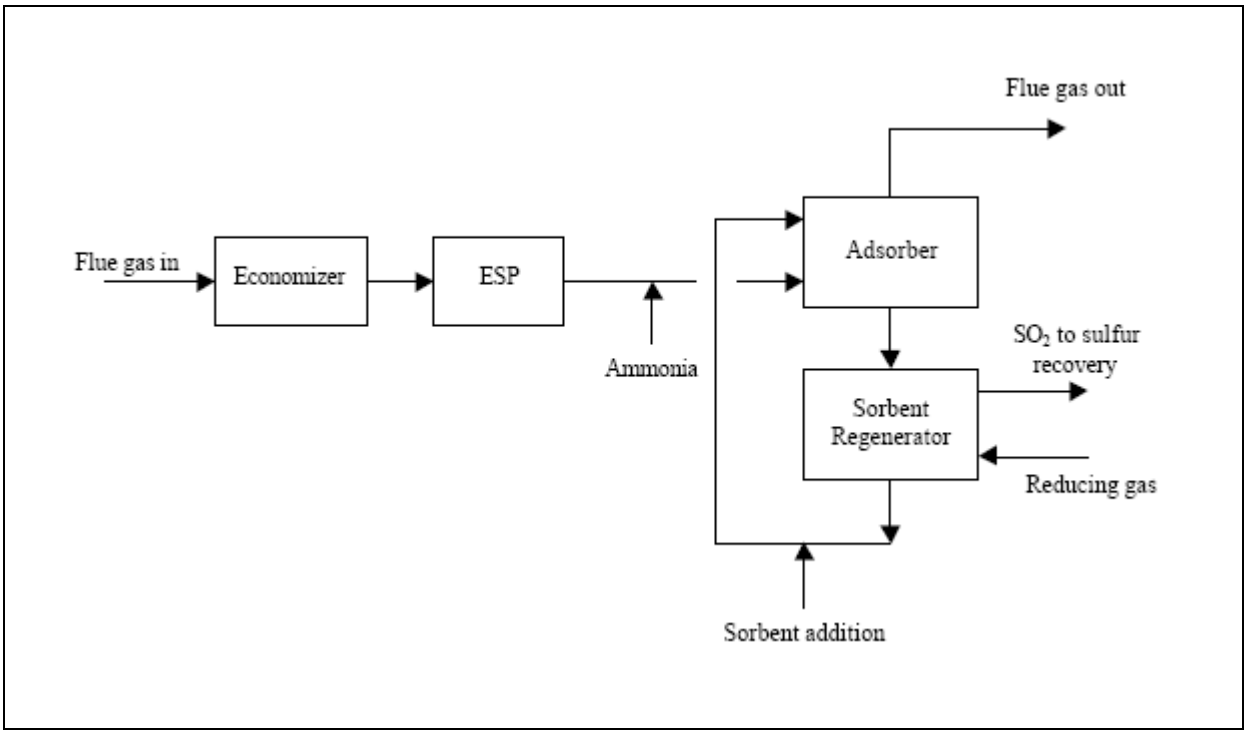

FIGURE 2.3**:** CuO desulphurization process

The sulphated sorbent can be thermally regenerated at temperatures of 700 ˚C and higher. The problem of this approach, besides requiring additional energy input, is the loss of absorption efficiency and of sorbent granule strength because of thermal stress. Regeneration by reduction is more attractive as it can be done in the same temperature range used for sulphation. The regeneration is done with a reducing gas stream such as methane or carbon monoxide at about 400 ˚C. Reduction using methane follows the reaction (Piotrowski et al., 2005):

$$CuSO_{4(s)} + \tfrac{1}{2}CH_{4(g)} \rightarrow Cu_{(s)} + SO_{2(g)} + \tfrac{1}{2}CO_{2(g)} + H_2O_{(g)} \qquad (2.13)$$

The copper can then be oxidized to copper oxide using oxygen. The concentration of SO_2 in the regeneration off-gas is high enough for further processing to generate sulphuric acid or elemental sulphur (Lin & Deng, 1998).

2.4 COMBINED SO_X/NO_X REMOVAL SYSTEM

Both SO_2 and oxides of nitrogen (NO_x) are present in flue gases. Since emissions of both is regulated, it would, in principle, be highly desirable to remove both using the same process. However, despite the fact that both are acidic (and therefore amenable to reaction with a range of alkaline substances), in practice, separate methods are normally used for the control of each; conventional FGD processes are used to restrict SO_2 emissions and NOx are limited either by combustion measures or selective catalytic reduction (SCR). One reason for this is that any combined SO_x/NO_x removal (SNOX) system would have to be sufficiently effective at removing both species that no further system is required. There are only a few plants operating worldwide that can remove both NO_x and SO_2 and those that are running are complex and expensive, although efficiencies over 90 % for both emissions can be achieved. Combined processes in operation include the activated carbon process, Wet-Gas Sulphuric Acid integrated with SNOX (WSA – SNOx) process, Degussa-SNOX (DESONOX) process, and NOXSO. These type of plants are currently in operation in Denmark (1 retrofit), Germany (2 new, 7 retrofit), Italy (1 retrofit) and the USA (1 new, 9 retrofit).

Typical reactions for the SNOX process are (Schoubye et al., 2001):

SO_2 Removal:

$$SO_{2(g)} + \tfrac{1}{2}O_{2(g)} + H_2O_{(l)} \rightarrow H_2SO_{4(aq)} \quad (2.14)$$

NO_x Removal:

$$2NO_{(g)} + \tfrac{1}{2}O_{2(g)} + 2NH_{3(g)} \rightarrow 2N_{2(g)} + 3H_2O_{(l)} \quad (2.15)$$

Sub reactions

$$NH_{3(g)} + H_2SO_{4(aq)} \rightarrow NH_4HSO_{4(aq)} \quad (2.16)$$

$$2NH_{3(g)} + H_2SO_{4(aq)} \rightarrow (NH_4)_2SO_{4(aq)} \quad (2.17)$$

2.4.1 Electron Beam Ammonia (EBA) Process

The electron beam flue gas treatment technology is one of the most advanced technologies among new generation processes for air pollution control. The process which has been developed in Japan, the United States, Germany and Poland allows simultaneous removal of SO_2 and NO_x. Over the last 20 – 25 years, research on the process has been done in many laboratories and pilot plants. The EBA process consists of three main stages: gas cooling, ammonium injection and electron beam irradiation, and by-product collection and treatment. After ash collection, the flue gas is passed through a spray cooler where it is cooled by water sprays. The cooled gas is then introduced into the process vessel and irradiated with electron beams after the injection of ammonia (Figure 2.4). The powder by-product is collected by the ESP and the treated clean gas is discharged into the atmosphere through the stack.

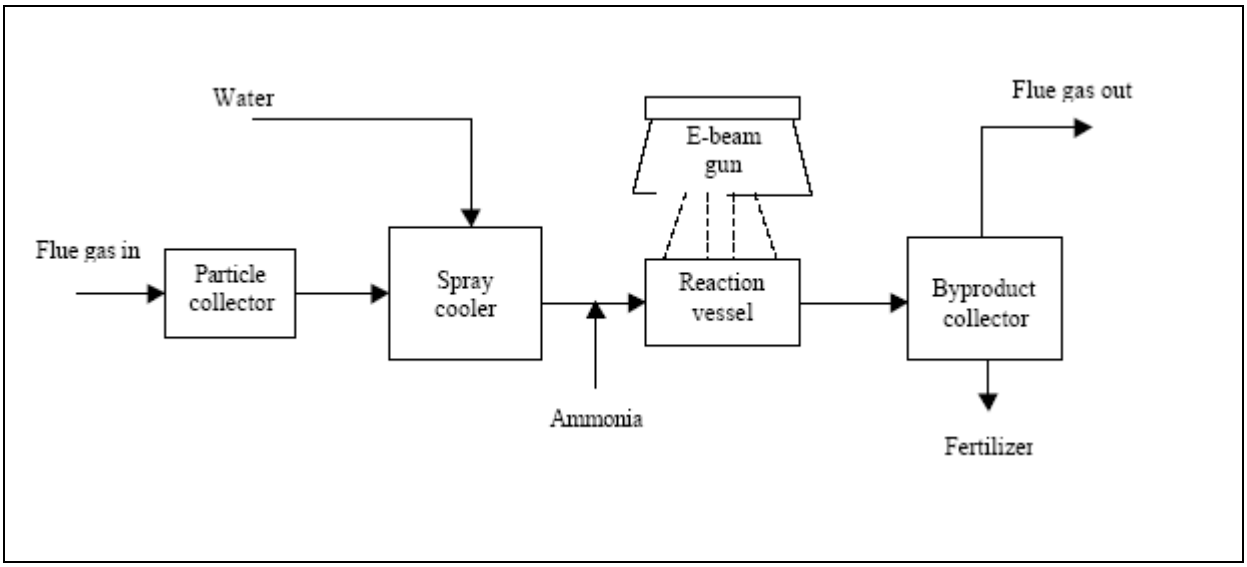

FIGURE 2.4: Electron Beam Ammonia process (Quijada, 2001)

EBA reaction mechanism; The core of the EBA process is a "Process vessel" where electron beam irradiation causes the main reactions to occur in three stages (Doi, Nakanishi, & Konno, 2000). The first stage is the formation of active radicals such as OH, O and HO_2. The second stage is the oxidation of SO_x and NO_x by free radicals to form sulphuric acid and nitric acid respectively. The third stage is the neutralization of these acids by the injection of ammonia to form dry ammonium sulphate and ammonium nitrate solids. Three big pilot plant were installed in coal-fired electric power stations (EPS) at Indianapolis (USA), Nagoya (Japan) and Kawêczyn (Poland). The experience gained during their operation have allowed the preparation of full-scale industrial plant designs. The first such installation was built at EPS Chengdu (China). This is the first full scale EBA desulphurisation unit to operate in the world. Its designed flue gas treatment capacity is 300,000 N m^3/h. The plant demonstrated a SO_2 removal efficiency of 80 % and a NOx removal efficiency of 10 % (Doi, Nakanishi, & Konno, 2000; Yuqing, 2003). Another plant is located in EPS Pomorzany in Szczecin in Poland and treats a maximum of 270,000 N m^3/h of flue gas from two boilers. Removal

efficiencies of up to 95 % for SO_2 and up to 70 % for NO_x have been achieved in this plant (Andrzej et al, 2004). In 2001, the Chubu Electric Power Company Inc. (Japan) put into operation another unit at its EPS Nishi-Nagoya for treating 620,000 N m^3/h of flue gas from a 220 MW_e oil-fired boiler (Licki et al., 2003). The energy consumption in this kind of technology has been estimated at 2-4 % of the total energy produced at the plant (Radoiu et al., 1998).

2.5 EFFECT OF OPERATING PARAMETERS DURING THE FGD PROCESS

2.5.1 Factors Affecting the Wet FGD process

A proper understanding of the factors that influence the desulphurisation process is necessary for the proper design and operation of any FGD process. These include the operating parameters and the reactivity of the sorbent under varying conditions as encountered in full-scale FGD processes. In the wet FGD process, a limestone slurry is used to absorb SO_2 to form solid products. The dissolution of the limestone provides the calcium and carbonate ions necessary for the removal of the SO_2. Below are some of the factors that influence the dissolution process.

2.5.1.1 Effect of the limestone particle size

The particle size may be the single most influential parameter on the reactivity of a sorbent. Hosten and Gulsan (2004) have shown that finer particles show better desulphurisation characteristics than coarse ones. This is possibly due to the higher surface area available for the dissolution reaction making available the necessary alkalinity for desulphurisation. In their

study of spray dry absorption with a lime slurry, Scala, D'Ascenzo, and Lancia (2004) also agree that careful control of the particle mean size is a key to obtain a good spray dry performance. Frandsen, Kiil, and Johnsson (2001) have experimentally shown that by changing limestone size from one of 20 μm mean particle size to one of 4 μm increased the overall measured degree of desulphurisation from 83 % to 87 % and reduced the residual limestone level from 4.6 to 1.3 wt.%. Similar results have also been reported elsewhere (Xiaoxun et al., 2000, Davini, 2000).

2.5.1.2 Sorbent Preparation

Ahlbeck et al. (1995) have identified the grinding and separation procedure as an important factor to be considered when manufacturing sorbents for wet FGD processes. Hosten and Gulsen (2004), obtained bond grindability work indices ranging from 6.2 to 11.2 kWh/ton while using natural limestone from five deposits in Turkey. This implies that the energy requirement for the preparation of the sorbent will vary from region to region and needs to be experimentally determined for a specific case. The type of production process also has a direct bearing on the reactivity of a particular sorbent. Using three different types of pulverizers (hammer mill, rolls crusher, and ball mill) Brown, Miles, and Hall (1994) determined that the different particles produced by the three had different reactivity characteristics. The particles produced by the hammer mill were more ragged and had a better reactivity than for the other two types of pulverizers.

2.5.1.3 Effect of the Ca/S molar ratio

Several researchers have investigated the effect of this parameter on the SO_2 removal. Scala, D'Ascenzo, and Lancia (2004) have shown that, the overall SO_2 removal efficiency increases with the Ca/S ratio up to about 1.2 above which there is no appreciable change. Xioaxun et al. (2000) have also reported a similar trend where SO_2 removal efficiency increases rapidly with increasing Ca/S molar ratio and then tends to level off as the molar ratio becomes larger. Further increase of the Ca/S ratio cannot enhance SO_2 removal efficiency effectively. Rather a too large Ca/S molar ratio certainly results in a low utilization rate of the sorbent. It is thus important to determine the optimum Ca/S molar ratio for any particular sorbent experimentally.

2.5.1.4 Effect of chloride (Cl^-) and fluoride (F^-) ions

Due to the heterogeneous composition of fossil fuels, coal combustion can generate other harmful acid gases besides SO_2. The two most important, disregarding NOx, are hydrogen chloride (HCl) and hydrogen fluoride (HF). A typical coal chlorine (Cl) concentration is 0.1 wt% and in the case of fluorine (F), a typical concentration in coal is 0.015 wt.% (Kiil, Nygaard, & Johnson, 2002). Following combustion, a typical flue gas concentration of HCl and HF is 100 and 10 ppmv respectively (though this would not necessarily be the case in South Africa, where coal halogen concentrations are relatively low). In wet FGD scrubbers, HCl and HF can be absorbed simultaneously with SO_2, whereby they dissociate to form Cl^- and F^- ions according to:

$$HCl_{(aq)} \leftrightarrow Cl^-_{(aq)} + H^+_{(aq)} \qquad (2.18)$$

$$HF_{(aq)} \leftrightarrow F^-_{(aq)} + H^+_{(aq)} \quad (2.19)$$

The absorption of HCl and HF is desirable because the pollutants should not be emitted to the atmosphere, but in the scrubber, the presence of these species can cause problems. HCl will, upon absorption, produce H^+ ions according to reaction (2.18) and thereby contribute to a large pH drop in the absorber. This may reduce the amount of SO_2 that can be absorbed because the SO_2 dissociation equilibrium, reaction (2.20), is shifted to the left:

$$SO_{2(g)} + H_2O_{(l)} \leftrightarrow HSO^-_{3(aq)} + H^+_{(aq)} \quad (2.20)$$

Additionally, due to the internal recirculation of the slurry, the concentration of Cl^- may rise to a high steady state concentration. High concentrations of Cl^- reduce the rate of limestone dissolution and too high concentrations of Cl^- in the gypsum by-product make it useless for commercial purposes. The steady state slurry concentration of chlorine should not exceed 25-30 g/l (Kiil, Nygaard, & Johnson, 2002) and this concentration is typically maintained in wet FGD plants by continuously withdrawing a sufficient amount of slurry liquid for wastewater treatment.

2.5.1.5 Effect of trace elements

The presence of small amounts of iron have been found to increase the reactivity of limestone in close relation with the eventual presence of NO_x in the treated gas. It is thought that the presence NO_x and iron acts to catalyze the sulphation reaction (Malaga-Starzec et al., 2003, Davini, 2000). Other elements that influence the sulphurisation are fluoride (F^-) and aluminium (Al^{3+}) ions. Al^{3+} ions originate from the fly ash and F^- ions is absorbed as HF from

the flue gas. When present in sufficiently high concentrations, these two will react to form complexes, AlF_x, which may 'blind' the limestone surface and inhibit dissolution.

2.5.1.6 Effect of additives

The SO_2 removal efficiency of wet FGD plants using $CaCO_3$ can be improved by the addition of various organic acids (Frandsen, Kiil, & Johnsson, 2001). An organic acid with a buffering capacity between the pH of the gas/liquid interface and the pH of the bulk liquid phase would provide optimum enhancement. The organic acid acts as a buffer in the absorber. Organic acid addition improves both the limestone dissolution and the solubility of calcium in the slurry liquid, thereby enhancing SO_2 absorption efficiency, reducing limestone consumption, improving energy efficiency, improving by-product gypsum quality, and reducing wastewater production (Clean Coal Technology, 1999).

At a performance testing at the Milken Clean Coal Technology Demonstration Project located at Lansing New York, SO_2 removal efficiency was shown to increase from 83 % without formic acid to 95 % with formic acid (Clean Coal Technology, report 12 1999: 22). At the same removal efficiency, using formic acid results in a 75 % reduction in energy required for circulating the sorbent slurry. Seventy five percent of the operating costs of a power plant are spent on the fuel purchases (Hammack & Gohara, 1997) therefore any minor reduction in the unit fuel price translates into major annual savings in power plant costs. The use of the organic additives is thus a very attractive option. The use of organic acids has also been done at the Ghent Generating Station, Ghent, Kentucky USA. The station used DiBasic Acid (DBA) to enhance the system's SO_2 removal efficiency from 90%, to as high as 96% particularly when high sulphur content fuel was used (Hammack & Gohara, 1997). Their

experience showed that the DBA and the magnitude of pH depression depend on the concentration of the DBA in the slurry tank and can vary from 0.2 pH units at 200 ppm to more than 1 pH unit at 3000 ppm.

Stergarsek et al. (1999) have investigated the effect of ammonium salts on the limestone dissolution. Using a pilot plant unit at the Sostanj coal-fired power station, Slovenia, they observed that the introduction of the ammonium ion does increase the buffer capacity to absorber slurry and that this increase corresponds to a decrease in the required liquid/gas (L/G) ratio for the same absorber performance. The increased buffer capacity was thought to be caused by the increased concentration of the HCO_3^- ion. Their experimental measurement in a pH-stated apparatus show that the introduced ammonium ion significantly promotes the limestone dissolution rate. The results indicated that the linear dissolution rate constant can be increased by upto 30 times. Takashina et al. (2002) have also investigated the effect of the ammonium concentration on the SO_2 absorption rate into a limestone slurry using a stirred tank reactor at a constant pH and high temperature (50 ^oC). Their results indicate that the SO_2 absorption rate was improved by the increase in the ammonium concentration in the limestone slurry.

Frandsen, Kiil, and Johnsson (2001) observed that there is a large increase in the degree of desulphurisation when increasing the feed tank concentration of adipic acid to 5 mM. They theorised that adipic acid and other organic buffers provide enhanced transport of H^+ in the liquid film between gas/liquid and gas/solid. When SO_2 dissociates in the liquid film between gas and liquid phase, H^+ is produced. The H^+ is taken up by the adipate (A^{2-}) and the hadipate (AH^-) ion and transported to the liquid bulk phase. Here it may be released and react with, e.g.

HCO_3^-, producing CO_2 (aq) and H_2O (l). The transport of H^+ from liquid film to the bulk phase promotes the dissociation of SO_2, increasing the overall removal rate. The dissociation of limestone is dependent on the diffusion of H^+ to the surface of the particles. Adipic acid can provide additional transport of H^+, as AH^- or H_2A, from the liquid phase to the liquid film surrounding the limestone particles. The hadipate-ion will release the H^+ close to the limestone surface where it can react CO_3^{2-}, thereby increasing the limestone dissolution rate.

2.5.2 Factors Influencing the sulphation reaction in the fixed bed reactor

2.5.2.1 Effect of SO_2 Concentration

Ho and Shih (1993) reported a low influence of SO_2 concentration on the reaction rate at 30 % relative humidity but reported an increased reaction rate and final conversion with increasing SO_2 concentration at 70 % relative humidity. Liu, Shih, and Lin (2002) reported a very weak influence of the SO_2 concentration on the total conversion and the reaction when testing $Ca(OH)_2$/fly ash sorbents at 30 – 80 % relative humidity and 1000 – 5000 ppm SO_2 concentration. At a reactor temperature of 71.5 ^oC and 38 % relative humidity, Izquierdo et al. (2000) concluded that the reaction rate between SO_2 and calcium hydroxide does not depend on the SO_2 partial pressure for sulphur dioxide concentration of less than 3000 ppm. Lee et al. (2005) observed a linear correlation between the concentration and the time the sorbent can maintain 100 % SO_2 removal. Varying the SO_2 concentration in the range 271 – 15047 ppm Krammer et al. (1997) observed that the initial reaction rate is independent of the SO_2 concentration. After the initial reaction rate, SO_2 shows an increasing influence on the reaction rate but only during the first period of the reaction. Afterwards, the SO_2 concentration shows negligible influence on the reaction.

2.5.2.2 Effect of Relative Humidity/Approach to Saturation temperature

The approach to saturation temperature (ΔT_a) is defined as the difference between the gas temperature (T_b) and the adiabatic saturation temperature (T_s). (If t_2 is the flue gas temperature at the semi-dry FGD reactor outlet, supposing that the flue gas at outlet would go along the adiabatic humidification process and reach the saturation status with the adiabatic saturation temperature (t_{as}), then $\Delta T_a = t_2 - t_{as}$). ΔT_a provides an indirect measure of the relative humidity of the flue gas. The smaller the value of ΔT_a, the closer the approach to saturation, that is, the higher the relative humidity. Since relative humidity has a considerable impact on SO_2 removal, the approach to saturation temperature is a key factor for the removal efficiency (Xiaoxun, et al. 2001).

Experimental investigations by Xiaoxun et al. (2000) in a powder-particle sprouted bed reactor have shown that decreasing the approach to saturation temperature enhances the SO_2 removal efficiency of an FGD. In their investigation of the efflorescence on thin sections of calcareous stones, Malaga et al. (2003) have shown that the presence of moisture is a critical factor influencing the rate of reaction between SO_2 and limestone. It was suggested that the water creates a concentration gradient between the wet limestone surface and the air, which is important in the transfer of gases by diffusion. The thinner the moisture film, the greater the dissolution of gases and consequently the higher the reactivity. In a demonstration project carried out on a 10 MW_e plant located at West Paducah, McCracken county, tests over a 10 year period (1988-1998) indicated that after the Ca/S ratio, the approach to saturation temperature had the greatest effect on the SO_2 removal efficiency (DOE Project Fact Sheets 2003).

However, there is a minimum practical approach to saturation temperature due to increased risk of solid deposition on the absorber walls and on the internal parts of the process equipment, electrostatic precipitator (ESP) efficiency decrease or induced fan corrosion (Gutierrez et al., 2002). The optimum value of the approach to saturation temperature has been found to be 10 ^{o}C (Yuzhong Li et al. 2004). Investigations by Karatepe et al. (1999) have also shown a strong dependence of the sulphation reaction on the relative humidity. The obtained conversion – time curves of sorbents show an initial increase before gradually flattening out after some conversion value depending on the relative humidity of the gaseous mixture used. These conversion values were determined to be 0.03, 0.16, and 0.35 for the relative humidities of 25 %, 55 % and 90 % respectively. The adsorption of water vapour on the free surface of the sorbent and the number of water monolayers is considered to be critical for the reaction yield. Thus at low relative humidities, no reaction occurs because insufficient water molecules are available. However, at high relative humidities, the number of water monolayers formed is large enough to provide a symmetrical configuration of H_2O ligations around an SO_2 molecule and therefore the reaction rate increases with the increasing relative humidity and becomes independent of the partial pressure of SO_2. Adsorption isotherms on a sorbent at 60 – 80 ^{o}C obtained by Liu, Shih and Lin (2002) showed that the amount of water adsorbed increased with increasing relative humidity and decreased with increasing temperature. Similar results have been reported elsewhere (Ho and Shih, 1993; Izquierdo, 2000).

2.5.2.3 Effect of reaction Temperature

Several researchers have studied influence of reaction temperature on the sorbent conversion. Liu, Shih and Lin (2002) observed a weak dependence of sorbent conversion on reaction temperature. They postulated that though increasing temperature could raise the chemical reaction rate constant, it could simultaneously reduce the adsorption amounts of water vapor and reaction gas. Ho and Shih (1993) have also reported a mild influence of the reaction temperature on the conversion as the temperature was increased from 60 to 90 ºC. Raymond-Ooi et al. (2004) observed a modest increase in the SO_2 capture capacity when they increased the reaction temperature from 60 to 80 ºC. Results of Krammer et al. (1997) indicate that the influence of the reaction temperature (70 – 90 ^oC) on the reaction rate was small, and differences were within experimental error range.

2.5.2.4 Effect of sorbent surface area

The specific surface area plays an important role in the SO_2 capture capacity of calcium based materials. Lee et al. (2006) showed that the SO_2 capture by sorbents prepared from fly ash/$Ca(OH)_2$ increased linearly from 83.3 to 163.5 min (g CaO)$^{-1}$ as the specific surface area increased from 22.5 to 133.3 m^2g^{-1} (Figure 2.5). Ho et al. (2002) investigated the influence of the initial BET specific surface area on the reaction. They used samples of the same material but different initial particle size. The different size fractions had specific surface areas varying from 7.8 to 12.3 m^2/g and mean diameter 10 to 96 μm. Their results indicated that the samples of the smallest particle size d_p = 10 μm were the least reacted. However, upon consideration of the initial BET specific surface areas of the samples, their conversions per unit initial specific surface area X/S_{g0} versus time could be represented by the same curve with a standard deviation of the data around the curve of 0.02.

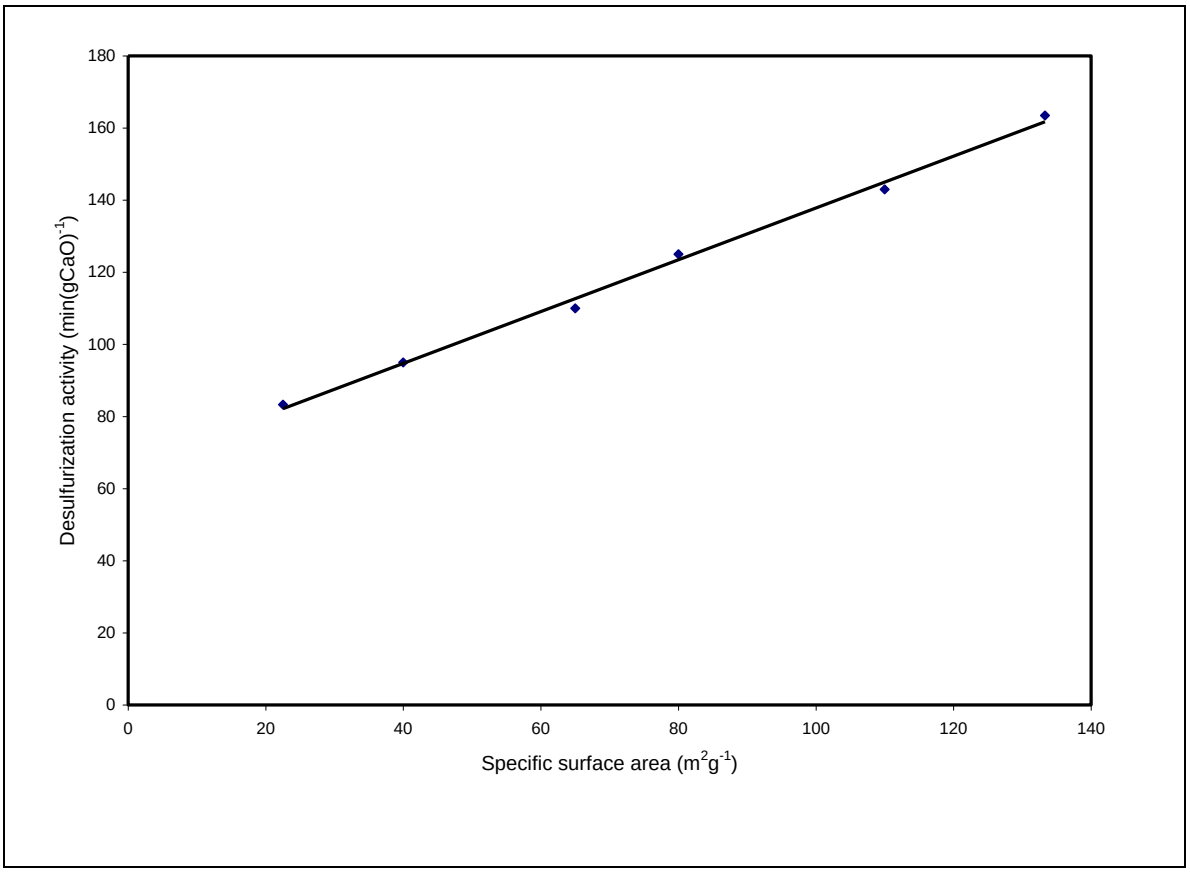

FIGURE 2.5: Effect of specific surface area on the desulfurization activity of selected fly ash/CaO/$CaSO_4$ sorbents. Feed gas: 1000 ppm SO_2, 5% O_2, 12 % CO_2, (Lee et al., 2006)

2.5.2.5 Use of additives to enhance reactivity

The use of additives to enhance the $Ca(OH)_2$ reactivity with SO_2 have been explored by a number of researchers. The type of additives explored to date may be classified as deliquescent inorganic salts and related inorganic salts, sodium containing basic compounds, or oxidation catalysts. The majority of the compounds tested fall into the first category above, although there is some cross classification among the compounds evaluated to date. For example, sodium hydroxide (NaOH) is capable of reacting directly with SO_2 as a basic solution but it is also a deliquescent compound.

Izquierdo et al. (2000) tested the effectiveness of sodium chloride (NaCl), calcium chloride ($CaCl_2$) and NaOH as additives to enhance the reactivity of calcium hydroxide towards sulphur dioxide. Their experiments were performed at 71.5 ºC and 36.7 % relative humidity. The amount of additives ranged from 10 to 31.2 wt.%. This study found that the reaction rate increases with increasing concentration of calcium chloride and sodium hydroxide. $CaCl_2$ was found to be more effective than NaOH despite the poor alkaline and hygroscopic properties of $CaCl_2$. No significant enhancement on the reaction rate was found when different amounts of sodium chloride were used. Its hygroscopic character was not enough to significantly improve the desulfurization power of calcium hydroxide. It was concluded that deliquescence is a desirable property for sulphur removal since $CaCl_2$ is a deliquescent salt. Liu, Wey, and Lin (2005) have also observed a significant increase in SO_2 removal efficiency when they added p to 30 wt. % $CaCl_2$ in spray dryer experiments (Figure 2.6). Stein, Kind and Schlünder (2002) observed that adding $CaCl_2$ to a lime slurry up to a mass fraction of 1.2 wt. %, enhances the SO_2 removal in spray dry absorption. They ascribed this to the influence of the additive on the drying behavior of the droplets. At high excess of calcium hydroxide in the spray drying process, the absorption efficiency of sulphur dioxide is limited by the drying conditions (Hill & Zank, 2000). The $CaCl_2$ prolongs the drying process and therefore enhances the absorption efficiency.

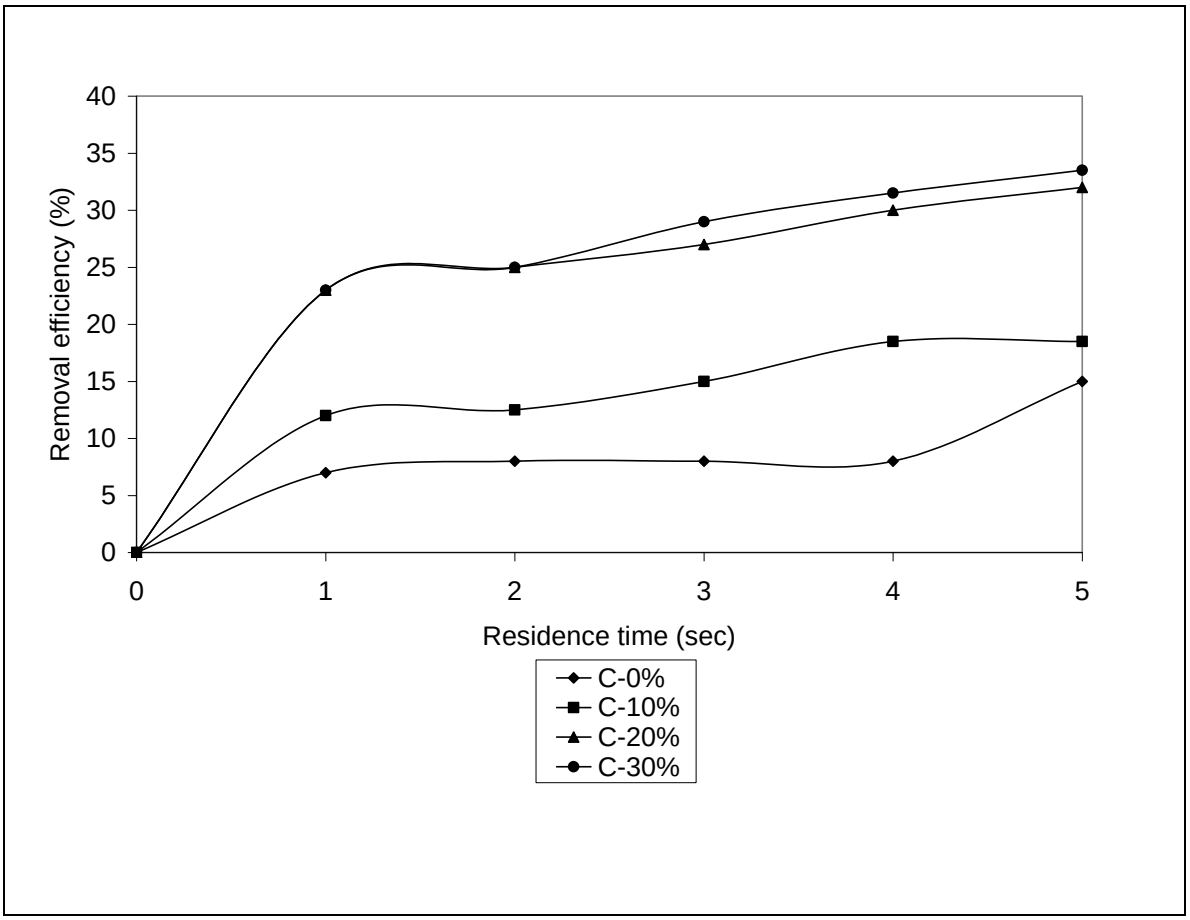

FIGURE 2.6: SO_2 removal profiles with the addition of different amounts of calcium chloride (C) (Liu, Wey, & Lin , 2005).

2.6 CHALLENGES FACING FUTURE FGD TECHNOLOGIES

There are three major challenges that face research and development in FGD systems namely to; reduce FGD costs, increase desulphurisation efficiencies, and improve system reliability. Currently, the FGD system increases the cost of electricity by about 10% (IEA, 2001). Greater in-depth knowledge can reveal the factors that control process performance, and lead to substantial enhancement of FGD processes. Basic research is needed in three broad

categories: reaction mechanisms and sorbent material, transport effects and modeling, and process development.

More knowledge of the inherent kinetics and controlling resistances in all areas of the SO_2 capture process is needed in order to improve the capture efficiency and reduce costs. For example, there is a need to elucidate the chemical mechanism(s) that allow successful sorbent additives to be effective. Recent researchers have shown that the use of organic and formic acids can improve the sorbent utilization and process efficiency in wet FGD applications (CCT, 1999; Frandsen, Kiil, & Johnsson, 2001; Gohara & Strock, 1997). The use of ammonium salts has also been shown to be beneficial to the limestone utilization and performane efficiency in wet FGD processes (Stergarset et al., 1999; Takashina et al., 2002). These additives act as buffers in the absorber and increase the limestone dissolution. Additional research will be necessary in order to make the use of additives commercially viable.

Poor sorbent utilization in the dry and semidry processes limits their economic feasibility. Sorbent preparation techniques used today have generally been adapted from those traditionally used in the lime industry. These preparation techniques need to be examined with an eye to the optimization of the properties important to the SO_2 capture process. Further, little attention has been paid to the selection of limestones for the SO_2 capture process (Kadambi et al., 1998). Criteria must be established for limestone selection so that locally available limestones can be evaluated and used. The improved utilization of new sorbents such as calcium silicate sorbents formed from lime and fly ash has been demonstrated in laboratory scale FGD units (Karatepe et al., 1998; Lee et al., 2006; Liu, Shih, & Lin, 2002;

Renedo & Fernandez, 2002). Further research is needed on its viability in large scale industrial operations. In cases where low one-pass utilizations are inevitable, unreacted sorbent separation and recycle can serve to give high overall utilizations and reduce the volume of solid products. Davini (2002) showed that sorbents sulphated at high temperature can be partly regenerated by a suitable steam treatment. Innovative separation technologies such as membrane separation and electrochemical processes may lead to new process concepts applicable to FGD processes.

Opportunities exist to find methods of improving the efficiency of contacting operations between the flue gas and the sorbent, for example by using countercurrent rather than cocurrent contacting. The use of smaller, more effective scrubbers is another area that is currently being pursued to reduce FGD capital and operating costs. One approach that is being evaluated is the design of systems that can operate at high flue gas velocities (Gohara & Strock, 1997; Williams, 1999). The higher flue gas velocity has the additional advantage of improving SO_2 absorption rate as a result of increased turbulence, increased time that the slurry droplets remain suspended, and a decrease in the film thickness of the droplets.

2.7 REACTIVITY MEASUREMENT TECHNIQUES

Many researchers have carried out laboratory experiments aimed at determining the reactivity of different calcium-based sorbents. In each case, the experimental set-up adopted aims at testing the reactivity of the sorbents when used in a particular process i.e wet, dry, or semi-dry processes. Testing models can be either on a laboratory-scale, pilot-plant, or industrial scale.

2.7.1 Wet FGD Process

In wet FGD processes, two kinds of experimental set-ups are used in determining the reactivity of the sorbent material under conditions that approximate to those found in industrial scale FGD units. These experiments can be described either as batch experiments or continuous experiments.

2.7.1.1 Batch Processes

In the wet limestone FGD process, an absorbent slurry consisting of the sorbent i.e. limestone, $CaCO_3$, and water reacts with gaseous SO_2 and air producing $CaSO_4.2H_2O$. If the reactivity of an absorbent slurry is measured with gaseous SO_2 directly, there is both a gas diffusion process in the liquid and complex surface kinetics to take into account when modeling the absorption process. Instead of gaseous SO_2, strong acids like sulphuric acid or hydrochloric acid can be used (Ahlbeck et al., 1995). In this case, the reactivity of the limestone particles is measured directly as the dissolution rate of the absorbent in an acidic environment at a constant pH. This technique is sometimes referred to as the pH-Stat method. pH-Stat is a powerful technique which maintains a constant pH as hydrogen ions are released or consumed during the reaction. The basic principles behind pH-Stat are as follows:

- The pH of a reaction is measured continuously.
- Any deviation in pH from the set pH-Stat value is quickly compensated by reagent addition.

- The speed and the volume of reagent addition is measured continuously and controlled with a wide range of flow rates to match the reaction rate.

- The temperature of the reaction is continuously measured and the pH compensated accordingly.

- The kinetics of the studied reaction are calculated based on the consumption of the reagent required to keep the pH constant

The technique was first used by Knaff-Lenz in 1923 to study an esterase. At that time, the reagent was added manually by the operator who had to keep watching and adjusting the pH of the substrate. In recent years, the growing technological know-how has enabled the process of maintaining the pH constant to be done automatically and thus opening this technique to more widespread application. It has found application in the pharmaceutical and biomedical industries, food and beverage industry, and in geochemistry where it is used in determining the dissolution or precipitation kinetics of various minerals. In the field of flue gas desulphurisation, the process is gaining acceptance as a more convenient method for determining the reactivity of different calcium-based materials as sorbents for the sulphur dioxide emissions reduction from power plants. Several researchers have used this technique in this way. Holsten and Gulsun (2004) used this technique to investigate the reactivity of limestones from different sources in Turkey. Their findings indicated that the conversion rates/reactivity of natural limestones composed mainly of calcite were independent of the sample source but the presence of dolomite inhibited the dissolution rate. Particle size was also shown to be an influential parameter on the reactivity of a particular sorbent. Using the same technique, Fellner and Khandl (1999) concluded that the reactivity of limestone powder

samples of a similar size distribution depends remarkably on the reaction surface area of the samples. They related this reaction surface area to the apparent porosity of the powder samples as measured using a porosimeter. Shih, Lin, & Shiau (2000) used the same technique to model the dissolution rates of limestones from different sources. Using a reactor temperature of 60 ^{o}C and pH values of 4 and 6, and assuming a shrinking core model for the limestone dissolution, they concluded that the dissolution rates of the limestones are controlled by the mass transfer of hydrogen ions with chemical reactions in the liquid film surrounding the limestone particle. The measured value of mass transfer coefficient increased with increasing pH value and stirrer speed and remained constant with particle size. Ahlbeck et al. (1995) used a similar procedure to obtain the differences in direct reactivity between limestone samples. They concluded that by calculating the reactivity coefficient for the shrinking particles, the differences in chemical reactivity can be obtained independent of the particle size. Stergarsek et al. (1999) used the pH-stated technique to determine the influence of ammonium sulphite additive on limestone dissolution rate. Their results showed that the ammonium ions significantly increase the buffer capacity of the absorbing slurry and promotes the dissolution rate of the limestone.

If an absorbent slurry sample in a stirred beaker is neutralized by a strong acid, the dissolution rate can be ascertained by measuring the absorbent conversion as a function of time at constant pH.

$$CaCO_{3(s)} + 2\ HCl_{(aq)} \rightarrow CaCl_{2(aq)} + H_2O_{(l)} + CO_{2(g)} \qquad (2.21)$$

The amount of acid consumed at any given time is a measure of the limestone dissolution rate and thus the reactivity.

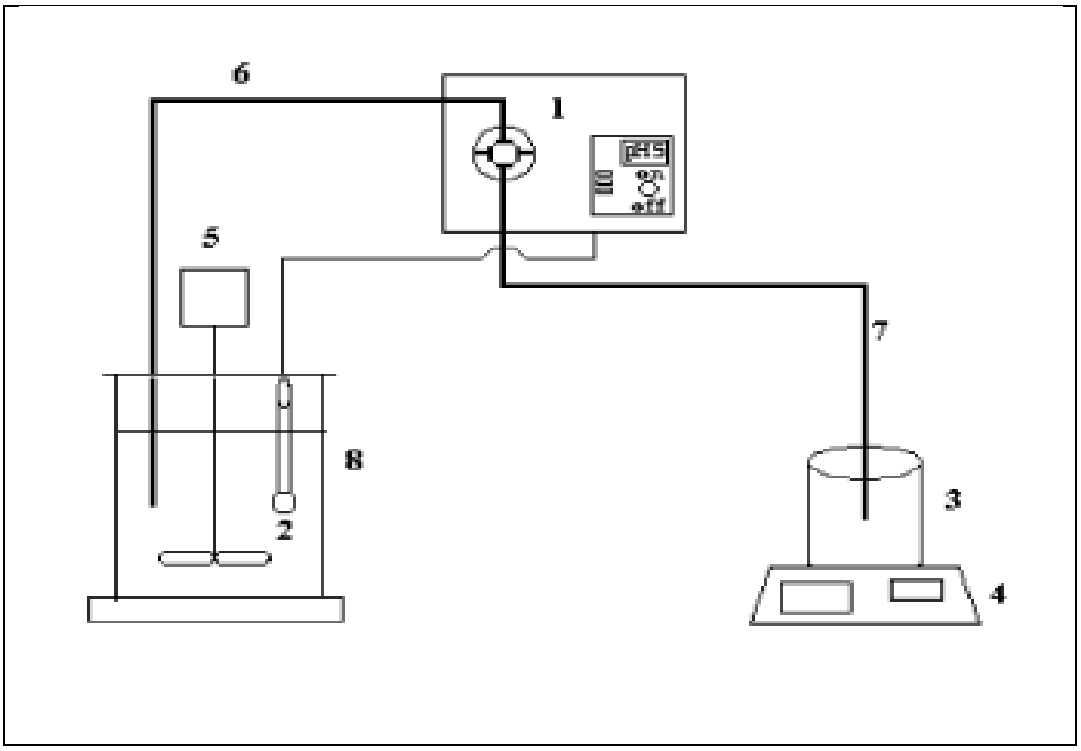

FIGURE 2.7: pH-Stat experimental set-up: (1)pH control pump; (2) pH electrode (3) HCl solution beaker; (4) electronic balance; (5) stirrer; (6,7) plastic tubing; (8) reaction vessel.

Different absorbent parameters that influence the reactivity, such as chemical composition, specific surface, or particle diameter distribution function can be investigated using this method (Hosten & Gulsun, 2004). The experimental set-up used by Hosten and Gulsun is shown in Figure 2.7. The conversion rates determined by batch laboratory tests can be used to reliably rank the performance of sorbents in the industrial full-scale processes. Recently, ASTM developed a standard test method for determination of total neutralizing capability and dissolved calcium and magnesium oxides in lime for flue gas desulphurisation (ASTM C:1318-95). This method also recommends an acid titration procedure.

2.7.1.2 Pilot plant processes

Several researchers have used pilot plants to simulate full-scale FGD industrial processes in order to obtain information on the degree of desulphurisation of different sorbent materials. Fransen et al have simulated a co-current packed tower (Figure 2.8).

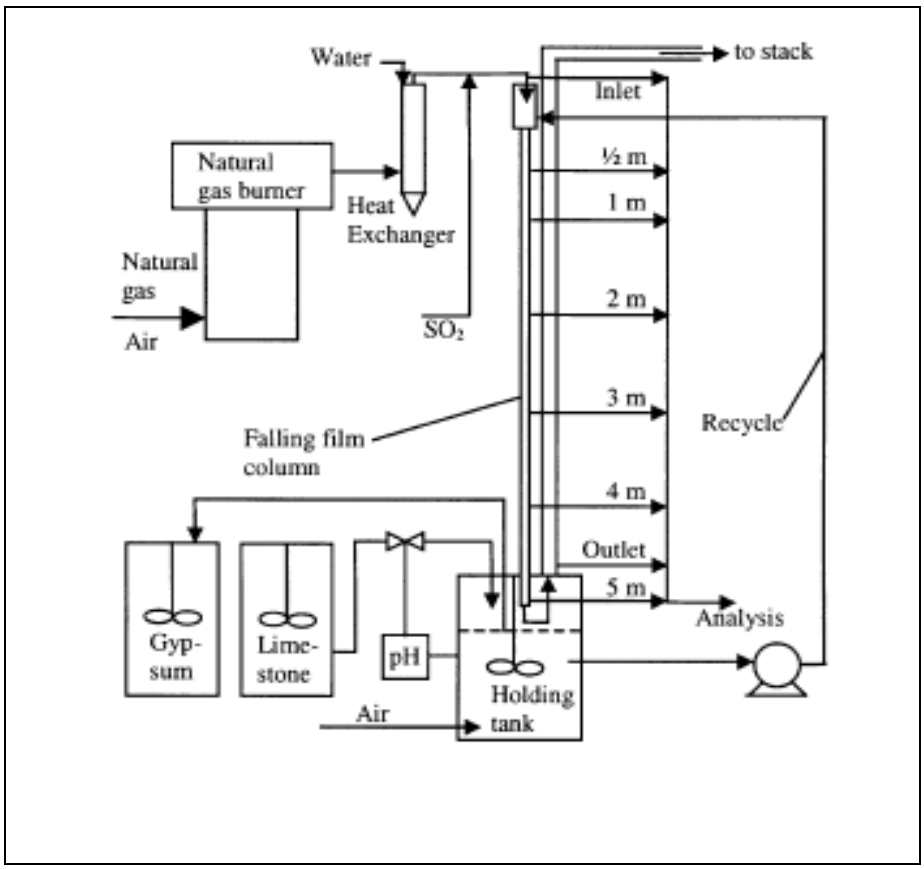

FIGURE 2.8: Schematic of wet FGD pilot plant (Frandsen et al., 2001)

The pilot plant was designed to resemble a single channel in a full-scale co-current packed tower. The main components are a natural gas burner, a falling film column and a holding tank. Pure SO_2 is added to the flue gas produced by the gas burner before it enters the falling film column, a 5 m PVC tube with an inner diameter of 3.3 cm. The SO_2 is absorbed mainly in the column, but also in the holding tank. The addition of feed mixture (limestone, distilled

water, and in some cases, organic acid) to the holding tank is controlled by a pH unit which ensures a fixed pH in the range 5 – 6 in the holding tank. A timer controlled pump maintains a constant level in the holding tank by removing gypsum slurry once an hour. Air is supplied to the holding tank for the oxidation of the sulphite ion (HSO_3^-). Gas samples for measurement of SO_2 concentration can be withdrawn through sampling probes at the inlet and outlet of the pilot plant and at six positions in the falling film column.

Zheng et al. (2002) fabricated a pilot scale jet bubbling reactor (JBR) to test this kind of process. The JBR pilot plant is downscaled from a full-scale wet FGD plant cleaning the flue gas from a 285 MW_e coal fired power plant. A typical flue gas flow rate from the full scale power plant is 285 Nm^3/s and the number of sparging tubes in the full scale JBR is about 2000. The diameter of the JBR is 17m and the volume of the gypsum is 1300 m^3. A schematic of the pilot plant is shown in Figure 2.9. The main components are the JBR, the feed and product tanks, and the natural gas burner. All pipes and vessels are made from PVC or stainless steel to avoid corrosion. The absorber is a stirred vessel with continuous feeding of both the gas and liquid phases. The reactor temperature is controlled by means of a heat exchanger. The reactor vessel is a cylinder with an inner diameter of 52 cm and a height of 101 cm, fitted with four vertical baffles, a pH probe and a floating contact system for slurry level control. To avoid plugging, the level control was flushed with N_2 for 30s every 10 min. An axial four-blade stirrer (diameter 20 cm), with adjustable speed from 0 to 1420 rpm, creates a high degree of mixing in the liquid phase.

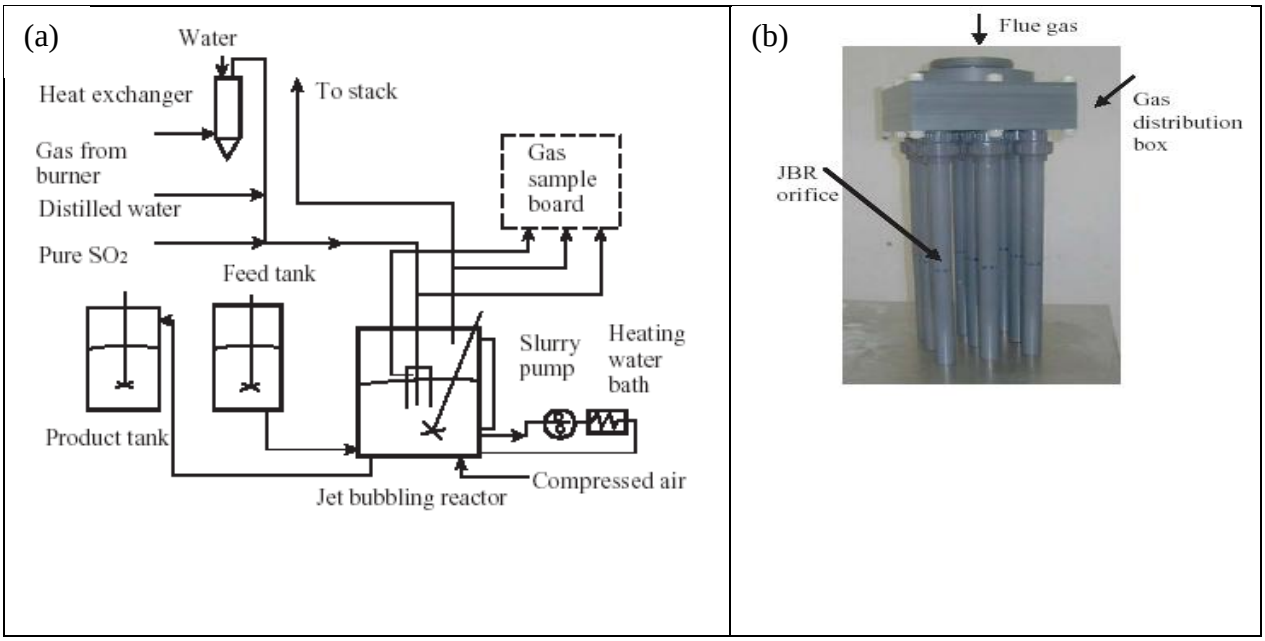

FIGURE 2.9: (a) Schematic illustration of the experimental pilot-scale JBR (b) Photo of gas distribution box with nine spargers (Zheng et al., 2002)

The feed gas is supplied from a natural gas burner. The gas mixture enters a heat exchanger where it is cooled from burner temperatures to 74 ^{o}C. The gas enters the JBR through a gas cooling duct where the temperature is reduced further to 50 ^{o}C and the gas is saturated by injection of distilled water. In order to simulate a coal combustion flue gas, SO_2 is added to the saturated gas just before it enters the absorber. The flue gas is then distributed through nine gas sparger tubes (Figure 2.9 (b)) with an internal diameter of 27.2 mm and a length of 436 mm. The tubes are immersed 5 cm below the stagnant surface of the gypsum/limestone slurry. The treated flue gas finally flows to the stack.

Air is introduced into the reactor through a probe to oxidize HSO_3^- to SO_4^{2-}. The SO_4^{2-} ions combine with the Ca^{2+} originating from the dissolved limestone, and crystallize as gypsum.

The addition of fresh limestone slurry is controlled by maintaining the holding tank pH at a constant value (typically 4.5)

2.7.2 Semi-dry Processes

The powder particle sprouted bed (PPSB) is a kind of semidry FGD system. Figure 2.10 gives a schematic of the pilot plant used by Xiaoxun et al (2000).

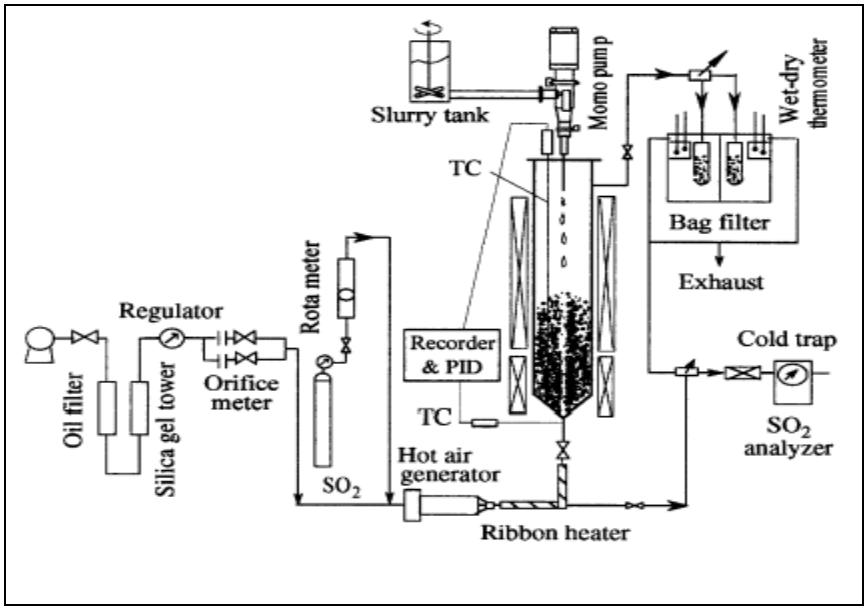

FIGURE 2.10: Schematic of the PPSB experimental apparatus (Xiaoxun et al, 2000)

Air available from a central compressor was passed through an oil filter and a dehydrating tower. The air was then mixed with SO_2 to form simulated flue gas. The flow of air was measured by an orifice meter and the feeding rate of SO_2 was adjusted by a rotameter. After heating to the desired temperature, the flue gas went through a powder sprouted bed. The sprouted bed, used as a reactor, is a 5.35 cm ID, 64.5 cm high stainless steel column. Its cone angle and inlet diameter are 60^o and 1.43 cm respectively. Silica sand particles of 460 μm were used as sprouting media. Limestone and hydrated lime were used as SO_2 sorbents.

2.7.3 Dry FGD Processes

Garea et al. (2001) have carried out experiments on a laboratory scale dry FGD apparatus, Figure 2.11. The experiments were carried out at laboratory scale in a glass-made tubular reactor of dimensions 2.5 x 10^{-2} m inlet diameter and 0.29 m long.

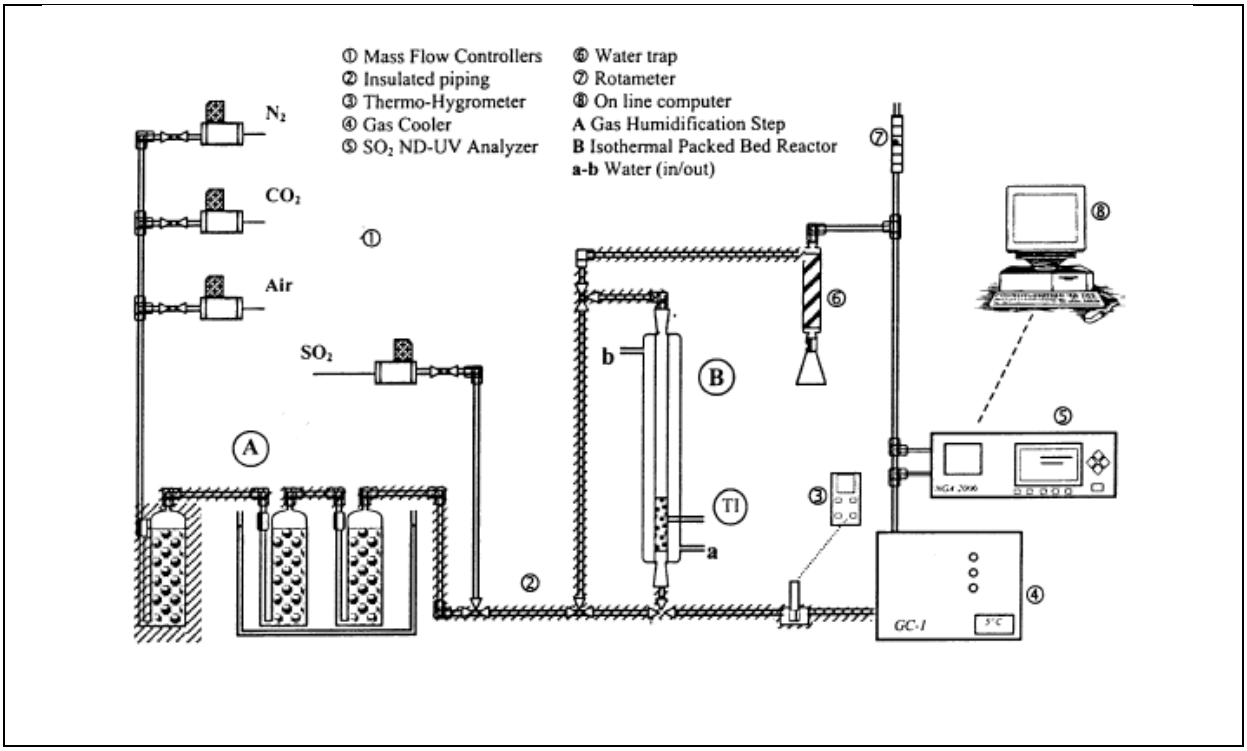

FIGURE 2.11: Experimental set-up of the laboratory scale fixed-bed reactor (Garea et al., 2001)

The packed-bed reactor was formed with commercial-grade $Ca(OH)_2$ dispersed into an inert silica sand bed, supported by glass wool. The dispersion in the silica sand helps to avoid channeling, improves gas/solid contact and ensures isothermal conditions. The sorbent load in the packed bed reactor was ranged from 200 to 600 mg in a series of experiments. Synthetic flue gas was used with a composition of 4000 ppmv SO_2 on a dry basis, 12 % CO_2, 5 % O_2

and balance N_2 resulting in a total of 900 N cm^3 min^{-1}. Water vapour was added by bubbling the gas stream into pure water at a selected temperature in order to reach the required level of relative humidity. From this point, the gas stream was sent to the reactor through heated and insulated piping. The water content was checked downstream of the reactor by means of a thermohygrometer with capacitive sensor. The SO_2 concentration in the gas phase leaving the reactor was continuously analyzed and the data trends of SO_2 concentration versus time were sent to an on-line computer and saved to a data file. After the experiment the entire bed was removed and sieved to recover the solid reacted sorbent. The chemical composition of the solid reacted sorbent was determined by the thermogravimetric technique. In each experiment, the breakthrough curve was recorded until the dimensionless concentration (C/C_o) reached the 0.95 value. Experimental error from breakthrough curves was estimated to be around 6.48 %.

2.8 SUMMARY OF FGD PROCESSES

- FGD is the most widely used technology for the control of SO_2 emissions from fossil-fired boilers. A wide variety of FGD technologies are available. Worldwide, there are currently 678 FGD systems operating on a total capacity of 229 GW_e. The most commonly used are the limestone /gypsum (and its variations) and the spray-dry process, but newer technologies such as the CFB, sea water washing and the Electron Beam Ammonia (EBA) are rapidly gaining acceptance.

- A steady improvement in process design over the years means that modern designs can achieve more than 95% sulphur removal efficiency. Costs have fallen steadily as the process become better understood and are now equivalent to \$100-125 kW^{-1}. Additionally,

better knowledge of the process has made it possible to design units with high availability rates and thus eliminate the need for spare modules.

- Several new processes are under development, many of which are designed to remove both SO_x and NO_x. In recent years researchers have been investigating the design and operation of wet FGD modules with high gas velocities. This will help in making future FGDs smaller and more reliable.

- There are several sorbent reactivity measurement techniques available. Performance in wet FGD processes can be simulated using the pH-stat method or a pilot-plant design. Performance under dry processes can be simulated through the use of differential or integral fixed-bed reactors.

2.9 CONCLUSIONS

In all the test procedures encountered in literature, the reactor is the one difference and is constructed to approximate the performance of a particular process. All the pilot plants consist of a gas supply system, a reactor, and a gas analysis equipment. Different reactors can be built in order to simulate their performance with the South African calcium-based sorbents. The wet FGD process is the most widespread among all the FGD processes. For the purposes of this study, a pH-stat method will be used to simulate the limestone performance in wet FGD processes. The dry FGD process has low installation and operational costs and is easily adapted as a retrofit to existing plants. In the present study, a fixed-bed reactor will be used to simulate performance in the dry FGD processes. The sorbent composition and crystallinity, sorbent particle size, Ca/S molar ratio, reactor temperature, use of additives, SO_2

concentration, as well as the presence of trace elements have an influence on the performance of any FGD system and must be investigated.

CHAPTER 3

3. KINETIC STUDY AND PROCESS MODELLING

3.0 INTRODUCTION

This chapter gives an overview of the rate expressions for the sorbent dissolution and the desulphurisation reaction between the hydrated sorbent materials and the simulated flue gas containing SO_2. An analysis of the existing methods for the calculation of the kinetic parameters such as global reaction rate constant, activation energy and frequency factor of the dissolution and sulphation experiments is also presented.

3.1 SORBENT DISSOLUTION

3.1.1 Introduction

The dissolution kinetics of calcium carbonate has been widely studied for many years. However, a large number of papers published have been concerned with how the dissolution process affects geological processes such as diagenesis of calcareous deep-sea sediments, formation of karst in limestone terranes, the evolution of water chemistry in calcite depositing stream systems, and the global CO_2 cycle (Eisenlohr et al., 1999, Plan, 2005, Liu & Dreybrodt, 1997). Pokrovsky, Golubev, & Schott (2005) investigated the effect of CO_2 partial pressure up to 55 atm on the rate of dissolution of calcite, dolomite and magnesite at 25 ºC, pH 3 to 4 and solution constant ionic strength. The experiments were carried out using the rotating disc technique. For the three minerals, the effect of the pCO_2 was found to be insignificant compared to that of pH. They described the dissolution rate within the

framework of the surface complexation model assuming carbonate sites protonation (CO^{-}_{3} + H^{+} = CO_3H^o) without explicit pCO_2 effect. Gautelier, Oelkers, & Schott. (1999) used the rotating disc mixed flow reactor to measure dolomite dissolution rates in HCl solutions. The dissolution rates were determined at 25, 50 and 80 ºC, disk rotation speeds ranging between 210 to 1000 rpm, and at pH between -0.39 and 4.44. Their measured rate of dissolution were consistent with $r = k_1 a^{n_1}_{H^+,surf}$, where exponent n_1 increases from 0.63 at 25 ºC to 0.80 at 80 ºC. They further observed that the rates tend towards pH dependence at more acidic conditions, suggesting that the surface becomes saturated with rate controlling protonated surface species at these conditions. The apparent activation energy of dolomite dissolution decreased dramatically from 46 kJ mol^{-1} at pH = 1 to 15 kJ mol^{-1} at pH = 5. The overall dissolution process was found to be surface reaction limited at pH < 1, but the effect of diffusional transport becomes increasingly significant with increasing pH.

Recently, several researchers have studied the dissolution of limestone with special reference to the conditions encountered in the wet type FGD process. Shih, Lin, and Shiau (2000) investigated the dissolution rate of six limestone samples from different sources in a pH-Stat apparatus at pH 4 and 6. Their results indicated that the dissolution rate was controlled by the mass transfer of hydrogen ions with chemical reactions in the liquid film surrounding the limestone particle. The measured value of the mass transfer coefficient increased with an increasing pH value and stirrer speed but remained constant with particle size. A model which assumes that the limestone particle dissolves according to the shrinking-core behaviour was used to describe the dissolution kinetics. Using a sequential pH-time derivative method, Ahlbeck et al. (1995) concluded that the dissolution rate of limestone is controlled by both liquid film diffusion and chemical reaction. There is a correlation between the apparent

limestone porosity and the dissolution kinetics. Using 8 limestone samples, Fellner and Khandl (1999) showed that the reaction half-time in pH-Stat apparatus reduced with an increase in the apparent porosity. Hosten and Gulsun (2004) also showed that the particle size and dolomite content of the limestone were the most influential parameters in the reactivity measurements.

The rate of carbonate mineral dissolution is determined by the physical and chemical characteristics of the stone, including the type and amount of impurities and mineral crystallography. The chemistry and temperature of the solution are also important.

3.1.2 Limestone Desulphurisation Chemistry

In the wet FGD process, limestone slurry is used to absorb SO_2 to form solid products. There are several reactions and physical steps which may affect the rate of SO_2 absorption within a limestone slurry. These include (Bravo et al., 2002; Takashina et al., 2002):

a) The diffusion of SO_2 through the gas film near the gas-liquid interface.

b) The dissolution of SO_2 in the liquid phase

$$SO_2(g) \rightarrow SO_2(aq) \tag{3.1}$$

c) The first dissociation of SO_2.

$$SO_2(aq) + H_2O \rightarrow H_2SO_3(aq) \tag{3.2}$$

$$H_2SO_{3(aq)} \rightarrow H^+_{(aq)} + HSO^-_{3(aq)} \quad (3.3)$$

d) The second dissociation of SO_2.

$$HSO^-_{3(aq)} \rightarrow H^+_{(aq)} + SO^{2-}_{3(aq)} \quad (3.4)$$

e) The dissolution of $CaCO_3$.

$$CaCO_{3(s)} \rightarrow CaCO_{3(aq)} \quad (3.5)$$

f) The dissociation of $CaCO_3$

$$CaCO_{3(aq)} \rightarrow Ca^{2+}_{(aq)} + CO^{2-}_{3(aq)} \quad (3.6)$$

$$H^+_{(aq)} + CO^{2-}_{3(aq)} \rightarrow HCO^-_{3(aq)} \quad (3.7)$$

$$H^+_{(aq)} + HCO^-_{3(aq)} \rightarrow CO_{2(g)} + H_2O_{(l)} \quad (3.8)$$

g) The diffusion of SO_2 and the different ions towards the reaction area of the liquid film.

h) Reaction of the different species

$$SO_{2(aq)} + HCO^-_{3(aq)} \rightarrow HSO^-_{3(aq)} + CO_{2(g)} \quad (3.9)$$

$$SO_{2(g)} + SO^{2-}_{3(aq)} + H_2O_{(l)} \rightarrow 2HSO^-_{3(aq)} \quad (3.10)$$

$$CO_3^{2-}{}_{(aq)} + HSO_3^-{}_{(aq)} \rightarrow HCO_3^-{}_{(aq)} + SO_3^{2-}{}_{(aq)} \quad (3.11)$$

At first, the SO_2 gas diffuses through the gas-liquid film, dissolves into the bulk liquid then finally dissociates. Simultaneously, the solid limestone also dissolves and then dissociates. Thereafter, the sulphite and carbonate ions react with each other in the liquid film according to step (h) above. Step (a) above depends largely on the operating conditions and the type of equipment used to obtain contact between the phases. Steps (b) – (d) are virtually instantaneous. It has been shown that the absorption rate increases with the surface area of the particles, the concentration of solids in the suspension and, when a stirred tank is used, with the stirring speed of the slurry (Bravo et al., 2002; Shih, Lin, & Shiau, 2000). Furthermore, the dissolution rate of a limestone is a strong function of its chemical composition/ quality (Fellner & Khandl, 1999; Ahlbeck et al., 1995). For example, Mg (in dolomite) significantly reduces the limestone reactivity. The dissolution rate of the $CaCO_3$ thus plays an important role in the overall kinetics. Accurately evaluating the dissolution rate of the limestone is important in the development and the efficient operation of the SO_2 wet scrubbing system.

3.1.3 Mathematical models of dissolution kinetics

A number of mathematical models have been developed for predicting the rate of calcium carbonate dissolution in aqueous systems. Some of these are entirely empirical (Fellner & Khandl, 1999) and some have a basis in fundamental principles (Shih, Lin, & Shiau, 2000; Bakan et al., 2006; Alkattan et al, 2002). The rate of reaction between a fluid and a solid can be expressed according to the heterogeneous reaction models. The dissolution of limestone is a *heterogeneous reaction* – it occurs at the interface between two phases, a solid and a liquid.

A basic concept in chemical kinetics is that reactions consist of a series of different physical and chemical processes that can be broken down into different "steps". For dissolution, these steps generally include at a minimum (Morse & Arvidson, 2002):

1. Diffusion of reactants through solution to the solid surface,

2. Adsorption of the reactants on the solid surface,

3. Migration of the reactants on the surface to an "active" site (e.g. a dislocation),

4. The chemical reaction between the adsorbed reactant and solid which may involve several intermediate steps where bonds are broken and formed, and hydration of ions occurs,

5. Migration of products away from the reaction site,

6. Desorption of the products to the solution,

7. Diffusion of products away from the surface to the bulk solution.

A central concept in reaction kinetics is that one of these steps will be the slowest and that the reaction cannot, therefore, proceed faster than this rate limiting step. Steps 1 and 7 involve the diffusive transport of reactants and products through the solution to and from the surface. When this process is rate-limiting, the reaction is said to be *diffusion controlled*. Steps 2-6 occur on the surface of the solid and when one of them is rate controlling, the reaction is said to be *surface controlled or chemically controlled*. Very soluble minerals tend to undergo

reactions that are diffusion-controlled, whereas relatively insoluble minerals have surface controlled reaction rates until very high degrees of disequilibrium are obtained. Carbonate minerals fall into the latter category. Surface controlled reactions tend to be non-linear with respect to saturation state while diffusion controlled reactions are linear with respect to saturation state (Morse & Arvidson, 2002).

Thus the overall reaction rate of a rapidly dissolving mineral, such as calcite under acidic conditions stems from two distinct effects: detachment from the mineral surface ('surface reaction' effect), and diffusional transport of dissolved aqueous species from this surface through an interfacial layer into the bulk solution ('transport' effect) (Alkattan et al., 1998). The variation of $CaCO_3$ detachment rate from the calcite surface (r_c) with the composition of the fluid immediately adjacent to the mineral surface can be quantified in terms of transition state theory. Calcite dissolution can proceed via a variety of mechanisms including the hydration of the calcite surface consistent with:

$$CaCO_{3(s)} \rightarrow Ca^{2+}_{(aq)} + CO_3^{2-}{}_{(aq)}, \tag{3.12}$$

The protonation of one or two hydrogen ions according to:

$$CaCO_{3(s)} + H^{+}_{(aq)} \rightarrow Ca^{2+}_{(aq)} + HCO_3^{-}{}_{(aq)}, \tag{3.13}$$

Or

$$CaCO_{3(s)} + 2H^{+}{}_{(aq)} \rightarrow Ca^{2+}_{(aq)} + H_2CO_3^{0}{}_{(aq)}, \tag{3.14}$$

And the carbonation of the calcite surface by the reaction:

$$CaCO_{3(s)} + H_2CO^0_{3(aq)} \rightarrow Ca^{2+}_{(aq)} + 2HCO^-_{3(aq)}. \quad (3.15)$$

Assuming that precipitation occurs by the single reaction:

$$Ca^{2+}_{(aq)} + CO^{2-}_{3(aq)} \rightarrow CaCO_{3(s)}, \quad (3.16)$$

A general equation for calcite dissolution rates can thus be expressed as:

$$r_c = k_1 + k_2 a_{H^+,s} + k_3 a^2_{H^+,s} + k_4 a_{H_2CO_3,s} - k_5 a_{Ca^{2+},s} a_{CO_3^{2-},s} \quad (3.17)$$

Where k_1, k_2, k_3, k_4, and k_5 stand for the chemical reaction rate constants of reactions, Equations 3.12 to 3.16 and a_i,s refers to the activity of the i^{th} aqueous species adjacent to the calcite surface. At acidic conditions (pH<5), the $k_2 a_{H^+,s}$ term dominates the right side of Equation 3.17.

The chemical reaction rate at these pH's and at far from equilibrium conditions is thus given by:

$$r_c = k_2 a_{H^+,s} = k_2 \gamma_{H^+,s} c_{H^+,s}, \quad (3.18)$$

Where $\gamma_{H^+,s}$ and $c_{H^+,s}$ represent the activity coefficient and concentration of hydrogen ions in the solution adjacent to the calcite surface

Proton consumption by calcite dissolution, in accordance to Equation 3.13, results in a dramatic decrease in hydrogen ion concentration in the fluid adjacent to the mineral surface relative to the bulk solution. This leads to the diffusional transport of hydrogen ions which can be described using:

$$r_t = k_t \left(c_{H^+,b} - c_{H^+,s} \right), \tag{3.19}$$

Where r_t represents the transport rate, $c_{H^+,b}$ refers to the hydrogen ion concentration in the bulk solution, and k_t denotes a transport rate constant. At equilibrium, the quantity of hydrogen ions transported to the surface equals that consumed by Equation 3.13 such that:

$$r = r_c = r_t, \tag{3.20}$$

Equations 3.18 to 3.20 can be combined to yield:

$$c_{H^+,s} = \frac{k_t c_{H^+,b}}{k_2 \gamma_{H^+,s} + k_t}, \tag{3.21}$$

And

$$r = \frac{k_t k_2 \gamma_{H^+,s}}{k_t + k_2 \gamma_{H^+,s}} c_{H^+,b}, \tag{3.22}$$

To the extent that $\gamma_{H^+,s}$ and k_t are independent of solution composition and $\gamma_{H^+,b} \approx \gamma_{H^+,s}$, the overall calcite dissolution rate is a linear function of the hydrogen ion activity in the bulk solution consistent with:

$$r = k_2^{'} \gamma_{H^+,s} c_{H^+,b} \approx k_2^{'} a_{H^+,b}, \tag{3.23}$$

Where $k_2^{'}$ designates an apparent rate constant defined by:

$$k_2^{'} = \frac{k_t k_2}{k_t + k_2 \gamma_{H^+,s}}, \tag{3.24}$$

This apparent rate constant has two limits, when $k_t >> k_2 \gamma_{H^+,s}$ then $k_2^{'} \approx k_2$, but when $k_t << k_2 \gamma_{H^+,s}$ then $k_2^{'} \approx k_t / \gamma_{H^+,s}$.

Experimental studies of calcite dissolution at acidic conditions are typically interpreted to generate $k_2^{'}$, which is a function of both the chemical and transport rate constant. In general, the transport constant depends on the hydrodynamics and geometry of the experimental system. Consequently, $k_2^{'}$ values generated from experimental data available in literature depend to a large extent on the experimental design.

One of the oldest classical models for describing fluid-solid heterogeneous reactions is the sharp interface or unreacted-core shrinking model which assumes that the reaction occurs initially at the particle outer surface then moves towards the centre of the particle by means of

a narrow reaction front. This model is suitable for a simple reaction of a fluid with a non-porous solid that does not undergo any structural change.

3.1.4 Shrinking core model (SCM)

The SCM is a theoretical model that considers the beginning of the reaction at the outer surface of the particle and the formation of a reaction front which moves towards the centre of the solid particle, leaving behind a solid product layer as the reaction progresses. This product layer is here referred to as the 'ash'. For a gas-solid reaction with a solid product (ash), the model visualizes the reaction to be occurring in three steps in succession:

i. Diffusion of the gaseous reactant A (SO_2 in the present case) through the film surrounding the particle to the surface of the solid,

ii. Penetration and diffusion of A (SO_2 in the present case) through the blanket of ash to the surface of the unreacted core,

iii. Reaction of gaseous A (SO_2 in the present case) with solid (sorbent particle) at this reaction surface.

The resistances of the different steps usually vary greatly one from the other; in such cases the step with the highest resistance may be considered to be rate-controlling. Taking ρ_B – particle density, R – particle radius, k_g – mass transfer coefficient between gas and particle, C_{SO_2} – SO_2 concentration, τ – time for complete reaction, X – solid conversion, D_e – effective diffusion coefficient of gas in the ash layer, K_s – first order constant for surface reaction, three cases may be considered.

Diffusion through gas film controls

If the fluid reactant diffusion through the fluid film surrounding the particle controls the overall reaction, then:

$$t = \frac{\rho_B R}{3 k_g C_{SO_2}} \left[1 - \left(\frac{r_c}{R} \right)^3 \right], \text{ or } \quad \frac{t}{\tau} = 1 - \left(\frac{r_c}{R} \right)^3 = X \tag{3.25}$$

Diffusion through the ash layer controls

If the reactant fluid diffusion through the ash layer surrounding the unreacted particle core controls the overall reaction, then:

$$t = \frac{\rho_B R^2}{6 D_e C_{SO_2}} \left[1 - 3\left(\frac{r_c}{R} \right)^2 + 2\left(\frac{r_c}{R} \right)^3 \right], \text{ or } \frac{t}{\tau} = 1 - 3(1 - X)^{\frac{2}{3}} + 2(1 - X) \tag{3.26}$$

Chemical reaction controls

If the chemical reaction at the unreacted surface is the rate limiting step, then

$$t = \frac{\rho_B R}{k_s C_{SO_2}} \left[1 - \left(\frac{r_c}{R} \right) \right], \qquad \frac{t}{\tau} = 1 - (1 - X)^{\frac{1}{3}} \tag{3.27}$$

In general, it may not be reasonable to consider that just one step controls throughout the reaction. The relative importance of the fluid film, ash layer, and reaction step will vary as conversion progresses. For a constant size particle, the fluid film resistance remains unchanged, the resistance to reaction increases as the surface area of the unreacted core

decreases, while the ash layer resistance is nonexistent at the beginning because no ash is present, but becomes progressively more and more important as the ash layer builds up. To account for the simultaneous action of these resistances is straightforward since they act in series and are all linear in concentration.

Combined chemical reaction and ash diffusion control

The model commonly tested for the sulphation activity combines the chemical and diffusion through the ash layer as the controlling mechanisms. The rate equation for the combined steps is:

$$r_s = \frac{4\pi R^2 C_{so_2} (1 - X)^{\frac{2}{3}}}{\frac{1}{k_s} + \frac{R(1 - X)^{\frac{1}{3}}}{D_e}\left[1 - (1 - X)^{\frac{1}{3}}\right]} \qquad (3.28)$$

3.2 SORBENT SULPHATION IN A FIXED-REACTOR

A study of the absorption in the fixed-bed reactor is based on determining the exhaust SO_2-time concentration curves which are a function of the reactor geometry, the conditions of operation, the type of sorbent, and also the equilibrium absorption data. The exhaust SO_2-time concentration curve is generally known as the "breakthrough curve" and is obtained by passing the flue gas with an initial concentration, C_0, through a bed packed with the sorbent particles. As the flue gas passes through the bed, the SO_2 is retained and the sorbent becomes saturated until the SO_2 concentration at the outlet is equal to the initial inlet concentration, establishing a distribution of the concentration inside the bed as shown in Figure 3.1.

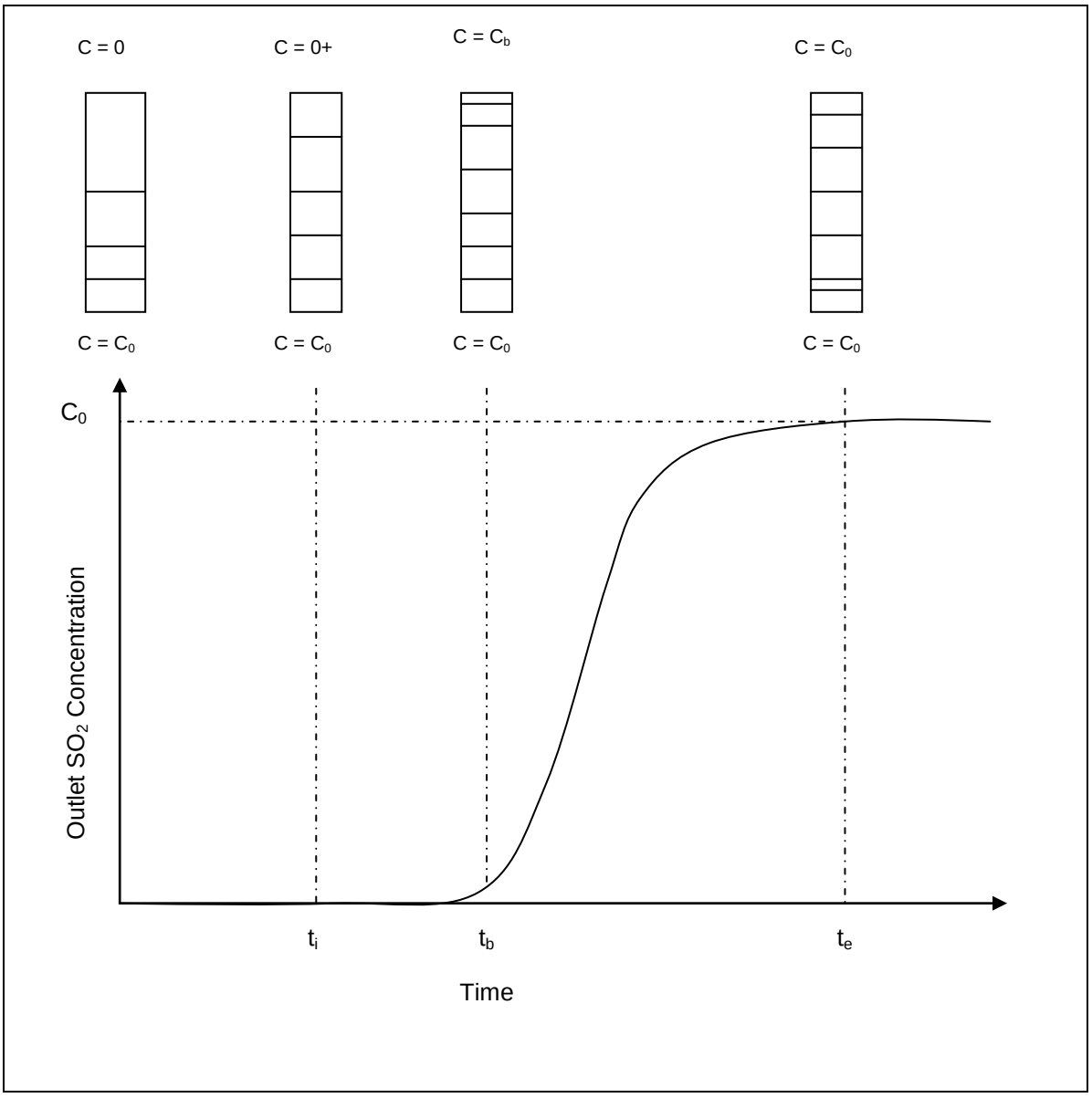

FIGURE 3.1: SO_2 Breakthrough Curve in a Fixed-bed

After a time t_i, SO_2 starts to appear at the outlet of the fixed bed. Time t_b is defined as the time necessary to reach the changeover point concentration as indicated by C_b. This is the maximum permissible SO_2 concentration in the outlet flue gas. Time t_e is the time after which the sorbent in the fixed-bed has been exhausted. The time period t_i to t_e is the thickness of the

absorption area or mass transfer zone in the bed and is related to the absorption capacity of the sorbent.

3.2.1 Reactor Model

The mathematical model used to describe the desulphurisation process in a fixed bed reactor with calcium-based sorbents is based on the microscopic mass balance of the sulphur in the gas and solid phase of the reactor. The following assumptions are taken into account in the model development:

i. The fixed bed is operating under isothermal conditions.

ii. The SO_2 is the only adsorbable gas in the flue gas.

iii. The concentration of the SO_2 is small enough so that when much or most of it has adsorbed, velocity does not change significantly.

iv. Plug flow conditions for the gas phase.

v. There is no axial or radial dispersion

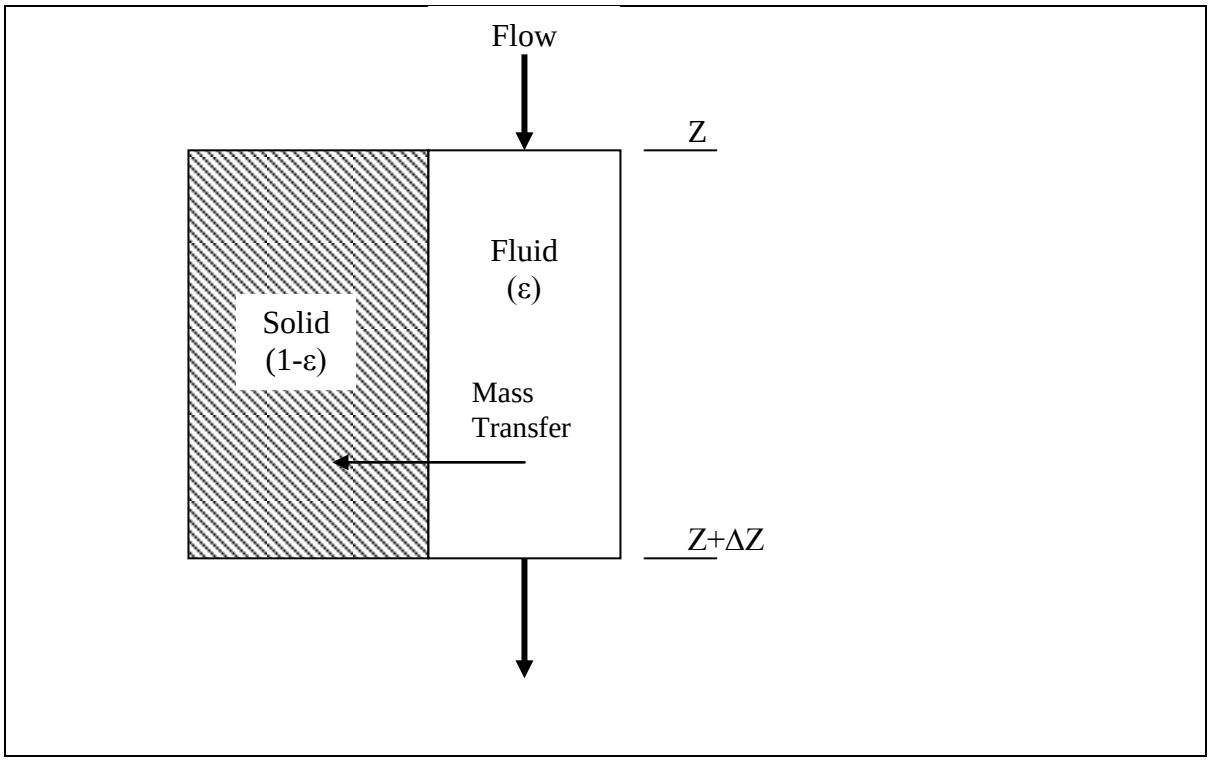

FIGURE 3.2: Schematic diagram of a fixed-bed adsorber

The differential mass balance equation for SO_2 in a fixed-bed adsorber is easily derived through a consideration of a short length ΔZ of a fixed-bed of cross-sectional area A, as shown in the Figure 3.2. Considering the elemental section and the model assumptions, the following set of equations are obtained:

- Gas phase mass balance

$$\frac{\partial C_{SO_2}}{\partial t} = -v\frac{\partial C_{SO_2}}{\partial Z} + \left(\frac{1-\varepsilon_{fb}}{\varepsilon_{fb}}\right) f_{v,s}(-r_s) \qquad (3.29)$$

Where: C_{SO_2} - is the SO_2 concentration (mol m^{-3}), v – is the gas velocity (m s^{-1}), ε_{fb} – fixed bed porosity, $f_{v,s}$ – volume fraction of sorbent in the bed, r_s – average reaction rate in the particle (mol $m^{-3}s^{-1}$).

The z-coordinate indicates the axial position in the bed, with z = 0 at the gas inlet point, i.e. the upper limit of the bed.

- Solid phase mass balance

$$\frac{\partial X}{\partial t} = S_e M r_s \qquad (3.30)$$

where: X – conversion of the solid reagent (-), M – molecular weight (g mol^{-1}), S_e – specific surface area of the reagent (m^2 g^{-1})

These equations are solved using the following initial and boundary conditions:

$$C_{SO_2}\big|_{Z=0} = C_{SO_2,in} \;, \quad C_{SO_2}\big|_{Z>0} = 0 \quad \text{and} \quad X = 0 \quad \text{at} \quad t = 0$$

$$C_{SO_2}\big|_{Z=0} = C_{SO_2,in} \quad \text{at} \quad t > o$$

The equation can be used together with the particle reaction model to show how the concentration of SO_2 in both the flue gas and solid phases varies with time and position, and to show more specifically how the flue gas concentration at the absorber outlet varies with time (the so-called breakthrough curve).

3.2.2 Particle reaction model

3.2.2.1 Insight into the reaction mechanism

The description of the kinetics of gas-solid non-catalytic reaction usually comprises of a number of physical and chemical steps. In this way, a sequence of the steps involved in the reaction between $Ca(OH)_2$ and SO_2 in the presence of water vapor can be proposed. This scheme not only takes into account typical steps involved in gas-solid reactions, but it also constitutes a first approximation to describe the relevant role of water vapor in the kinetics of the reaction. The following steps are considered:

1. Adsorption of water on the solid surface (pores and external), which can be described as:

$$H_2O_{(g)} \xleftrightarrow{k_{ads}^{H_2O}} H_2O_{(ads)} \tag{3.31}$$

Liu, Shih, and Lin (2002) showed that the amount of water adsorbed increased with increasing relative humidity (water vapour) and decreased with increasing temperature. They also estimated the monolayer (ML) adsorption capacity at being 1.6 ML thick at 30% relative humidity and about 3.2 ML at 80% relative humidity. Ch'un-S. and Shin-M. (1993) observed that the monolayer capacity decreased from 8.7 to 4.0 g/kg (Table 3.1) as the temperature increased from 60 to 90^{o}C. Additionally, the number of monolayers, being nearly independent of the temperature, increased from 1.5 to 2.4 as the relative humidity increased from 30 to 70%.

TABLE 3.1: Monolayer capacity and the number of monolayers for water adsorption on hydrated lime, BET surface area 10 m^2/g (Ch'un-Sung & Shin-Min, 1993)

T (^oC)	Monolayer capacity, V_m (g/kg)	$V/V_m \left(= \frac{\text{water adsorption on hydrated lime (g/kg)}}{\text{monolayer capacity (g/kg)}} \right)$		
		30 %	50%	70%
60	8.65	1.60	1.80	2.27
70	7.21	1.50	1.77	2.33
90	4.04	1.46	1.53	2.45

2. Hydration of SO_2 with adsorbed water molecules on the solid surface.

In the presence of water, SO_2 can be hydrated forming $SO_2.zH_2O$ species with different z values according to the following expression:

$$SO_{2(g)} + zH_2O_{(ads)} \overset{k_c}{\longleftrightarrow} SO_2.zH_2O_{(ads)} \quad (3.32)$$

3. Reaction of $SO_2.zH_2O$ with $Ca(OH)_2$ and formation of the reaction product according to the reaction:

$$SO_2.zH_2O_{(ads)} + Ca(OH)_{2(s)} \rightarrow CaSO_3.(z-½)H_2O_{(s)} + (z+½)H_2O_{(g)} \quad (3.33)$$

4. Once a product layer forms on the solid reagent, a diffusion step might be hypothesized. Taking into account the crystalline nature of $Ca(OH)_2$, the lattice parameters of its unit cell and the BET surface area, the ratio between surface and inner Ca^{2+} or OH^- ions can be

roughly estimated. In this way, solid conversions of only 1.5% would be attained if only the most superficial $Ca(OH)_2$ reacted. However, as higher conversions are experimentally obtained, inner solid reagent should also react. Moreover, because the molar volume of the solid product ($CaSO_3$) is slightly higher than that of $Ca(OH)_2$ reagent (ratio of 1.6:1), it seems reasonable to consider that a non-porous product layer will be formed, which might be crossed by diffusion by at least one of the reactants (SO_2 or Ca^{2+} and OH^- ions) for the reaction to go on.

All the kinetic models proposed to describe experimental data of the reaction under study are based on one or more of the above stages. Below is a review of kinetic models that have been proposed by previous researchers.

3.2.2.2 Evaluation of kinetic models

The models applied to the reaction at high temperature fall into the following categories: (1) grain or particle-pellet model, (2) pore, and (3) deactivation models, most of which incorporate mathematical equations to consider structural variations.

Grain model: The concept of the grain theory is useful for the analysis of gas-solid reactions. According to this theory, a porous particle is comprised of spherical grains of uniform size separated by pores through which the reacting gases diffuse to reach the various grains. The reaction occurs at the surface of each grain according to the sharp interface model (SCM). As the reaction proceeds, a shell of the reaction product is formed on the surface of the grains and this will in turn offer some resistance to diffusion.

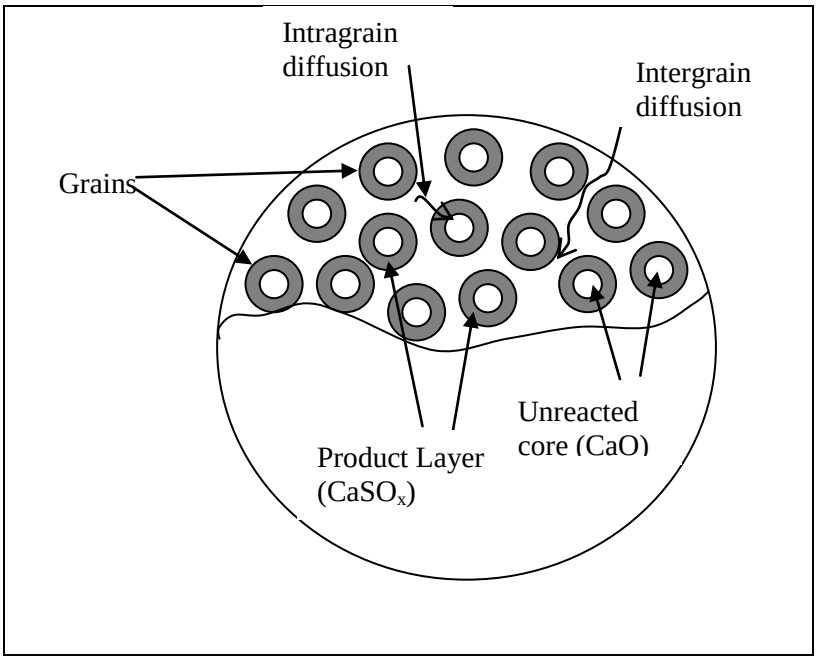

FIGURE 3.3: Schematic representation of the grain model

Hartman and Trnka (1980) have used this modified version of theory to model the sulphation process. They developed their model based on the unreacted shrinking core mechanism of the reaction between the gas and grains of calcium oxide. The overall reaction is governed by three individual processes: diffusion through the pores of particles, diffusion through an expanding shell of sulphate formed on the grains, and the chemical reaction taking place at the active interface of the grains. Figure 3.3 shows a schematic representation of the grain model (Ramachandran & Doraiswmy, 1982).

One feature of most models based on an average pore or grain size is a sudden cut off of the reaction at the point of pore closure. The experimental data do not show this type of behaviour but the rate tends to gradually decrease as the outer layer is plugged. Hartman and Coughlin (1976) overcame this problem with their grain model by noting that a certain amount of residual porosity associated with the largest pores remained after the bulk of the outer shell

was plugged. By using this residual porosity as an adjustable parameter, they obtained a smooth decrease in the reaction rate up to the ultimate conversion. Karatepe *et al*. (1999) assumed that the effective diffusion coefficient of gaseous reactant through product layer was conversion dependent and calculated it from experimental conversion-time data using the following semi-empirical equation.

$$D_e = D_{e,0}.e^{-bx} \tag{3.34}$$

Where D_e is the effective diffusion coefficient, $D_{e,0}$ is the effective diffusion coefficient at t = 0, x is the conversion, and b is a constant.

Pore model: The single-pore model approaches the problem in an entirely different manner. In this case, the model focuses attention on the changes taking place in a single pore which is supposed to be representative of the changes taking place in the pellet. The single pore can be assumed to be cylindrical with a concentric ring of solid B associated with it. Petersen (1957) analyzed the gasification of a solid by assuming it to be comprised of long cylindrical pores of uniform radius. A schematic representation of this is shown in Figure 3.4. The model parameters are: (1) average pore radius; (2) radius of associated solid; (3) effective pore length; (4) effective diffusivity through the product later; and (5) reaction rate constant. The first three parameters can be obtained independently by measuring the surface area and the pore volume of the initial pellet. Thus the main advantage of this model is the small number of independent model parameters. A disadvantage of this model is that it does not take into account the intersections of the reaction surfaces as the various pores present in the pellet react.

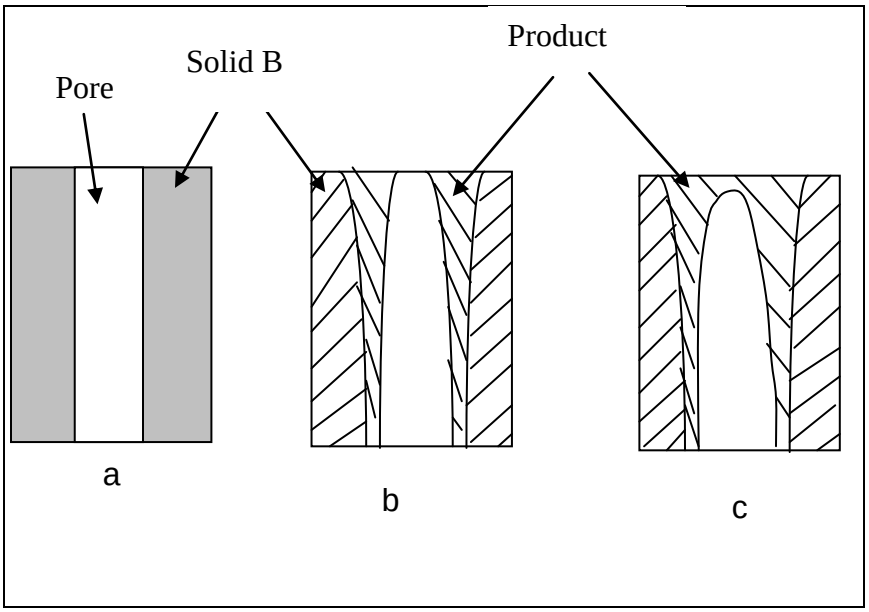

FIGURE 3.4: Schematic representation of the single-pore model with pore mouth plugging. (a) unreacted particle, (b) partially plugged pore, (c) plugged pore.

Distributed Pore Models: These models are similar in concept to the single pore model but take into account the effect of pore size distribution. Bhatia and Perlmutter (1980) presented a random pore model that accounts for the random overlap of reacting surfaces as they grow by extending a theory originally developed by Avrami (1940) for the analysis of the geometry of crystal aggregates. In their analysis, they visualize the reaction between a solid and a fluid as starting at the surface of the pores. As further reaction occurs, a layer of the product is formed around each pore which separates the growing reaction surface of the solid from the fluid reactant within the pores. The reaction surface is the interface between the non-overlapped portion of the cylindrical surface and the unreacted solid (Figure 3.5). The product layer that is deposited as the reaction surface moves is not shown on this figure.

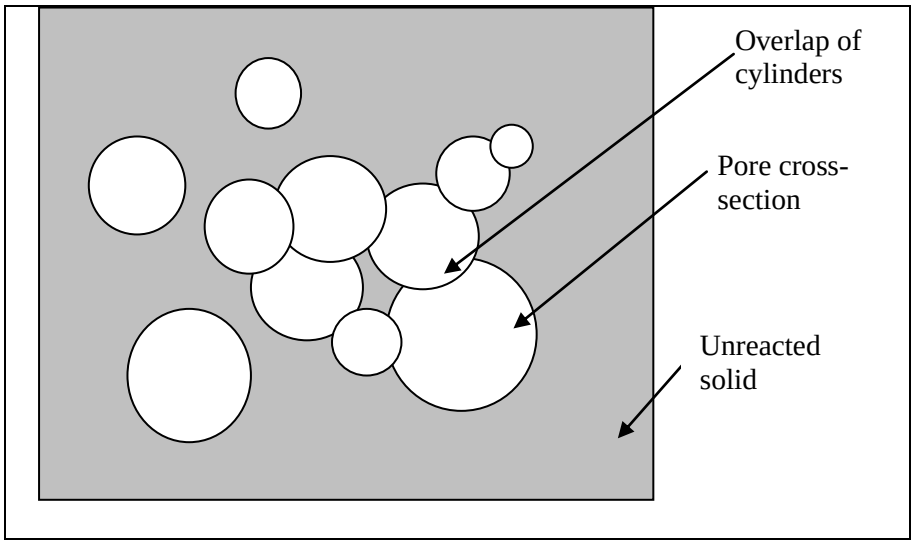

FIGURE 3.5: Overlapping of cylindrical surfaces. The grey area shows the unreacted solid.

As the reaction progresses, each pore of the particle has associated with it a growing reaction surface which initially corresponds to the inner surface of the pore. As the various reaction surfaces in the particle grow, it is inevitable that the neighbouring surfaces will intersect with one another as the solid separating them is consumed and replaced by the product. Figure 3.5 shows a schematic of the overlapped system. A balance over the size distribution of the growing cylinders yields the expression (Bhatia & Perlmutter, 1980; Christian & Edgar,1983):

$$\frac{\partial f}{\partial t} + \frac{\partial}{\partial r}\left[f \frac{dr}{dt} \right] = 0 \qquad (3.35)$$

Where f is the pore size distribution function, r radial position of unit surface, and t time. Equation 3.35 is the standard population balance equation which assumes that there is no net fractional increase in the number of pores by “birth” or “death” mechanisms; that is, it assumes that the total number of pores are conserved. Based on these assumptions, Bhatia and

Perlmutter (1980) derived an expression for the conversion at each dimensionless time in terms of the initial pore structure parameter ψ and the particle size parameter σ:

$$\frac{S}{S_0} = \frac{1-X}{\left(1-\frac{\tau}{\sigma}\right)^3}\sqrt{1-\psi \ln\left[\frac{1-X}{\left(1-\frac{\tau}{\sigma}\right)^3}\right]} \qquad (3.36)$$

And

$$X = 1-\left(1-\frac{\tau}{\sigma}\right)^3 \exp\left[-\tau+\frac{\psi\tau}{4}\right] \qquad (3.37)$$

where S is the reaction surface area per unit volume, S_0 is S at t = 0, X is conversion, $\tau = k_g C^n S_0 t / (1-\varepsilon_0)$, $\psi = 4\pi L_0 (1-\varepsilon_0)/S_0^2$, $\sigma = R_0 S_0 / (1-\varepsilon_0)$, k_g is rate constant for surface reaction, C is concentration of gaseous reactant, t is time, ε_0 is initial porosity, n is reaction order with respect to gas reactant, L_0 initial length of overlapped system, and R_0 is the initial particle radius.

This equation is similar to other models; for example, if ψ = 0 it reduces to the volume reaction model with n = 1. Similarly the grain model behavior can be closely approximated if ψ = 1. This also leads to the conclusion that the concept of reaction order with respect to solid is closely related to the structure of the pores of the solid. A relationship between the order of reaction n and the structural parameter ψ has also been obtained (Bhatia and Perlmutter, 1980). Thus the random pore model is able to offer a rational meaning to the reaction order

with respect to the solid. In subsequent papers, Bhatia and Perlmutter (1981a, 1981b) extended this model to consider the case of ash diffusion.

Christian and Edgar (1983) applied the single pore model for a pore of radius r_0. As reaction occurs, a product layer will form on the walls of the cylinder, creating new radii r_1 at the solid-gas interface, and r_2 at the solid-solid interface between reactant and product. The characteristic radii of the pore are related by:

$$r_1^2 = \alpha r_0^2 + (1-\alpha) r_2^2 \tag{3.38}$$

where α is the ratio of molar volumes of the solid product to solid reactant.

Deactivation Models: Structural changes that occur during the reaction between a porous solid and a gaseous reactant cause significant variations on the rates and the mechanism of gas-solid non-catalytic reactions. The formation of a product layer causes a diffusion resistance through the layer and hence a significant decrease in the reactivity of the solid. Changes in the pore structure and in the active area of the solid reactant with reaction extent are also observed in a number of reactions. The changes in pore structure, active surface area, and active site distribution are expected to cause significant deactivation of the solid. Deactivation models are used for breakthrough analysis of gas-solid reactions taking into account these structural changes (Turkan & Sefa, 2004). Orbey et al. (1982) used the deactivation model to derive analytical expressions for the breakthrough curves of the reaction between pre-calcined limestone and SO_2. Effects of film mass-transfer, pore diffusion and structural changes on the observed rate were investigated and it was shown that the experimental results and the predictions of the model agree well. The expression which

represents the *S*-shaped breakthrough curves of sulphur dioxide tracer concentration at the bed outlet is as follows (Orbey et al., 1982):

$$\frac{C}{C_0} = \left[e^{Nv} \frac{\sinh \phi_0 \exp(-N\theta)}{\sinh \phi_0 \exp N(-\theta)} \right]^{\frac{\delta}{N}} \tag{3.39}$$

Where, $Ø_0$ is the initial Thiele Modulus defined by,

$$\phi_0 = R\left(\frac{\rho_{P,0} S_{g,0} k_{s,0}}{D_{eff}} \right)^{1/2} \tag{3.40}$$

N is a dimensionless parameter given by,

$$N = \frac{\beta \tau}{2} \tag{3.41}$$

Where τ is the time after which no significant conversion occurs and β is an empirical parameter. The formation of the solid product on the active reactant solid surface and the additional diffusion resistance caused by the formation of product layer on active surface change the value of reaction rate constant. All the factors which would change the value of reaction rate constant are dumped into an empirical parameter, β in this model. *v* is a dimensionless parameter defined by,

$$v = \frac{L\varepsilon_b}{tu_0} \tag{3.42}$$

δ is a dimensionless parameter as defined below,

$$\delta = 3(1-\varepsilon_b)\frac{D_{eff}\tau}{R^2\varepsilon_b} \tag{3.43}$$

and θ is the dimensionless time (t/τ). Regression analysis of the breakthrough data reported using Equation 3.39 gave the model parameters. Yasyerli et al. (2002) sought to improve the deactivation model of Orbey et al. (1982) by considering the concentration dependence of the deactivation rate. Neglecting pore diffusion resistance, species conservation equation for the packed column was written as:

$$-Q\frac{dC_A}{dW} - k_0 a C_A = 0 \tag{3.44}$$

Rate of change of activity, *a*, of the solid reactant was expressed by the following equation in this model:

$$-\frac{da}{dt} = k_d C_A a \tag{3.45}$$

Using an iterative procedure, the expression given below was proposed for the breakthrough curve:

$$\frac{C_A}{C_{A0}} = \exp\left\{\frac{1-\exp(-k_0 W/Q(1-\exp(-k_d t)))\exp(-k_d t)}{1-\exp(-k_d t)}\right\} \tag{3.46}$$

This is a two parameter model. The agreement of the model with experimental data was also observed to be quite good. The presence of only two adjustable parameters, namely initial rate constant k_0 and the deactivation rate constant k_d is the main advantage of this model. Both of

these constants showed an increasing trend with an increase in temperature. The activation energies of k_0 and k_d were found as 5.2 and 4.7 kJ/mole, respectively.

Suyadal et al. (2005) analyzed the breakthrough curves of SO_2 in the presence of O_2, CO_2 and H_2O vapour in a fluidized bed (FBC) reactor using the deactivation model. In order to formulate the SO_2 adsorption to calcined limestone, they assumed that: the system is isothermal; the external and internal mass transfer limitations can be neglected; the FBC can be approximated to a pseudo-homogeneous stirred tank reactor. Based on these assumptions, the mass balance for SO_2 in solid phase can be given by the following form:

$$k_g (C - C_S) S_0 - k_S C_S S_0 e^{-k_d t} = 0 \tag{3.47}$$

Which can be rearranged as:

$$\frac{C_S}{C} = \frac{1}{1 + (k_S / k_g) e^{-k_d t}} \tag{3.48}$$

Mass balance of SO_2 in fluid phase is given by:

$$Q_0 C_0 - Q_0 C - k_g (C - C_S) S_0 = 0 \tag{3.49}$$

The ratio S_0 to Q_0 may be called the surface-time (τ):

$$\tau = \frac{S_0}{Q_0} \tag{3.50}$$

Substituting equation (3.48) and (3.50) in (3.49) gives:

$$\frac{C}{C_0} = \frac{1}{1 + \frac{\tau}{(1/k_g) + [1/k_S e^{-k_d t}]}} \tag{3.51}$$

By considering assumption 2, Eq. (3.54) becomes:

$$\frac{C}{C_0} = \frac{1}{1 + k_S \tau e^{-k_d t}} \tag{3.52}$$

Hence:

$$\ln\left[C_0/C - 1\right] = \ln(k_S \tau) - k_d t \tag{3.53}$$

Thus, if the left hand side of Equation 3.53 is plotted against reaction time (t), a straight line should be obtained with a slope equal to $-k_d$ and intercept giving $ln(k_s\tau)$, from which k_s can be obtained. Table 3.2 gives a comparison between model parameters from literature.

TABLE 3.2: Comparison of Deactivation Model parameters

Material Properties/Operating Conditions				
Literature	Material	Gas Composition	Condition	Model Parameters
Dogu T.(1981)	Pre-calcined limestone at 950ºC; d_p, 1.5 cm; ε_0, 0.52	C_{SO2} = 0.5% C_{O2} = 99.5%	Fixed Bed; 101.3 kPa; 900ºC	$k_s=0.034\times10^3 s^{-1}$; $k_d=0.64\times10^{-3} s^{-1}$; E_a=27.2 kJmol^{-1}; E_d=50.2 kJmol^{-1}
Zheng et al. (1982)	Calcined limestone; S_0, 4×10^4 m^2m^{-3}; d_p, 150μm	C_{SO2} = 0.15%, air/balance N_2	Fluidized bed; 101.3 kPa; 850ºC	$k_s=3.044\times10^3 s^{-1}$; $k_d=4.640\times10^{-3} s^{-1}$
Orbey et al. (1982)	Pre-calcined limestone: R_0, 845μm; ε_0, 0.56	C_{SO2}=1.0%; C_{O2}=99%	Fixed Bed; 101.3 kPa; 900ºC	$k_s=0.260\times10^3 s^{-1}$; $k_d=0.750\times10^{-3} s^{-1}$ E_a=53.5 kJmol^{-1}; E_d=55.2kJmol^{-1}
Suyadal et al (2005)	Hydrated lime; S_0, 7.199×10^7 m^2m^{-3}; d_p, 186μm; ε_0, 0.44	C_{SO2}=0.6%; C_{O2}=6%; C_{CO2}=10%; C_{H2O}=5%; balance N_2	Fluidized bed; 101.3 kPa; 850ºC	$k_s=7.235\times10^3 s^{-1}$; $k_d=3.633\times10^{-3} s^{-1}$ E_a=87.4 kJmol^{-1}; E_d=0.9 kJmol^{-1}

SURFACE COVERAGE MODEL. The hypothesis of the surface coverage model is that the sorbent is made up of plate grains and that the reaction is controlled by chemical reaction on the surface of a grain and the reacting surface area of the grain decreases with the deposition of solid product. According to this model, the reaction of a sorbent reaches a maximum conversion when its reacting surface is fully covered by the product (Liu & Shih, 2002). Thus the reaction rate of sorbent per unit initial surface area, r_s, can be expressed as:

$$r_s = k_s \Phi, \tag{3.54}$$

where k_s is a function of temperature, concentrations of the reacting species, and relative humidity, Φ is the fraction of surface area which is not covered by product. The rate of conversion of sorbent is:

$$\frac{dX}{dt} = S_{g0} M r_s = S_{g0} M k_s \Phi, \tag{3.55}$$

where S_{g0} is the initial specific surface area of the sorbent and M is the sorbent weight per mole of Ca. How Φ changes with reaction time depends on the reaction rate and the way by which the product deposits on the surface; one may assume that:

$$-\frac{d\Phi}{dt} = k_p r_s = k_p k_s \Phi, \tag{3.56}$$

where k_p is a constant of proportionality, which is a function of temperature, concentrations of the reacting species, and the relative humidity. Equation 3.56 can be integrated to get Φ as a function of time:

$$\Phi = \exp\left(-k_1 k_2 t\right), \tag{3.57}$$

Where

$$k_1 = k_s S_{g0} M, \tag{3.58}$$

$$k_2 = k_p / \rho_{g0} M \quad (3.59)$$

By substitution of Equation 3.57 into Equation 3.55 and integrating, the relationship between conversion and timecan be obtained as:

$$X = 1 - \exp(-k_1 k_2 t / k_2) \quad (3.60)$$

From Equations 3.55, 3.60, and 3.60, the rate of conversion can be expressed as a function of conversion:

$$\frac{dX}{dt} = k_1 (1 - k_2 X) \quad (3.64)$$

3.3 CONCLUSIONS

From the discussion of the previous sections, it is seen that a number of models have been proposed to predict the desulphurisation reaction both under wet and dry conditions. Each of these models is usually applicable to a particular type of desulphurisation reaction. A sharp interface or shrinking core model (SCM) which assumes that the reaction occurs initially at the particle outer surface then moves towards the centre of the particle by means of a narrow reaction front is one of the oldest classical models. This model has been found to be suitable for a simple reaction of a gas with a non-porous solid that does not undergo structural changes and for liquid-solid reactions. Thus for the dissolution experiments, this model will adopted in determining the reaction rate constants for the different sorbent materials and thus ranking their reactivity for use in flue gas desulphurisation.

For the particle reaction models proposed for the desulphurisation in the fixed-bed reactor, a complete set of experimental data is necessary for their application, and this is often lacking in literature. From the discussion, an important conclusion that emerges is that the structure of the sorbent material plays a key role in characterizing the reaction rate. Hence a complete characterization of the sorbent must be undertaken in addition to obtaining the usual conversion – time data. The porosity and the pore size distribution of the sorbent are important parameters in many of the models and therefore such measurements are of great importance. In addition, the characterization of the sorbent at various stages of reaction and that of the final product are very valuable in fitting models which predict the evolution of pore structure with time. A second important quantity is the effective intraparticle diffusivity. This can be measured under nonreacting conditions at various extents of reaction in order to note any changes as a function of reaction. In high temperature processes, sintering of the sorbent reactant or product can significantly alter the effective diffusivity and its influence should be factored. Determination of the order of reaction with respect to the gas is necessary for a complete model fitting. Such data can easily be obtained by varying the partial pressure of the gas phase (i.e. SO_2 concentration) over a wide range.

Having obtained the experimental data, one can then proceed to model verification and parameter estimation. Here, the choice of model is often important. The most widely used model has been the sharp interface model due to its mathematical simplicity. However, the model may not be satisfactory especially for relatively porous particles. The volume reaction models are suitable for porous particles but these models account for changes that occur in the particle in a purely empirical way. The single pore models have mathematical simplicity and very few adjustable parameters but have the disadvantage of inherent assumption of uniform

pore size. The distributed pore size model and the random pore model incorporate the structural characteristics in greater detail and hence are useful in fitting data for pellets of differing pore structures. However, for the sulphation tests, this study will adopt the surface coverage model to obtain the kinetic rate constants.

CHAPTER 4

4. EXPERIMENTAL MATERIALS, EQUIPMENT, AND PROCEDURES

4.0 INTRODUCTION

This chapter describes the experimental equipment, procedures, and materials used in the study. Two experimental techniques were used in the determination of the reactivity of the samples. The first was by the pH-stat method to simulate performance in the wet FGD while the second was using a fixed-bed reactor to simulate the behaviour of the sorbents under dry FGD conditions. The main research materials used in this study were calcium-based materials from different mines in South Africa. The materials' physical and chemical properties were determined using standard methods.

4.1 MATERIALS

4.1.1 Location and selection of natural sorbents

The South African limestone and dolomite deposits are massive, remotely located and of high grade. Deposits of economic significance are hosted in five sedimentary units: (1) the Campbell Rand subgroup and the Malmani subgroup, the former in the Northern Cape province and the later in the Gauteng, Limpopo, Mpumalanga and Northwest provinces, (2) the Mapumulo Group, outcropping at Marble Delta in southern KwaZulu-Natal, (3) the Nama Group in the Vanrhynsdorp area of the Western Cape, (4) the Malmesbury Group in the Western and Eastern Cape, and (5) the Tertiary and Quatermary coastal limestone along the Cape coast (Agnello, 2003). The South African limestone and dolomite industry comprises of

41 quarries – 27 limestone and 10 dolomite quarries, 4 operations mining limestone and dolomite, 4 major lime and 2 dolomite manufacturers. Figure 4.1 shows the distribution of sorbent deposits and power plants in South Africa.

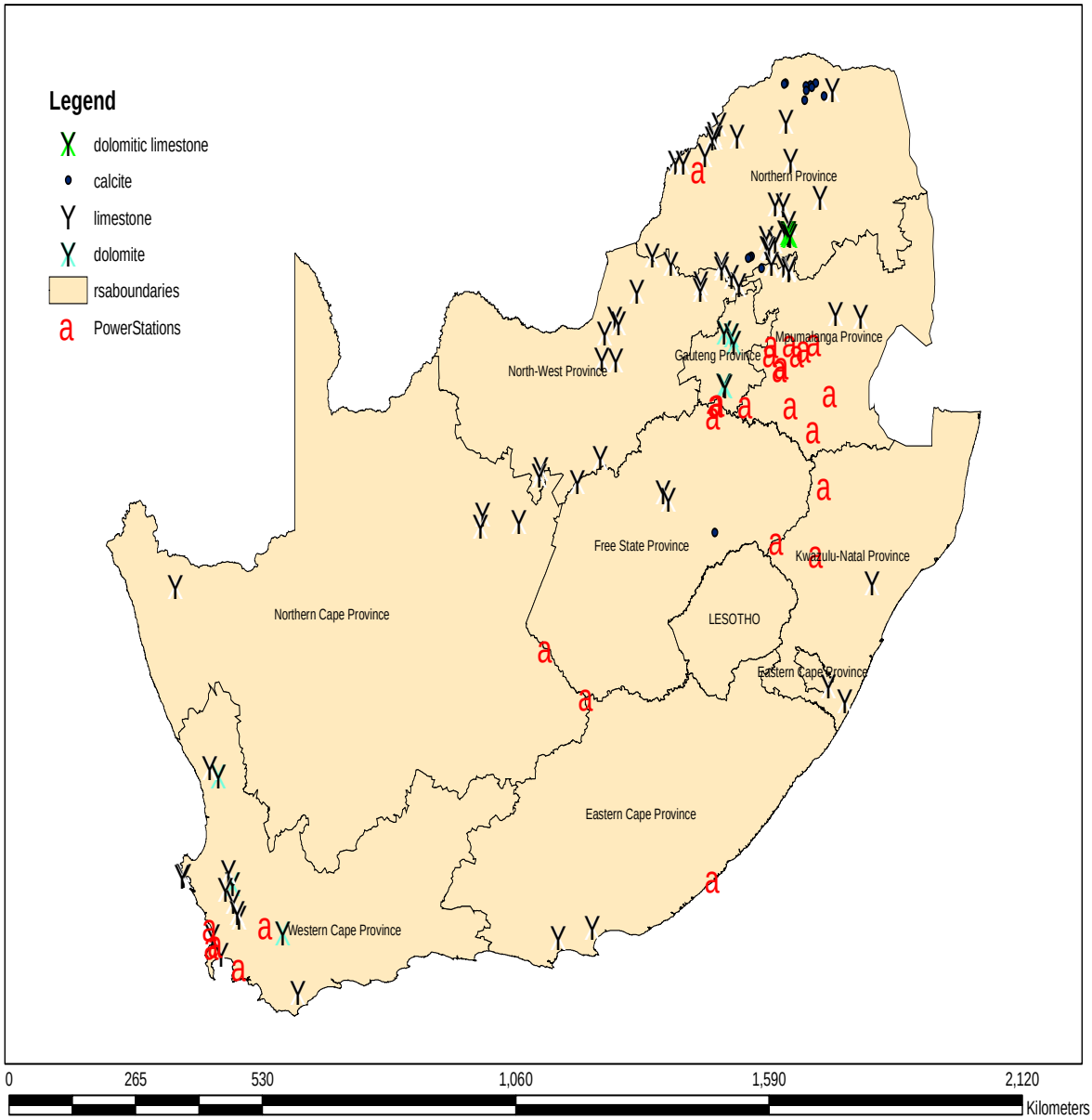

FIGURE 4.1: Sorbent and power plant locations in South Africa. (Haripersad, 2006)

Presently, limestone and dolomite products in South Africa are used in five principal industries: cement manufacturing, metallurgy (steel refining), agriculture (fertilizers, fungicides, animal feed), aggregate and lime manufacture.

The selection of limestone and dolomite samples was based on several reports of the council of Geoscince of South Africa and locations of coal – fired power stations. 15 samples were collected from different deposits situated close to coal-fired power stations around South Africa. The aim was to obtain samples with various crystalline structure and geological age at the shortest distance from the power stations. The reagent costs can be considerably influenced by the location of the plant. The total cost of the regent to the plant will include a transport cost, and so the proximity (or otherwise) of a suitable limestone mine, for example can be an important consideration. In general, the samples are not the representative mean samples of the deposits, but their composition remains within the characteristic margins of a definite deposit.

4.1.2 Sorbent preparation

For each limestone or dolomite sample used, about 0.5 kg of the sample (particle size of about 10 mm) was ground and sieved using a three-step procedure (Fig. 4.2). The sample from the step 3 was dried at 120^{o} C in a vacuum oven for 24 hours sieved to sizes of >200, 200x250, 250x275, 275x325, <325 meshes. The 200x250 mesh size fraction was for reactivity tests. The sorbents used in the pH-stat reactivity tests were used in their raw form while the samples used in the fixed bed underwent a calcination and hydration process.

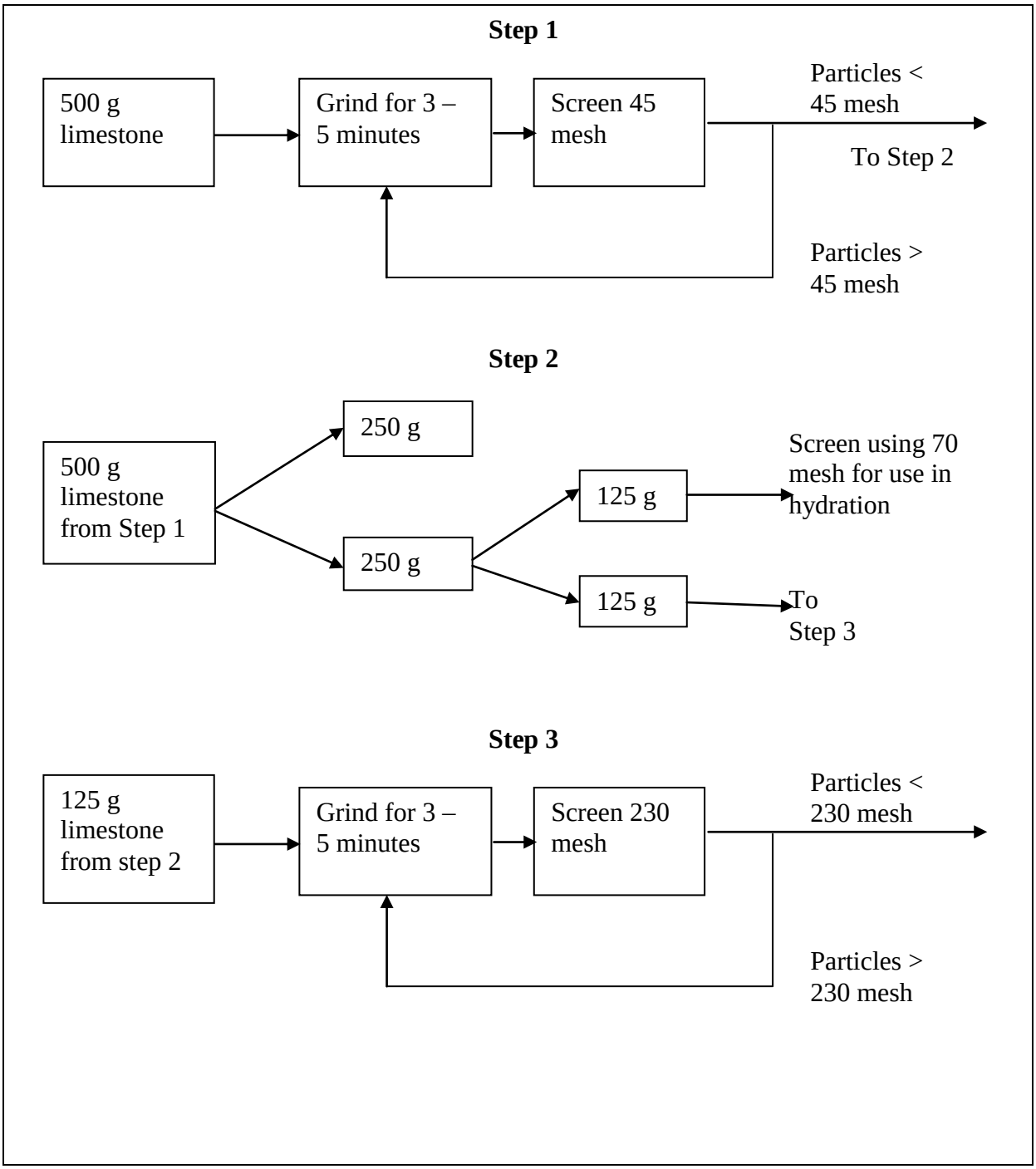

FIGURE 4.2: Procedure of sorbent sampling and grinding

4.1.3 Chemical Characterization

Limestones are mostly calcium carbonate ($CaCO_3$). Some rocks also have significant fractions of magnesium carbonate ($MgCO_3$). According to the MgO content of a calcined limestone rock, it can be classified as calcitic (0-1.1% MgO), magnesian (1.1 to 2.1% MgO), or dolomitic (2.1 to 10.8% MgO) limestone (Carmago, Pagliuso, & Milioli, 2003). Besides $CaCO_3$ and $MgCO_3$, natural limestone may contain varying amounts of impurities. The impurities can be classified as either homogeneous or heterogeneous. Homogeneous impurities are usually silt, sand or clay (or other forms of silica such as quartz) that entered the stone when it was first deposited and are therefore uniformly distributed throughout the formation. Heterogeneous impurities are contaminants that have accumulated between the strata or are loosely embedded in the stone.

The most common impurities in limestone are silicon and aluminium followed by iron. Silicon is usually present as silica or aluminum in alumino-silicate materials. Aluminium may also be present as alumina. Iron may exist as an iron carbonate or iron oxide, distributed heterogeneously from minerals such as pyrite or limonite. Other usually much less significant contaminants include manganese, copper, titanium, sulphur, phosphorous, zinc, chromium sodium and potassium (Carmago, Pagliuso, & Milioli, 2003).

The sorbents were subjected to a series of analyses including X-Ray Diffraction (XRD) for mineralogical composition, XRF for a quantitative analysis of the amounts of the individual elements in the sorbents, Scanning Electronic Microscopy (SEM) for morphology and semi-quantitative composition, N_2 absorption for the determination of pore size and distribution and the specific surface area.

4.1.3.1 XRD Analysis

X-ray diffraction (XRD) is a versatile, non-destructive technique that reveals detailed information about the chemical composition and crystallographic structure of natural and manufactured materials. Even though XRD is a qualitative technique, it can be used to obtain a rough quantitative approximation of the composition of a material.

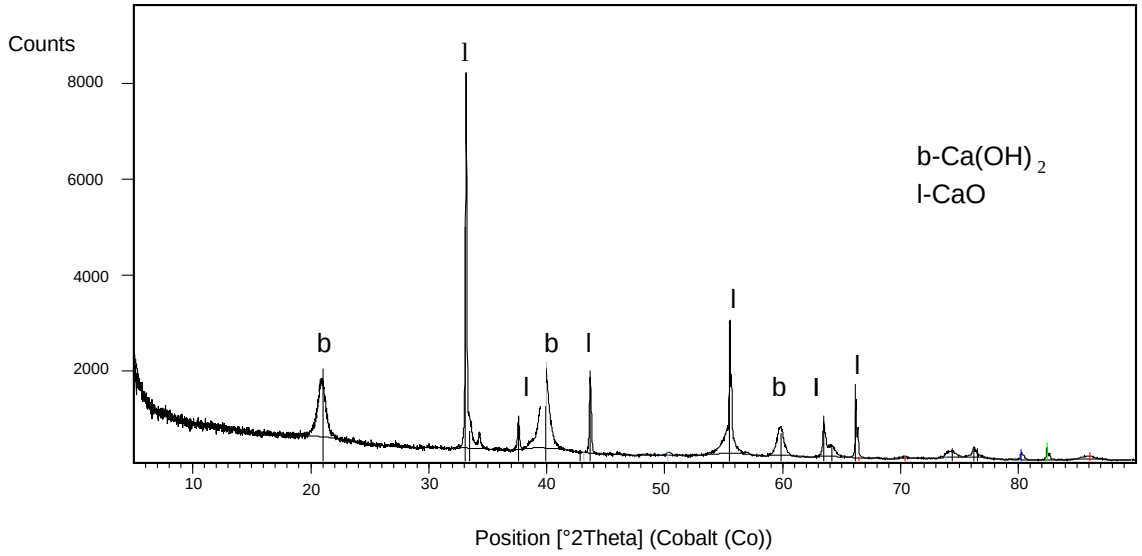

FIGURE 4.3: XRD pattern of limestone calcined at 900°C

In this study, an automated X-ray diffractometer (XRD) was used for mineralogical analysis. Samples were prepared using standard operating procedures (SOPs). 60-100g of sample were ground into a powder of <250µm with a *Shatterbox*. 4g of the sample were then milled down to <2µm with a *McCrone Micronizing Mill*. A *SCINTAG* x-ray diffractometer with a germanium detector and copper x-ray source was used to analyze the <2µm powder. The interpretation of the obtained patterns were done by comparison with data published by the "Joint Commission of Powder Diffraction Standards (2002)". Figure 4.3 shows a typical

example of an XRD pattern that is obtained for calcinated limestone. The figure shows only the presence of two major peaks; calcium oxide and calcium hydroxide. The exact quantitative analysis cannot be obtained but an approximation can be made based on the strength of the peaks.

4.1.3.2 XRF Analysis

The XRF was carried out at the Eskom laboratories (ESKOM Method No. 121 Rev 2 Accredited) . Wavelength-dispersive X-ray fluorescence spectrometry (XRF) was used to determine the concentrations of major and minor elements in the samples. Elements that were determined include silicon (Si), aluminum (Al), iron (Fe), potassium (K), calcium (Ca), magnesium (Mg), sodium (Na), titanium (Ti), phosphorus (P), and manganese (Mn) and trace elements barium (Ba), chromium (Cr), copper (Cu), nickel (Ni), lead (Pb), rubidium (Rb), strontium (Sr), vanadium (V), zinc (Zn), and zirconium (Zr). This is a whole-rock analysis and the results will reflect the purity of limestone samples being examined. The combustible matter was determined according to ESKOM Method 126 Rev 1. Table 4.1 shows the chemical analysis of the sorbents used as determined by XRF analysis.

TABLE 4.1: Chemical Composition of selected materials.

Sorbent Type	**Component**					
	SiO_2	**Al_2O_3**	**Fe_2O_3**	**CaO**	**MgO**	**Combustible matter**
A	5.95	1.53	1.83	88.39	1.26	38.3
B	13..33	1.67	0.67	81.87	1.67	37
C	nm	nm	nm	44	39.0	37
D	4.48	0.36	1.61	53.54	36.52	45.6
E	nm	nm	nm	92.5	1.75	40.2
F	7.93	0.50	2.87	66.2	22.1	43.9
G	6.85	0.01	1.65	72.5	18.3	43.2
H	7.69	0.01	2.34	87.8	2.15	44.2
J	4.26	0.09	0.61	94.2	0.77	39.0
K	4.45	0.16	1.96	73.8	19.6	43.3
L	36.0	2.32	1.89	39.7	19.1	37
M	22.5	2.42	0.01	72.9	2.10	41.6
N	11.8	1.27	0.50	80.3	6.70	40.6
P	8.84	0.12	1.23	77.0	11.65	40.0
Q	4.37	0.97	1.85	61.3	32.0	39.0

nm: not measured

As can be seen from the table the calcium content of the samples (as CaO) varies from 39.7 to 94.2 %. There is also a wide variation in the magnesium oxide from as low as 0.60 to 39%. Silicon oxide is also present in appreciable amounts in all the samples with the variation being

from 4.26 to 36.0 %. Al_2O_3, and Fe_2O_3 are also reported at quantities less than 3 % while P_2O_5, Na_2O, K_2O, and SO_3, are present in trace amounts (<0.5%) in all the samples.

4.1.3.3 Porosity and specific surface area

The BJH procedure (Barret, Joyner, & Halenda, 1951), which permits a better characterization of mesoporosity, was applied to obtain the pore-size distribution from nitrogen desorption data. The pore-size distribution is represented by the derivative $d(V_p)/d(d_p)$ as a function of pore diameter, where, V_p is the pore volume and d_p is the pore diameter. The samples were tested by the Protechnik Laboratories according to their test method 7300.101. Prior to measurement, the samples were degassed at 105ºC for 10 h in the degas pot of the adsorption analyzer in order to remove moisture and other contaminants. The samples were characterized using low temperature (77.35 K) nitrogen adsorption isotherms measured over a wide range of relative pressures from 10^{-6} to 1. High purity nitrogen (99.99%) was used. Adsorption measurements were performed on a Micromeritics ASAP 2020 Surface Area and Porosity analyzer by the principle of physical adsorption.

By IUPAC classification, pores are classified as micropores, mesopores and macropores. In porosity measurements, macropore is used to denote pores of diameter more than 50 *nm*, mesopore denotes pores of diameter between 2 *nm* and 50 *nm*, while micopore means pores of diameter less than 2 *nm* (IUPAC). There are six kinds of adsorption isotherms by the IUPAC classification with reference to pore size (Collet et al, 2007), and each indicates a distinct pore structure. A hysteresis may appear between the adsorption and the desorption branches. This hysteresis is often explained qualitatively by capillary condensation, by existence of ink-bottle shaped pores or, more generally, interconnected pore spaces. IUPAC classifies hysteresis

loops in four types (H1, H2, H3, and H4) and relates them with pore structure. Type H1 hysteresis loops are generally associated with pores of cylindrical geometry while type H3 are associated with slit-shaped or parallel plate-like pores (Adanez, Garcia-Labiano, & Fierro, 2000). Carbonate derived sorbents are usually associated with cylindrical pore geometries while hydroxide derived sorbents exhibit plate-like or slit geometries (Fierro , Adanez, & Garcia, 2004).

Due to cost constraints, only two representative samples of dolomitic (C and D) and calcitic (A and B) limestone each were submitted for the analysis of porosity and Specific surface area. Table 4.2 presents the results obtained:

TABLE 4.2: Specific surface area, pore volume, and average pore size of two calcitic and two dolomitic limestones tested.

Hydrated Sample	Surface Area (m^2/g)	Micro-pore (cm^3/g)	BJH Volume (cm^3/g)	Average pore width (Å)
A	33.2	Not detected	0.174	164
B	29.7	0.002	0.176	187
C	13.0	Not detected	0.108	257
D	23.7	Not detected	0.173	232

As can be seen from the results, the specific surface area of the samples vary over a wide area. However, the specific surface area is observed to be higher for the calcitic limestones than for the dolomitic ones. Except for sample C, all the samples tested appear to have the same BJH pore volume (0.174 cm^3/g).

4.1.3.4 Scanning Electron Microscope (SEM) analysis

A leica Cambridge S360 scanning electron microscope with 15 kV of accelerating voltage (located in The School of Biological Sciences, Universiti Sains Malaysia) was used to examine the sorbent surface morphologies. The absorbent was spread evenly on top of an aluminum stub attached with a double sided carbon tape. The sample was then placed into the specimen chamber under vacuum condition and was subsequently bombarded with an electron beam at 15 kV. The image of the sample was recorded by a Phillips model GP-850 graphic video recorder.

4.2 pH-STAT METHOD

Reactivity of limestone particles measured as the conversion or dissolution-reaction rate of the particles at a constant acidic pH value is an important tool for the design and operation of wet FGD processes. The conversion rates determined by batch laboratory tests can be used to reliably rank the performance of different limestones materials in industrial full-scale applications (see section 2.7.1.1).

4.2.1 Experimental set-up

For the current research, the proposed experimental apparatus is shown in Figure 4.4. Agitation of the sorbent particles in the solution is provided by a three blade propeller rotating at a variable speed that can be easily set between 50 and 1300 r.p.m.

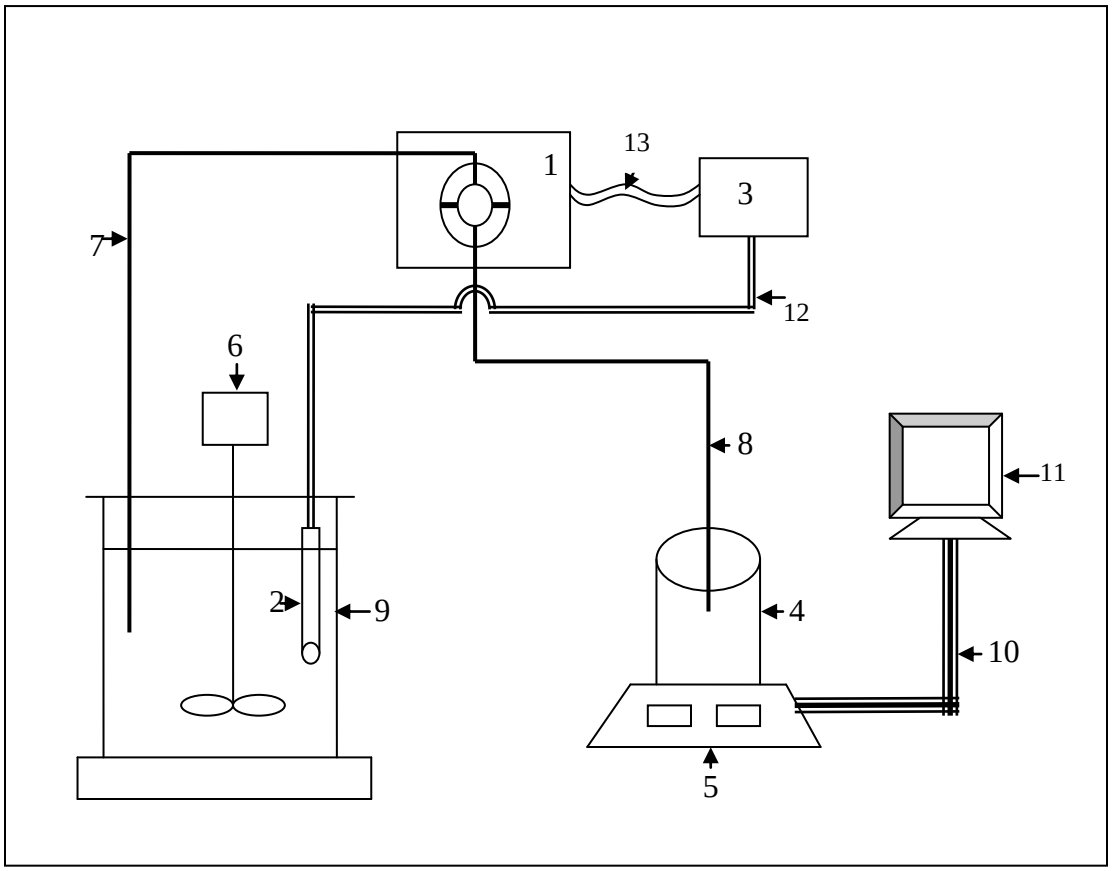

FIGURE 4.4: A schematic drawing of the experimental set-up. (1) Peristaltic pump, (2) pH electrode, (3) pH controller, (4) Acid solution Beaker, (5) Electronic balance, (6) Stirrer, (7,8) Plastic tubing, (9) Reaction vessel,(10) RS232 Cable, (11) Computer work station, (12) wiring for pH electrode, (13) Connection between pump and controller

The pH value in the reaction vessel is sensed by a pH electrode which is connected to an alpha pH 200 1/8 DIN pH/ ORP controller supplied by Eutech Instruments. Any variation from the pH stated value causes the controller relay to send a signal to a peristaltic pump which delivers a quantity of reagent to bring the pH to the set value. The reagent vessel is placed on an external weighing balance which records the amount of reagent remaining at

any given instant. The weighing balance is an Explorer Pro balance from Ohaus with a rated capacity of 2100g and a measurement accuracy of 0.001g. It is equipped with a bi-directional RS232 compatible interface for communication with serial printers and computers. Connecting the balance to a computer enables one to operate the balance from the computer, as well as receive and store data such as displayed weight, weighing mode, stability status, e.t.c. The balance is programmed to record the weight after every five (5) seconds and the information is transmitted to the computer where it is saved.

4.2.2 Experimental Procedure

1.5g of sample was dissolved in 200 mL of distilled water in a covered 500 mL glass beaker and the mixture agitated by a three bladed stirrer at a stirrer speed of 100 rpm. The temperature of the reaction vessel was kept at $50^{o}C$ by immersing the reaction vessel in a temperature controlled water bath. A constant pH of 5 was maintained throughout the experiment. The dissolution process was carried out by titrating with a 1M solution of hydrochloric acid. The amount of acid added was noted after every five seconds and the result recorded on an online computer. The cumulative dissolution was determined directly from a recording of HCl added vs. time. The fraction of dissolution was obtained by the ratio of the HCl added volume to that required for complete dissolution.

4.2.3 Experimental Design

Experiments were done to evaluate the reactivity of the different sorbent materials in the pH-stat apparatus. Additional experiments were carried out to determine the influence of the pH, temperature, particle size as well as sorbent type on the dissolution rate. Most wet FGD

processes operate at a temperature of less than 70°C (see Figure 2.1). Thus to determine the influence of the temperature on the dissolution process, the reactor temperature was varied in the range $30 \leq T \leq 70$°C. The pH in commercial FGD installations is maintained at a constant value, pH = 5.0, and to investigate the influence of this parameter, the pH was varied in the range $4 \leq T \leq 6$. For the influence of sorbent type, all the sorbents were tested at the average commercial FGD conditions of pH and temperature. One calcitic limestone (A) and one dolomitic limestone (C) were used to determine the influence of particle size, pH, and reactor temperature. Table 4.3 shows the type of experiments performed. For each experiment, 3 runs were performed and the average dissolution curve used for analysis.

TABLE 4.3: Type of pH-stat experiments, operating conditions, and type of sorbent used. (HCl concentration = 1M).

Type of Experiment	The operating conditions				Sorbent type used
	Static pH	Temp. (ºC)	Particle size (μm)	Stirrer (rpm)	
pH	4, 4.5, 5, 5.5, 6	50	-25	500	A, C
Temperature	5	30, 40, 50, 60, 70	-25	500	A, C
Particle size	5	50	-25, -45, -63	500	A, C
Sorbent	5	50	-25	500	All

4.2.4 Analysis of Results

Batch dissolution rates for various calcium – based materials were measured at constant pH by using the pH – stat apparatus (Figure 4.2). 1.5 g of sample material was dissolved in 200 mL of distilled water. The pH was automatically controlled by titrating with 1M HCl. The limestone dissolution rate was related to the titration rate by the stoichiometric equation:

$$CaCO_{3(s)} + 2HCl_{(aq)} \rightarrow CaCl_{2(aq)} + H_2O_{(l)} + CO_{2(g)} \quad (4.1)$$

The cumulative dissolution was determined directly from a recording of HCl added vs. time.

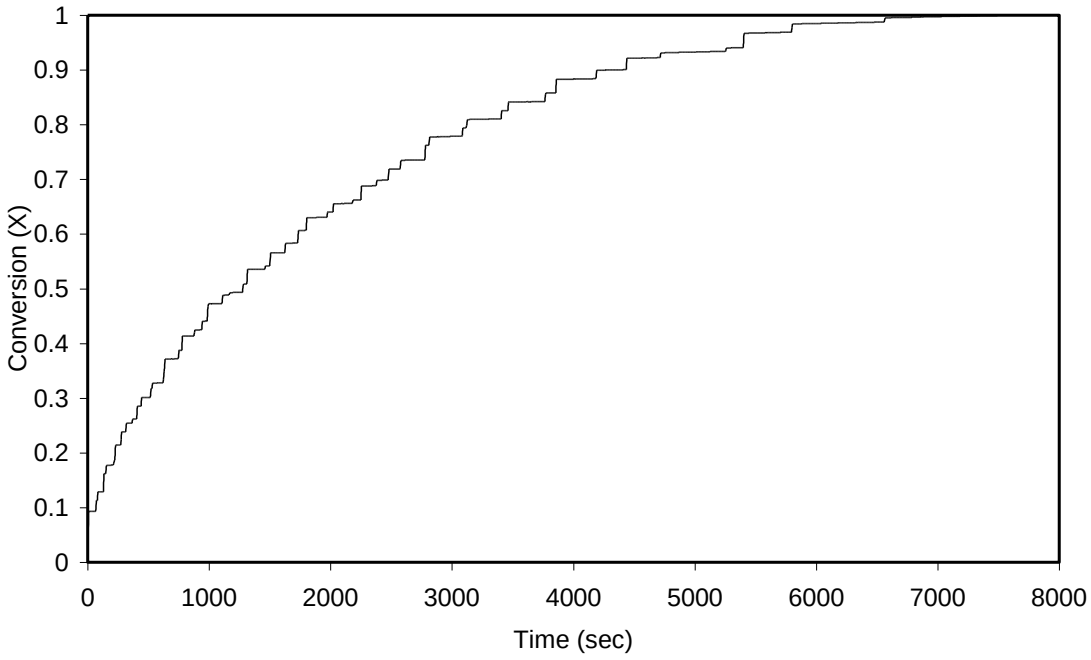

FIGURE 4.5: Plot of conversion (X) vs. time for Leo dolomite dissolution at pH 5.0 and 30ºC, 1.5 g dissolved in 200 mL distilled water. (<44um).

The fraction of dissolution was obtained by the ratio of the HCl added volume to that required for complete dissolution. Figure 4.3 shows an example of the conversion curve obtained for Leo Dolomite at a pH of 5.0 and 30ºC.

4.3 FIXED-BED METHOD

4.3.1 Introduction

The induct FGD process can be simulated by the use of the fixed-bed reactor. The evaluation of kinetic data from fixed beds of calcium-based sorbents is usually based on the assumption of plug flow of gases. However, channeling and back mixing of gases in the fixed beds, especially in short beds, is a major problem leading to low utilization of solid material. Therefore, preventing the gas channeling and back mixing effects through the fixed bed of solid reactant particles is necessary for obtaining proper gas-solid contact.

Dilution of solid reactant with inert materials in fixed beds is one option for good gas-solid contacting. The premise of this method is that inert solids would not influence the course of the reaction. However, some authors found that solid diluents affected the extent of conversion in a fixed bed of reacting particles by changing the residence time distribution or by creating shortcut effects, which are predominant in beds with small ratio of bed length to particle diameter. The fixed bed performance has been shown to increase with the degree of dilution up to about 10 kg inert per kg of sorbent (Akosman, & Walters, 2004). Mercader (2005) has shown experimentally that the dilution beyond a ratio 30:1 has no effect on the resulting breakthrough curves. Izquierdo *et al*. (2000) have used a ratio of 8:1 in their investigation in a fixed bed. Garea et al. (2001) have used a ratio of 90:1 to avoid the

channeling. In the experiments performed for this study, a sand to sorbent ratio of 30:1 was selected.

4.3.2 Sorbent preparation

The most important chemical property of limestones is their thermal decomposition and their conversion to quicklime (CaO). This reaction is called calcination and is carried out at a temperature of about 900°C (Kantiranis, 2003; Irfan & Gulsen, 2001). The calcination reaction is endothermic and it can be represented by the equation:

$$CaCO_{3(s)} \xrightarrow{heat} CaO_{(s)} + CO_{2(g)} \qquad (4.2)$$

$$\Delta H = +182.1 kJmol^{-1}$$

Similarly, in a carbon dioxide-free atmosphere, dolomite decomposes in one endothermic step to the mixture of oxides:

$$CaMg(CO_3)_{2(s)} \xrightarrow{heat} CaO_{(s)} + MgO_{(s)} + 2CO_{2(g)} \qquad (4.3)$$

$$\Delta H = 295.6 \text{ kJmol}^{-1}$$

TGA results by Hartman *et al*. (1996) demonstrate that the dolomite decomposition starts at about 600ºC and end at about 760ºC. The sorbent used widely in the humidified duct injection processes is hydrated lime (Karatepe *et al*., 1998). At temperatures less than 350°C, quicklime (CaO) rapidly reacts with water, exothermically, to produce hydrated lime according to the following equation (Kantiranis, 2003):

$$CaO_{(s)} + H_2O_{(l)} \rightarrow Ca(OH)_{2(s)} \quad (4.4)$$

$$\Delta H = -1138 kJ/kg\ of\ CaO$$

During the hydration of quicklime, two simultaneous phenomena are usually observed; the temperature increases (exothermic reaction) and the volume of the paste is expanded.

In the present study, the raw samples were heated at 900^{o}C for 3 hours obtaining the relevant calcines, which were cooled and slowly hydrated to obtain the required test material. The weight of the samples before and after calcination were recorded to determine the percentage weight loss due to calcination. Hydration was achieved by weighing 10 g of the calcinated sample and mixing, while stirring, with 20 mL of water. A thermometer immersed in the hydrating mixture recorded the maximum temperature attained for each sample. The resulting slurry was dried off in an oven maintained at 105^{o}C to produce a dry solid. All samples were then milled and sieved to a particle size below 200 μm before being used in the fixed bed.

4.3.3 Experimental set-up

A fixed-bed desulfurization test rig at the School of Chemical Engineering of the Universiti Sains Malaysia (Plate 4.1) was used to analyze the desulfurization activity. The schematic diagram of the test rig is shown in Figure 4.6. The experimental rig consists of the following sections:-

i. A system consisting of a series of mass flow controllers (Aalborg, Model: AFC 2600D) for mixing the various gases to obtain the simulated flue gas.

ii. A humidification system for the addition of water vapor into the flue gas. This system consists of two 250 ml conical flasks immersed in a water bath (Tempette TE-8D) at constant temperature.

iii. A fixed-bed absorber/reactor fitted with thermocouple (Patos, Model: DE-305, Type K) and heating arrangement (Thermolyne, Model: 21100) for monitoring the reactor temperature and heating the reactor respectively.

iv. A gas analyzer (Portable Flue Gas Analyzer IMR2800P) to obtain the flue gas composition before and after reaction.

The reaction zone is contained in a 0.008 m inner diameter stainless steel tube fitted in a furnace for isothermal operation. 0.1 g of the sorbent material is dispersed in 3 g of inert silica sand, packed in the centre of the reactor and is supported by 0.05 g of borosilicate glass wool

PLATE 4.1 Experimental Test Rig

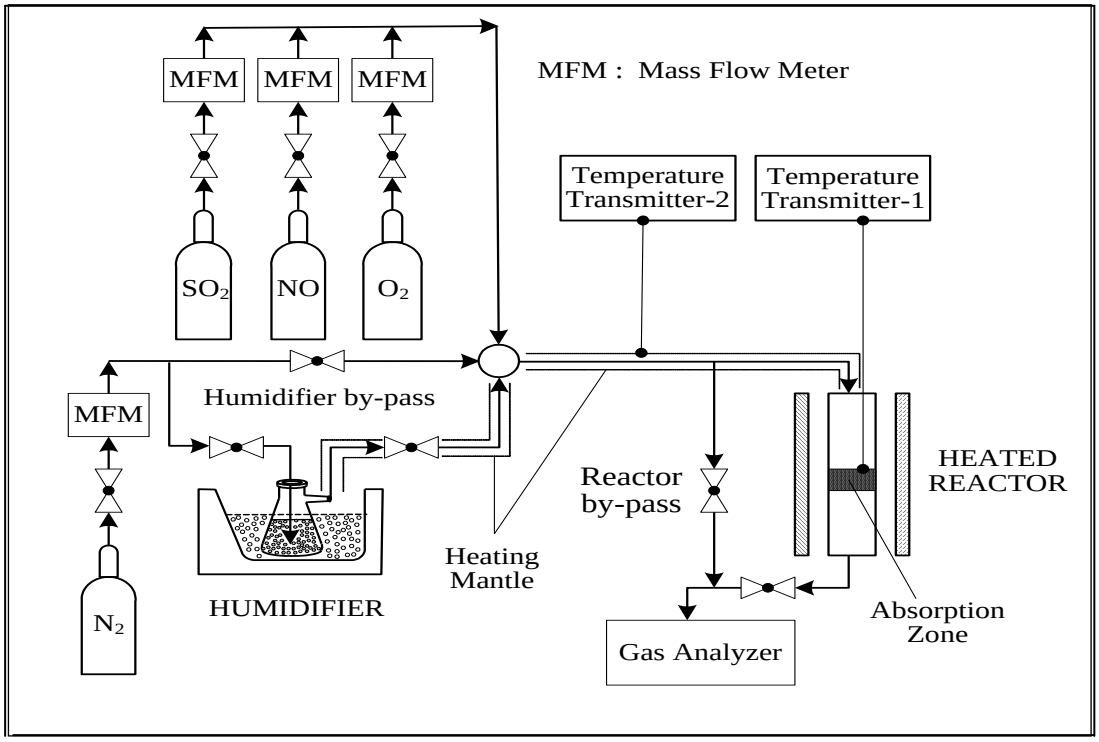

FIGURE 4.6: Schematic diagram of the experimental rig for fixed bed desulfurization

as shown in Figure 4.7. The inert silica sand helps to ensure isothermal operation, improve gas solid contact and avoid channeling of the flue gas. A N_2 stream is passed through a humidification system consisting of two 250 mL conical flasks immersed in a water bath maintained at constant temperature. After humidification, the N_2 stream is mixed with a gas stream consisting of SO_2, NO, and O_2. The simulated flue gas then flows through the reactor at a flow rate of 150 ml/min. The SO_2 concentration of the effluent gas is continuously monitored by an IMR 2800P flue gas analyzer.

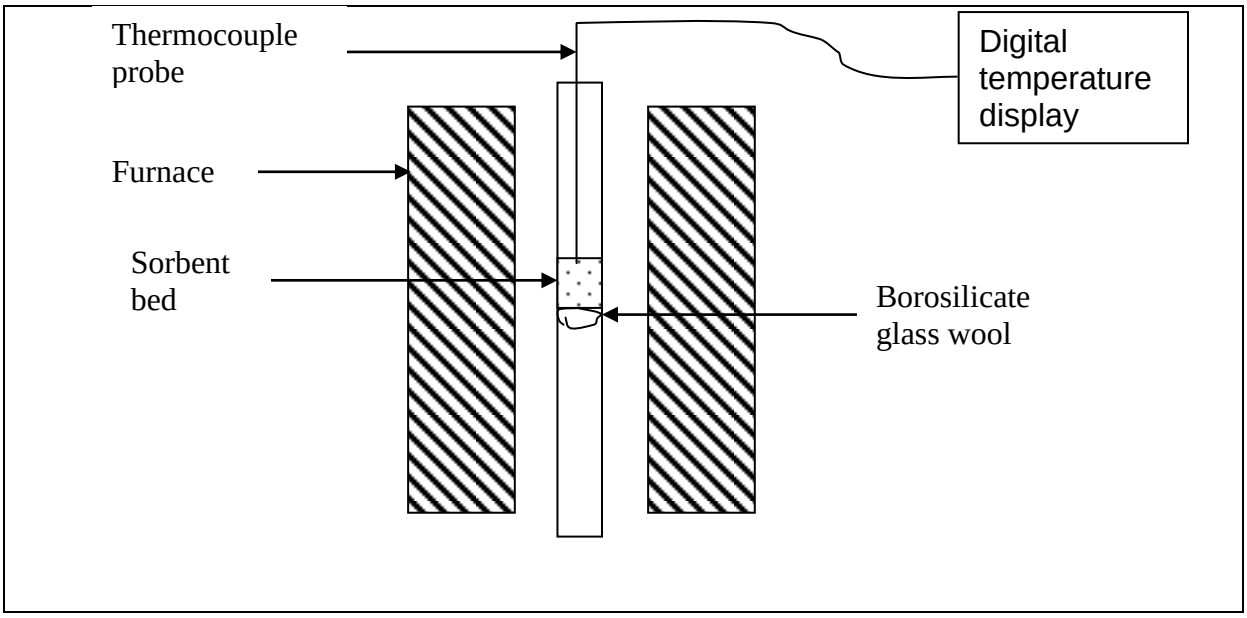

FIGURE 4.7: Reactor system showing location of sorbent bed

4.3.4 Experimental Procedure and analysis

After powering up, the desired reactor temperature and water bath temperature for a required relative humidity are selected. The reactor is loaded with 3 g of silica sand and fixed to the experimental set-up. Prior to the experimental run, the sand bed was humidified at the desired relative humidity for about 20 minutes by passing the humidified N_2 gas through the reactor. After humidification, the SO_2 gas was admitted into the reactor to start the run. After the blank run, 0.1g of the sample material is dispersed in the sand bed and the bed is left to stabilize before the experimental run. Figure 4.8 shows an example of the obtained blank and experimental runs. The amount of SO_2 retained per mole of sorbent is given by :

$$mol\ SO_2\ retained/\ mol\ sorbent\ =\ (A_{bl} - A_{\exp})C_0 10^{-6}\ \frac{\varphi_v}{22400}\ \frac{M_{sorbent}}{m_{sorbent}} \qquad (4.5)$$

Where, A_{bl} is the area under the blank run, A_{exp} is the area under the reaction curve, C_0 is the inlet SO_2 concentration, C is the outlet SO_2 concentration, $Ø_v$ is the volumetric flow rate ($mLmin^{-1}$), $M_{sorbent}$ is the molar mass of the sorbent, and $m_{sorbent}$ is the mass of the sorbent used in the experiment (Mercader, 2005). This method of estimating the sorbent activity has also been used by Izquierdo et al. (2000) with good results. When all the SO_2 that enters the reactor is retained, the ratio C/C_0 becomes zero. In the same way, when C/C_0 tends to one, no reaction can be expected.

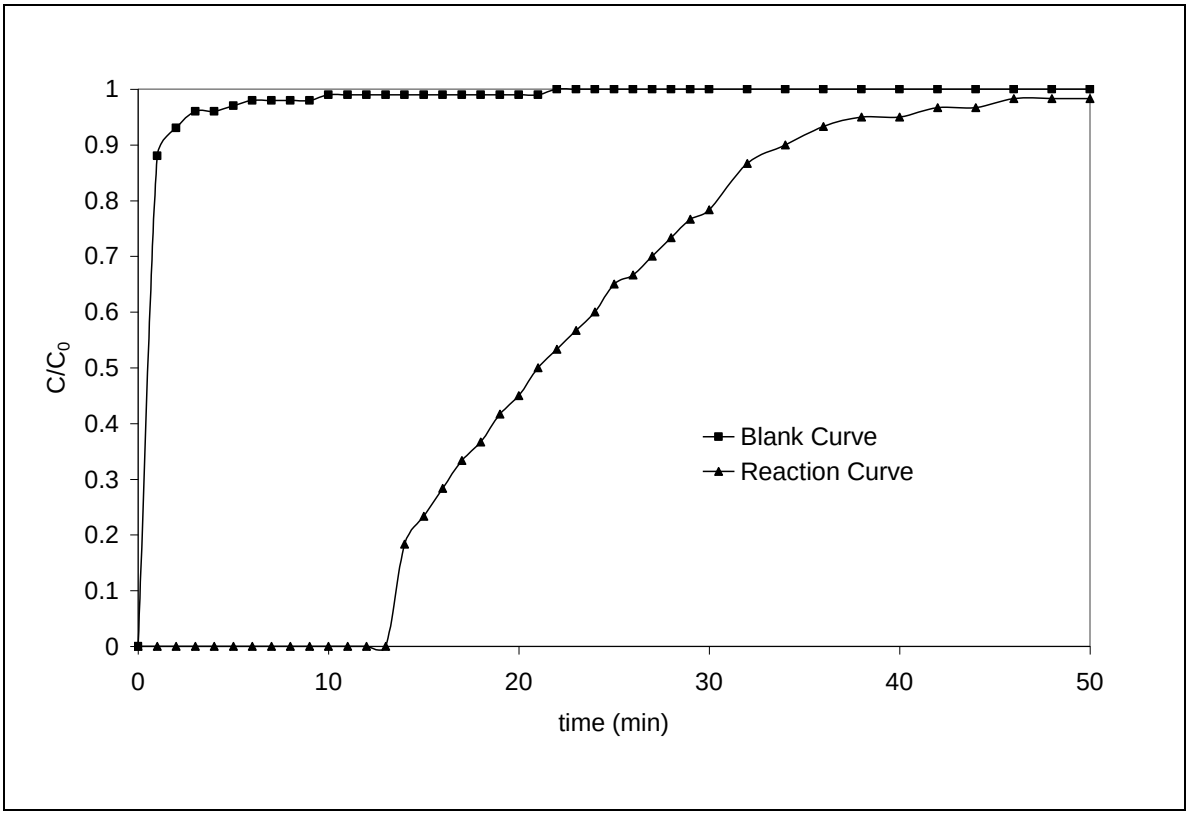

FIGURE 4.8: Example of reaction and blank breakthrough curves

The solid conversion was obtained from the stoichiometric equation as:

$$X = \frac{mol.SO_2.retained}{mol.Ca} \times 100 \qquad (4.6)$$

CHAPTER 5

5. RESULTS AND DISCUSSION

5.0 INTRODUCTION

This chapter presents the results of the dissolution experiments in the pH-Stat equipment, the sulphation tests performed in a fixed-bed reactor, and the results of kinetic modeling.

In the first part of the chapter, results on the preparation of the respective hydroxides from the parent raw materials are reported. Identification of specific sorbent properties that have significant influence on the dissolution process (origin, particle size, chemical composition) as well as important process parameters (solution pH and the reaction temperature) are also reported here.

The second part of this chapter reports the comparison of the desulphurization activity of sorbents from different sources in a fixed-bed reactor. The effect of the various operating conditions such as SO_2 inlet concentration, reaction temperature, and relative humidity on the desulphurisation activity are reported. A comparison is also done between the performance of the different sorbents in the pH-stat equipment and in the fixed-bed apparatus.

The last part of the chapter presents the results of kinetic modeling. The dissolution process was modeled according to the shrinking core model while the sulphation process was modeled according to the surface coverage model. The reaction rate constants obtained were used as a basis for ranking the different sorbents.

5.1 SORBENT PREPARATION

5.1.1 pH-Stat materials

Limestone and dolomite materials used in the pH-stat apparatus were used in their raw form. The materials used to determine the influence of particle size on the dissolution behaviour were ground and sieved to three particle sizes; -25 μm, -45 and -63. Materials used to determine the influence of type and origin were ground to -25μm.

5.1.2 Fixed-bed materials

Table 5.1 shows the maximum temperature recorded from a room temperature of 30 ºC during hydration and the weight loss recorded on calcination for eight calcitic and seven dolomitic limestones. The calcitic limestones were selected because of their high content of $CaCO_3$ while the dolomitic limestones were selected for their low $CaCO_3$ and high $MgCO_3$ content. In the case of samples A, B, E, H, J, N, and P (calcitic limestone), the hydration process was accompanied by a rapid expansion of the paste and the evaporation of the hydration water such that the result was a thick paste that was almost dry. Samples C, D, F, G, L, and Q (dolomitic limestone) however, gave a very light slurry. For the ASTM C110 (1995) standard, the parameters that describe the reactivity of quicklime are the increase in hydration temperature in the first 30 s (T_{30sec}), the maximum hydration temperature (T_{MAX}) and the time that it is observed. In terms of the BS 6463 reactivity test (1997), lime reactivity can be classified based on temperature rise as: Low – below 40ºC, Moderate – 40 to 55 ºC, High – above 55 ºC, and Very high – above 65 ºC.

TABLE 5.1: Calcination and hydration of South African calcium-based sorbents.

Sorbent	Type	CaO (%)	Weight loss (%)	Maximum temperature (°C)	Temperature rise (°C)	Lime reactivity
A	Calcitic	88.39	38.3	95	65	Very high
B	Calcitic	81.87	37	94	64	High
C	Dolomitic	44	37	35	5	Low
D	Dolomitic	53.54	45.6	54	24	low
E	Calcitic	92.5	40.2	92	62	High
F	Dolomitic	66.2	43.9	75	35	Low
G	Dolomitic	72.5	43.2	57	27	Low
H	Calcitic	87.8	44.2	96	66	Very High
J	Calcitic	94.2	39.0	98	68	Very High
K	Dolomitic	73.8	43.3	85	55	High
L	Dolomitic	39.7	37	34	4	Low
M	Dolomitic	72.9	41.6	65	35	Low
N	Calcitic	80.3	40.6	88	58	High
P	Dolomitic	77.0	40.0	50	30	Low
Q	Dolomitic	61.3	39.0	52	22	Low

On average the results obtained in Table 5.1 show that the calcitic limestones have a higher reactivity than the dolomitic limestones. This is, nevertheless, not unexpected since the MgO existing in most types of dolomite is virtually insoluble (0.0086 g/g) and does not hydrate under atmospheric pressure (Al-Shawabkeh, Matsuda & Hasatani, 1997). Moreover, during calcination of dolomitic limestone, the $MgCO_3$ is first decomposed at much lower

temperatures compared to $CaCO_3$ and, as a result, the MgO components are hard-burned before the CaO is formed. It follows that when dolomite is hydrated under atmospheric conditions, almost all its CaO components hydrate, but very little of MgO does. The heat of hydration for fully calcined dolomite is 880 kJ/kg of CaO.MgO (Oates, 1998). This is low compared to 1138 kJ/kg reported for CaO (Kantiranis, 2003).

5.2 CHEMICAL REACTIVITY OF THE SORBENTS

5.2.1 Chemical reactivity of the sorbents using pH-Stat method[2]

The study of the dissolution behaviour of the sorbent materials was studied in a pH-Stat apparatus at conditions normally encountered in wet FGD processes. The influence of various parameters such as the reaction temperature ($30 \leq T \leq 70$ºC), sorbent particle size ($25 \leq dp \leq 63$μm), solution acidity ($4 \leq pH \leq 6$), and chemical composition as well as sorbents source and origin, were studied in order to determine the kinetics of $CaCO_3$ dissolution.

5.2.1.1 Effect of particle size

Three size fractions of sample A (calcitic limestone) and sample C (dolomitic limestone) were used to determine the influence of the particle size on the dissolution rate. The size fractions are -25 μm, -45 μm and -63 μm. Figure 5.1 shows the data of HCl volume added vs. time at 50 ^{o}C and pH 5 for the three size fractions of sample A. The results show that the limestone conversion is a strong function of the particle size; the finer the particle size is, the higher the conversion within the same time period. For all the three size fractions investigated, there was

[2] Based on: Siagi Z.O. & Mbarawa M. Dissolution rate of South African Calcium Based materials. Journal of Hazardous Materials. Article in Press, 2008.

a high initial consumption of acid before a more gradual trend was established. This was thought to be due to the presence of very fine particles in all the size fractions which react fast with the HCl during the initial stages. After these particles have been consumed by the acid solution, the bigger particles will then proceed with the reaction at a gradual rate.

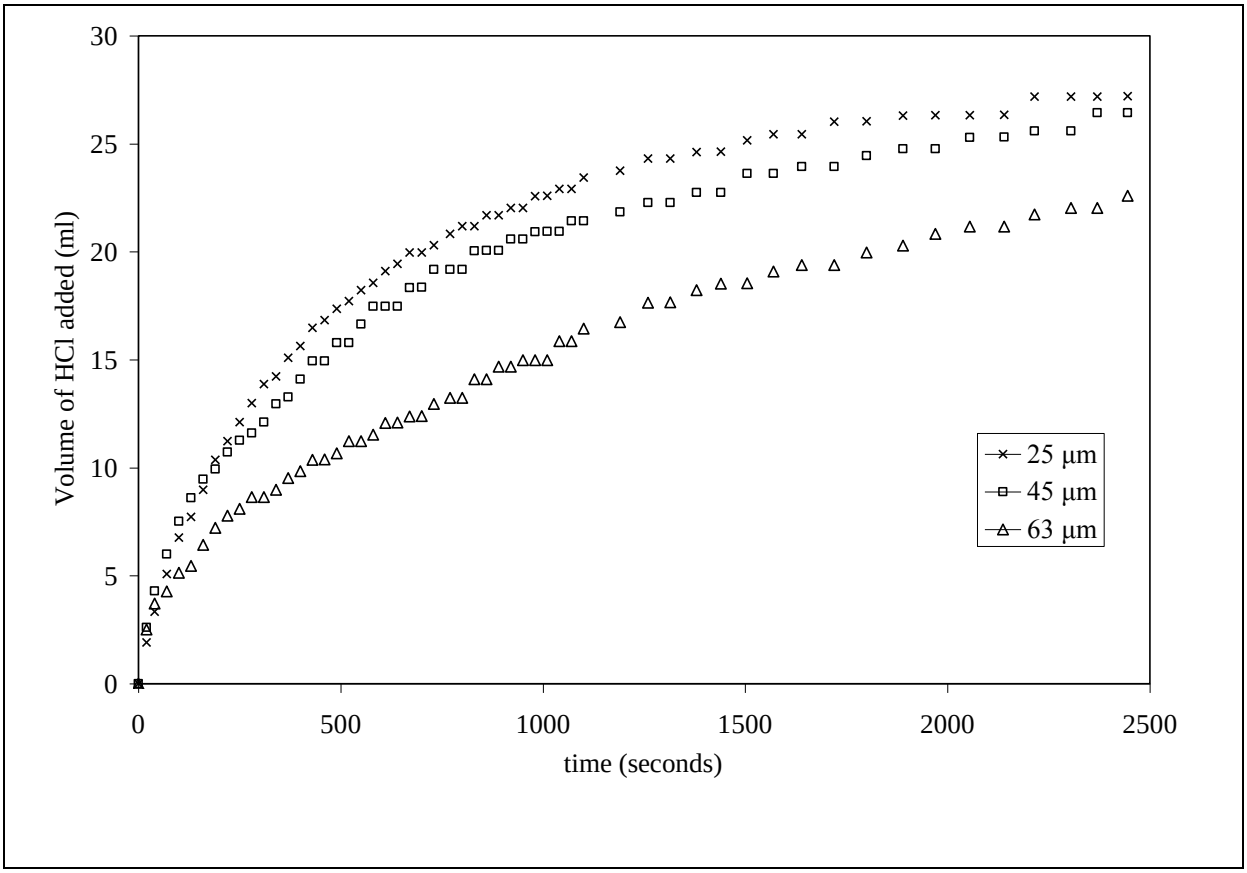

FIGURE 5.1: Effect of particle size on the limestone conversion as a function of time for sample A

Various studies have concluded that the particle size may be the single most influential parameter on the reactivity of a sorbent. Hosten and Gulsan (2004) have shown that finer particles show better desulphurisation characteristics than coarse ones. This is possibly due to the higher surface area available for reaction. In their study of spray dry absorption with a lime slurry, Scala, D'ascenzo and Lancia (2004) also agree that careful control of the particle

mean size is a key to obtain a good spray dry performance. Frandsen, Kiil and Johnsson (2001) have experimentally shown that by changing limestone type from one of 20 µm mean particle size to one of 4 µm increased the overall measured degree of desulphurisation from 83 % to 87 % and reduced the residual limestone level from 4.6 to 1.3 wt.%. Similar results have also been reported elsewhere (Xiaoxun M. et al., 2000; Alvarez & Gonzalez, 1999; Davini, 2000).

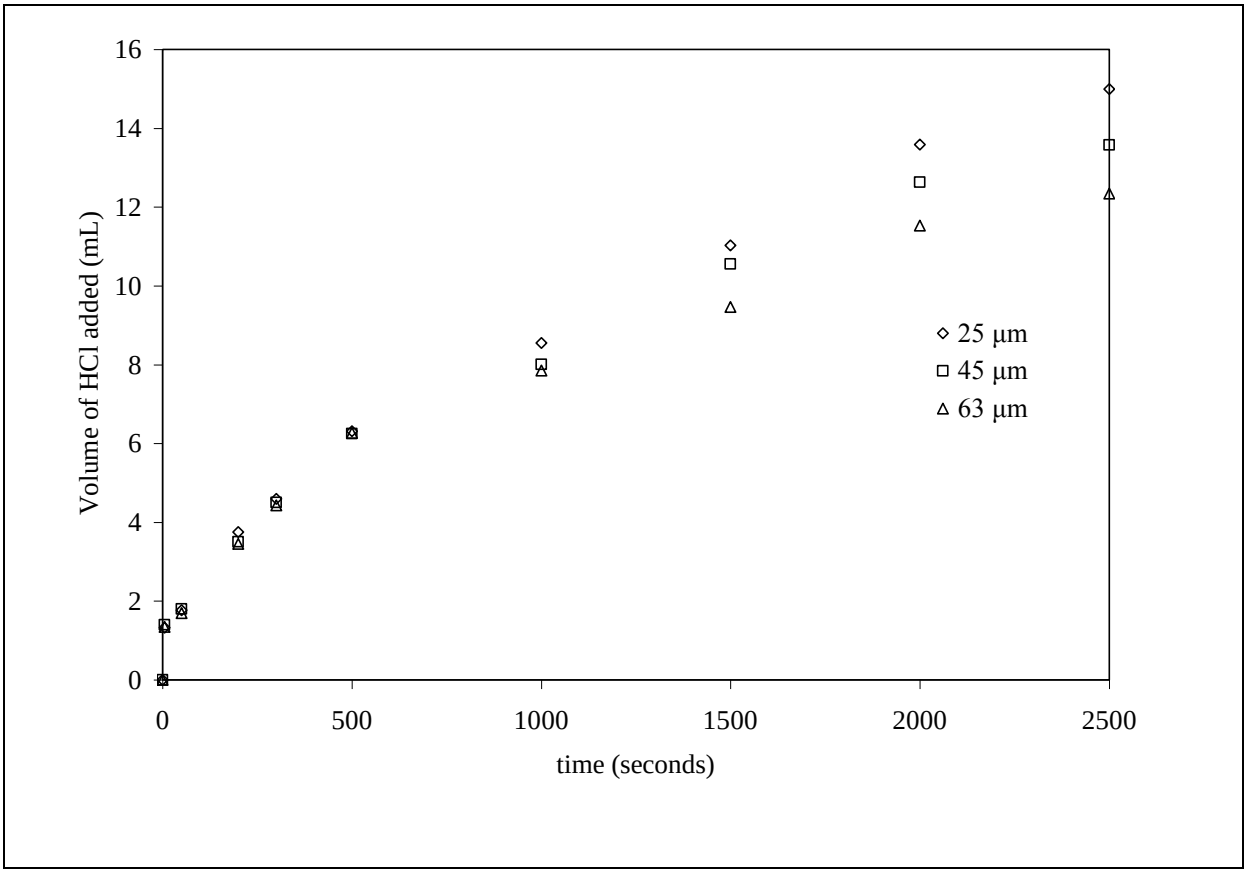

FIGURE 5.2: Effect of particle size on the limestone conversion as a function of time for sample C

Results obtained for the sample C (Figure 5.2) show that the conversion is also a strong function of particle size for the dolomitic limestones.

5.2.1.2 Effect of Origin

This experiment was carried out to measure the batch, constant pH reactivity of limestone samples obtained from different sources in South Africa. The limestone samples used had differing chemical and mineralogical compositions (Table 4.1).

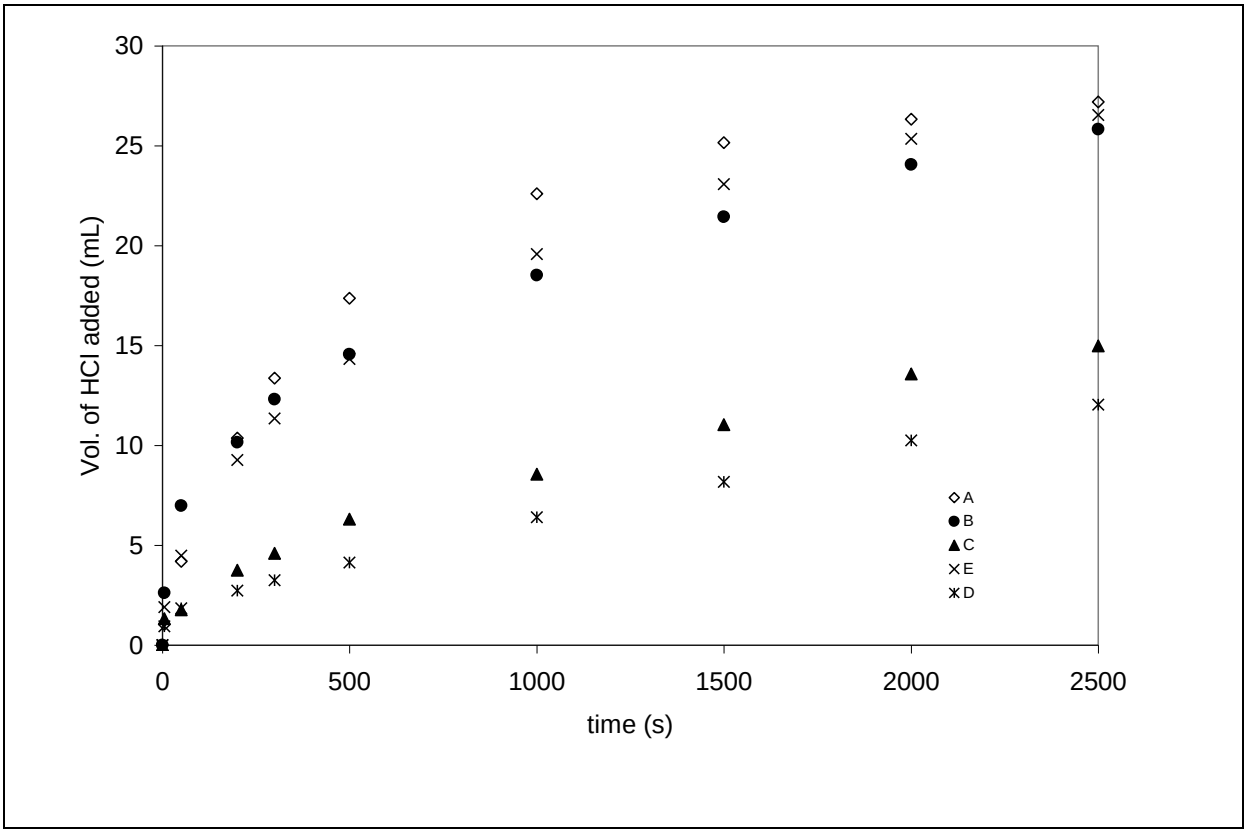

FIGURE 5.3: Conversion versus time for limestone from different sources in South Africa

All the samples were ground to fine particle size (-25 μm). Figure 5.3 shows the sorbent conversion versus time plots for three calcitic limestones and two dolomitic limestones. From the results obtained, the B and E samples display an initial short region of high dissolution before this settles to a more gradual dissolution rate. This could possibly be due to a higher amount of fine particles in both samples than for sample A. Other than this high initial rate,

the samples A, B, and E display an amount of conversion which is comparably close. On the other hand the C and D samples show a lower dissolution rate than the other three. A possible explanation could be found from an examination of their chemical analysis (Table 4.1). Whereas the A, B, and E samples have a magnesium carbonate content of less than 2 wt.%, the C and D samples have a high content of magnesium carbonate (>35 wt.%). Previous work by Ahlbeck et al. (1995) have associated the presence of Mg with a reduced activity of the sorbent material. Figure 5.3 also tends to confirm this observation as sample A which has a lower $CaCO_3$ content than sample E nevertheless displays a higher dissolution at any given instant. This could possibly be due to the higher $MgCO_3$ content of the latter. A comparison of C and D samples also tends to confirm that the source of the sample could as well play an important role in the dissolution rate. C which has a lower $CaCO_3$ and a higher $MgCO_3$ content shows a higher dissolution rate than D contrary to expectation.

For purposes of clarity, Figure 5.3 only gives the comparison between two dolomitic and three calcitic limestones. As can be seen from the figure, the amount of acid consumed gives an indication of the sulphur capture capacity of the particular sorbent being studied. In this investigation, fifteen samples from different sources were studied. Table 5.2 gives the amount of acid consumed after 10, 20, 30, and 40 minutes for all the samples. Based on the amount of acid used, a ranking of the materials can be obtained. The sorbents that consume more acid in a given time are deemed to be more reactive.

TABLE 5.2: Amount of 1M HCl added (50°C, pH =5.0)

Sorbent Type	10 minutes	20 minutes	30 minutes	40 minutes	Ranking
A	19.11	21.32	24.82	27.19	2
B	15.43	19.73	23.18	25.80	5
C	7.2	9.87	12.71	14.51	13
D	4.61	7.27	9.36	12.03	15
E	15.74	23.77	26.04	26.54	3
F	8.54	12.01	14.58	16.31	11
G	9.53	13.61	16.51	17.88	10
H	17.08	21.84	24.65	26.39	4
J	22.16	26.35	28.10	29.14	1
K	10.13	14.25	17.62	19.53	9
L	6.87	9.74	12.29	13.69	14
M	10.21	15.33	18.74	19.93	8
N	13.92	19.23	22.65	24.5	6
P	14.81	19.08	21.13	23.40	7
Q	6.52	8.52	10.80	15.07	12

5.2.1.3 Effect of pH

Five experimental runs were made of sample A and sample C, at pH values of 4.0, 4.5, 5.0, 5.5 and 6.0 to try and analyze the effect of the pH on the dissolution rate. Figure 5.4 shows the results of the experiments obtained for sample A. As can be seen from the results, the dissolution is very fast for the sample dissolved in the pH 4 solution with the dissolution being complete in about 12 minutes. As the pH is increased, the dissolution rate decreases. For the test carried out at pH 5.0, the dissolution rate is much slower and the process reaches completion after about 90 minutes. For the test carried out at pH 6.0, the dissolution is not complete even after a test period of 2 hours. The effect of pH on the dissolution rate for sample C (Figure 5.5) shows a similar trend. Previous work by Shih, Lin, and Shiau (2000) have given similar results. The explanation of pH dependence is thought to be as follows. When a strong acid is added to a stirred limestone slurry, the acid completely dissociates and hydrogen ions are formed. The limestone in water dissolves to a low degree according to the equation:

$$CaCO_{3(s)} \rightarrow Ca^{2+}{}_{(aq)} + CO_3^{2-}{}_{(aq)} \qquad (5.1)$$

The carbonate ions react with hydrogen ions to form HCO_3^-, CO_2(aq) and CO_2(g) as follows:

$$CO_{3(aq)}^{2-} + H_{(aq)}^{+} \rightarrow HCO_{3(aq)}^{-} \qquad (5.2)$$

$$HCO_{3(aq)}^{-} + H_{(aq)}^{+} \rightarrow CO_{2(aq)} + H_2O_{(l)} \qquad (5.3)$$

$$CO_2(aq) \leftrightarrow CO_2(g) \tag{5.4}$$

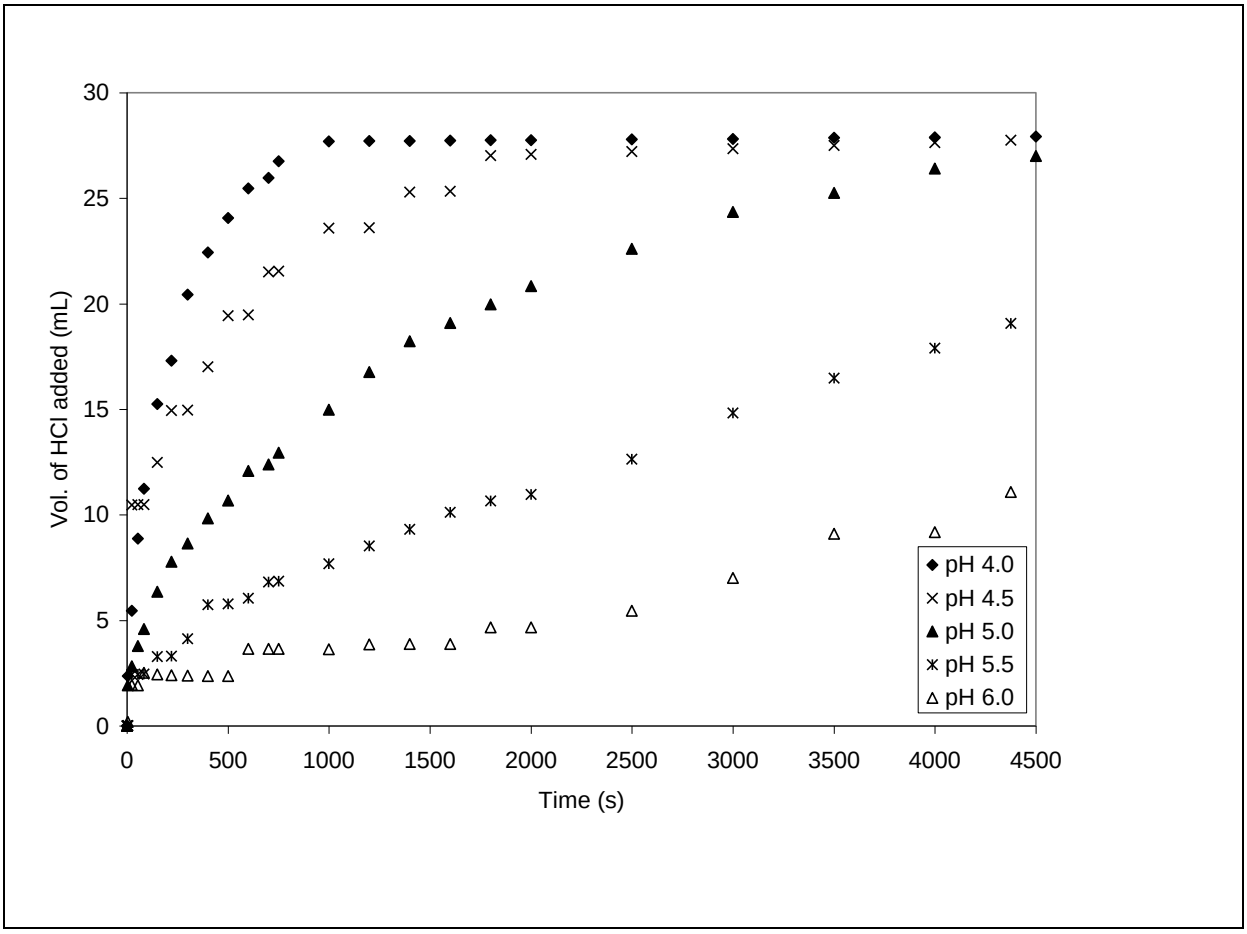

FIGURE 5.4: Influence of the solution pH on the dissolution rate for sample A.

It may be assumed that reaction (5.1) reaches equilibrium at the surface of the limestone and reaction (5.2) is replaced by the following two reactions

$$CO_3^{2-}(aq) + H_2O(l) \rightarrow HCO_3^-(aq) + OH^-(aq) \tag{5.5}$$

$$H^+(aq) + OH^-(aq) \rightarrow H_2O(l) \tag{5.6}$$

due to the low concentration of H^+ in the vicinity of the surface. Reaction (5.5) is instantaneous and, since water is available on the surface, reaction (5.5) can also be assumed to reach equilibrium at the surface.

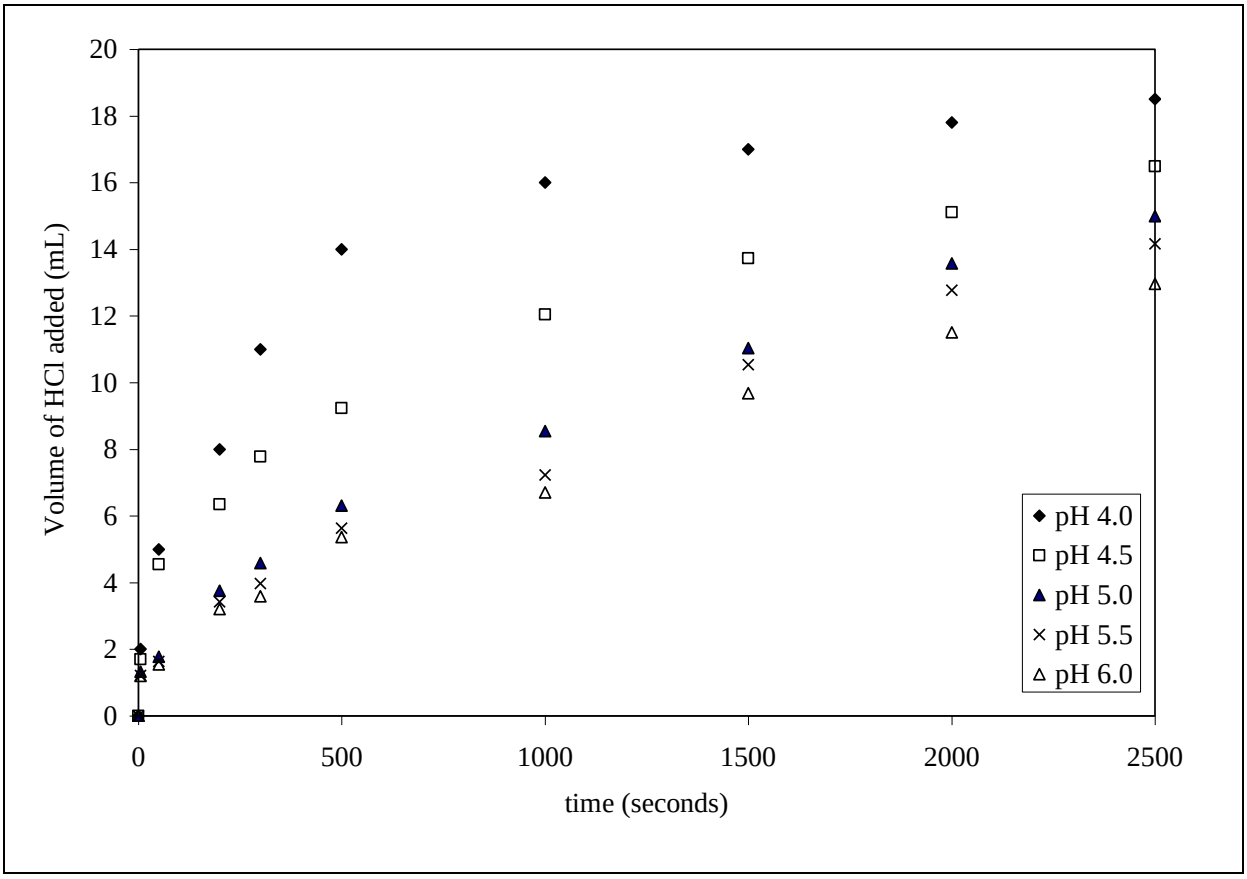

FIGURE 5.5: Influence of the solution pH on the dissolution rate for sample C

Reaction (5.6) is instantaneous and its equilibrium constant is very large, but H^+ has to move into the boundary layer from the bulk solution or OH^- has to move outward from the surface for their reaction to take place. Thus the actual rate of reaction (5.6) and the place where it occurs depends on the inward diffusion of H^+ and the outward diffusion of OH^-. Since the reaction of H^+ with OH^- is faster than that with HCO_3^-, it may be assumed that at higher pH, the H+ ions diffusing into the boundary layer are consumed entirely by the reaction with OH-

and that the dissolution rate equals the rate of H^+ or OH^- consumption in the boundary layer. Thus, for mass transfer of H^+ across the boundary layer accompanied with reaction (5.6), the dissolution rate constant, k, can be expressed as

$$k = k_{H^+}^0 \left(1 + \frac{D_{OH^-}}{D_{H^+}} \frac{[OH]_s}{C_b} \right) \tag{5.7}$$

where $k_{H^+}^0$ is the physical mass transfer coefficient for H^+; D_{OH^-} and D_{H^+} are the diffusivities of OH^- and H^+, respectively; $[OH]_s$ is the equilibrium concentration of OH- at the surface of the limestone. It is obvious that the enhancement factor, the terms in the bracket of equation (5.7) increases with increasing pH while other experimental variables are kept constant.

5.2.1.4 Effect of Temperature

Experiments were carried out in the 30ºC - 70ºC temperature range for sample A to investigate the influence of temperature on the dissolution rate. Figure 5.6 shows the rate curves obtained. From the figure, it can be observed that the reaction rate is a strong function of the reaction temperature with an increase in temperature resulting in an increased reaction rate. The temperature effect on the dissolution rate is often a unique indication of the reaction mechanism itself. For example, diffusion-controlled reactions in solutions have activation energies (E_a < 20 kJ/mol) that are lower than those for surface controlled reactions (40 – 80 kJ/mol). Therefore the accurate estimation and interpretation of the activation energy value is important (Cama, Ayora, & Lasaga, 1999).

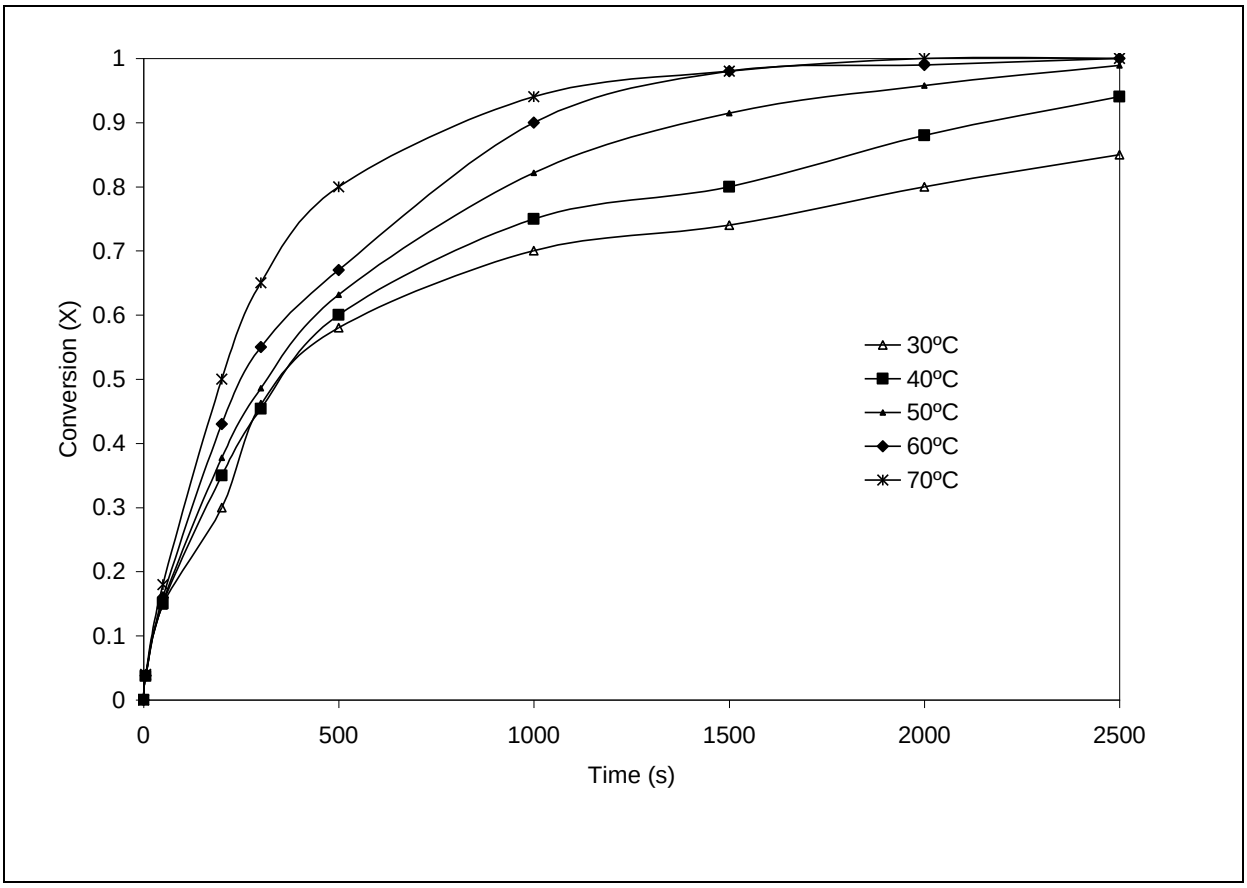

FIGURE 5.6: Effect of temperature on the dissolution rate of sample A

A number of recent studies have analyzed the temperature dependence of mineral dissolution rates. The temperature dependence of the dissolution rate typically follows the Arrhenius law:

$$Rate = Ae^{\frac{-E_a}{RT}} \tag{5.8}$$

which is grounded in statistical mechanics and quantum theory. In this equation, A is the pre-exponential factor, E_a is the apparent activation energy of the overall mineral-fluid reaction, R is the gas constant, and T is the temperature. Activation energy is currently estimated from experimental rate values of dissolution reactions conducted at different temperatures. The values of A and E_a can be obtained from the straight line plot of *ln Rate vs. 1/T*.

5.2.1.5 Conclusion of reactivity in the pH – stat method experiments

Experiments were carried out on five samples from different sources in South Africa. The results indicate that a higher content of calcium carbonate supports the expectation of increased activity (Figure 5.7).

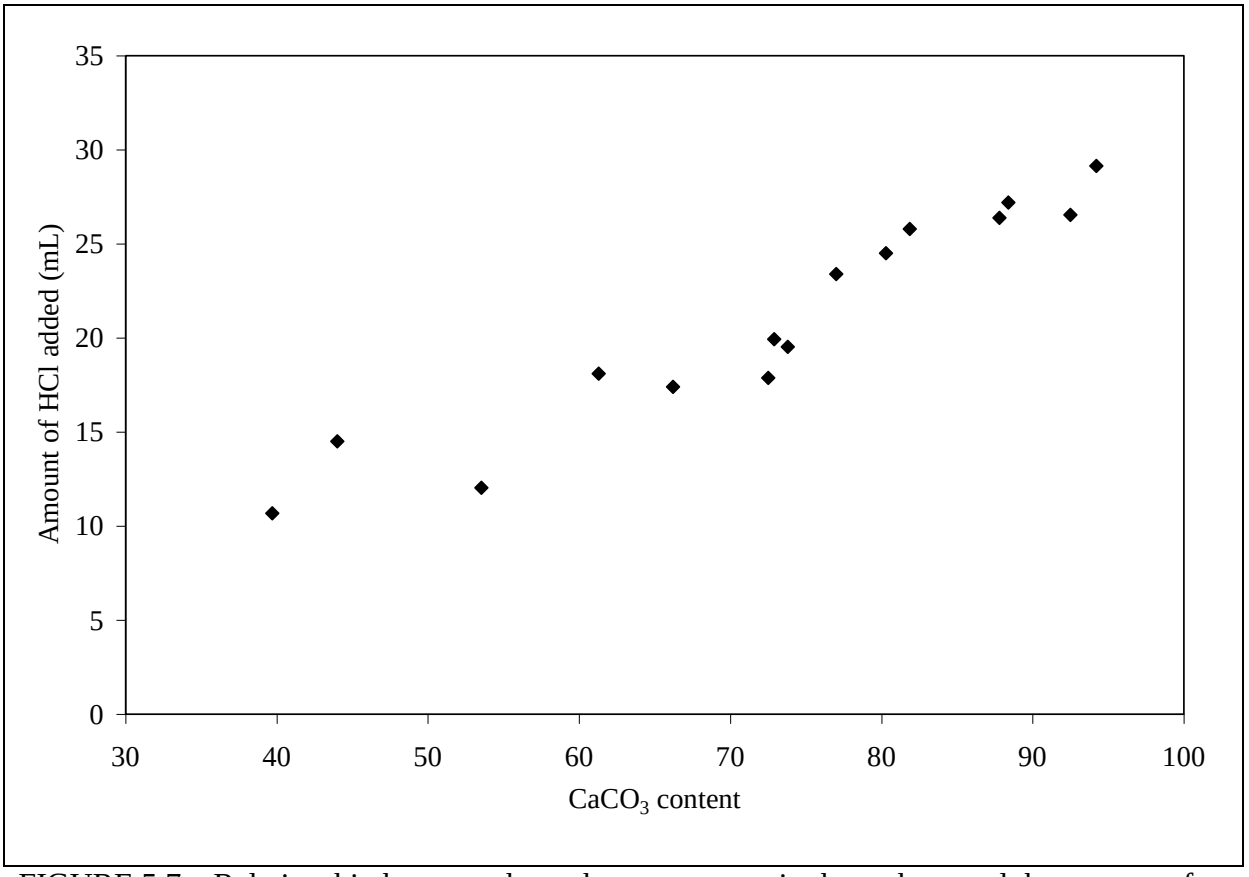

FIGURE 5.7: Relationship between the carbonate content in the sorbent and the amount of acid consumed in 40 minutes

The presence of magnesium in the sorbent was observed to decrease the measured reactivity of the sorbent. Further investigations show that the conversion rate is a strong function of the particle size; the finer the particle size is, the higher the conversion within the same time period. The results for samples C and D lead us to conclude that the origin of the sample has a

bearing on the expected reactivity of the sorbent. The pH also showed a marked influence on the dissolution rate with lower pH showing a higher rate of dissolution. Finally, an analysis of the influence of the reactor temperature shows that the dissolution rate increases with an increase in the temperature.

5.2.2 Chemical reactivity in the Fixed-Bed Reactor[3]

5.2.2.1 Effect of Sorbent Type and Source

The sulphation of several sorbent samples have been investigated to ascertain whether the source and type of material plays any significant role in the sulphur capture capacity. Figure 5.8 gives a comparison of the breakthrough curves for the hydrates of two dolomitic and two calcitic limestones, and a commercial calcium hydroxide sample (LC) at 10% relative humidity. From the figure, it can be seen that the capacity of the slaked samples to maintain 100% SO_2 removal vary from one material to the other. Applying equation (4.5) to the results, the amount of SO_2 retained by A, B, C, D and LC are 0.1823, 0.1478, 0.0274, 0.0798 and 0.1081 mol SO_2 per mol of sorbent respectively for the 30 minute duration considered. The limestone samples (A and B) thus have a better capture capacity than the commercial calcium hydroxide while the capacity of the dolomite samples (C and D) is lower than that of the commercial sample. The sulphation capacity of the raw samples can be related to their CaO contents. The higher CaO content samples show a higher sulphation capacity while the lower CaO content samples display a lower capacity. The sulphation of the commercial calcium hydroxide, however, does not fall into this neat generalization. Despite having the highest

[3] Based on: Siagi Z.O., Mbarawa M., Mohamed A.R., Lee K.T., & Dahlan I. 2007. The effects of limestone type on the sulphur capture capacity of slaked lime. Fuel 86: 2660-2666.

CaO content of the tested samples, its capacity falls in between those of the dolomites and those of the limestones. A possible explanation for this anomaly could be in the iron oxide content of the samples.

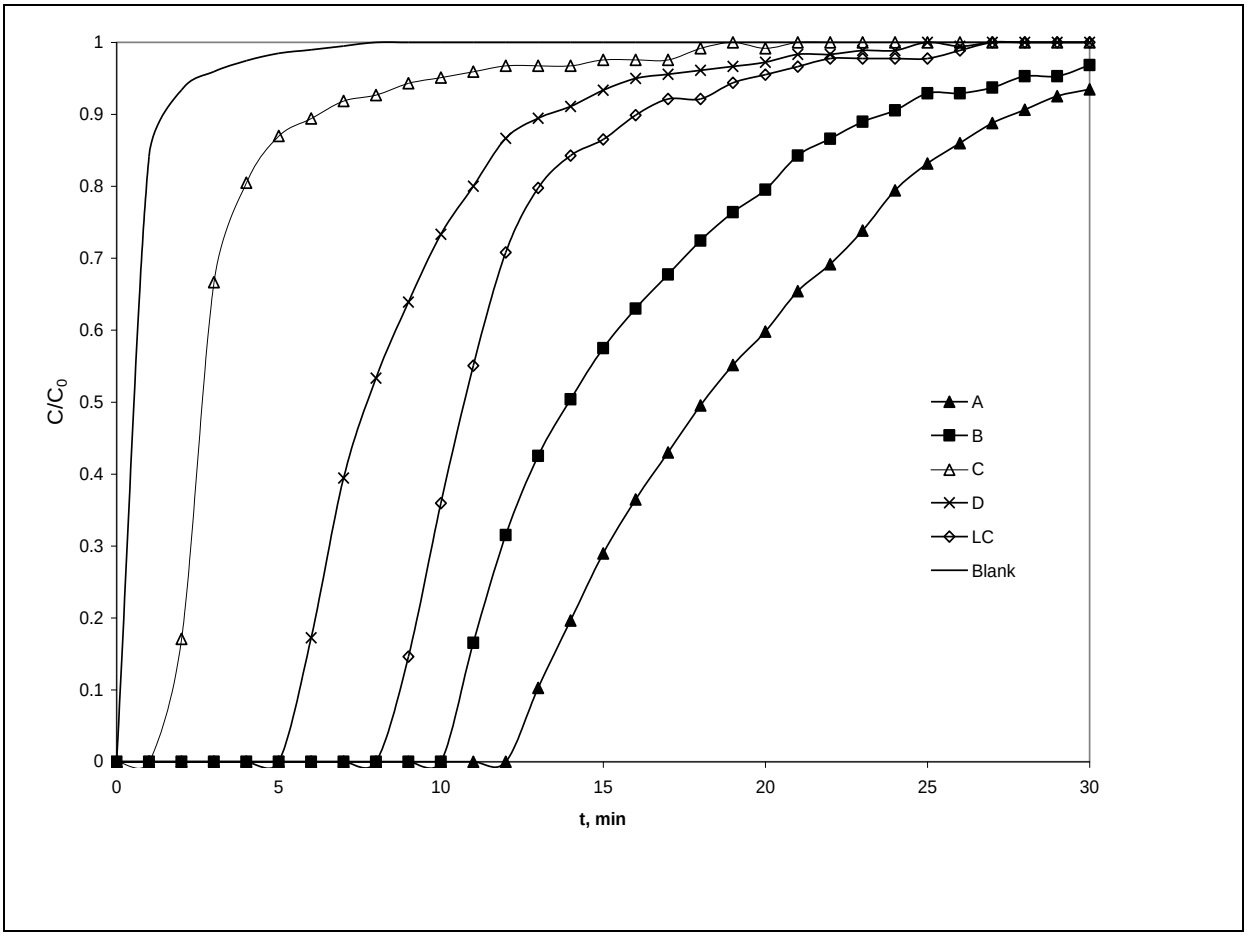

FIGURE 5.8: SO_2 breakthrough Curves for Four SA Calcium-Based Samples and Commercial Calcium Hydroxide. (C_0 = 2000ppm, T_R=80ºC, RH=10%)

The commercial calcium hydroxide sample has less than 0.05% Fe_2O_3, while samples A and B have 1.83 and 0.67% Fe_2O_3 respectively. Iron oxide plays an important role in the $CaSO_4$ formation, probably related to the catalytic activity that the iron itself can have in the oxidation process of SO_2 to SO_3, which when reacting with solid CaO particles, favoring $CaSO_4$ formation. Previous researchers have obtained similar results. Using three marble by-

products and a commercial limestone material, Davini (2000) showed that the maximum conversion of the sulphation reaction of the calcium oxides has an increasing relationship with the percent content of the iron oxide in the original carbonaceous material. The amount of SO_2 retained by all the samples used in this study is shown in Table 5.3 below.

TABLE 5.3: Amount of SO_2 retained per mol of sorbent for study materials

Sample	Amount of SO_2 retained/ mol of sorbent
A	0.1823
B	0.1478
C	0.0274
D	0.0798
E	0.1960
F	0.1120
G	0.1126
H	0.2032
J	0.2113
K	0.1282
L	0.0175
M	0.1064
N	0.1773
P	0.0839
Q	0.0588

5.2.2.2 Effect of SO_2 Concentration

Figure 5.9 gives the results of the amount of SO_2 retained per mole of sample A for flue gas concentrations 1000, 1500, 2000 and 2500 ppm. Although the total amount of SO_2 retained for the different concentrations is approximately the same (0.1071, 0.1051, 0.1116 and 0.1115 for 1000, 1500, 2000 and 2500 ppm respectively) the time taken to reach maximum conversion seems to be dependent on the concentration. The higher the concentration, the faster the conversion proceeds.

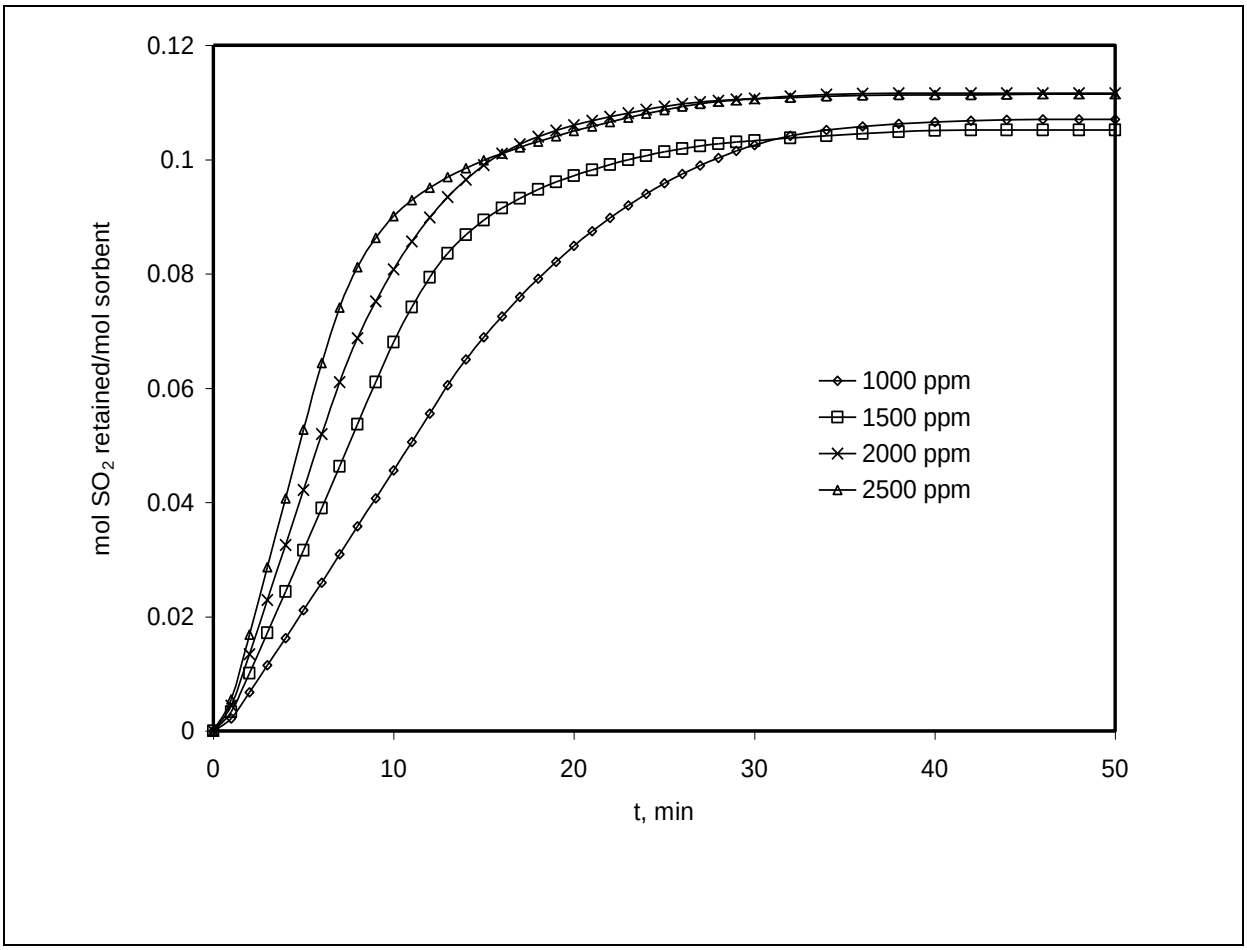

FIGURE 5.9: Influence of SO_2 concentration; Sample A, T_R = 80ºC, RH = 0%, Flow rate = 150 mL min^{-1}, dp < 200 μm.

These results agree with those obtained by Lee et al. (2005) who observed a linear correlation between the concentration and the time the sorbent can maintain 100 % SO_2 removal. Ch'un-Sung and Shin-Min (1993) have reported a low influence of SO_2 concentration on the reaction rate at 30% relative humidity but reported an increased reaction rate and final conversion with increasing SO_2 concentration at 70% relative humidity. Liu, Shih and Lin (2002) reported a very weak influence of the SO_2 concentration on the total conversion and the reaction when testing $Ca(OH)_2$/fly ash sorbents at 30-80% relative humidity and 1000-5000 ppm SO_2 concentration. At a reactor temperature of 71.5^oC and 38% relative humidity, Izquierdo *et al.* (2000) concluded that the reaction rate between sulphur dioxide and calcium hydroxide does not depend on the sulphur dioxide partial pressure for sulphur dioxide concentration of less than 3000 ppm.

5.2.2.3 Effect of Relative Humidity

Figure 5.10 shows the amount of SO_2 retained/mol of sample D (dolomitic limestone) as a function of relative humidity. From the results, the relative humidity is a major factor in the ability of the sorbent to capture SO_2. Regression analysis of the results shows the amount of SO_2 retained in one hour to be related to the percentage relative humidity by an exponential expression of the form:

$$mol\ SO_2\ retained/\ mol\ of\ SampleD = 0.0549e^{0.0405RH} \qquad (5.9)$$

The regression coefficient for the curve fitting was high at R = 0.998.

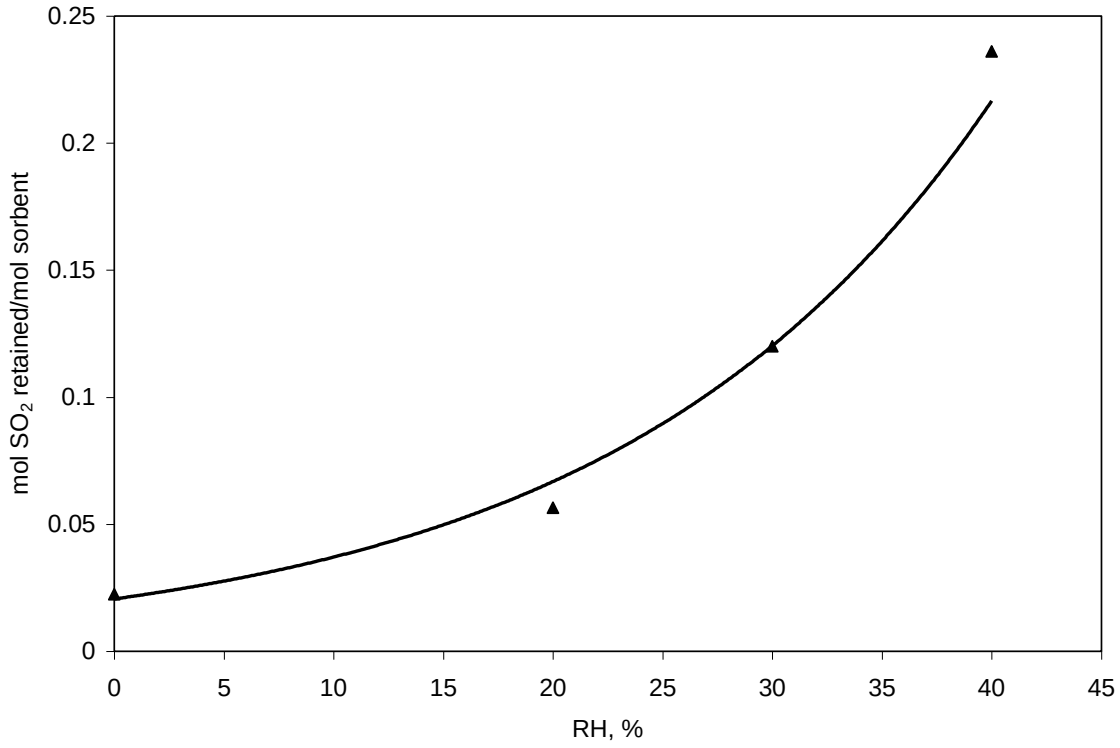

FIGURE 5.10: Influence of relative humidity on the amount of SO_2 retained/mol of sample D. T_R = 80ºC, C_0 = 2000 ppm

Figure 5.11 shows the amount of SO_2 retained/mol of sample B (calcitic limestone) as a function of relative humidity. From the results, the relative humidity is a major factor in the ability of the sorbent to capture SO_2. Regression analysis of the results shows the amount of SO_2 retained in one hour to be related to the percentage relative humidity by a linear expression of the form:

$$mol\ SO_2\ retained\ /\ mol\ of\ sample\ A = 0.0066\,RH + 0.0672 \qquad (5.10)$$

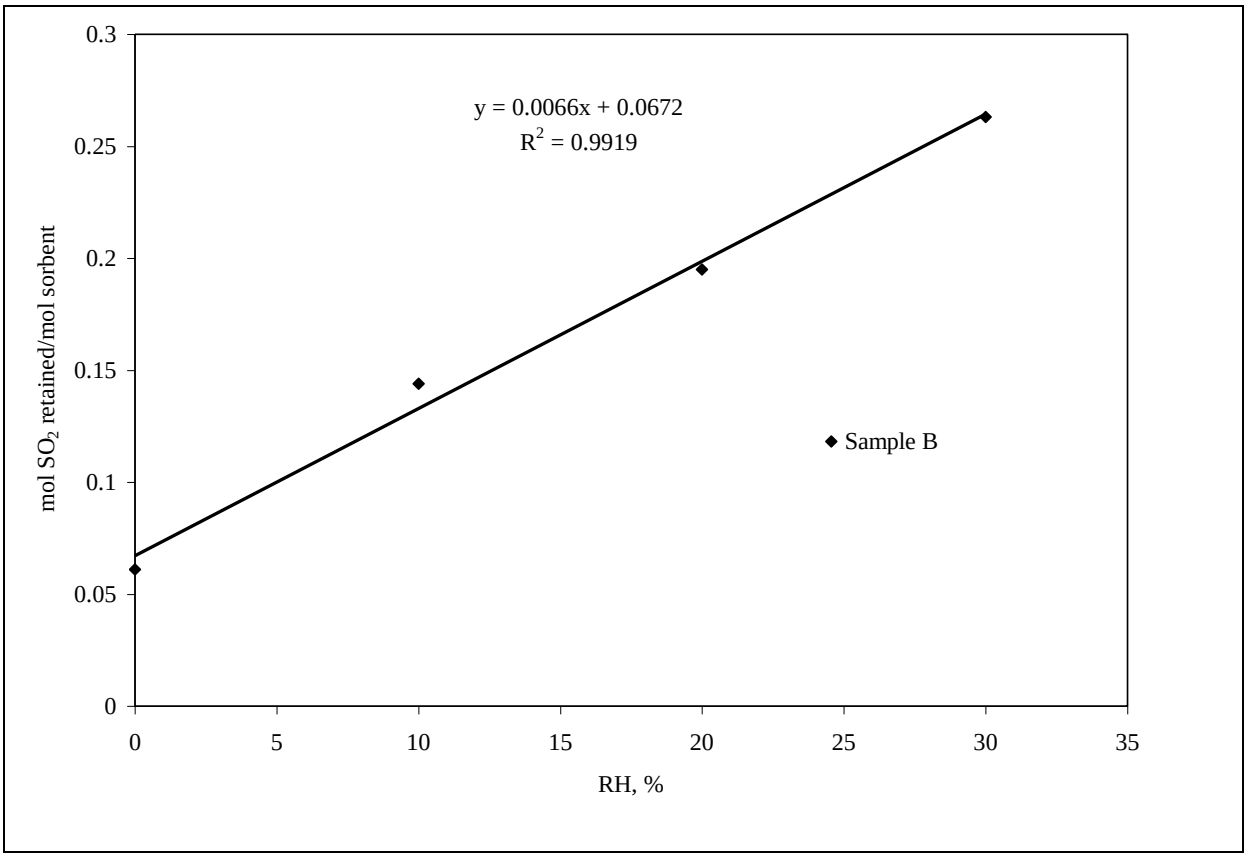

FIGURE 5.11: Influence of relative humidity on the amount of SO_2 retained/mol of sample B. T_R = 80ºC, C_0 = 2000 ppm

The breakthrough curves and the calculated conversion versus time data for the other samples used in this study are presented in the appendix (Figure A.1 to A.10). Generally, the results show a strong influence of the relative humidity on the conversion of all samples.

The water adsorbed on the sorbent surface plays an important role in the reaction. Adsorption isotherms on a sorbent at 60 – 80 ^{o}C obtained by Liu, Shih and Lin (2002) showed that the amount of water adsorbed increased with increasing relative humidity and decreased with increasing temperature. They hypothesized that the fundamental processes taking place at the water adsorption surface could include: (a) Adsorption of SO_2 on the outer surface of water layer, (b) Hydration of SO_2 to form $SO_2.H_2O$ (c) Diffusion of $SO_2.H_2O$ inward (d) Dissolution of $Ca(OH)_2$ to form Ca^{2+} and OH^- (e) Diffusion of Ca^{2+} and OH^- outward (f) Reaction of OH^-

and $SO_2.H_2O$ to form HSO_3^- and SO^{2-}_3 (g) Reaction of Ca^{2+} and SO^{2-}_3 to form calcium sulphite precipitate. They further hypothesized that since the overall reaction rate of the sorbent decreases with conversion and is slightly affected by SO_2 concentration, the rate controlling step may be that involving OH^- or Ca^{2+} ions, which are generated by the dissolution of the sorbent surface i.e. process (f) or (g). The rate of either process (f) or (g) will increase with increasing relative humidity because the higher amount of adsorbed water can produce higher amounts of reactant to react. Similar results have been reported by Ch'un-Sung and Shin-Min (1993). Chu and Hwang (2005) observed a SO_2 removal efficiency (RE) of 100 % at a relative humidity (RH) of 80 % for up to 140 minutes. They attributed this to the fact that the reaction rate was very high at such a high RH and therefore all of the inlet SO_2 was absorbed/ adsorbed and reacted at the surface of the calcium sorbent. RE decreased dramatically after that because a low porosity product layer ($CaSO_3$. ½ H_2O) began to form at the surface of the sorbent. Consequently, the diffusion resistance of SO_2 from the gas phase to the inner unreacted calcium sorbent increased, which results in a decrease in RE. At last, RE was quite low due to the formation of a thick product layer on the sorbent surface.

5.2.2.4 Effect of Reaction Temperature

Table 5.2 shows the amount of SO_2 retained per mol of Sample A as a function of temperature and relative humidity. From the results, temperature does not appear to significantly influence the sorbent conversion. As can be confirmed from the table, the conversion (area between experimental and blank curve) depends on the relative humidity but is largely independent of the reaction temperature.

TABLE 5.4: SO_2 Retained/mol of A at 60 and 80^oC (0 and 20% RH)

Temperature, ^oC	Relative Humidity, %	Mol SO_2 retained/mol SA9
80	0	0.111
	20	0.213
60	0	0.100
	20	0.210

Several researchers have studied influence of reaction temperature on the sorbent conversion. Liu, Shih and Lin (2002) observed a weak dependence of sorbent conversion on reaction temperature. They postulated that though increasing temperature could raise the chemical reaction rate constant, it could simultaneously reduce the adsorption amounts of water vapor and reaction gas. Ch'un-Sung and Shin-Min (1993) have also reported a mild influence of the reaction temperature on the conversion as the temperature was increased from 60 to 90 ºC. Raymond-Ooi, Lee and Mohamed (2004) observed a modest increase in the SO_2 capture capacity when they increased the reaction temperature from 60 to 80 ºC. Similar observations have been reported by Chu and Hwang (2005). Using a bubbling fluidized bed reactor, they found out that the sulphur dioxide removal efficiency was not significantly affected by the bed temperature ranging from 40 to 65 ^oC.

5.2.2.5 SEM Analysis

The surface morphology of sample A in its raw form, after calcination, after hydration, and after the SO_2 capture was studied through SEM. As shown in Figure 5.12a, the parent raw material consists of irregular particles with relatively smooth surfaces. Figure 5.12b, shows

the formation of lumps of unevenly shaped particles formed after the calcination process. In Figure 5.12c, agglomerates have been formed after the hydration process and the surface appears to be more porous than for either the raw or calcinated sample.

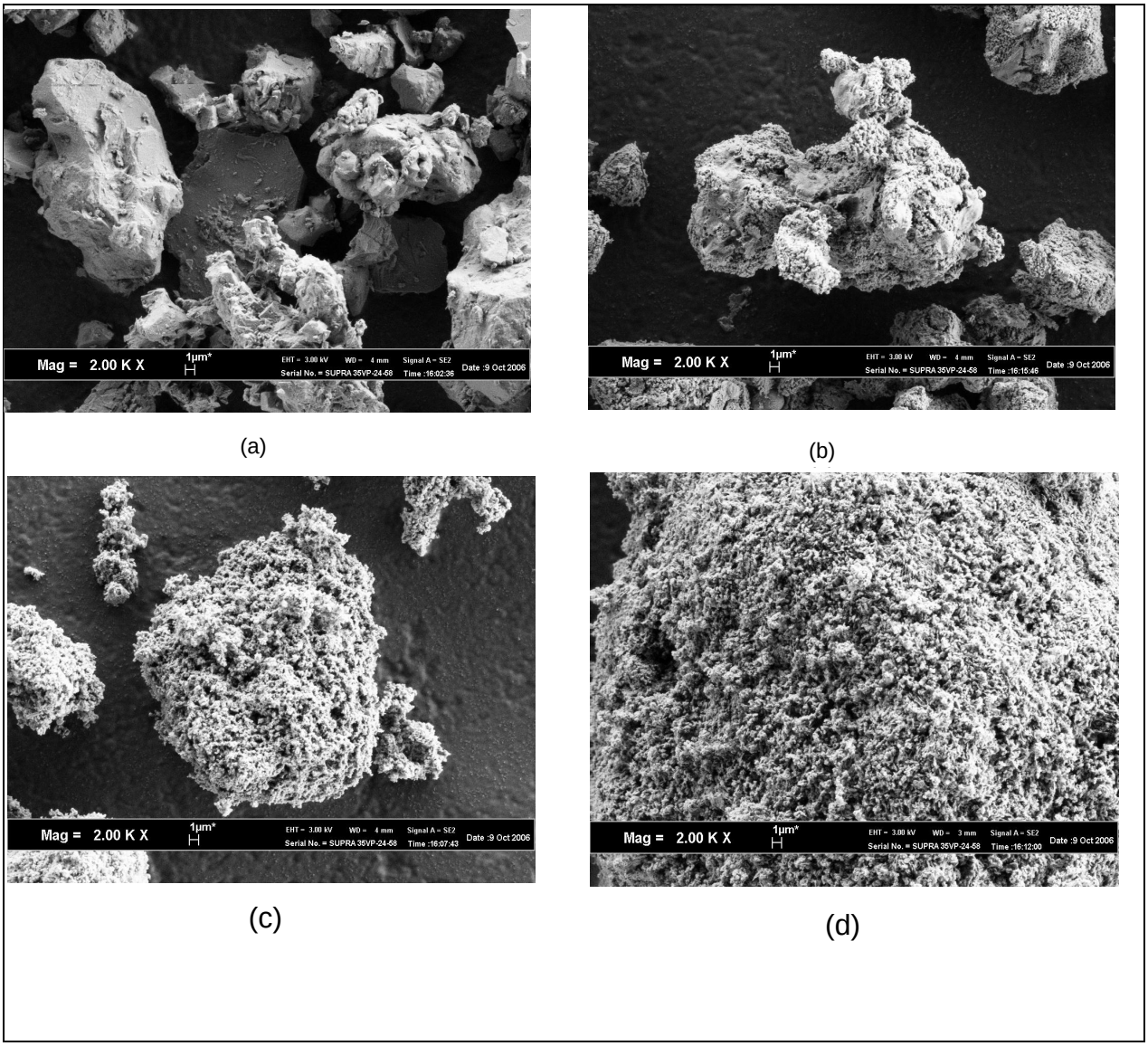

FIGURE 5.12: SEM micrographs of (a) The parent sample A, (b) Calcinated sample, (c) Hydrated sample, and (d) Reacted sample

The SEM micrograph of the reacted sample, Figure 5.12d shows a more compact structure that is wrapped with reaction products compared to the other samples and the porous surface of the sorbent is no longer discernible.

5.2.2.6 XRD Spectra

The chemical composition of sample A, before and after desulphurization, was studied through XRD analysis. The XRD spectra are shown in Figure 5.13. The peaks in the spectra can be assigned as follows; Peaks a = calcium hydroxide ($Ca(OH)_2$), peaks b = silica/quartz, low ((SiO_2)9H), peaks c = magnesium hydroxide ($Mg(OH)_2$), peaks d = aluminium oxide (Al_2O_3), e = calcium sulphite hydrate ($CaSO_3.1/2H_2O$), peaks f = magnesium sulphite hydrate ($MgSO_3.6H_2O$). $Ca(OH)_2$ and $Mg(OH)_2$ are the products of slaking CaO and MgO while the $CaSO_3.1/2H_2O$ and $MgSO_3.6H_2O$ are the reaction products with SO_2.

Even though XRD is a qualitative technique, it is used to obtain a rough quantitative approximation of the purity of the produced $Ca(OH)_2$ reagent. The absence of calcium carbonate ($CaCO_3$) and calcium oxide (CaO) in Figure 5.13a, the major compounds in the raw sorbent material and the calcination product respectively, suggests that the calcination and the subsequent hydration processes were complete. Further, the absence of MgO suggests that the hydration of this component was also complete. From an observation of Figure 5.13b, both the $Mg(OH)_2$ and the $Ca(OH)_2$ take part in the SO_2 capture producing the respective sulphite hydrates. The presence of $Ca(OH)_2$ peaks in Figure 5.13b lead to the conclusion that this compound is not fully utilized in the sulphation process.

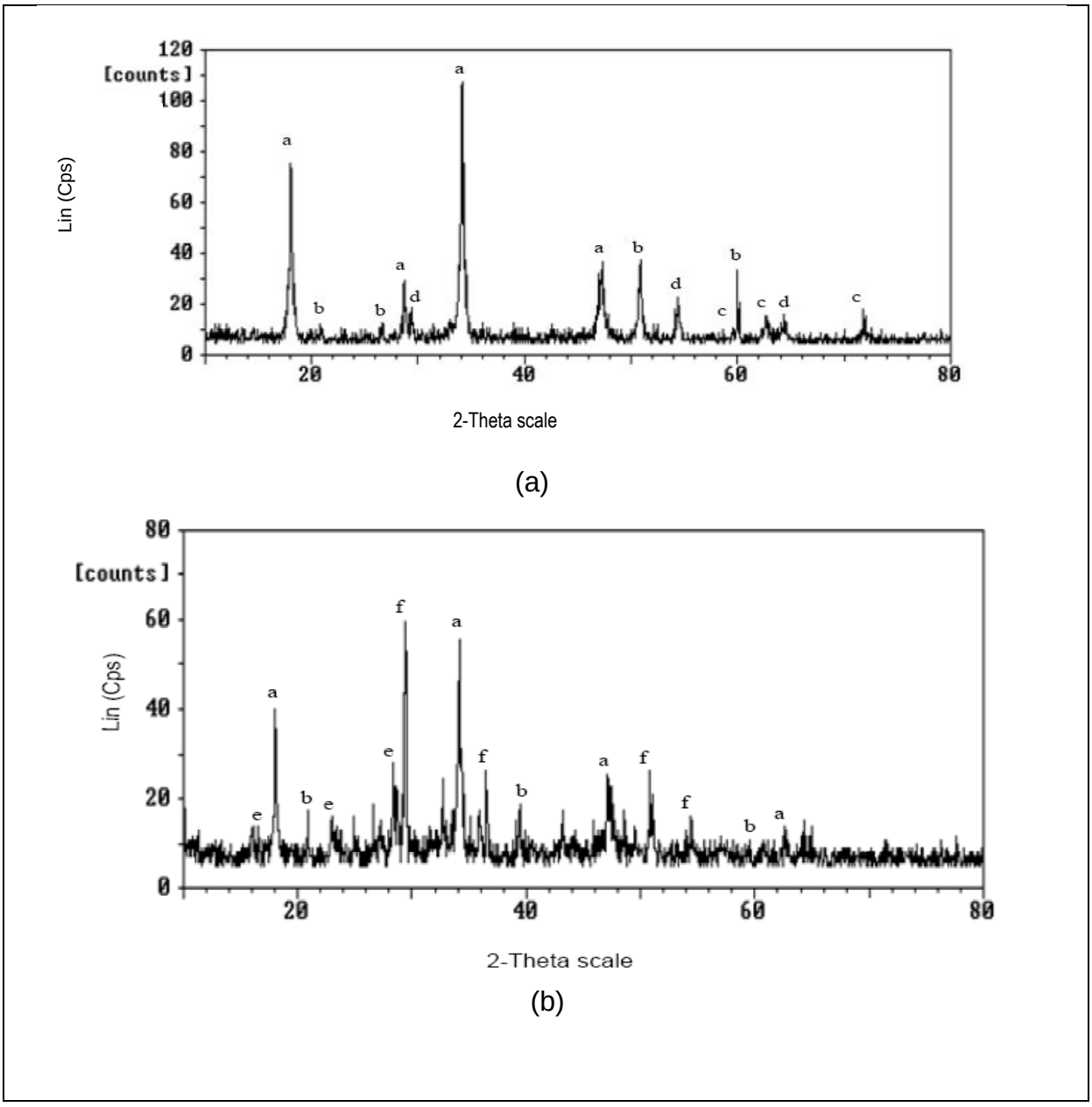

FIGURE 5.13: XRD spectra of sample A (a) before and (b) after sulphation.

5.2.2.7 Conclusion of the sulphation in fixed-bed experiments

The evaluation of the dissociation completion was performed by measuring the mass loss of the sample before and after calcination. The mass loss corresponds to the released amount of CO_2 during the calcination process. The results (Table 5.1) are considered satisfactory in conjunction with the data on the sample chemistry given in Table 4.1. During the hydration process, two simultaneous phenomena were observed: the temperature increases (exothermic reaction), and the volume of the paste expands. The higher the temperature increase recorded, the greater the expansion observed. Another phenomenon which was observed was that, for calcitic samples, which displayed a high final temperature after hydration, the process was accompanied by the evaporation of some of the water used. This phenomenon was so evident that the resulting paste was almost dry.

The evaporation of the water is likely to have an impact on the resulting structure of the sorbent material. The escaping steam will leave a structure that is more porous and an accompanying higher specific surface area will result. This observation is supported by the SEM micrographs for the calcinated and hydrated samples, Figure 5.12a – Figure 5.12d. Whereas there is not a lot of literature on the difference in the specific surface area between quicklime and slaked lime, Antonio, Asterios and Eleni (2001) have related the rate of increase in temperature to the specific surface area of the quicklime. In their investigation of two limestones calcinated at varying temperatures, they concluded that the larger the specific surface area, the higher the rate of temperature increase. This is likely to account for the higher capacity for samples A and B as observed in Figure 5.8.

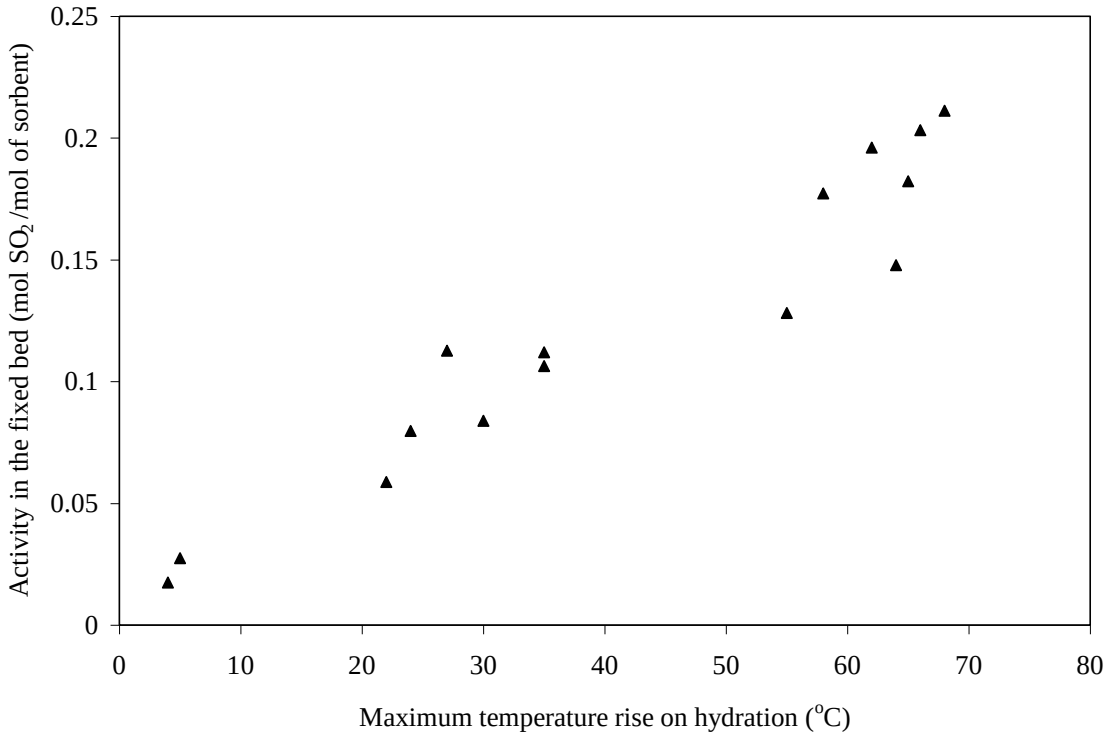

FIGURE 5.14: Relationship between the temperature rise on hydration and the activity in a fixed bed reactor for the study sorbents

Figure 5.14 shows the relationship between the recorded temperature rise during hydration and the amount of SO2 retained during the fixed-bed experiments. As can be seen, there is a general increase in the activity with the reported hydration temperature. Several studies have been carried out on the calcium utilization of commercial calcium hydroxide by various researchers. The calcium utilization has been defined as the moles of SO_2 retained per mole of calcium in the sorbent. Renedo and Fernandez (2002) observed a value of 18 % calcium utilization for 100 % $Ca(OH)_2$ under isothermal conditions of 57 ^oC and 52 % relative humidity. In their experimental protocol, 0.5g of sorbent was dispersed in 30g of an inert silica sand bed (particle size range 250-300 μm). Lin, Shih and Liu (2003) observed the reactivity of $Ca(OH)_2$ as 0.197 moles of SO_2/mole of Ca at 60 ^oC and 70 % relative humidity. On a gravimetric basis, their value was 0.170 g of SO_2/g of sorbent. Using commercial

$Ca(OH)_2$ ($18m^2/g$ BET area) in an isothermal fixed bed reactor, Martinez et al. (1991) observed a SO_2 capture of 18.2 mg SO_2/g of solid at a reactor temperature of 60 ºC and 60 % relative humidity. They also observed that the SO_2 removal for $Ca(OH)_2$ did not change when the temperature was increased from 60 to 80 ºC. The dolomitic samples tested in the present study compare favorably to the results that have been reported in the literature.

The relative humidity of the flue gas was the single most influential operating parameter on the maximum conversion obtained by all the sorbents. An increase in the relative humidity resulted in an increase in the sorbent conversion. Experiments done on the effect of temperature showed that the conversion achieved has a very weak relationship to the reaction temperature for the range used. The initial sorbent conversion rate was seen to be dependent on the SO_2 concentration although the final conversion remained independent of the SO_2 concentration

5.3 KINETIC ANALYSIS[4]

5.3.1 Sorbent Dissolution

Assuming that the limestone particle is nonporous and spherical and dissolves according to shrinking-core behavior, and as no ash covers the unreacted core as the reaction proceeds, there can be only two controlling steps, namely, fluid film diffusion or chemical reaction (see section 3.1.4). If the process were controlled by the fluid film diffusion, then the conversion would vary linearly with the elapsed time (Equation 3.25). An analysis of the conversion curves, however, shows a non-linear dependence on the elapsed time. The dissolution curves will thus be analyzed on the basis of the shrinking core model with chemical control. In the current study, the fit of all the experimental data into the integral rate is tested and the multiple regression coefficients obtained for the integral rate expression are calculated.

5.3.1.1 Reaction Rate constant (k)

A plot of $1-(1-X)^{1/3}$ vs. time for each sorbent material can be represented by a straight line if the reaction is chemically controlled. The value of k is then calculated from the slope of the straight line corresponding to each material. Figure 5.15 shows the plots obtained for three calcitic and two dolomitic limestones. From the results it can be seen that that the data points for each sorbent can be represented by a straight line up to the corresponding X value of about 0.936 or the R/R_0 value of about 0.4. This result indicates that Equation 3.27 is valid not only for the early period of dissolution, but also for the latter period in which the reduction of

[4] Based on: Siagi, Z.O and Mbarawa, M. Experimental investigation of the SO_2 abatement capacity of south african calcium – based materials. *ASME Energy Sustainability 2007*. June 27-30, 2007, Hilton Long Beach, California.

particle size is appreciable. This result also implies that the dissolution rate constant *k* is insensitive to particle size. Table 5.4 shows the values of *k* obtained for the five samples. As can be seen, the k value of the dolomitic limestones (0.0057 and 0.00415) is much less than that of the calcitic samples (0.0175, 0.0181, and 0.0190) indicating that their expected dissolution rate will be much lower. Table 5.5 also shows the values obtained for the other samples used in this study. Generally, it can be seen that the dolomitic limestones have a much lower reaction rate constant than their dolomitic counterparts. The variation of the reaction rate constant with the percentage calcium in the sample has been presented in Figure 5.16. The results show that, save for a few exceptions, the reaction rate increases almost linearly with the amount of calcium in the sample.

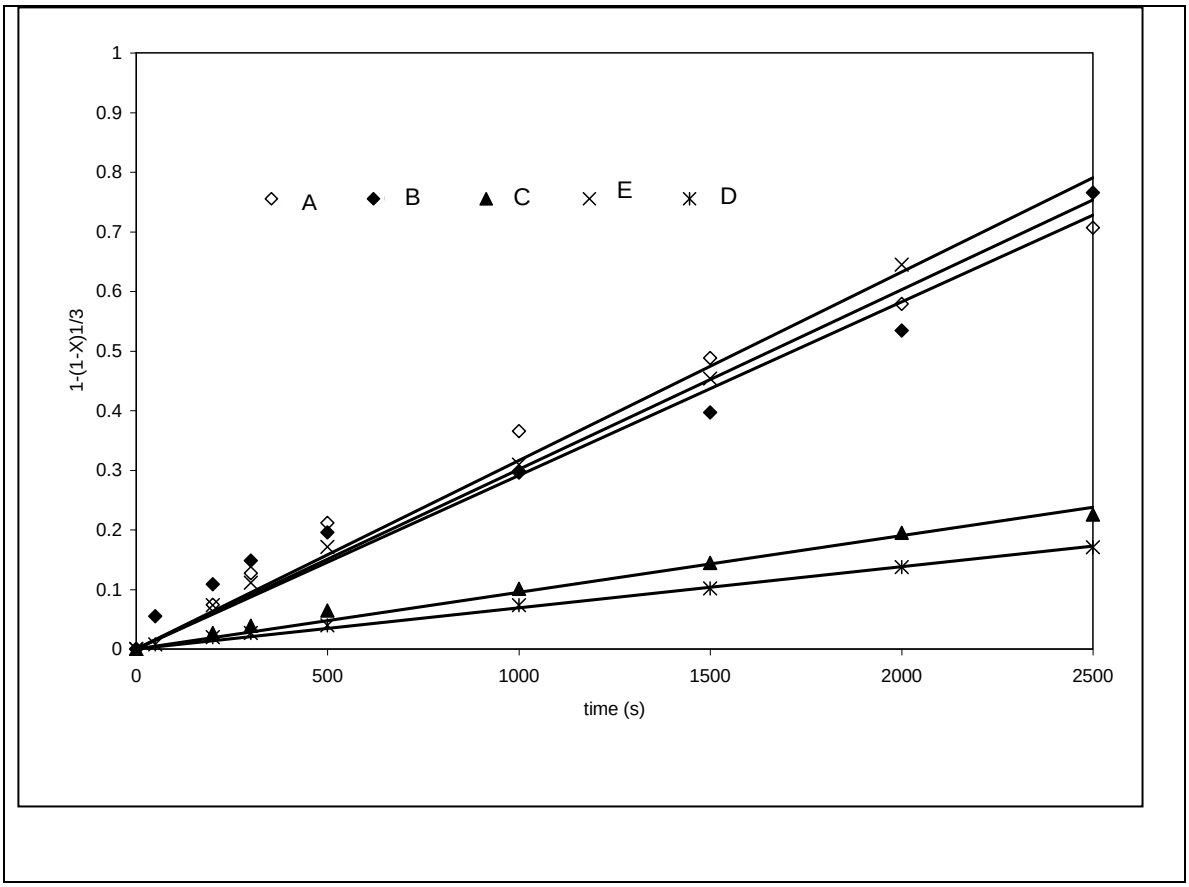

FIGURE 5.15: Plot of 1-(1-X)1/3 vs time for limestone dissolution at pH 5.0 and 50ºC.

TABLE 5.5: Reaction rate constants (k) and activation energy (E_a) for the tested sorbents.

Sample	**Constant, k (min^{-1})**	**E_a (kJ/mol)**
A	0.0181	26.1
B	0.0175	25.0
C	0.0057	20.3
D	0.00415	18.4
E	0.0190	25.7
F	0.0079	22.6
G	0.0093	23.5
H	0.0175	25.6
J	0.0181	27.5
K	0.010	21.5
L	0.006	16.4
M	0.0108	22.2
N	0.0163	24.0
P	0.0153	24.6
Q	0.0061	14.7

The plots used to generate these rate constants are tabulated in Appendix A, Figures A.11 – A.20

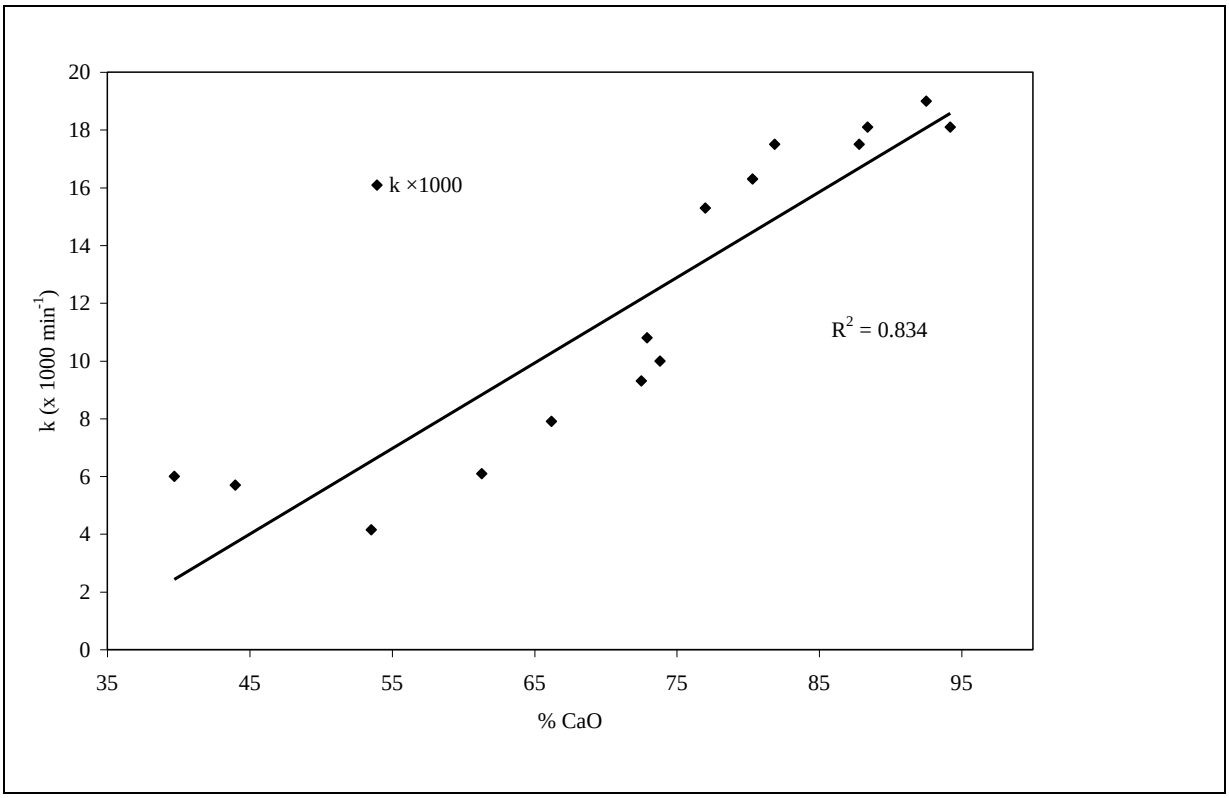

FIGURE 5.16: Variation of the reaction rate constant, K, with the % Calcium in the sample

5.3.1.2 Activation energy and frequency factor

Figure 5.17 shows the plot of $1-(1-X)^{1/3}$ against time for dissolution tests done for sample A at various reaction temperatures. As can be seen by the straight lines, the dissolution follow the shrinking core model between the temperatures 30 ºC to 70 ºC. Using the *k* values obtained from the slopes at the different temperatures in Figure 5.17, a plot of *lnk* against the reciprocal of the reaction temperature (1/T) is obtained, Figure 5.18. From the Arrhenius equation, the frequency factor is obtained using the intercept of the *ln k* axis, while the activation energy is obtained from the slope of the graph. From Figure 5.18, the values obtained for sample A are:

E = 26.1 kJ mol^{-1}, and k_0 = 242. Following the same procedure, the activation energy of the other samples used in the study are included in Table 5.5

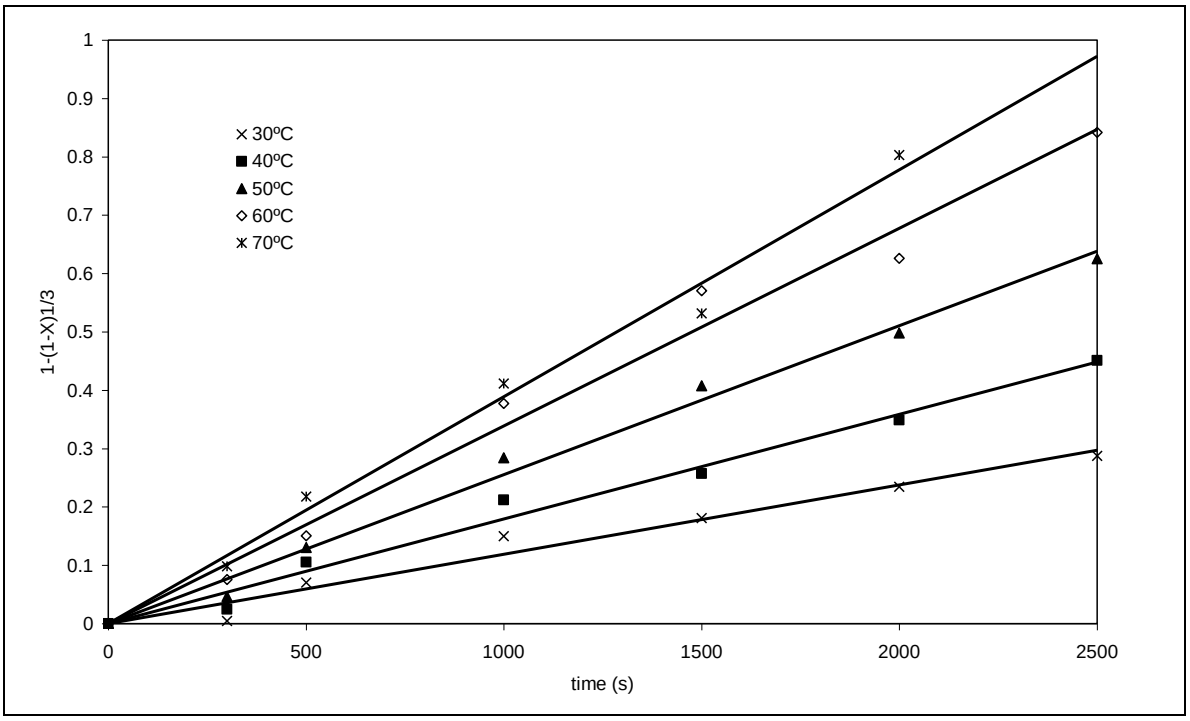

FIGURE 5.17: Plot of $1-(1-X)^{1/3}$ vs. time for various reaction temperatures for sample A

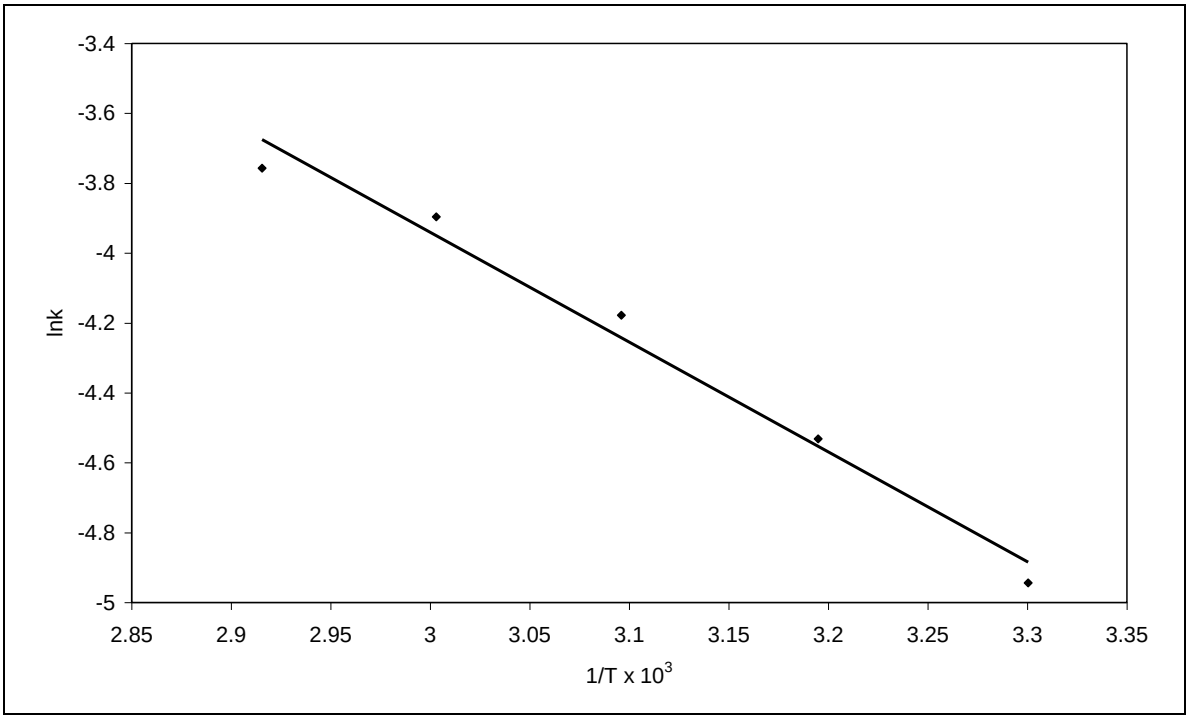

FIGURE 5.18: Arrhenius plot for the dissolution of sample A1

5.3.2 Desulphurization activity in the fixed-bed reactor

Modeling of non-catalytic gas-solid reactions has received considerable interest in recent years mainly because of the unresolved questions concerning the removal of sulphur dioxide with dry sorbents. Many models have been developed to describe the solid conversion versus time relationship observed during the course of the reaction (see section 3.2.2.2). Each of these models is usually applicable to a particular type of gas-solid reaction. In the current study the surface coverage model proposed by Liu and Shih (2002) has been used to predict the sorbent conversion observed in a fixed bed reactor.

The hypothesis of the surface coverage model is that the sorbent is made up of plate grains and that the reaction is controlled by chemical reaction on the surface of a grain and the reacting surface area of the grain decreases with the deposition of solid product. According to this model, the reaction of a sorbent reaches a maximum conversion when its reacting surface is fully covered by the product (Liu, & Shih, 2002). The relationship between conversion and time for this model is given by the Equation:

$$X = 1 - \exp\left(-k_1 k_2 t\right) / k_2 \qquad (5.11)$$

where

$$k_1 = k_s S_{g0} M, \qquad k_2 = k_p / S_{g0} M,$$

k_s is the initial reaction rate of solid, k_p is a proportionality constant between the rate of change of unreacted surface and the reaction rate, S_{g0} is the initial specific surface area, and M is the sorbent weight per mole of calcium. The two parameters, k_1 and k_2, in Equation 5.11 can be obtained by least-squares fitting of Equation 5.11 to the experimental data. One can easily see from Equation 5.11 that k_2 is the reciprocal of the maximum conversion. According to the

definitions of k_1 and k_2, they are functions of initial specific surface area, temperature, SO_2 concentration, and relative humidity. These functions can be derived by analyzing the values of k_1 and k_2 obtained at different experimental conditions.

5.3.2.1 Dependence of the reaction rate on sorbent type

Figure 5.19 shows the experimental as well as the calculated conversion curves for two dolomitic (A and B) and two calcitic (C and D) limestones at 80 ºC, 2000 ppm SO_2 concentration and 10 % relative humidity.

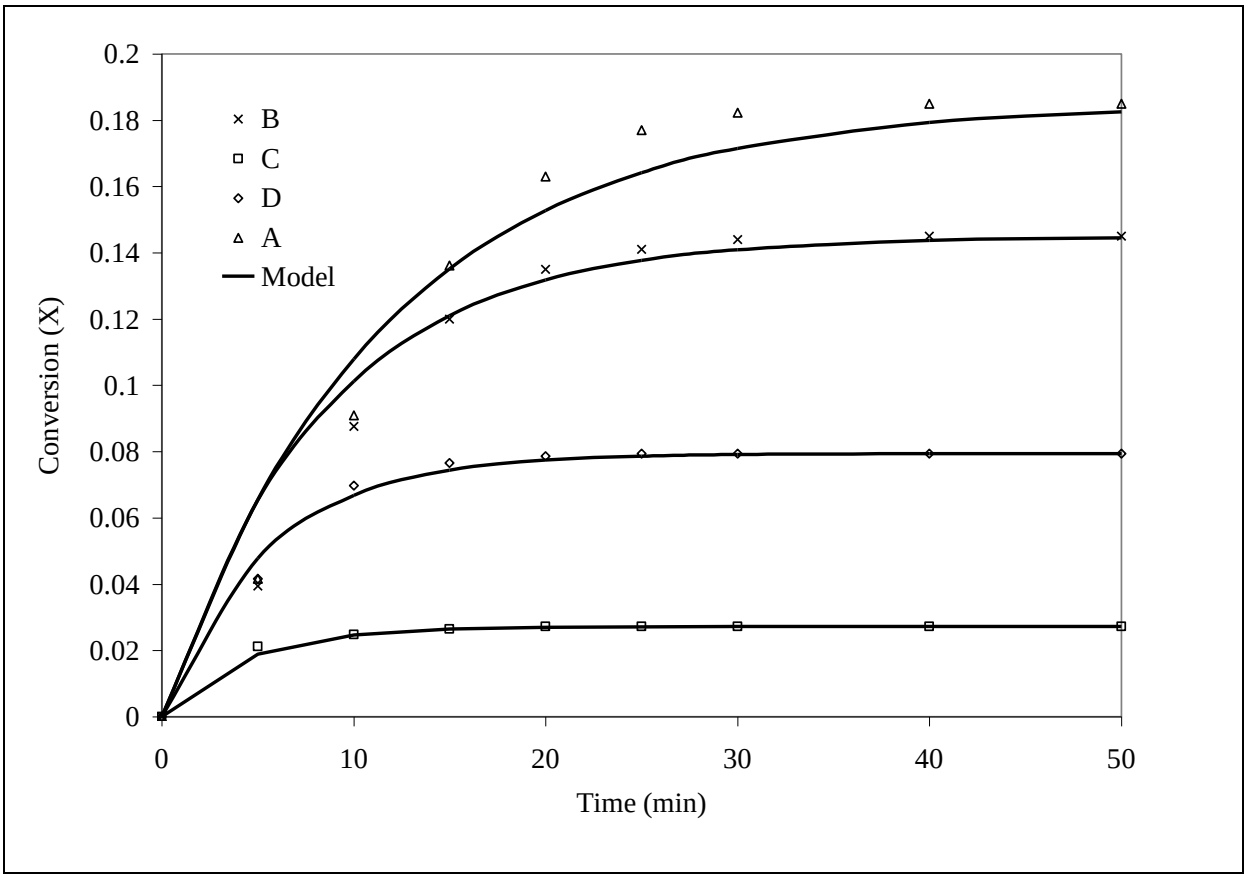

FIGURE 5.19: Comparison of model predictions with experimental data for two calcitic and two dolomitic limestones reacted at 80 ºC, 2000 ppm SO_2, and 10 % RH

It can be seen that the experimental data are described by Equation 5.11 very well. However, the calculated values differ from the experimental results during the early part of the conversion but as the reaction proceeds, both the predicted value and the experimental value are in very good agreement. Table 5.6 shows the k_1 and k_2 values calculated for all the samples used in this study at 80 ºC, 2000 ppm SO_2, and 10 % RH.

TABLE 5.6: Values of k_1 and k_2 of Equation 5.10

Sorbent	k_1	k_2
A	0.0162	5.41
B	0.0174	6.90
C	0.00646	36.76
D	0.0146	12.59
E	0.0121	5.102
F	0.0142	8.929
G	0.007	8.881
H	0.0164	4.921
J	0.185	4.733
K	0.01261	7.800
L	0.00463	57.143
M	0.01344	9.398
N	0.01573	5.640
P	0.01397	11.920
Q	0.01103	17.007

5.3.2.2 Effect of the initial Specific surface area.

Each of the samples used has its own physical and chemical properties. In this section the effect of the initial specific surface area on the reaction is investigated. Table 5.2 shows the specific surface area of the sorbents used in this investigation.

Figure 5.20 presents the conversion per initial specific surface area versus time of two dolomitic (C and D) and two calcitic (A and B) limestones used in this study. Lee et al. (2006) showed that the SO_2 capture by sorbents prepared from fly ash/$Ca(OH)_2$ increased linearly from 83.3 to 163.5 min (g CaO)$^{-1}$ as the specific surface area increased from 22.5 to 133.3 m^2g^{-1}. Ho et al. (2002) investigated the influence of the initial BET specific surface area on the reaction. They used samples of the same material but different initial particle size. The different size fractions had specific surface areas varying from 7.8 to 12.3 m^2/g and mean diameter 10 to 96 μm. Their results indicated that the samples of the smallest particle size d_p = 10 μm were the least reacted. However, upon consideration of the initial BET specific surface areas of the samples, their conversions per unit initial specific surface area X/S_{g0} versus time could be represented by the same curve with a standard deviation of the data around the curve of 0.02. However, as can be seen from Figure 5.20, the conversion per unit specific surface area for the four samples used in this study vary from one to the other. This indicates that besides the initial specific surface area, the type of sorbent plays an important role in the reaction kinetics.

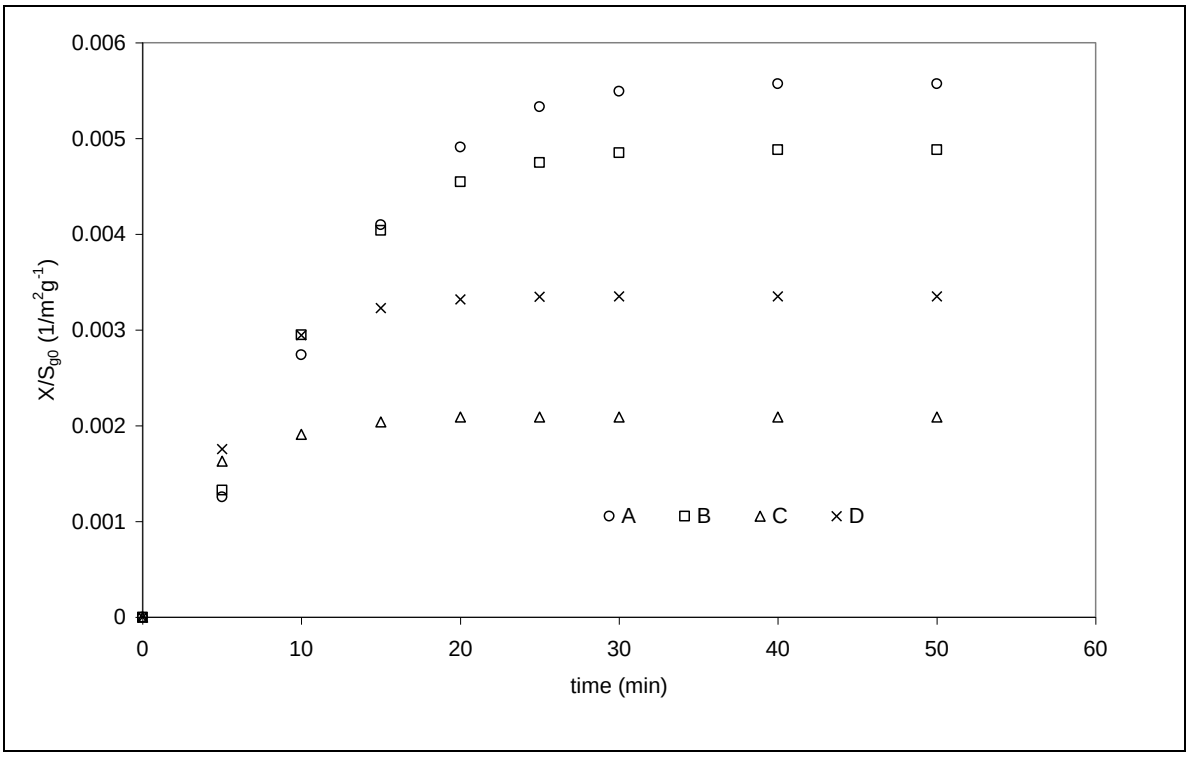

FIGURE 5.20: Conversion of sorbent per unit initial specific surface area of two dolomitic and two calcitic limestones. Reaction conditions: 80 ºC, 2000 ppm SO_2, and 10 % RH.

5.3.2.3 Effect of relative humidity

The parameters k_1 and k_2 (Equation 5.11) are functions of relative humidity, SO_2 concentration and temperature. Mathematically this can be written as:

$$k_1 = f(RH, C_{SO_2}, T), \qquad k_2 = f(RH, C_{SO_2}, T) \tag{5.12}$$

Where RH is the relative humidity, C_{SO_2} is the inlet SO_2 concentration in ppm, and T is the absolute temperature. The functional dependence of k_1 and k_2 can be evaluated by varying the experimental conditions and fitting Equation 5.11 to the experimental conversion versus time

(*X-t*) data. Figure 5.21 shows the fitting of experimental data to the *X-t* data for sample A at reactor temperature 80ºC and SO_2 concentration of 2000 ppm, and relative humidity 0-30%.

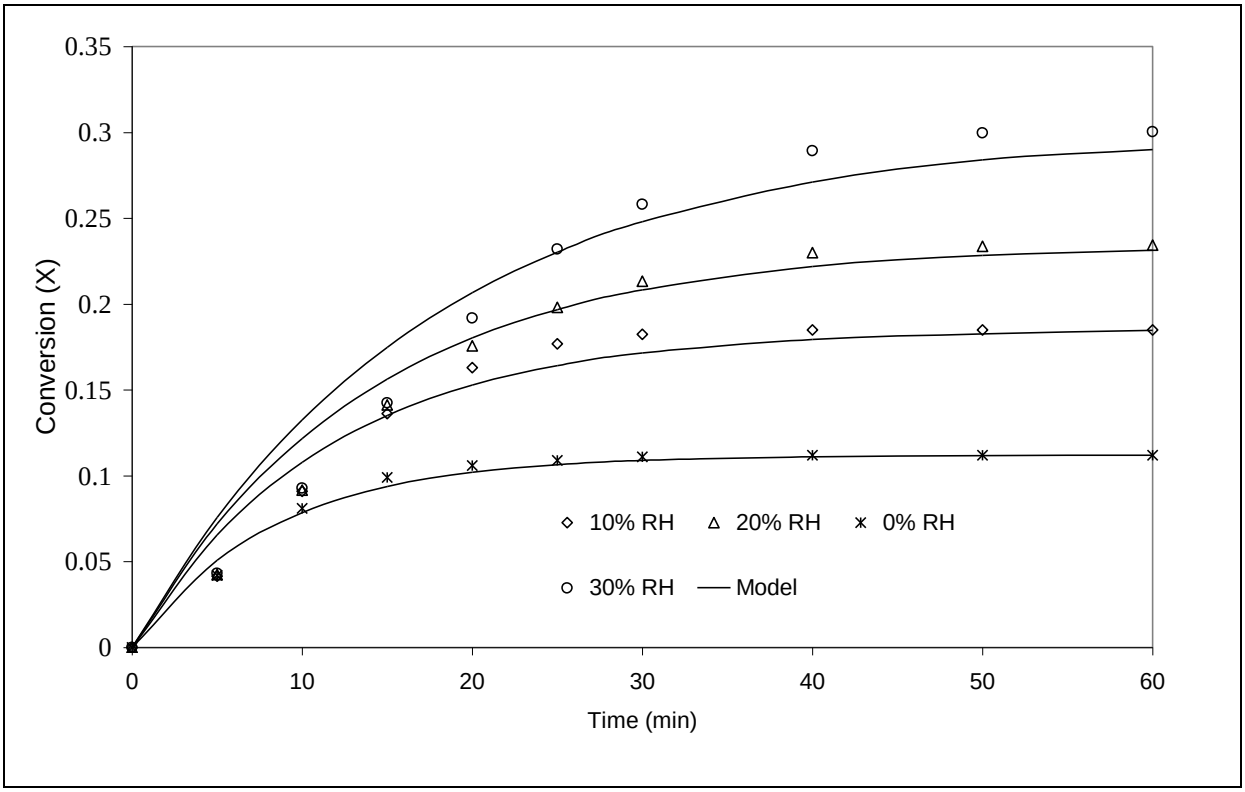

FIGURE 5.21: Comparison of model predictions with experimental data for sample A reacted at 80 ºC, 2000 ppm SO_2, and 0 – 30 % RH.

The variation of the k_1 parameter with relative humidity for the conditions given above is presented graphically in Figure 5.22. Regression analysis of the results shows the k_1 parameter can be related to the percentage relative humidity by an exponential expression of the form:

$$k_1 = 0.0136e^{0.0139RH} \qquad (5.13)$$

Equations 5.12 and 5.13 can be combined in the form

$$k_1 = 0.0136e^{0.0139RH} f(C_{SO_2}, T) \qquad (5.14)$$

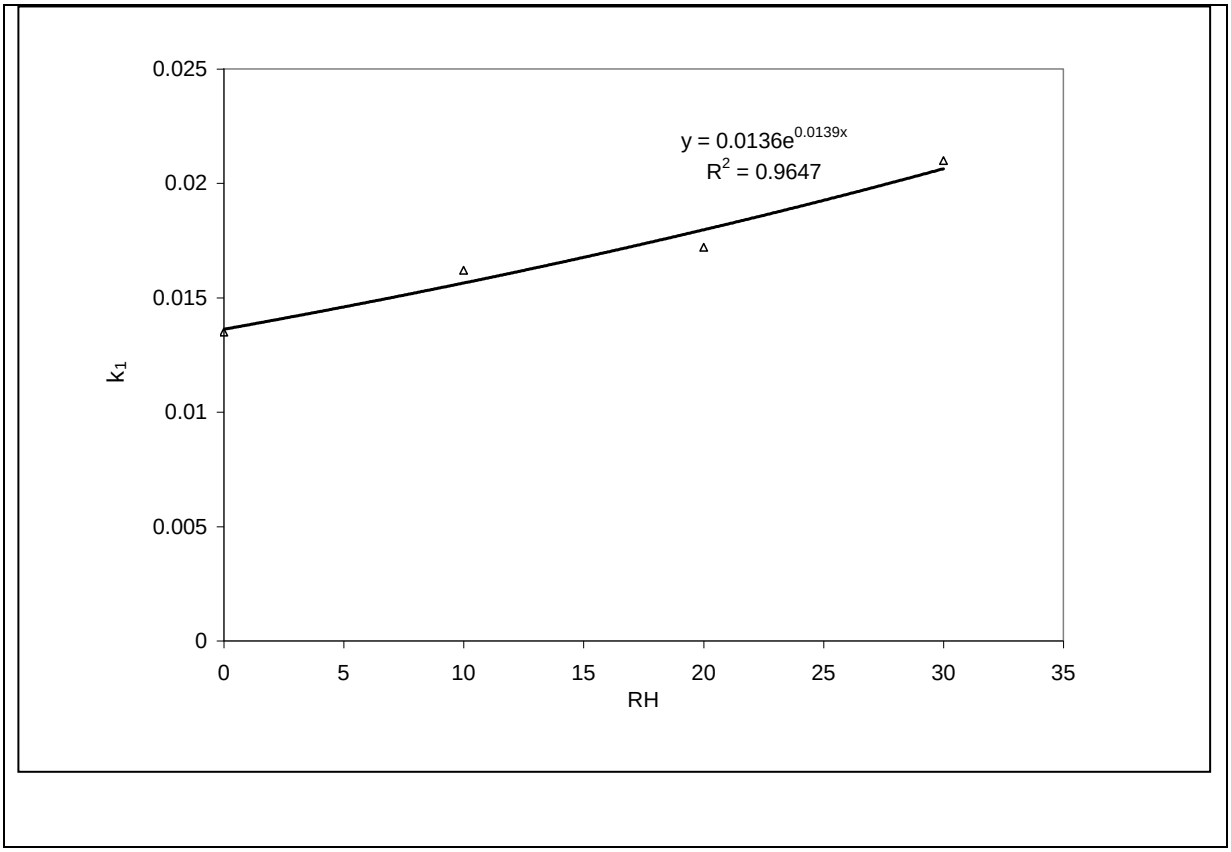

FIGURE 5.22: Relationship between k_1 and relative humidity for sample A reacted at 80 ºC and 2000 ppm SO_2.

The variation of the k_2 parameter with relative humidity for sample A at reactor temperature 80ºC and SO_2 concentration of 2000 ppm, is presented graphically in Figure 5.23. Regression analysis of the results shows the k_2 parameter can be related to the percentage relative humidity by an exponential expression of the form:

$$k_2 = 8.5719e^{-0.0374RH} \qquad (5.15)$$

Equations 5.12 and 5.15 can be combined in the form

$$k_2 = 8.5719e^{-0.0374RH} f(C_{SO_2}, T) \qquad (5.16)$$

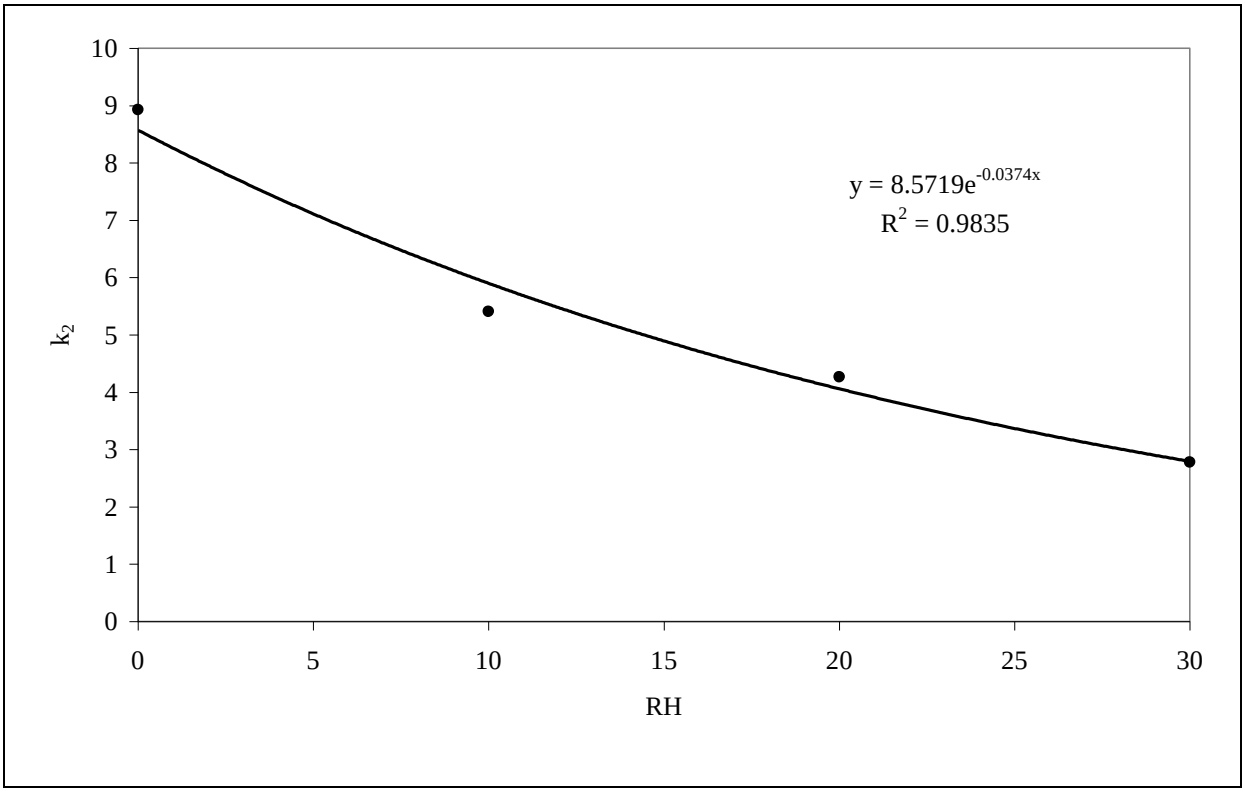

FIGURE 5.23: Relationship between k_2 and relative humidity for sample A reacted at 80 ºC and 2000 ppm SO_2.

5.3.2.4 Effect of SO_2 concentration

The effect of SO_2 concentration on the conversion of sample A has been presented in section 5.2.2.2. Application of Equation 5.11 on the results helps to obtain the constants k_1 and k_2 as a function of the SO_2 concentration. Figure 5.24 shows the relationship between the parameter k_1 and the SO_2 concentration at 0% RH and 80ºC reactor temperature. Using the slope of the straight line in Figure 5.24, the relationship between $k_1 e^{-0.0139}$ can be written as:

$$k_1 = e^{0.0139RH} C_{SO_2}^{0.864} f(T) \qquad (5.17)$$

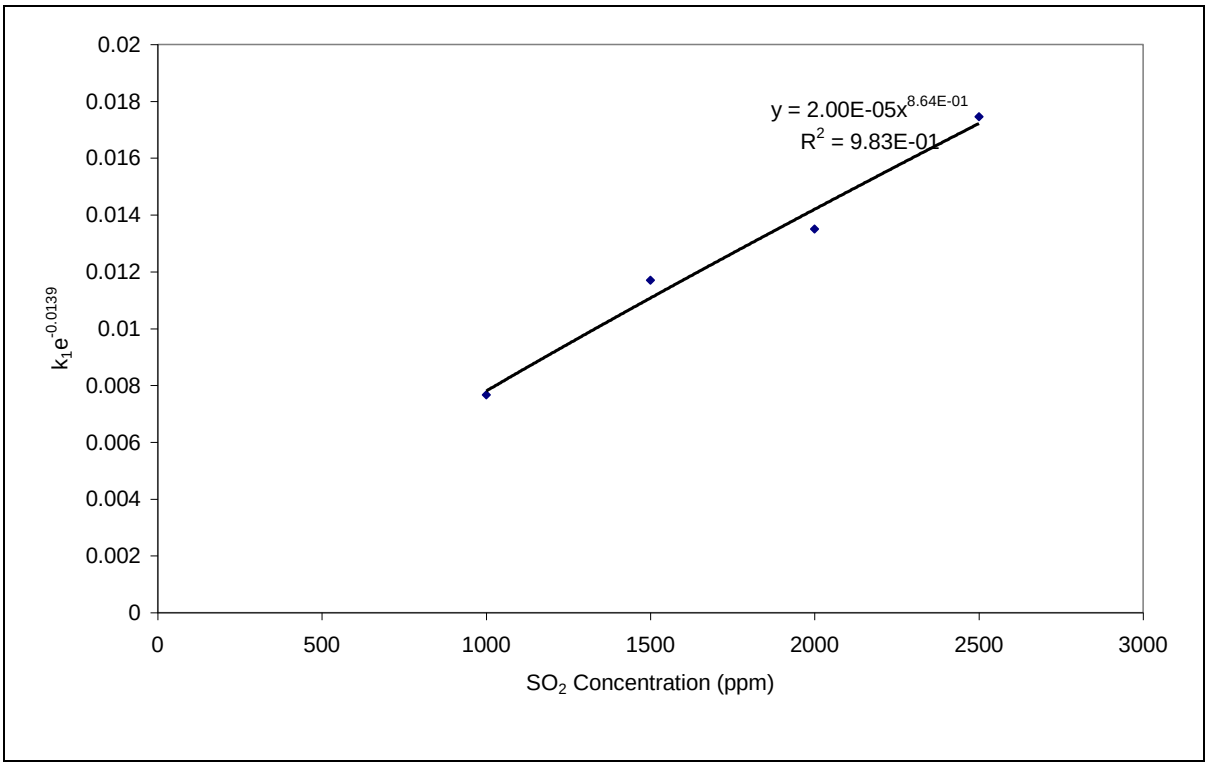

FIGURE 5.24: Relationship between k_1 and SO_2 for sample A reacted at 80 ºC and 0 % RH.

Variation of k_2 with SO_2 concentration is presented in Figure 5.25. From the results, it can be observed that k_2 is only a weak function of the SO_2 concentration in the flue gas; i.e. the final conversion is independent of the initial SO_2 concentration.

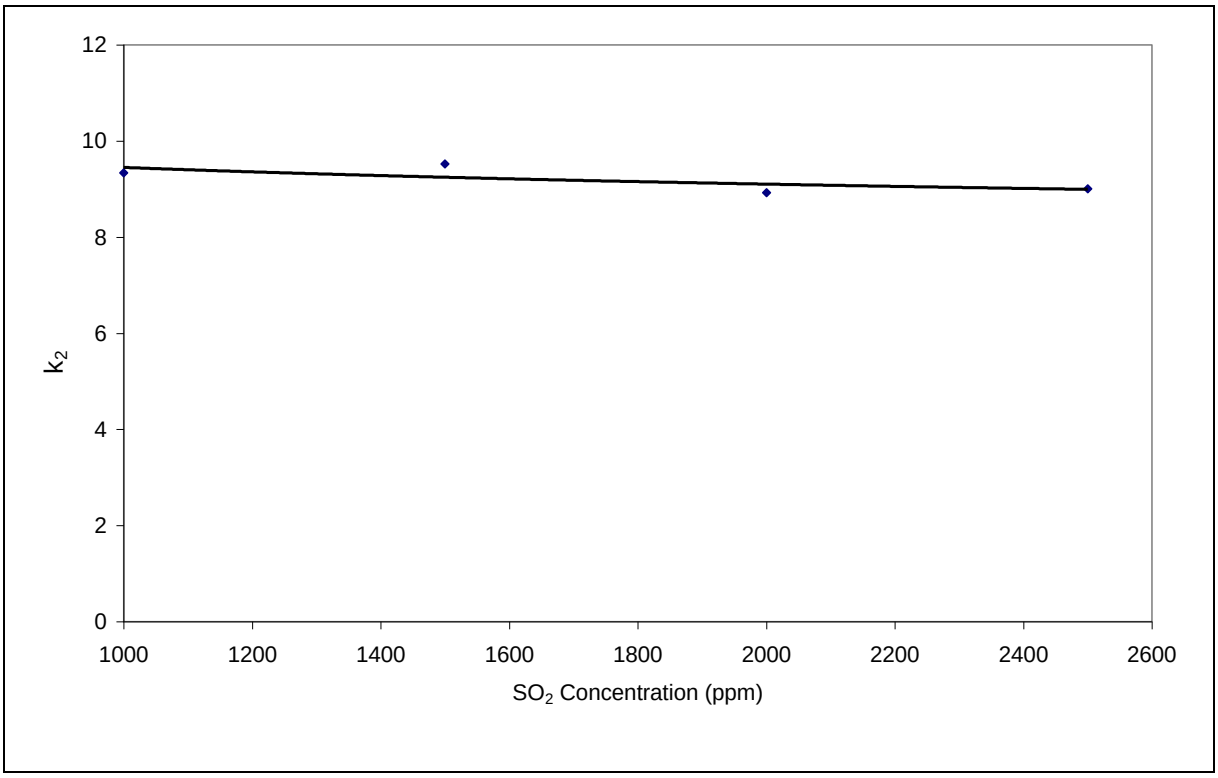

FIGURE 5.25: Relationship between k_2 and SO_2 for Sample A reacted at 80ºC and 0% RH.

Substituting for the concentration dependence in Equation 5.16, results in:

$$k_2 = 8.5719 e^{-0.0374RH} C_{SO_2}^{-0.0539} f(T) \qquad (5.18)$$

5.3.2.5 Effect of reactor temperature

The temperature dependence of the reaction rate can be determined by the use of the Arrhenius law. A plot of ln k_1 versus $1/T$ is shown in Figure 5.26.

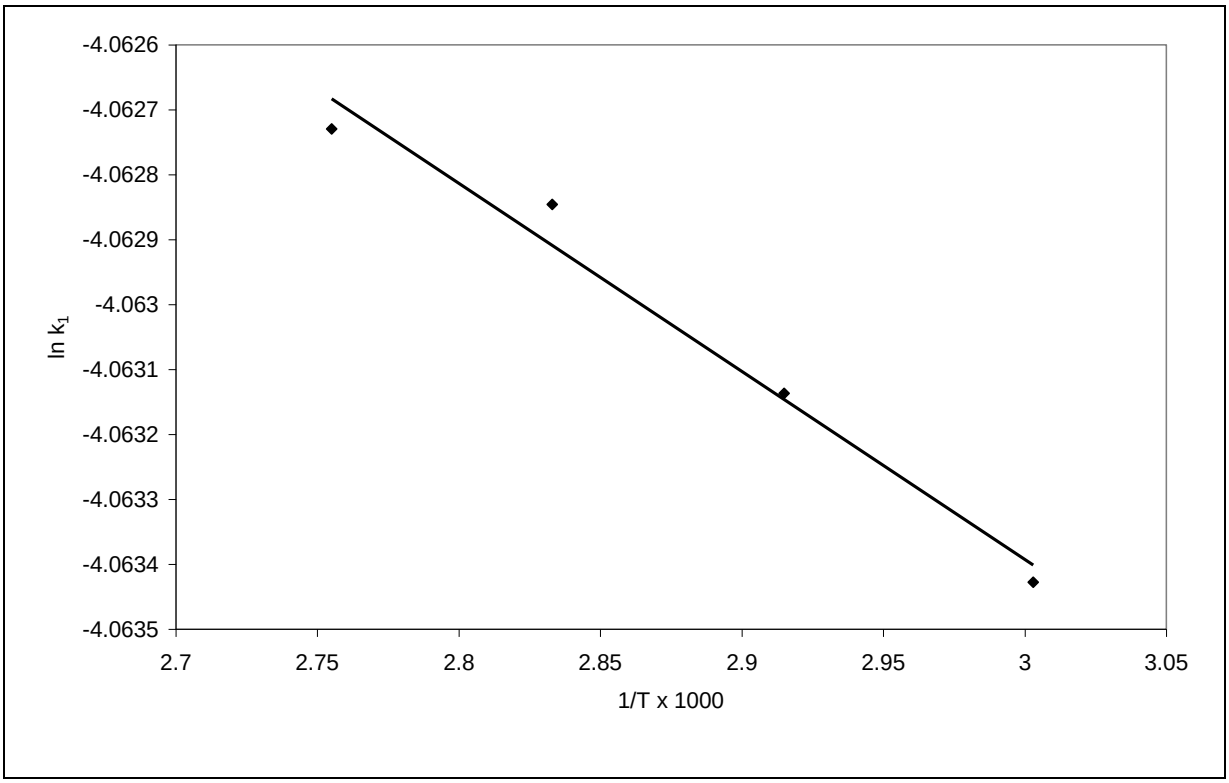

FIGURE 5.26: Arrhenius plot for k_1 for sample A

The slope of the straight line in Figure 5.26 allows us to determine the activation energy of the reaction. Taking into account the temperature dependence, Equation 5.17 can thus be written as:

$$k_1 = 1.846 \times 10^{-5} e^{0.0139RH} e^{\frac{-24000}{RT}} C_{SO_2}^{0.864} \qquad (5.19)$$

The small value of the apparent activation energy, *E = 24 kJ/mol*, indicates that the effect of temperature on the reaction is weak within the temperature range tested (60 ºC to 90 ºC)

Figure 5.27 shows the variation of k_2 as the temperature is varied from 60ºC to 90ºC. As can be seen from the figure, the temperature has only a small influence on the final conversion of

sample A. Taking into account the influence of the temperature, Equation 5.18 can be written in its final form as:

$$k_2 = 12.331 e^{-0.0374RH} C_{SO_2}^{-0.0539} e^{\frac{67.8}{T}} \tag{5.20}$$

Equations 5.19 and 5.20 together with Equation 5.11 constitute the kinetic model for the sulphation of sample A under fixed bed conditions in the operational range considered; i.e temperature 60ºC to 90ºC, relative humidity 0% to 40%, and SO_2 concentration of 1000 ppm to 2000 ppm.

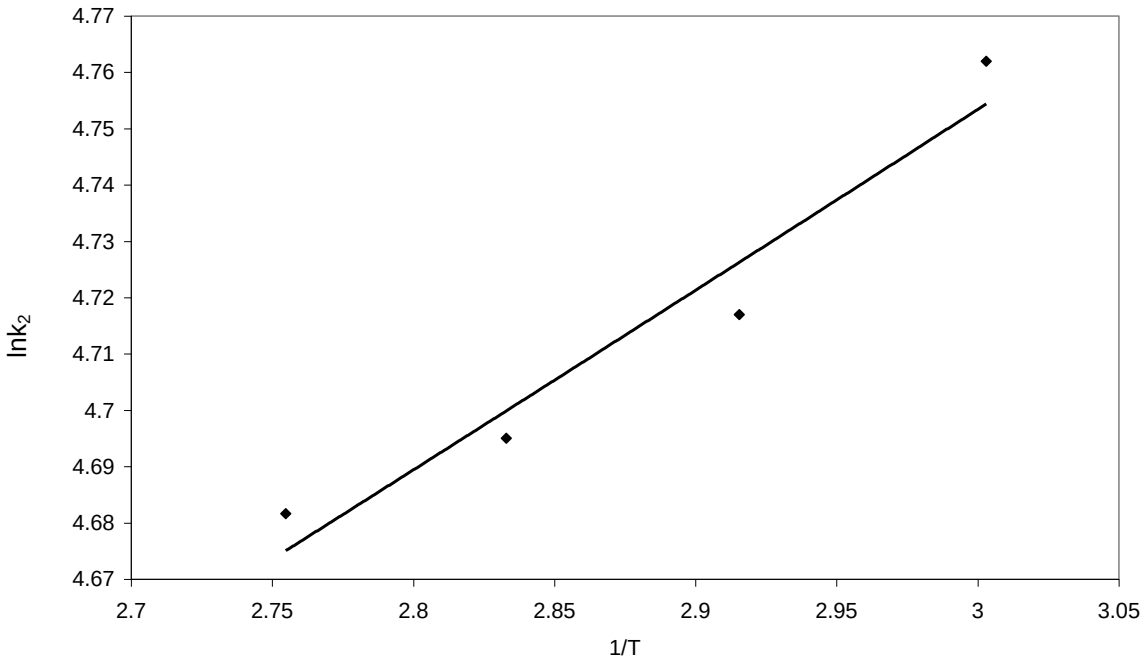

FIGURE 5.27: Arrhenius plot for k_2 for sample A

5.3.2.6 Kinetic model verification

The validity of the proposed mathematical model was verified by comparing the predicted conversion results with the experimental data. Figure 5.28 shows the comparison. The results demonstrate a very satisfactory prediction of the desulphurisation activity with an *R* value of 0.988.

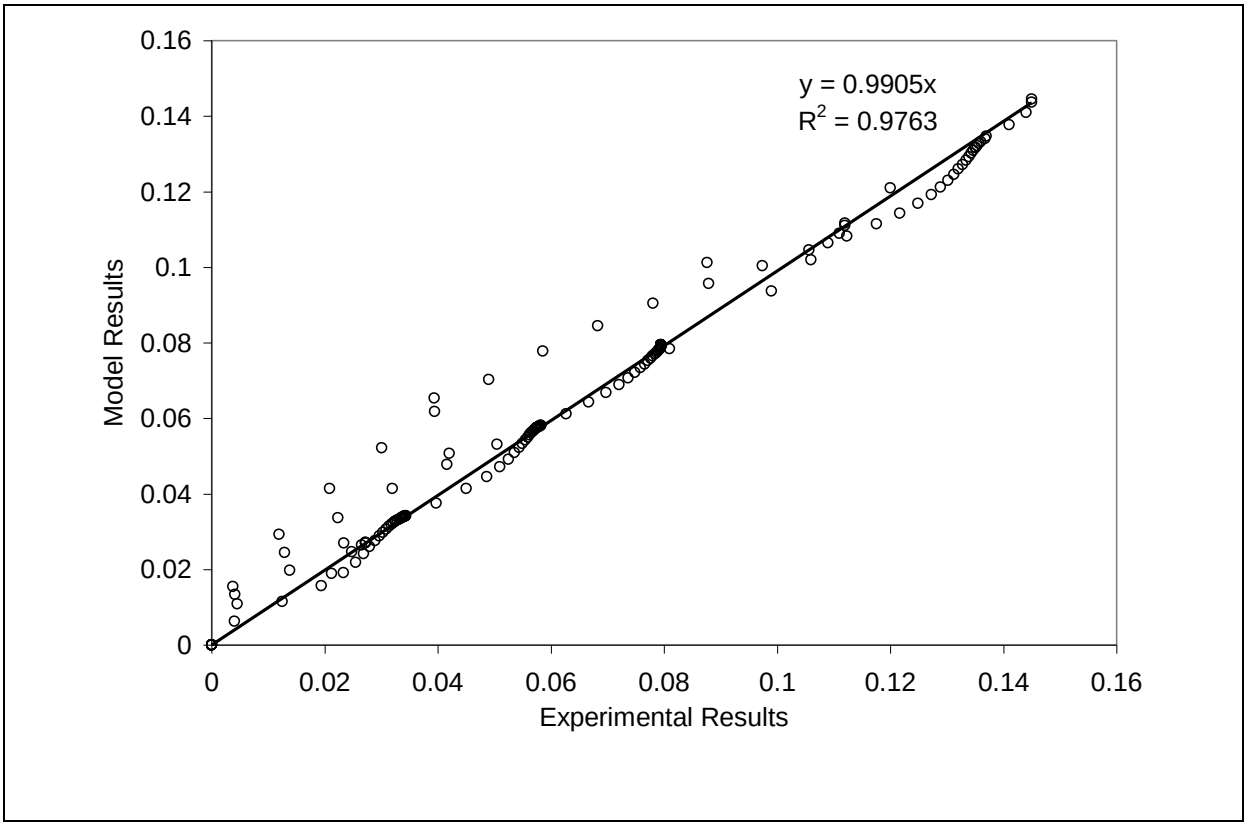

FIGURE 5.28: Predicted vs. experimental conversion

5.3.3 COMPARISON BETWEEN THE pH-STAT AND THE FIXED-BED RESULTS

In this chapter, results of the pH-stat and fixed bed reactor experiments have been obtained. The amount of acid consumed in 40 minutes under the pH-stat method and the amount of SO_2

retained over a period of 30 minutes in the fixed-bed can be used as a basis for the ranking of the sorbent materials in the respective reactors.

TABLE 5.7: Ranking of the sorbents using the pH-stat and fixed-bed methods

	HCL Added (mL)	pH-Stat rank	Mol SO_2 retained	Fixed-bed rank
A	27.19	2	0.1823	4
B	25.8	5	0.1478	6
C	14.51	13	0.0274	14
D	12.03	14	0.0798	12
E	26.54	3	0.196	3
F	17.4	12	0.112	9
G	17.88	11	0.1126	8
H	26.39	4	0.2032	2
J	29.14	1	0.2113	1
K	19.53	9	0.1282	7
L	10.69	15	0.0175	15
M	19.93	8	0.1064	10
N	24.5	6	0.1773	5
P	23.4	7	0.0839	11
Q	18.1	10	0.0588	13

A graphical representation of these results is given in Figure 5.29 below. Generally, the sorbents which show a higher reactivity in the pH-stat apparatus will have a higher capture capacity in the fixed bed reactor.

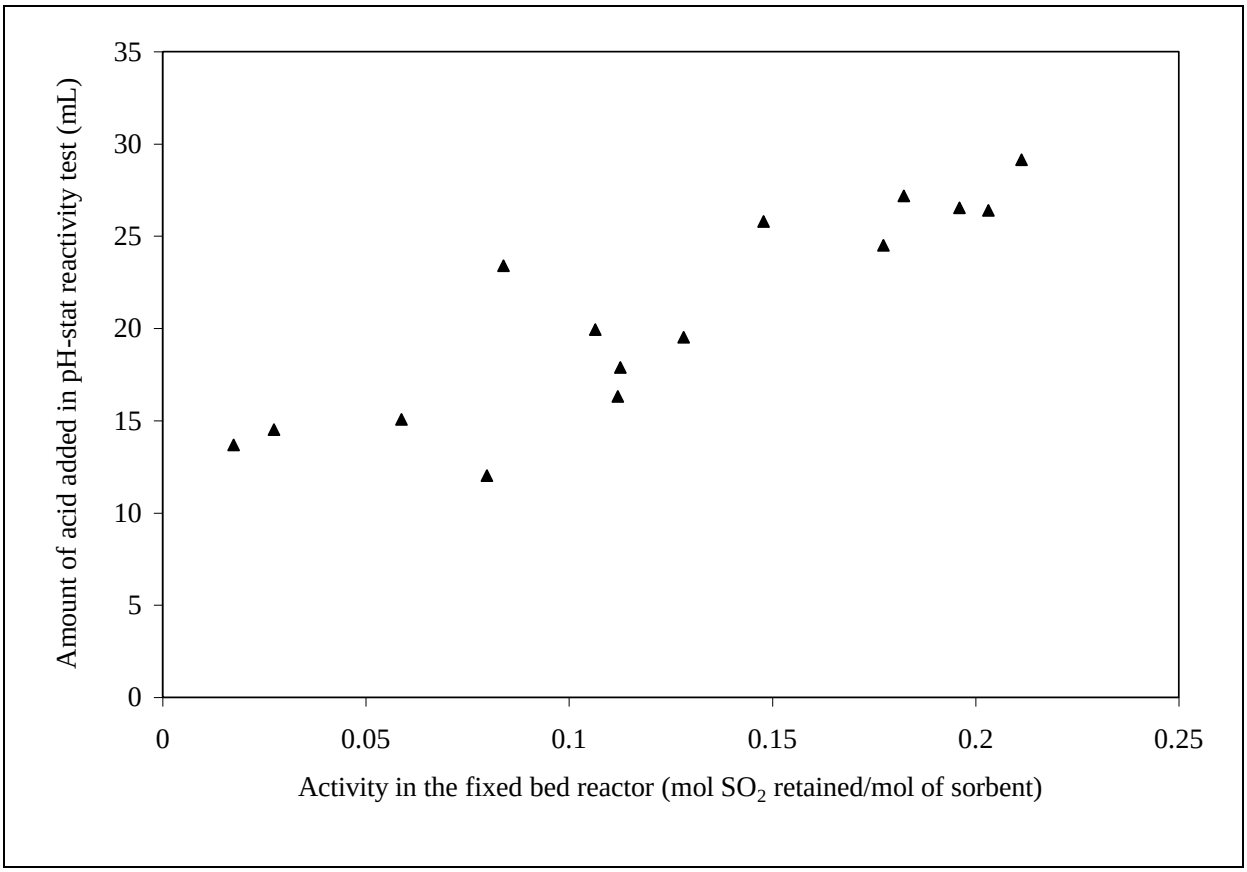

FIGURE 5.29: Comparison between the activity in the fixed bed reactor and the pH-stat method for the 15 samples tested in the study

Although the ranking in the fixed bed is somehow different from the ranking obtained in the pH-stat method, there is a general agreement and the differences may be explained by the presence of trance elements like iron oxide (see section 5.2.2.1). The reaction in the pH-stat method can be modeled according to the shrinking core model with chemical control while that in the fixed bed reactor is modeled satisfactorily using the surface coverage model.

CHAPTER 6

6. SUMMARISING CONCLUSIONS AND RECOMMENDATIONS

6.0 SUMMARY OF STUDY

The primary objective of this investigation was to study and rank the performance of locally available materials (i.e. limestone, dolomite, or calcrete) as sorbents in the capture of SO_2 emissions from coal-fired power plants. In achieving this objective an extensive literature review of the available FGD technologies worldwide was carried out. From the literature review, it was concluded that almost all commercial FGD processes are based on the fact that SO_2 is acidic in nature, and they remove the SO_2 from the flue gases by reaction with a suitable alkaline substance. The most commonly used alkaline materials were identified as limestone (calcium carbonate), quicklime (calcium oxide) and hydrated lime (calcium hydroxide). Limestone is an abundant and therefore relatively cheap material and both quicklime and hydrated lime are produced from limestone by calcination and hydration. Limestone is widely available from different mines in South Africa and to rank the performance of the material from different sources as sorbents for flue gas desulphurisation, it was necessary to carry out experimental testing at conditions similar to those which would be encountered in industrial scale flue gas desulphurisation devices in South Africa. The performance of the sorbents under wet FGD conditions were simulated under pH-Stat method while dry FGD was simulated using a Laboratory Scale fixed-bed FGD unit.

In the final part of the investigation, models were proposed to predict the performance of the sorbent materials under wet and dry FGD conditions. The dissolution of the sorbent material

under wet FGD conditions was found to be satisfactorily predicted by the Shrinking Core Model (SCM) and the reaction rate constants obtained from the application of this model were used to rank the SO_2 capture capacity of the different materials. The desulphurisation process of the sorbents in the fixed-bed reactor was found to be predicted closely by the Surface Coverage Model. From a regression analysis of the experimental data the model parameters were obtained. Application of the model equation to process variables showed a close agreement with experimental data. The initial reaction rate and final conversion of the sorbents can be used in the ranking of the different sorbent materials.

6.1 CONCLUSIONS

The results obtained in this work lead to the following conclusions:

6.1.1 pH-Stat Experiments

- In the dissolution process, it was observed that the reaction rate was very sensitive to the reaction temperature in the range 30ºC to 70º C. The solubility of the tested samples increased with an increase in the reaction temperature.

- The dissolution rate is a strong function of the particle size, i.e. the smaller the particle size, the higher the conversion within the same time period.

- The dissolution process showed a strong dependence on the solution pH with the dissolution rate being higher at lower pH values. This, together with the low calculated value of the activation energy, led to the conclusion that the dissolution process is surface reaction controlled.

- The type and source of sorbent had an influence on the dissolution rate. Calcitic limestones were observed to have a higher rate of dissolution than the dolomitic samples. The presence of impurities were also observed to have an influence on the dissolution behaviour with the presence of small amounts of iron as Fe_2O_3 being beneficial to the reaction.

- The dissolution data were successfully simulated by the Shrinking Core Model (SCM). This model assumes that the reaction takes place over a sharp interface. The reaction starts at the outer surface of the sorbent material and moves inward as the sorbent is consumed.

6.1.2 Fixed-bed experiments

- The type and source of sorbent had an influence on the maximum conversion of the sorbent observed. Calcitic limestones had a higher conversion than the dolomitic sorbents. The presence of iron in small amounts was thought to be beneficial to the conversion.

- The relative humidity of the flue gas was observed to be the single most influential parameter on the desulphurisation reaction. The maximum conversion recorded increased exponentially with an increase in the relative humidity for all the samples tested.

- The SO_2 concentration had only a weak influence on the maximum conversion observed in any of the sample but the initial conversion rate was observed to increase

with an increase in the SO_2 concentration indicating that the reaction is first order with respect to the SO_2 concentration.

- The maximum conversion calculated increased with an increase in the initial specific surface area, but the conversion per unit initial surface area was different for the different sorbents further reinforcing the influence of sorbent type.

- The reactor temperature had only a small influence on the final conversion of the sorbent. The beneficial contribution of temperature in reaction kinetics was thought to be negated by the increased evaporation of moisture from the sorbent surface.

- The conversion versus time data during desulphurisation process can be satisfactorily modeled using the surface coverage model. The model parameters are obtained by fitting the model to experimental data.

- The maximum sorbent conversion obtained during the desulphurisation reaction were very low for all the sorbent materials tested. This was attributed to the formation of an impervious layer on the surface during the reaction which prevents the inner material from taking part in the desulphurisation reaction.

6.1.3 Overall conclusions

- The pH-Stat process can be used to reliably rank the performance of the different sorbent materials as sorbents in the flue gas desulphurisation process. The materials that had a higher dissolution rate also showed a higher sulphur capture capacity in the fixed-bed reactor.

- The mechanism of desulphurisation can be postulated by considering the desulphurisation data in conjunction with the dissolution data to be as follows: (a) Adsorption of SO_2 on the outer surface of water layer, (b) Hydration of SO_2 to form $SO_2.H_2O$ (c) Diffusion of $SO_2.H_2O$ inward (d) Dissolution of $Ca(OH)_2$ to form Ca^{2+} and OH^- (e) Diffusion of Ca^{2+} and OH^- outward (f) Reaction of OH^- and $SO_2.H_2O$ to form HSO_3^- and SO^{2-}_3 (g) Reaction of Ca^{2+} and SO^{2-}_3 to form calcium sulphite precipitate. The rate controlling step may be that involving OH^- or Ca^{2+} ions, which are generated by the dissolution of the sorbent surface i.e. process (f) or (g). The rate of either process (f) or (g) will increase with increasing relative humidity because the higher amount of adsorbed water can produce higher amounts of reactant to react. The rate will also increase if the dissolution rate of the sorbent material is high.

- Sorbents from different sources exhibit different reactivities. Thus in considering any material as a sorbent in flue gas desulphurisation, its reactivity must be determined experimentally.

6.2 RECOMMENDATIONS

The desulphurisation experiments were carried out at the laboratories of the Universiti Sains Malaysia (USM). However, during the course of this research work, an FGD unit has been designed at the Laboratories of Mechanical Engineering of the Tshwane University of Technology. It is thus recommended that further study on the sorbent materials should be carried in these areas:

- The low sorbent utilization of the sorbents recorded in the present research is undesirable for the economic utilization of the materials. Several researches have studied this shortcoming and have recorded increased sorbent utilization when the material is mixed with flyash. It is thus recommended that research using flyash, and bottom ash from power stations in South Africa be used with the local sorbent materials to determine whether this can increase the sorbent utilization.

- The use of additives has been shown to increase the dissolution rate in the wet FGD process. Further work can be done on the use of locally available materials like urea and organic acids to determine their potential influence on the process.

REFERENCES

ABADIE, L.M., & CHAMORRO, J.M. 2006. Valuing Flexibility: The case of an integrated gasification combined cycle power plant. *Energy Economics*, Article in Press.

ACID RAIN. Downpour in Asia? Available at: www.wri.org. Accessed on 20/5/2007.

ADANEZ, J., GARCIA-LABIANO, F., & FIERRO, V. 2000. Modelling for the high-temperature sulphation of calcium-based sorbents with cylindrical and plate-like geometries. *Chemical Engineering Science*, 55: 3665-3683.

AGNELLO, V.N. 2003. A review of the dolomite and limestone industry in South Africa. Department of Minerals and Energy. Directorate: Minerals Economics (Minerals Bureau). Republic of South Africa. Report R43/2003

AHLBECK, J., ENGMAN, T., FALTEN, S., AND VIHMA, M. 1995. Measuring the reactivity of limestone for wet flue gas desulphurization. *Chemical Engineering Science*, 50, 1081-1089.

AKOSMAN, N., & WALTERS, J.K. 2004. The role of axial dispersion in fixed beds of reacting solid particles. *Chemical Engineering and Processing*, 43: 181-185.

ALKATTAN, M., OELKERS, E.H., DANDURAND, J.-L., & SCHOTT, J. 1998. An experimental study of calcite and limestone dissolution rates as a function of pH from -1 to 3 and temperature from 25 to 80ºC. *Chemical Geology*, 151: 199-214.

ALKATTAN, M., OELKERS, E.H., DANDURAND, J.-L., & SCHOTT, J. 2002. An experimental study of calcite dissolution rates at acidic conditions and 25ºC in the presence of NaPO3 and MgCl2. *Chemical Geology*, 190: 291-302.

AL-SHAWABKEH, A., MATSUDA, H., & HASATANI, M. 1997. Dry, high-temperasture De-SO_2 and De-H_2S via treated calcium-based materials. *Energy Conversion Management*, 38: 1389-1397.

ALVAREZ, E., & GONZALEZ, J.F. 1999. High pressure thermogravimetric analysis of the direct sulphation of spanish calcium based sorbents, *Fuel* 78: 341-348.

ANDRZEJ, G.C., JANUSZ, L., ANDRZEJ, P., BOGDAN, T., & ZIMEK, Z. 2004. Operational experience of the industrial plant for electron beam flue gas treatment. *Radiation Physics and Chemistry*, 71: 442-444.

ANTONIA, M., ASTERIOS, B., & ELENI, A. 2001. The effects of limestone characteristics and calcination temperature to the reactivity of the quicklime. *Cement and Concrete research*, 31: 633-639.

BAKAN, F., LAÇIN, O., BAYRAK, B., & SARAÇ, H. 2006. Dissolution kinetics of natural magnesite in lactic acid solutions. International Journal of Mineral Processing, 80: 27-34

BALINT, S.J. 1995. Flue gas desulphurization from Scottish perspective. *Inst. Chem. Eng. Symp. Ser.*, 138: 85-95.

BARRET, E.P., JOYNER, L.G., & HALENDA, P.P. 1951. The determination of pore volume area distributions in porous substances. *Journal of American Chemical Society,* 73: 373-380.

BHATIA, S.K., & PERMULTTER, D.D. 1980. The effect of pore structure on fluid-solid reactions: Applications to the SO_2-lime reaction. *AIChE Journal,* 27: 226-234.

BOUDON, J.P. 2003. Surface chemistry of a viscose-based activated carbon cloth modified by treatment with ammonia and steam. *Carbon,* 41: 1955-1963.

BOUDON, J.P., CHEHIMI, M., BRONIEK, E., SIEMIENIEWSKA, T., & BIMER, J. Adsorption of H2S or SO2 on an activated carbon carbon cloth modified by ammonia treatment. *Carbon,* 41: 1999-2007.

BRAVO, R.V., CAMACHO, C.F., MOYA, V.M., & GARCIA, A.I. 2002. Desulphurization of $SO_2 – NO_2$ mixtures by limestone slurry. *Chemical Engineering Science,* 57, 2047 – 2058.

BROWN, G.J., MILES, N.J., & HALL, S.T. 1994. Fractal assessment of finely ground limestone for flue gas desulphurisation. *Minerals Engineering,* 7: 1057-1067.

BUELNA, G., & LIN, Y.S. 2004. Characteristics and desulfurization-regeneration properties of sol-gel-derived copper oxide on alumina sorbents. Separation and Purification Technology, 39: 167-179.

CAMA, J., AYORA, C., & LASAGA, A. 1999. The deviation from equilibrium effect on dissolution rate and on apparent deviations in activation energy. *Geochimica et Cosmochimica Acta*, 63 (17): 2481-2486.

CARMAGO, F.L., PAGLIUSO, J.D., & MILIOLI, F.E. 2003. Conversion and global reaction rate coefficient in absorption of SO_2 by different types of limestone in a fluidized bed reactor. *Engenharia Térmica*, 3: 50-57.

CHAABAN, F.B., MEZHER, T. , & OUWAYJAN, M. 2004. Options for emissions reduction from power plants: an economic evaluation. *Electrical Power and Energy Systems*, 26: 57-63.

CHU, C.-Y, HWANG, S.-J. 2005. Flue gas desulfurization in an internally circulating fluidized bed reactor. *Powder Technology*, 154: 14-23.

CHU, C.-Y., HSUEH, K.-W., HWANG, S.-J. 2000. Sulfation and attrition of calcium sorbent in a bubbling fluidized bed. *Journal of Hazardous Materials*, B80: 119-133.

COAL. 2007. All about energy. Available from: http://www.planete-energies.com/. [Accessed: 05/11/2007]

COLLET, F., BART, M., SERRES, L., & MIRIEL JACQUES. 2007. Porous structure and water vapour sorption of hemp-based materials. *Construction and Building Materials*, Article in Press.

COMSTOCK, L.K., 1998. Partnering enhances New Mexico power plant project. 6(1) Communique, April.

COOPER, C.D., & ALLEY, F.C. 1994. Air pollution: A design approach. Second Edition, Waveland Press Inc. IL.

DAVINI, P. 2000. Investigation into the desulpharisation properties of by-products of the manufacture of white marbles of Northern Tuscany. *Fuel*, 79: 1363-1369.

DAVINI, P. 2002. Properties and the reactivity of reactivated calcium-based absorbents. *Fuel*, 81: 763-770.

DEPARTMENT of Energy see UNITED STATES.

DEPARTMENT of Trade and Industry see UNITED KINGDOM.

DEPRIEST, W. & GAIKWAD, R. 2003. Economics of Lime and Limestone for control of sulphur dioxide. National Lime association – http://www.lime.org/NLAdryFGD.Pdf

DIPEZ. 2007. The Cinergetica Desulphurisation Plant (Czech Repuplic) Available at: www.dipez.cz. Accessed on 17/5/2005.

DOE, US: Clean Coal Technology Demonstration Program. Environmental Control Devices. SO_2 Control Technologies: 10-MWe Demonstration of Gas Suspension Absorption. *Project Fact Sheets* 2003.

DOGU, T. 1981. The importance of pore structure and diffusion in the kinetics of gas-solid non-catalytic reactions: reaction of the calcined limestone with SO_2. *The Chemical Engineering Journal*, 21: 213-222.

DOI, Y., NAKANISHI, I., & KONNO, Y. 2000. Operational experience of electron beam purification of flue gas. *Radiation Physics and Chemistry*, 57: 495-499.

DOWNING, R.J., RAMANKUTTY, R., & SHAH, J. 1997. An assessment model for acid deposition in Asia. *RAINS-ASIA*. World Bank Report, Washington D.C.

DREYBRODT, W., LAUCKNER, J., LIU, Z., SVENSSON, U., & BUHMANN, D. 1996. The kinetics of the reaction $H_2O + CO_2 = H^+ + HCO_3^-$ as one of the rate limiting steps for the dissolution of calcite in the system $H_2O – CO_2 – CaCO_3$. *Geochimica et Cosmochimica Acta*, 60(18): 3375 – 3381.

EIA, 2001. World energy use and carbon dioxide emissions, 1980-2001: VI. Africa. Available from: http://www.eia.doe.gov/emeu/cabs/carbonemiss/chapter6.html [Accessed: 05/11/2007].

EIA. 2004. International Energy Outlook 2004. Available at: www.eia.doe.gov. DOE/EIA-0484(2004). Accessed on 20/5/2007.

EISENLOHR, L., METEVA, K., GABROVSEK, F., & DREYBRODT, W. 1999. The inhibiting action of intrinsic impurities in natural calcium carbonate minerals to their dissolution kinetics in aqueous $H_2O – CO_2$ solutions. *Geochimica et Cosmochimica Acta*, 63(7/8): 989-1002.

ELSEVIERS, W.F., & VERELST, H. 1999. Transition metal oxides for hot gas desulphurisation. *Fuel*, 78: 601-612.

El-Wakil, M.M. 1984. *Power Plant Technology*. *McGraw-Hill International Editions*. pp 719-722.

ENCYCLOPEDIA. 2000. Encyclopedia of the atmospheric environment.

ENERGY INFORMATION ADMINISTRATION. 2007. Country Analysis Briefs – South Africa. Available from: http://www.eia.doe.gov/emeu/cabs/South_Africa/pdf.pdf [Accessed: 05/11/2007].

ENGINEERING TOOLBOX. 2005. Classification of Coal. Available from: http://www.engineeringtoolbox.com/classification-coal-d_164.html [Accessed: 06/11/2007.

European Directive 2001/80/EC of the European Parliament and of the council of 23 October 2001 on the limitation of emissions of certain pollutants into the air from Large Combustion Plants.

FELLNER P., & KHANDL V. 1999. Characterization of limestone reactivity for absorption of SO_2 from Fume gases. *Chem. Papers*, 53, 238-241.

FIERRO,V., ADANEZ, J., & GARCIA-LABIANO. 2004. Effects of pore geometry on the sintering of Ca-based sorbents during calcination at high temperatures. *Fuel*, 83: 1733-1742.

FRANDSEN, J.B.W., KIIL, S., & JOHNSSON, J.E. 2001. Optimisation of a wet FGD pilot plant using fine limestone and organic acids. *Chemical Engineering Science*, 56, 3275-3287.

GAREA, A., HERRERA, J.L., MARQUES, J.A., & IRABIEN A. 2001. Kinetics of dry flue gas desulphurisation at low temperatures using $Ca(OH)_2$: competitive reactions of sulfation and carbonation. *Chemical Engineering Science*, 56: 1397 – 1393.

GAUTELIER, M., OELKERS, E.H., & SCHOTT, J. 1999. An experimental study of dolomite dissolution rates as a function of pH from -0.5 to 5 and temperature from 25 to 80ºC. *Chemical Geology,* 157: 13-26.

GOLESWORTHY, T.A. 1999. Review of industrial gas cleaning (3). *Filtration and Separation,* 36: 16-19.

GOORISSEN, H. 2000. Thermophilic methanol utilization by sulphate reducing bacteria. *PhD thesis, Department of Microbiology of the University of Groningen,* The Netherlands.

, F.J., OLLERO, P., CABANILLAS, A., & OTERO, J. 2002. A technical pilot plant assessment of flue gas desulphurisation in a circulating fluidised bed. *Advances in Environmental Research,* 7: 73-85.

HAMMACK D.L. & GOHARA W.F. Use of stack emissions to control DBA enhanced FGD systems burning fuel highly variable in sulfur content. *EPRI-DOE-EPA Combined Utility Air Pollutant Control Symposium*. BR-1641. August 25-29, 1997.

HARIPERSAD, N. (Naushaad.haripersad@eskom.co.za). 2006. Power Station Locations. [E-mail to:] Siagi, Z.O. (siagiz@tut.ac.za) October 7.

HARSTAD, A.O., & STIPP, S.L.S., 2007. Calcite dissolution: Effects of trace cations naturally present in Iceland spar calcites. *Geochimica et Cosmochimica Acta,* 71: 56-70.

HARTMAN M., TRNKA O., VESELY V., & SVOBODA K. 1996. Predicting the rate of thermal decomposition of dolomite. *Chemical Engineering Science* 51: 5229-5232.

HARTMAN, M., & COUGHLIN, R.W. 1976. Reaction of sulphur dioxide with limestone and the grain model. *AIChE Journal*, 22: 490-497.

HARTMAN, M., & TRNKA, O. 1980. Influence of temperature on the reactivity of limestone particles with sulphur dioxide. *Chemical Engineering Science*, 35: 1189-1194.

HARTMAN, M., TRNKA, O., VESELY, V., & SVOBODO, K. 1996. Predicting the rate of thermal decomposition of dolomite. *AIChE Journal*, 51: 5229-5232.

HEELEN, G. 2002. Thermophilic methanol utilization by sulphate reducing bacteria.PhD Thesis. *Department of Microbiology of the university of Groningen*, The Netherlands.

HILL, F.F., & ZANK, J. 2000. Flue gas desulphurization by spray dry absorption. *Chemical Engineering and Processing*, 39: 45-52.

HO, C.-S., & SHIH, S.M. 1993. Factors influencing the Reaction of $Ca(OH)_2$ with SO_2. *Journal of the Chinese Institute of Chemical Engineers*, 24 (4): 187-195.

HO, C.-S., SHIH, S.-M., LIU, C.-F., CHU, H.-M, & LEE, C.-D. 2002. Kinetics of sulphation of Ca(OH)2 at low temperatures. Ind. Eng. Chem. Res., 41: 3357-3364.

HOSTEN C., & GULSUN M. 2004. Reactivity of limestone from different sources in Turkey. *Minerals Engineering*, 17, 97-99.

IEA COAL RESEARCH. 2001. Air pollution control costs for coal-fired power stations. *The Clean Coal Centre*. PF 01-12.

IEA. 2001. International Energy Agency, Coal Information.

IEA. 2007. Clean Coal Technologies. Available from: http://www.iea-coal.org.uk/content. [Accessed: 09/11/2007].

IRFAN, A., & GULSEN, D. 2001. Calcination kinetics of high purity limestones. *Chemical Engineering Journal*, 83: 131-137.

IZQUIERDO, J.F., FITÉ, C., CUNILL, F., IBORRA, M., & TEJERO, J. 2000. Kinetic study of the reaction between sulfur dioxide and calcium hydroxide at low temperature in a fixed bed reactor. *Journal of Hazardous Materials*, B76: 113-123.

KADAMBI, J.R., PRUDICH, M.E., FAN, L.S., RAGHUNATHAN, K., KHANG, S.J., & KEENER, T.C. 1998. Flue gas desulphurization for acid rain control. *Dry technologies for flue gas scrubbing*. Editor: Barbara Toole-O'Neil.

KAMINSKI JACK. 2003. Technologies and costs of SO_2-emissions reduction for the energy sector. *Applied Energy*, 75, 165-172

KANTIRANIS, N. 2003. Hydration of high-calcium quicklime with methanol-water mixtures. *Construction and Building Materials*, 17: 91-96.

KANTRINAS, N. 2003. Hydration of high-calcium quicklime with methanol-water mixtures. *Construction and Building Materials*, 17: 91-96.

KARATEPE, N., AYSEGUL, E.-M., UGUR, D., & KUCUKBAYRAK, S. 1998. Determination of the reactivity of $Ca(OH)_2$ – fly ash sorbents for SO_2 removal from flue gases. *Thermochimica Acta*, 319: 171 – 176.

KARATEPE, N., AYSEGÜL, E.-M., YAVUZ, R., KÜCÜKBAYRAK, S. 1999. Kinetic model for desulphurisation at low temperatures using hydrated sorbent. *Thermochimica Acta*, 335: 127-134.

KIIL, S., NYGAARD, H., & JOHNSON, J.E. 2002. Simulation studies of the influence of HCl absorption on the performance of a wet flue gas desulphurisation pilot plant. *Chemical Engineering Science*, 57: 347-354.

KRAMMER, G., BRUNNER, CH., KHINAST, J., & STAUDINGER, G. 1997. Reaction of $Ca(OH)_2$ with SO_2 at low temperature. *Industrial Engineering & Chemistry Research*, 36: 1410-1418.

LEE, K.T. 2004. Flue gas desulfurization studies using absorbent prepared from coal fly ash. PhD thesis. University Sains Malaysia.

LEE, K.T., BHATIA, S., MOHAMED, A.R., & CHU, K.H. 2006. Optimizing the specific surface area of fly ash-based sorbents for flue gas desulfurization. Chemosphere, 62: 89-96.

LEE, K.T., MOHAMED, A.R., BHATIA, S., & CHU, K.H. 2005: Removal of sulfur dioxide by fly ash/CaO/$CaSO_4$ sorbents. *Chemical Engineering Journal*, 114: 171-177.

LEE, Y-W., KIM, H-J., PARK, J-W., CHOI, B-U., CHOI, D-K., 2003. Adsorption and reaction behaviour for the simultaneous adsorption of NO-NO2 and SO2 on activated carbon impregnated with KOH. *Carbon*, 41: 1881-1888.

LEVENSIEL O. 1972. Chemical Reaction Engineering. 2nd Edition. New York.

LICKI, J., CHMIELEWSKI, A.G., ILLER, E., ZIMEK, Z., MAZUREK, J., & SOBOLEWSKI, L. 2003. Electron-beam flue gas treatment for multi-component air-pollution control. *Applied Energy*, 75: 145-154.

LIN, R.-B., SHIH, S.-M., & AND LIU, C.-F. 2003. Structural properties and reactivities of $Ca(OH)_2$/Flyash sorbents for flue gas desulfurization. *Ind. Eng. Chem. Res*., 42: 1350-1356.

LIN, Y.S., & DENG, S.G. 1998. Removal of trace sulfur dioxide from gas stream by regenerative sorption process. *Separation and Purification Technology*, 13: 65-77.

LIU, C.-F., & SHIH, S.-M.. 2002. A surface coverage model for the reaction of $Ca(OH)_2$ with SO_2 at low temperatures. *Journal of the Chinese Institute of Chemical Engineers*, 33 (4): 407-413.

LIU, C.-F., SHIH, S.-M, & LIN, R.-B. 2002. Kinetics of the reaction of $Ca(OH)_2$/fly ash sorbent with SO_2 at low temperatures. *Chemical Engineering Science* 57: 93 – 104.

LIU, Z. & DREYBRODT, W. 1997. Disssolution kinetics of calcium carbonate minerals in H_2O-CO_2 solutions in turbulent flow: The role of the diffusion boundary layer and the slow reaction $H_2O + CO_2 = H^+ + HCO_3^-$. *Geochimica et Cosmochimica Acta*, 61(14), 2879-2889.

LIU, Z.-S, WEY, M.-Y, & LIN C.-L. 2002. Reaction characteristics of $Ca(OH)_2$, HCl and SO_2 at low temperature in a spray dryer integrated with a fabric filter. Journal of Hazardous Materials, B95: 291-304.

LIU, Z.S. 2005. Advanced experimental analysis of the reaction of $Ca(OH)_2$ with HCl and SO_2 during the spray dry scrubbing process. Fuel, 84: 5-11.

MALAGA-STARZEC, K., PANAS, I., LINDQVIST, J.E., & LINDQVIST O. 2003. Efflorescence on thin sections of calcareous stones. *Journal of Cultural Heritage*, 4: 313-318

MALLER, G., & HOLLIDEN, J. 2003. Status of flue gas desulphurization (FGD) technology, Available online at: http://apec-egcfe.fossil.energy.gov/7thtech/p112.pdf. [Accessed on 20/04/07]

MARTINEZ, J.C., IZQUIERDO, J.F., CUNILL, F., TEJERO, J., & QUEROL, J. 1991. Reactivation of flyash and $Ca(OH)_2$ mixtures for SO_2 removal of flue gas. Ind. Eng. Chem. Res. 30: 2143-2147.

MERCADER, M.B. 2005. Reactivity of Acid Gas Pollutants with $Ca(OH)_2$ at low temperature in the presence of water vapor. *PhD Thesis Universitat de Barcelona, Facultat de Quimica*.

MITRA, A.P., & SHARMA, C. 2002. Indian aerosols-present status. Chemosphere, 49: 1175-1190

MORSE, J.W., & ARVIDSON, R.S. 2002. The dissolution kinetics of major sedimentary carbonate minerals. Earth Science Reviews, 58: 51-84.

MORTSON, M., & TELESZ, R.W. 2001. Flue gas desulphurization using recycled sodium bicarbonate. *The U.S. EPA/DOE/EPRI Combined Power Plant Air Pollution Control Symposium "The Mega Symposium".* August 20-23.

NKOMO, J.C. 2005. Energy and economic development: Challenges for South Africa. *Journal of Energy in Southern Africa*.

Nolan, P.S. 2000. Flue gas desulphurisation technologies for coal-fired power plants. *Coal-Tech 2000 International Conference*. November 13-14, Jarkata Indonesia.

OATES, J.A.H. 1998. Lime and Limestone; Chemistry and Technology, Production and Uses. *Wiley-VCH*.

ORBEY, N., DOGU, G., & DOGU, T. 1982. Breakthrough analysis of non-catalytic solid-gas reactions: reactions of SO2 with calcined limestone. *The Canadian Journal of Chemical Engineering*, 60: 314-318.

ORTIZ, G.F.J., & OLLELO, P. 2001. A Pilot plant technical assessment of an advanced in-duct desulphurization process. *Journal of Hazardous Materials*, B83: 197-218.

OZAWA, S., HUANG, L., MATSUDA, H., & HASATANI, M. 2001. Dry gas cleaning of co-existing Sox and NOx by manganese ore. *Energy Conversion and Management*, 42: 15-17.

PEMBINA INSTITUTE RELEASE. 2001. A comparison of combustion technologies for electricity generation. Available from: http://pubs.pembina.org/reports/appendix4.pdf [Accessed: 09/11/2007].

PETERSEN, E.E. 1957. Reaction of porous solids. *AIChE Journal*, 3: 443-448.

PIOTROWSKI, K., WILTOWSKI, T., SZYMANSKI, T., MONDAL, K., RATHINASWAMY, V., BREAULT, R.W., & STONAWSKI, L. 2005. Cycling effects on the methane regeneration kinetics of CuO/γ-Al2O3. *Chemical Engineering Journal*, 108: 227-237.

PLAN, L. 2005. Factors controlling carbonate dissolution rates quantified in a field test in the Austrian Alps. *Geomophology*, 68, 201-212.

PLANT, W.H.D., & MATHAY, W.L. 1999 Nickel containing materials in flue gas desulphurisation equipment. CICIND Publications, 15 (2).

POKROVSKY, O.S., GOLUBEV, S.V., & SCHOTT, J. 2005. Dissolution kinetics of calcite, dolomite and magnesite at 25ºC and 0 to 50 atm pCO_2. *Chemical Geology*, 217: 239-255.

POWERWORKS. 2007. The Chemistry of brown coal. Available from: http://www.powerworks.com.au/chemistry.pdf [Accessed: 06/11/2007].

QUIJADA, G. B. 2001. Synthesis and properties of nanostructured Sol-gel sorbents for simultaneous removal of sulphur dioxide and nitrogen oxides from flue gas. PhD thesis, University of Cincinnati.

RADOIU, M., MARTIN, D., GEORGESCU, II., CALINESCU, I., BESTEA, V., INDREIAS, I., & MATEI, C. 1998. A laboratory test unit for exhausted gas cleaning by electron beam and combined electron beam-microwave irradiation. *Nuclear Instruments and Methods in Physics Research*, B 139: 506-510.

RAMACHANDRAN, P.A., & DORAISWAMY L.K. 1982. Modelling of noncatalytic gas-solid reactions. *American Institute of Chemical Engineers*.

RANDALL S.-F. AND MATIBE D.K. 2003. Electricity and externalities in South Africa, *Energy Policy,* 31, 721-734

RAYMOND-OOI, E.H., LEE, K.T., & MOHAMED, A.R. 2004. Activity study of absorbent prepared from CaO/$CaSO_4$/Coal fly ash for SO_2 Removal at low temperatures. *The Seventh Asia-Pacific International Symposium on Combustion and Energy Utilization,* December 15-17, Hong Kong SAR.

RENEDO, M.J., & FERNANDEZ J. 2002. Preparation, characterization, and calcium utilization of fly ash/Ca(OH)2 sorbents for dry desulfurization at low temperatures. Ind. Eng. Chem. Res. 41 (10): 2412-2417.

RUBIERA, F., MORAN, A., MARTINEZ, O., FUENTE, E., & PIS, J. 1997. Influence of biological desulphurization on coal combustion performance. *Fuel Processing Technology,* 52: 165-173.

SA, 2005. National Environmental Management: Air Quality Act. *South African Government Gazette,* (27318), 476, February 24, 2005.

SCALA, F., D'ASCENZO, & M, LANCIA, A. 2004. Modelling Flue gas desulphurisation by spray-dry absorption. *Separation and Purification Technology*, 34: 143-153

SCHOUBYE, P., ENEVOLDSEN, S., TOPSOE, H., & RICCI, R. 2001. The SNOX process for power plants using high sulphur fuels. *Sulphur International Conference*, Marakesh, Morocco. 28 October.

SHIH, S.-M., LIN, J.-P., SHIAU, G.-Y. 2000. Dissolution rates of limestones of different sources. *Journal of Hazardous Materials*, B79, 159-171.

Skaninavisk Miljø Service (SMS), Available online at: http://www.sms.dk/seawater.htm. [Accessed on 15/03/07]

SOUTH AFRICA. Year Book 2006/2007 – 16. Minerals, Energy and Geology. Available from: http://www.gcis.gov.za/docs/publications/yearbook/ [Accessed:05/11/2007]

SRIVASTAVA, R.K. 2000. Controlling SO_2 emissions: A Review of Technologies. US EPA/600/R-00/093.

STEIN, J., KIND, M., SCHLÜNDER, E.-U. 2002. The influence of HCl on SO_2 absorption in the spray dry scrubbing process. *Chemical Engineering Journal*, 86: 17-23.

STERGARSEK, A., GERBEC, M., KOCJANČIČ, R., & FRKAL, P. 1999. Modelling and experimental measurements of limestone dissolution under enhanced wet limestone FGD process conditions. *Acta Chim. Slov.*, 46(3): 323-338.

SULPHUR DIOXIDE. 2006. In: Encyclopedia of the Atmospheric Environment. Available from: http://www.ace.mmu.ac.uk/eae/english.html [Accessed: 05/11/2007]

SUYADAL, Y., EROL, M., & OGUZ, H. 2005. Deactivation model for dry desulphurization of simulated flue gas with calcined limestone in a fluidized bed reactor. *Fuel*, 84: 1705-1712.

TAKASHINA, T., HONJO, S., UKAWA, N, & IWASHITA, K. 2002. Effect of ammonium concentration on SO2 absorption in a wet limestone gypsum FGD process. *The Society of Chemical Engineers, Japan*, 35, 197-204.

TAYLOR, H.S., & NISCHT, W. 1998. San Juan Generating Station FGD retrofit project update, Power-Gen International '98, December 9-11, Orlando, Florida, USA.

TURKAN, K., & SEFA, K. 2004. Deactivation models for sulfur dioxide adsorption on silica gel. *Advances in Environmental Research*, 8: 417-424.

UNITED KINGDOM. Department of Trade and Industry. 2000. Technology Status Report 012: Flue gas desulphurisation technologies. CB013

UNITED STATES. Department of Energy. 1999 (1). Clean Coal Demonstration Program, Project Factsheets. DOE/FE-0402.

UNITED STATES. Department of Energy. 1999 (2). Clean Coal Technology: Advanced Technologies for the control of Sulphur Dioxide Emissions from Coal-Fired Boilers. Technical Report Number 12.

UNITED STATES. Department of Energy. 2003. Clean Coal Technology Demonstration Program. Environmental Control Devices. SO_2 Control Technologies: 10-MWe Demonstration of Gas Suspension Absorption. *Project Fact Sheets* 2003.

UNITED STATES. Department of Energy. 2006. Kentucky pioneer energy LLC integrated gasification combined cycle project 2 MW fuel cell demonstration. DE-FC21-95MC31262.

VAN DER RIET, M., & BEGG, J.H. 2003. Clean Coal Technologies for South Africa. ESI Africa, 2.

WILLIAMS, P.J. 1999. Wet flue gas desulphurization pilot plant testing of high velocity absorber modules. *EPRI-DOE-EPA Combined Utility Air Pollutant Control Symposium*. August 16-20, Atlanta, Georgia, USA.

XIAOXUN , M., KANEKO, T., XU, G., & KATO, K. 2001. *Influence of gas components on removal of SO_2 from flue gas in the semidry FGD process with a powder-particle sprouted bed*. Fuel, 80: 673-680.

XIAOXUN, M., KANEKO, T., TASHIMO, T., YOSHIDA, T, & KATO, K. 2000. Use of limestone for SO_2 removal from flue gas in the semidry FGD process with a powder-particle sprouted bed. *Chemical Engineering Science*, 55: 4643-4652

XIE, J., WANG, X., & DENG, J. 2004. Modifying the pore structure of Pit-ACF with the chemical vapor deposition of methane and propylene. *Microporous and Mesoporous Materials*, 76, 167-175.

XIE, W., LIU, K., PAN, W-P., & RLEY J.T. 1999. Interactions between emissions of SO_2 and HCl in fluidized bed combustors. *Fuel*, 78: 1425-1436.

YASYERLI, S., IRFAN, A., GULSEN. D., & TIMUR, D. 2002. Removal of hydrogen sulphide by clinoptilolite in a fixed-bed adsorber. *Chemical Engineering & Processing*, 41: 785-792.

YUQING, Y.2003. The status of FGD technology and its prospects in coal-fired power plants in Sichuan Province – China. Available online at: http://apec-egcfe.fossil.energy.gov/7thtech/p90.pdf. [Accessed on 10/04/07].

YUZHONG, L., HUILING, T., CHUNYUA, M., YUQUN, Z., & XUCHANG, X. 2004. Analytical study on approach to adiabatic saturation temperature and the control scheme for the amount of water sprayed in the semi-dry FGD process. *Fuel*, 83: 2255-2264.

ZHENG, J. YATES, G., & ROWE, P.N. 1982. A model for desulphurization with limestone in a fluidized bed combustor. *Chemical Engineering Science*, 37: 167-174.

ZHENG, Y., KIIL, S., JOHNSSON, J.E., & ZHONG, Q. 2002. Use of Spray dry absorption product in wet flue gas desulphurisation plants: pilot scale experiments. *Fuel*, 81: 1899-1905.

APPENDIX

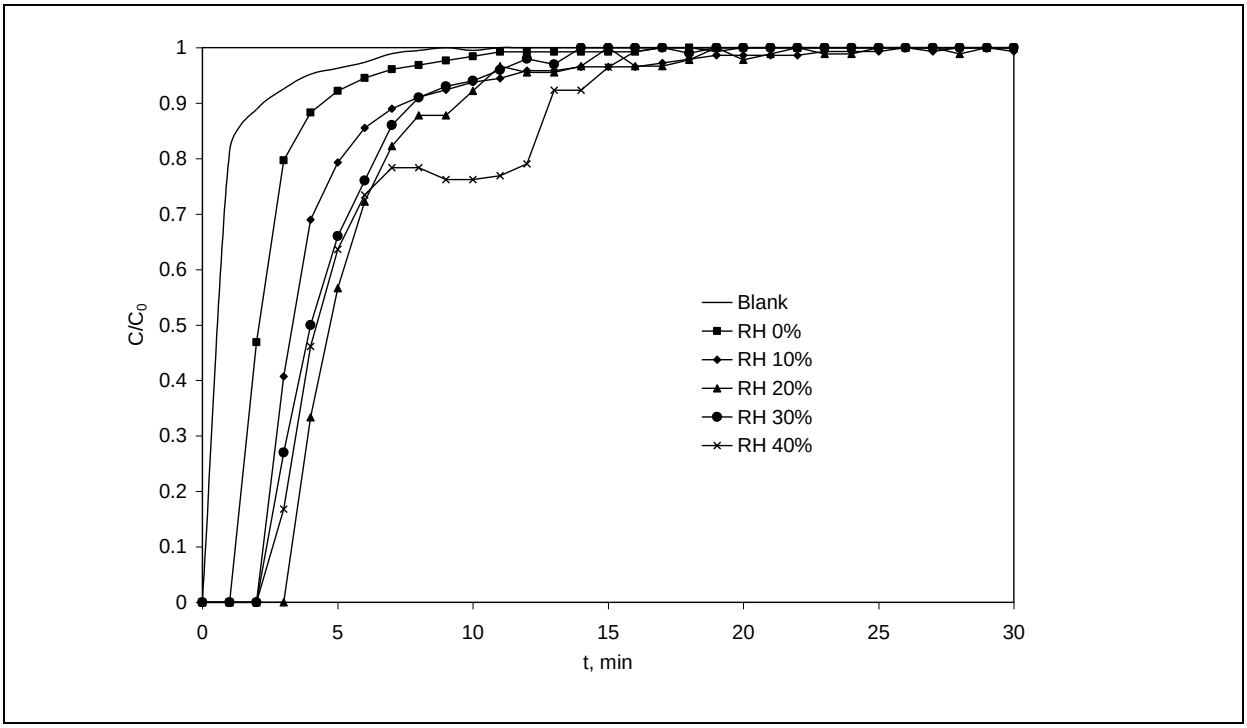

FIGURE A. 1: SO_2 Breakthrough curves for sample G at various relative humidities (RH). C_o = 2000 ppm, T_R = 80°C

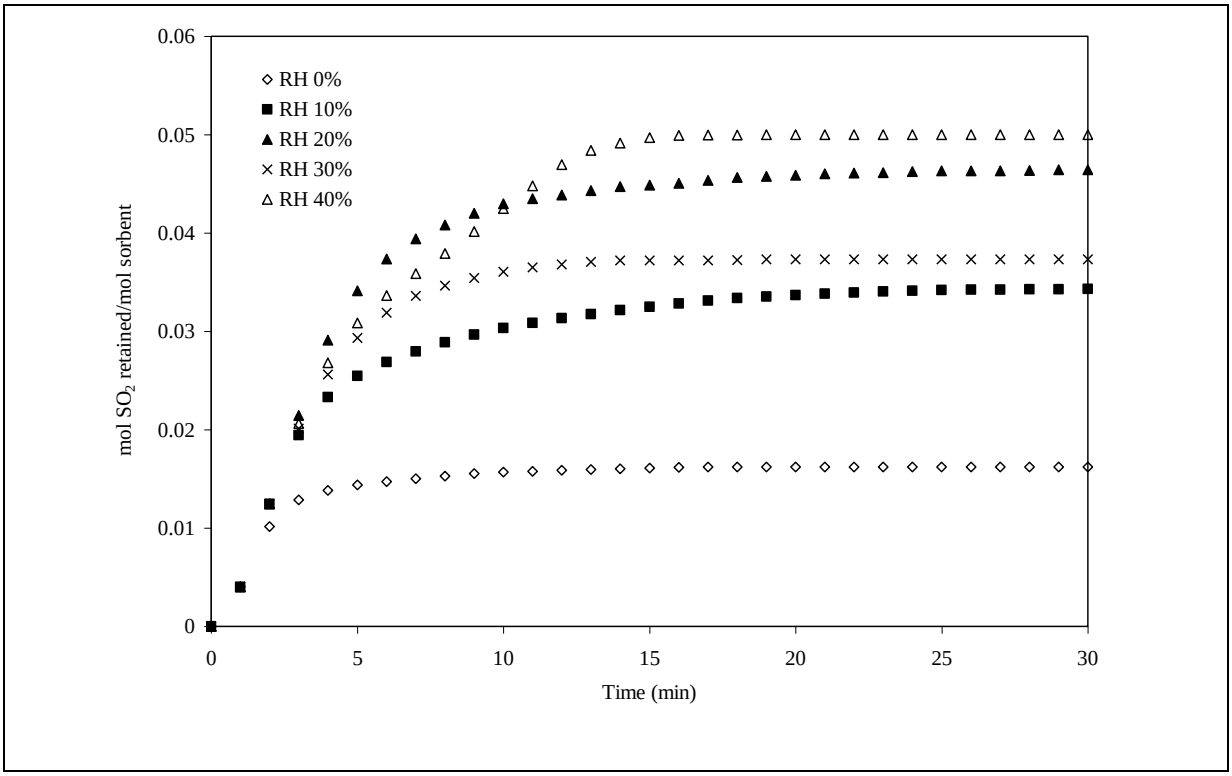

FIGURE A. 2: Effect of relative humidity on the conversion of sample E. Operating conditions: C_o = 2000 ppm, T_R = 80°C

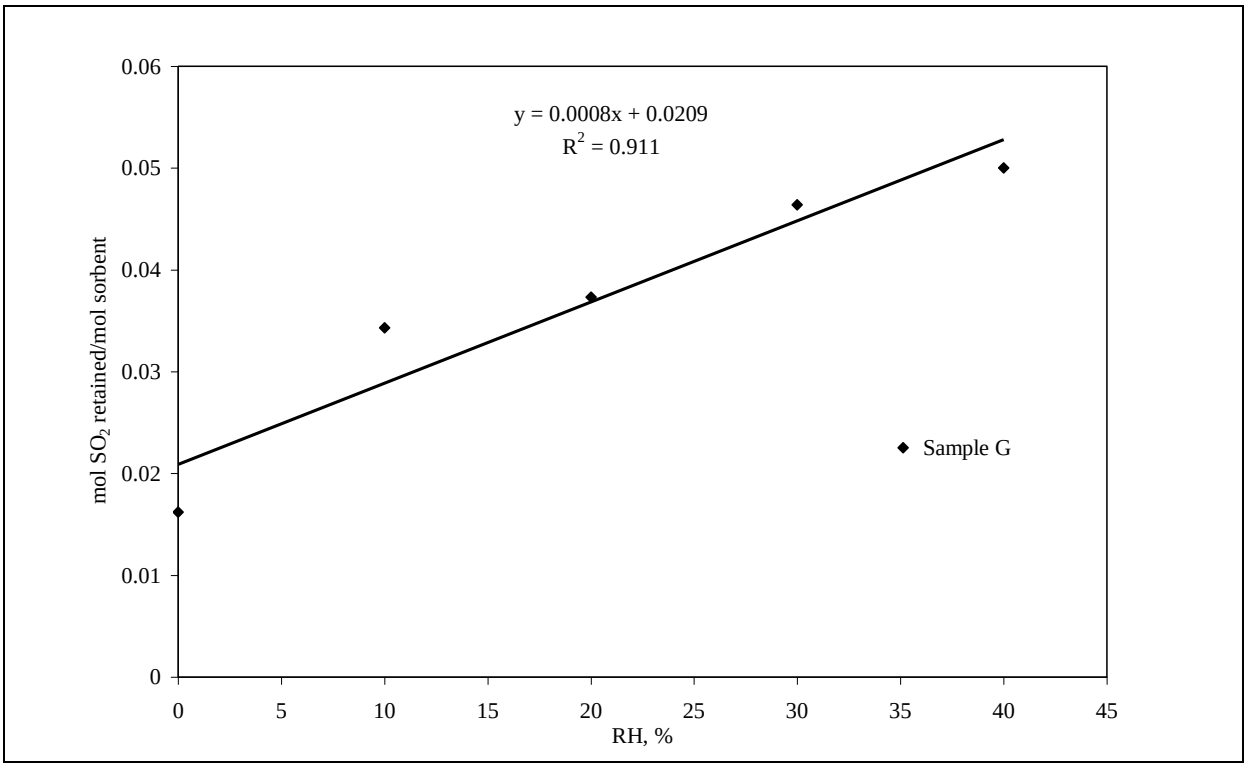

FIGURE A. 3: Influence of relative humidity on the maximum amount of SO_2 retained/mol of sample G. T_R = 80°C, C_0 = 2000 ppm

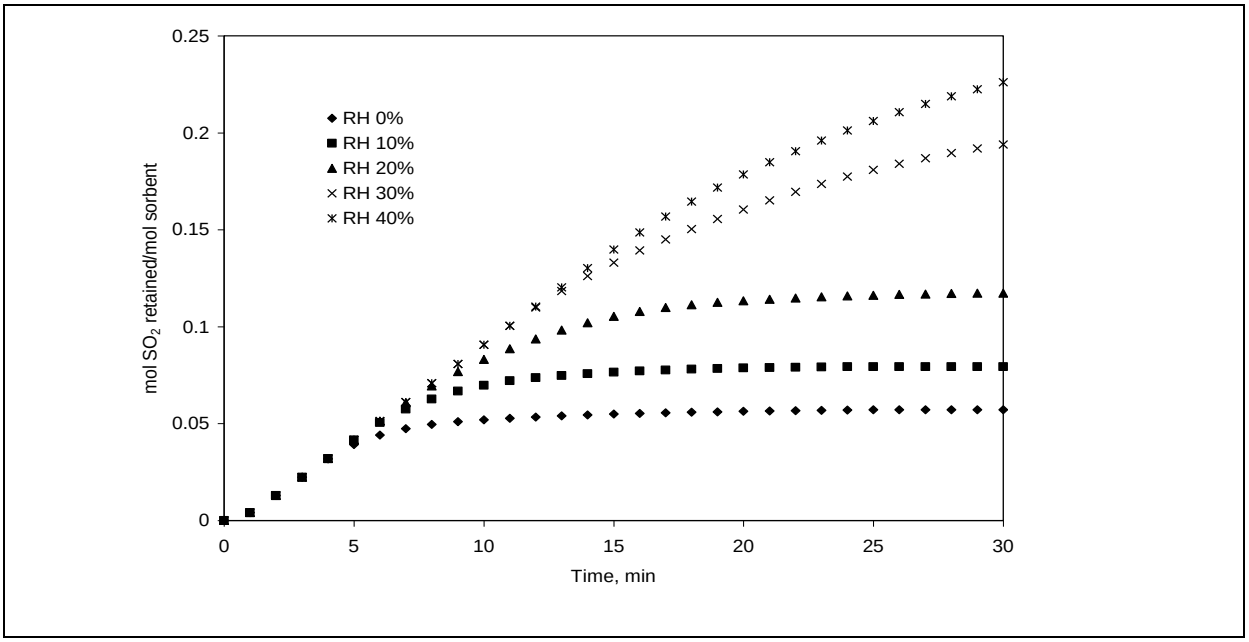

FIGURE A. 4: Effect of relative humidity on the conversion of sample E. Operating conditions: C_o = 2000 ppm, T_R = 80°C

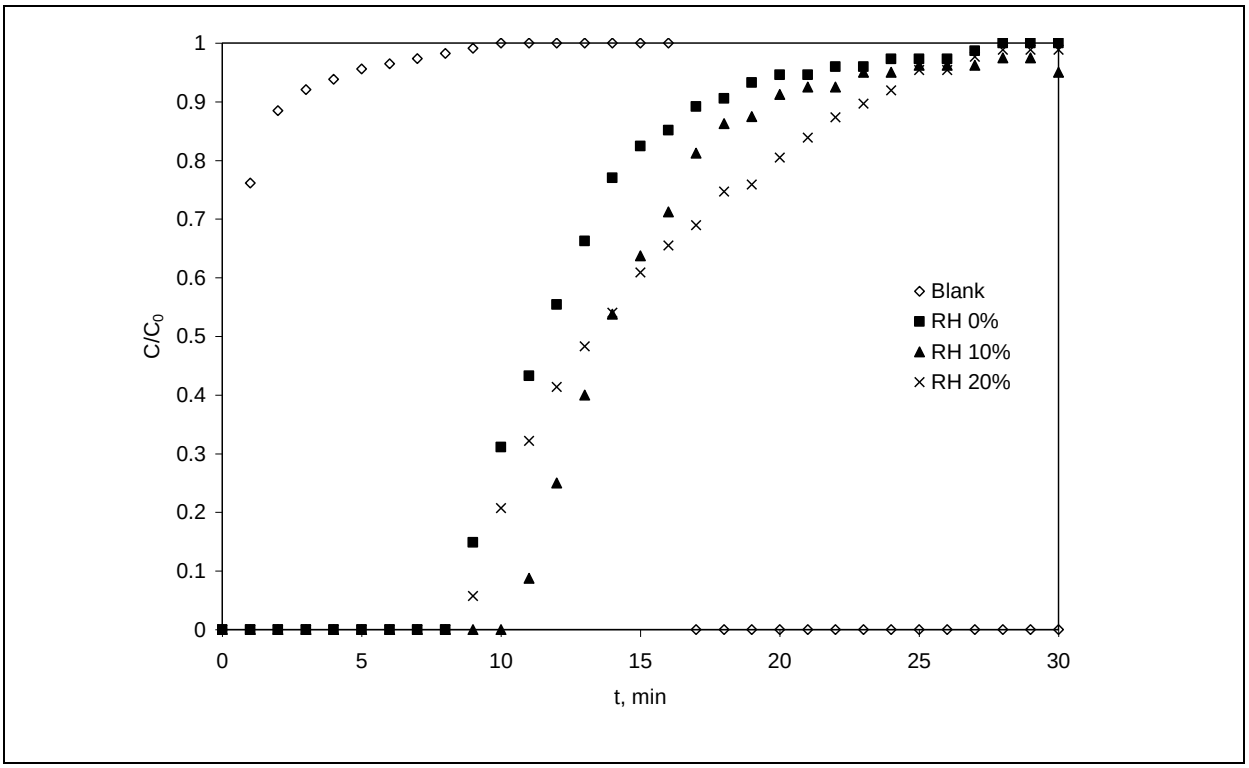

FIGURE A. 5: SO_2 Breakthrough curves for sample H at various relative humidities (RH). C_o = 2000 ppm, T_R = 80°C

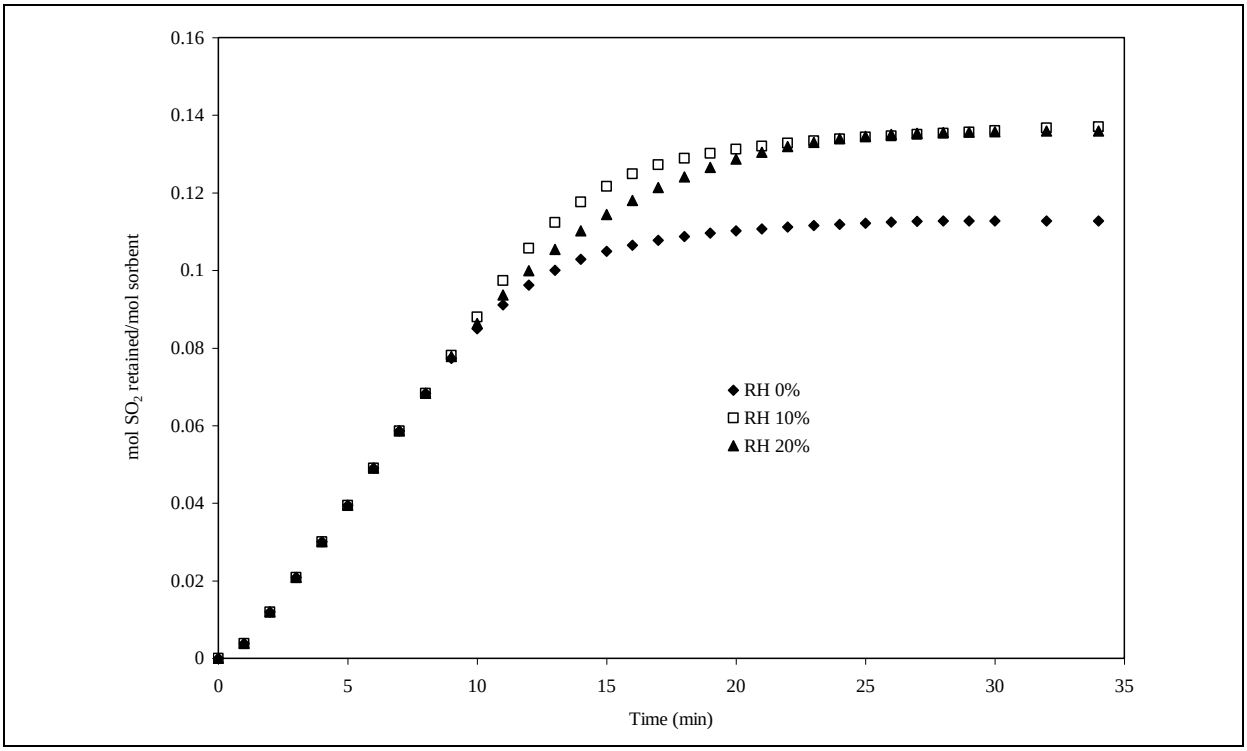

FIGURE A. 6: Effect of relative humidity on the conversion of sample H. Operating conditions: C_o = 2000 ppm, T_R = 80°C

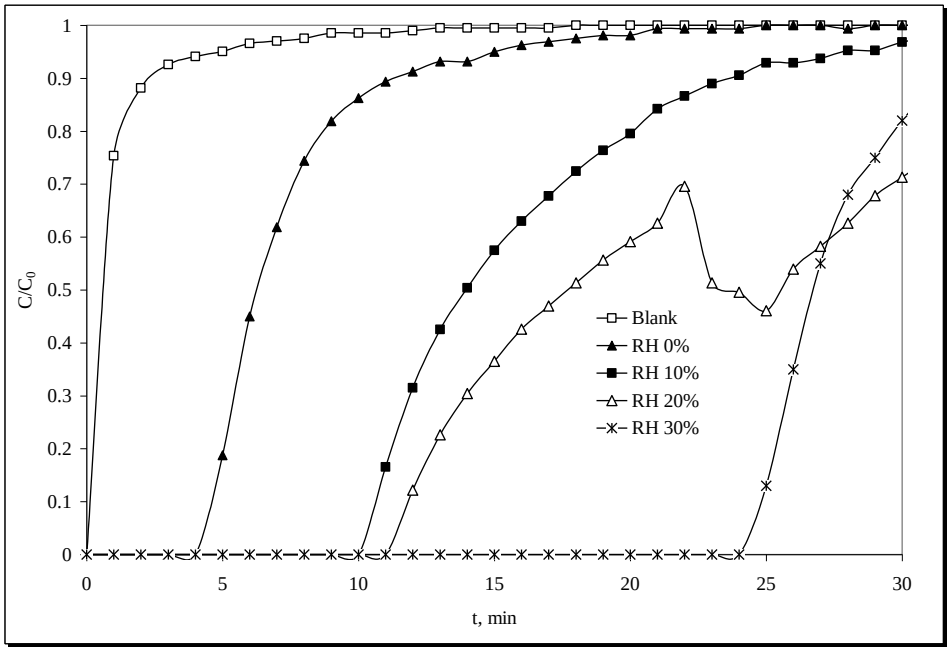

FIGURE A. 7: SO_2 Breakthrough curves for sample B at various relative humidities (RH). C_o = 2000 ppm, T_R = 80°C

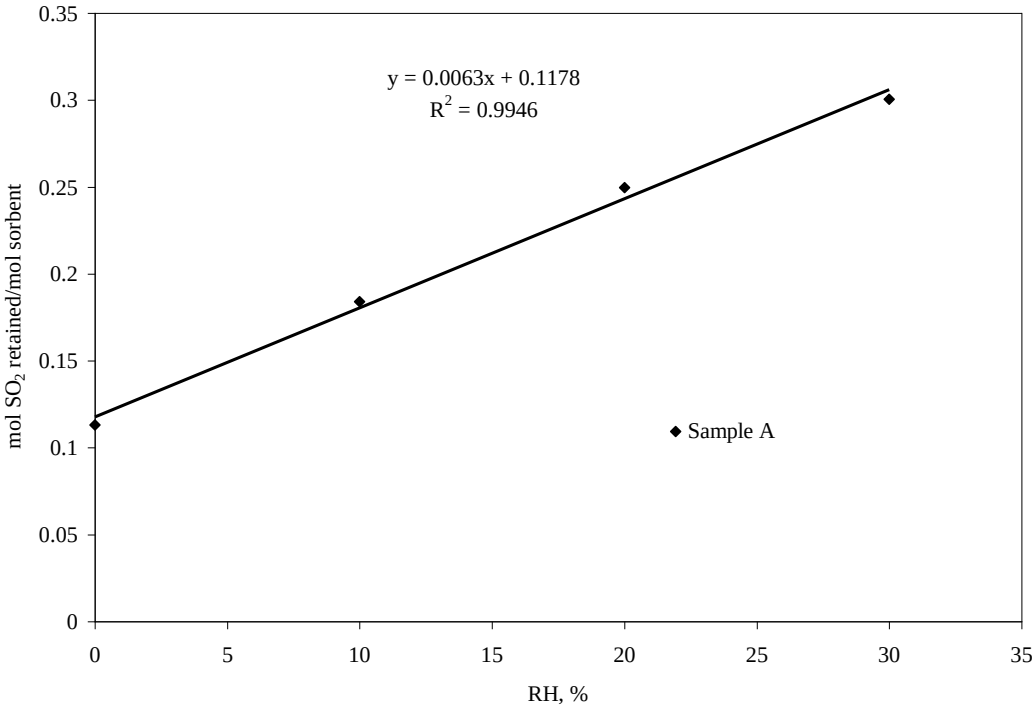

FIGURE A. 8: Influence of relative humidity on the maximum amount of SO_2 retained/mol of sample A. T_R = 80°C, C_0 = 2000 ppm

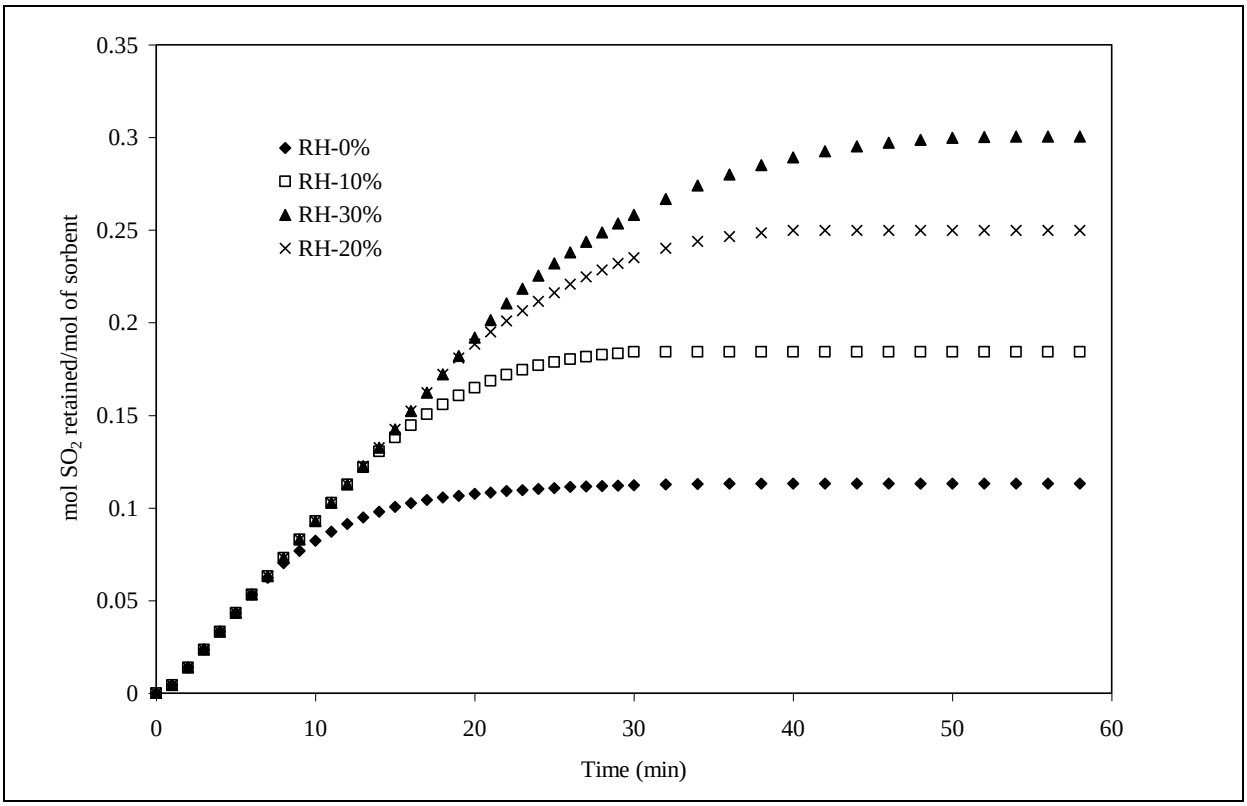

FIGURE A. 9: Conversion of sample A as a function of relative humidity and reaction time. T_R = 80°C, C_0 = 2000 ppm

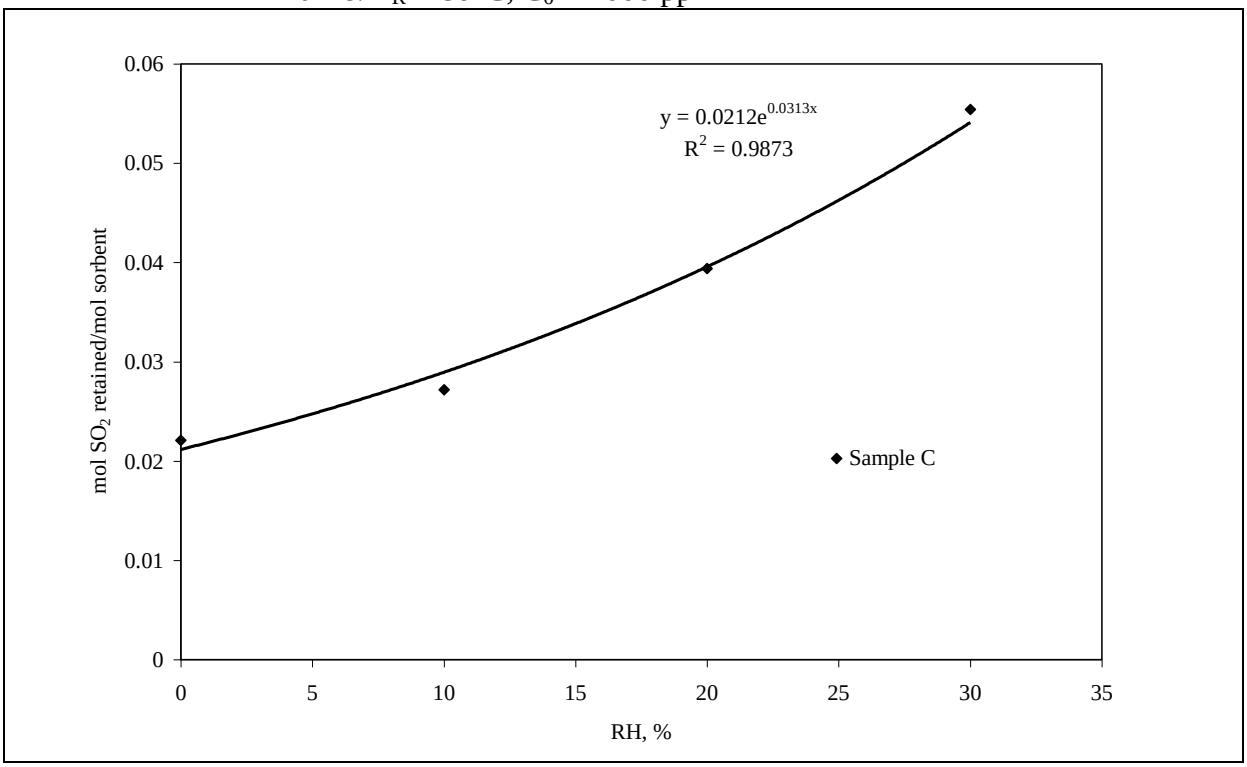

FIGURE A. 10: Influence of relative humidity on the maximum amount of SO_2 retained/mol of sample C. T_R = 80°C, C_0 = 2000 ppm

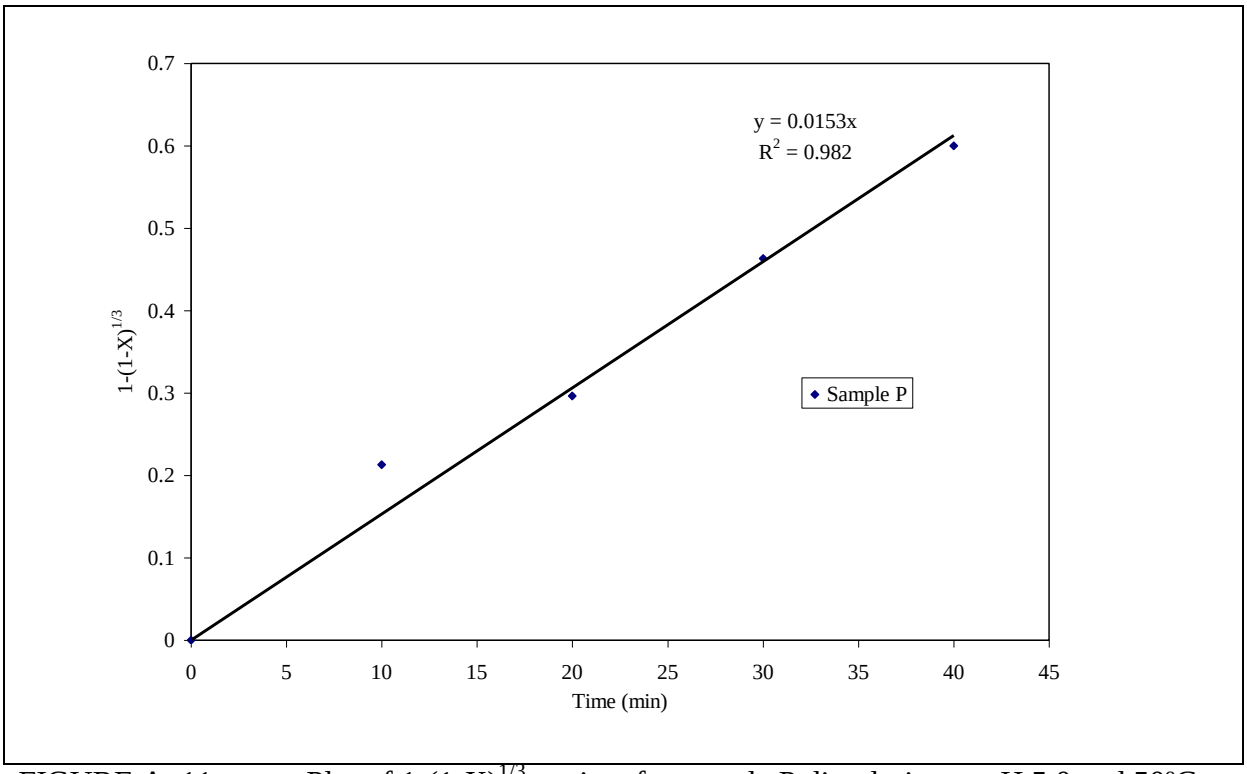

FIGURE A. 11: Plot of $1-(1-X)^{1/3}$ vs time for sample P dissolution at pH 5.0 and 50ºC

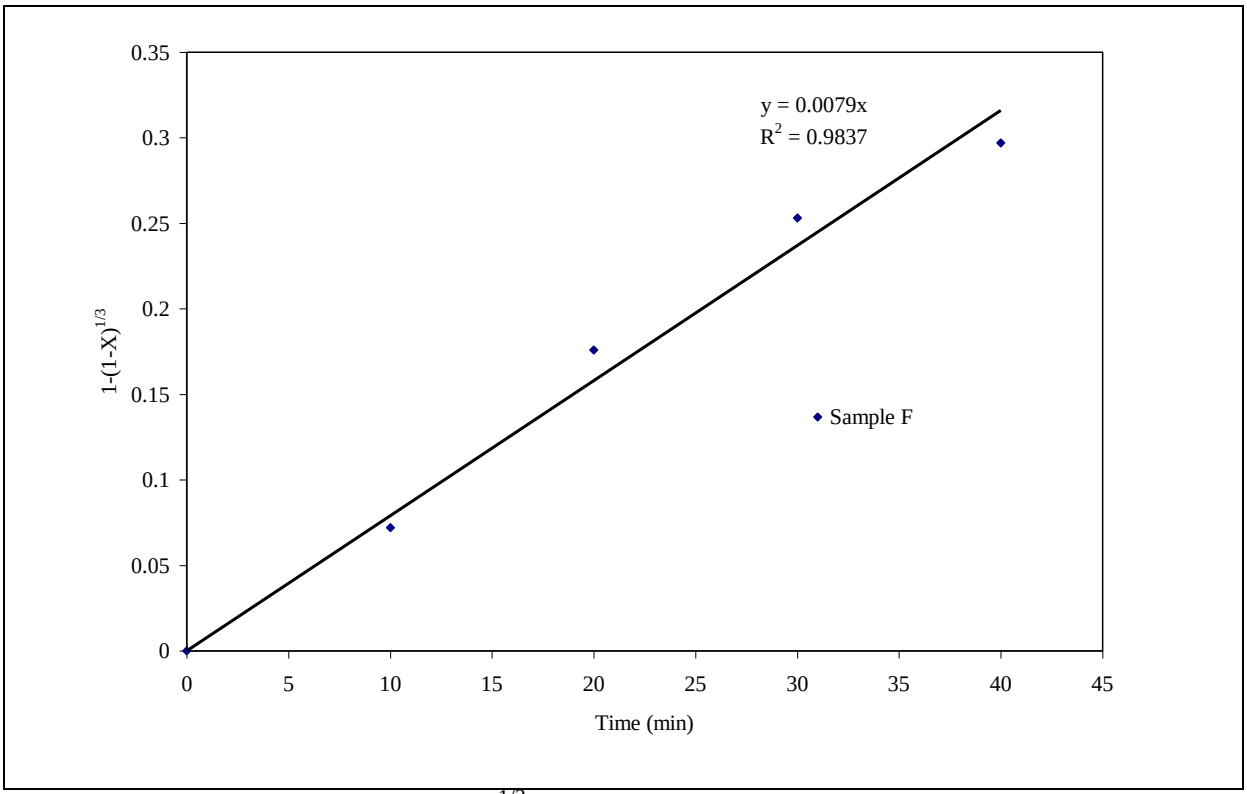

FIGURE A. 12: Plot of $1-(1-X)^{1/3}$ vs time for sample F dissolution at pH 5.0 and 50ºC

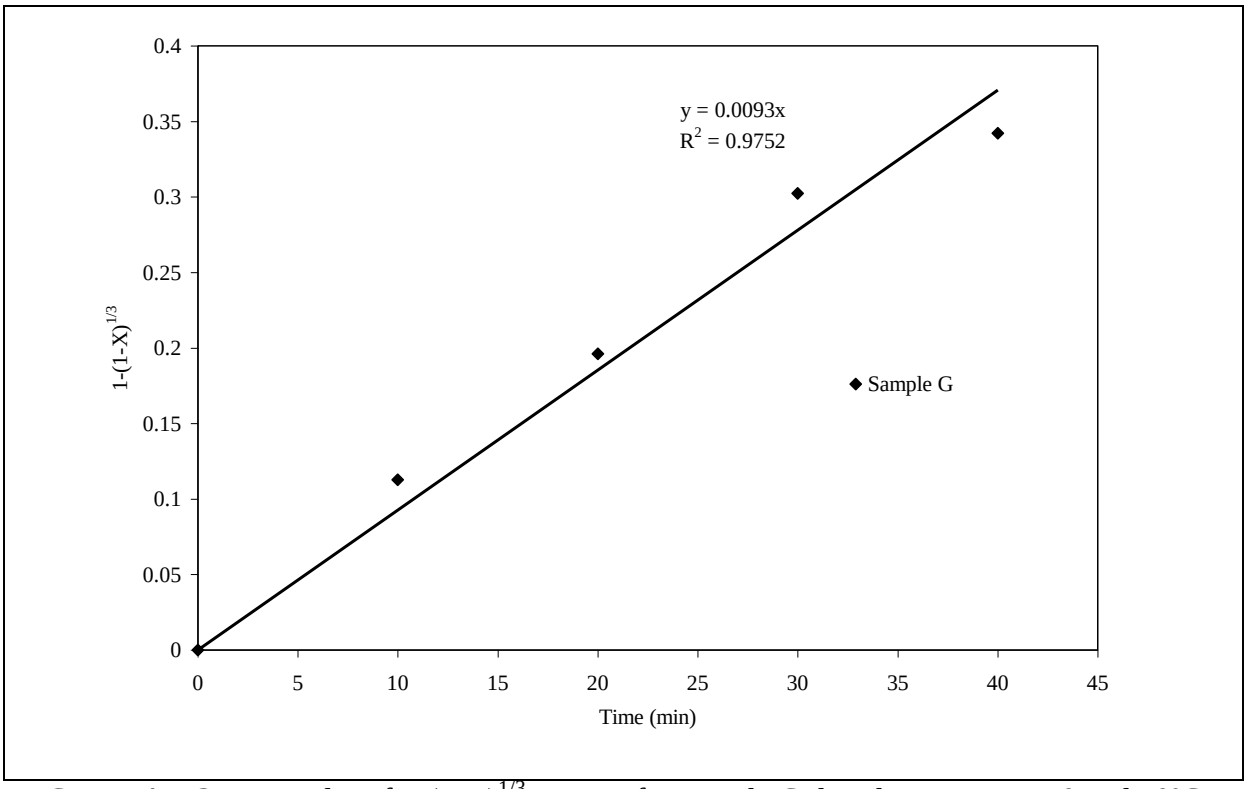

FIGURE A. 13: Plot of $1-(1-X)^{1/3}$ vs time for sample G dissolution at pH 5.0 and 50ºC

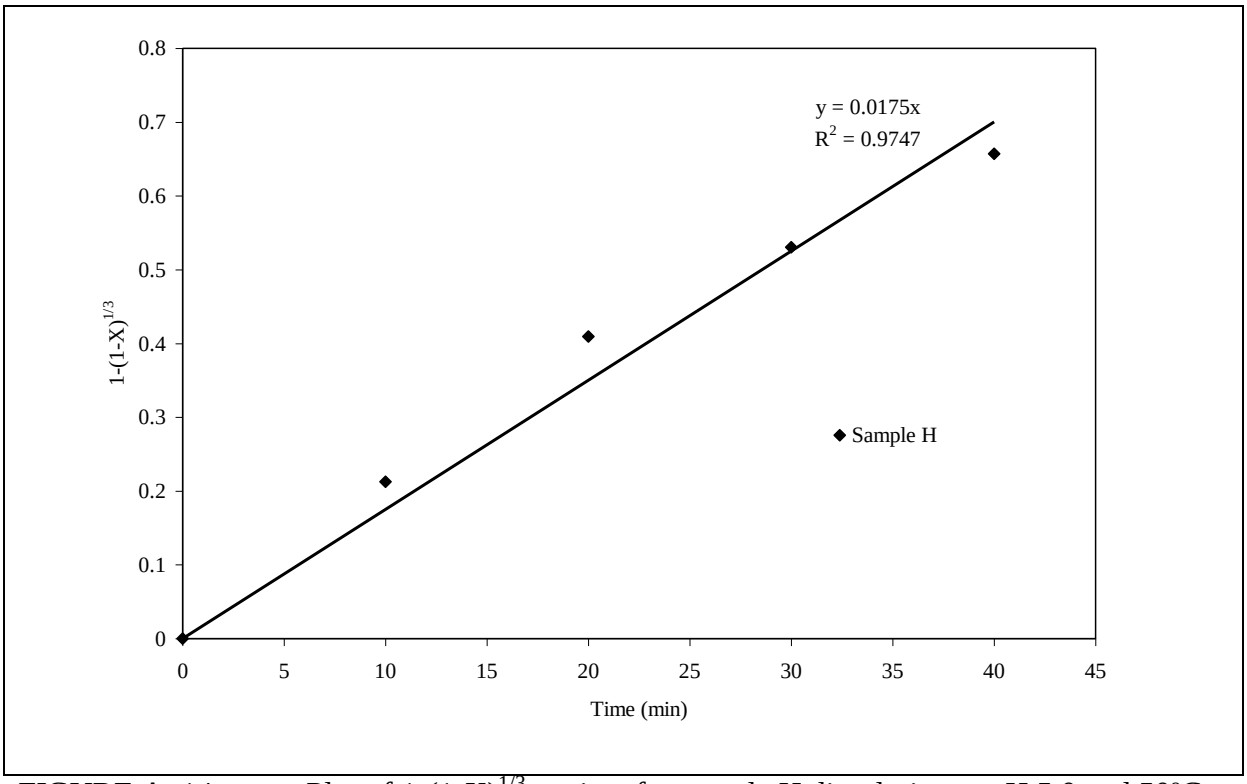

FIGURE A. 14: Plot of $1-(1-X)^{1/3}$ vs time for sample H dissolution at pH 5.0 and 50ºC

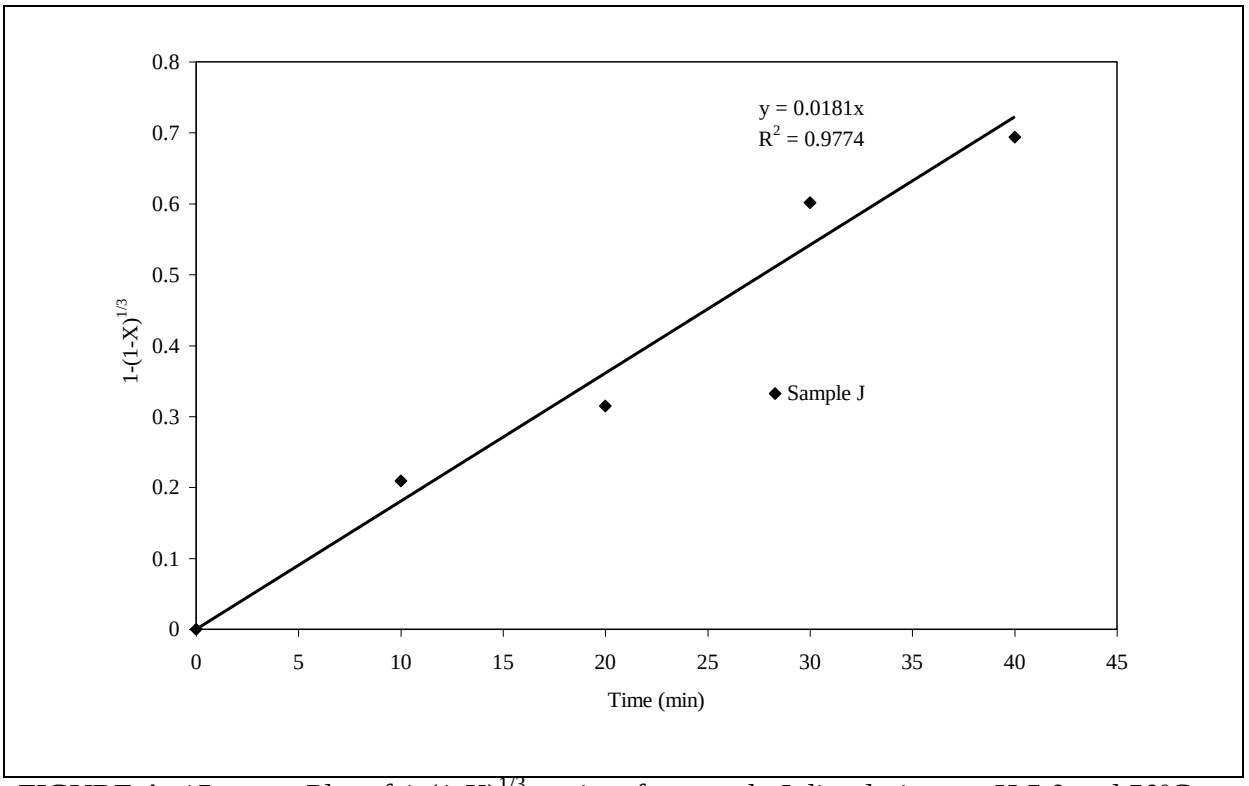

FIGURE A. 15: Plot of $1-(1-X)^{1/3}$ vs time for sample J dissolution at pH 5.0 and 50ºC

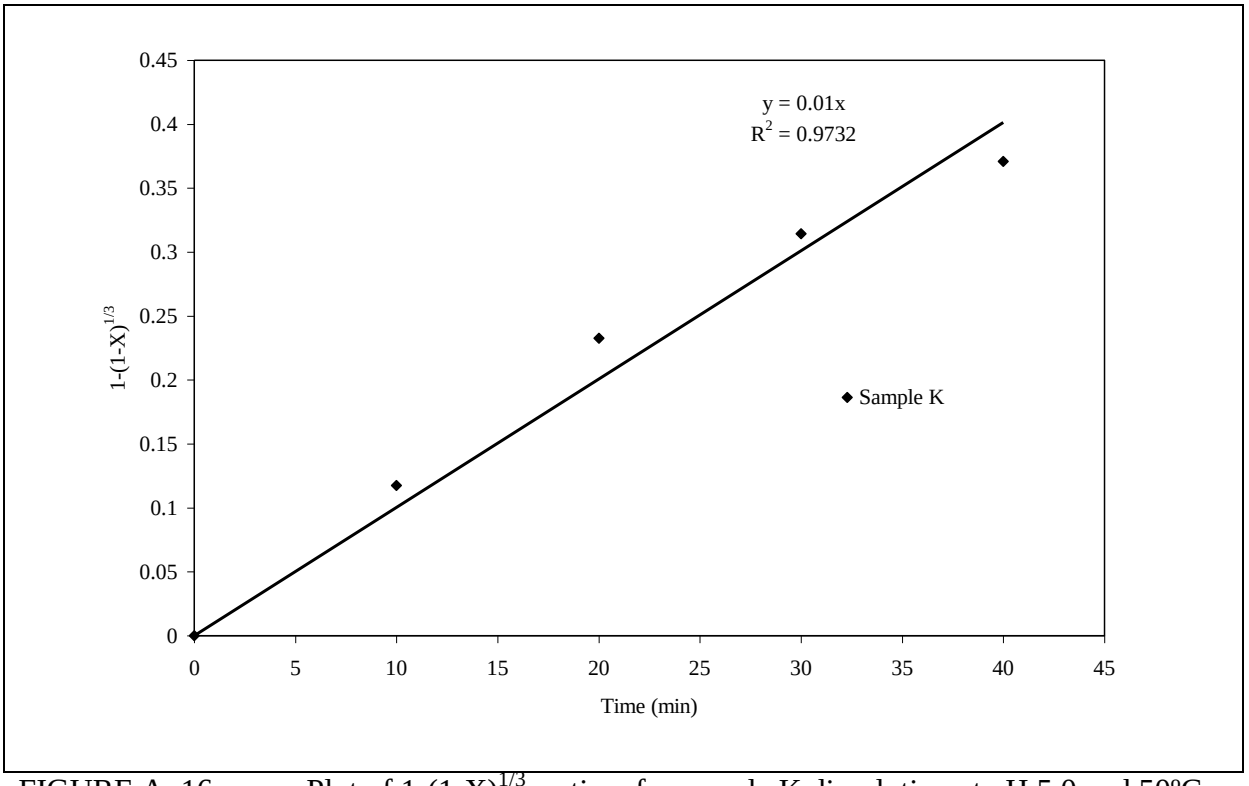

FIGURE A. 16: Plot of $1-(1-X)^{1/3}$ vs time for sample K dissolution at pH 5.0 and 50ºC

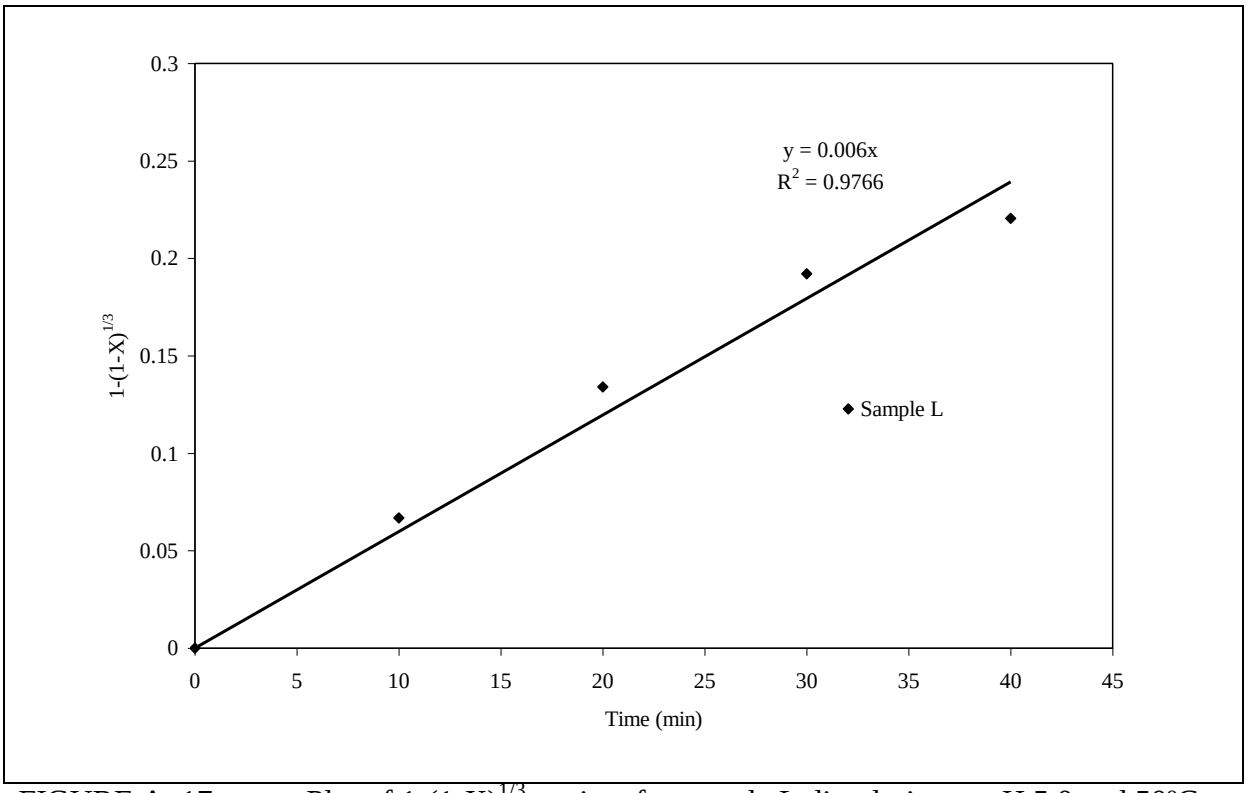

FIGURE A. 17: Plot of $1-(1-X)^{1/3}$ vs time for sample L dissolution at pH 5.0 and 50ºC

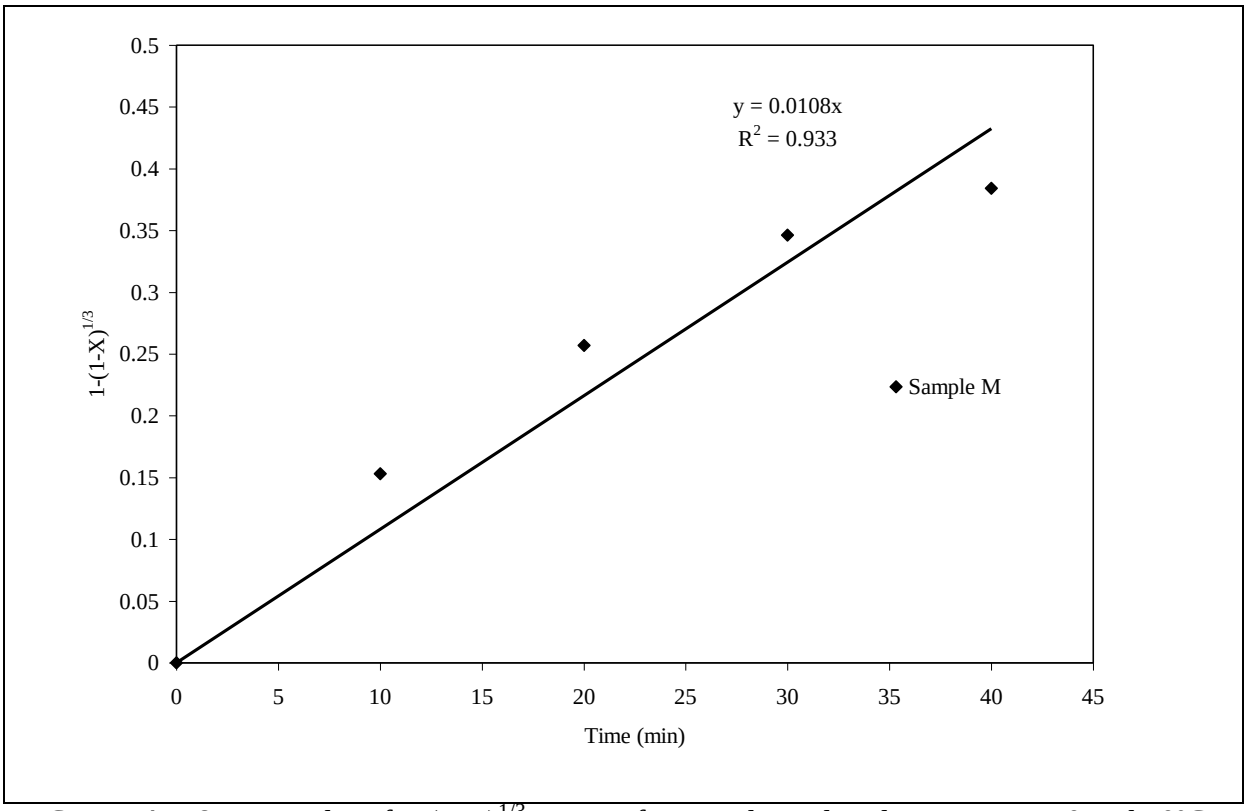

FIGURE A. 18: Plot of $1-(1-X)^{1/3}$ vs time for sample M dissolution at pH 5.0 and 50ºC

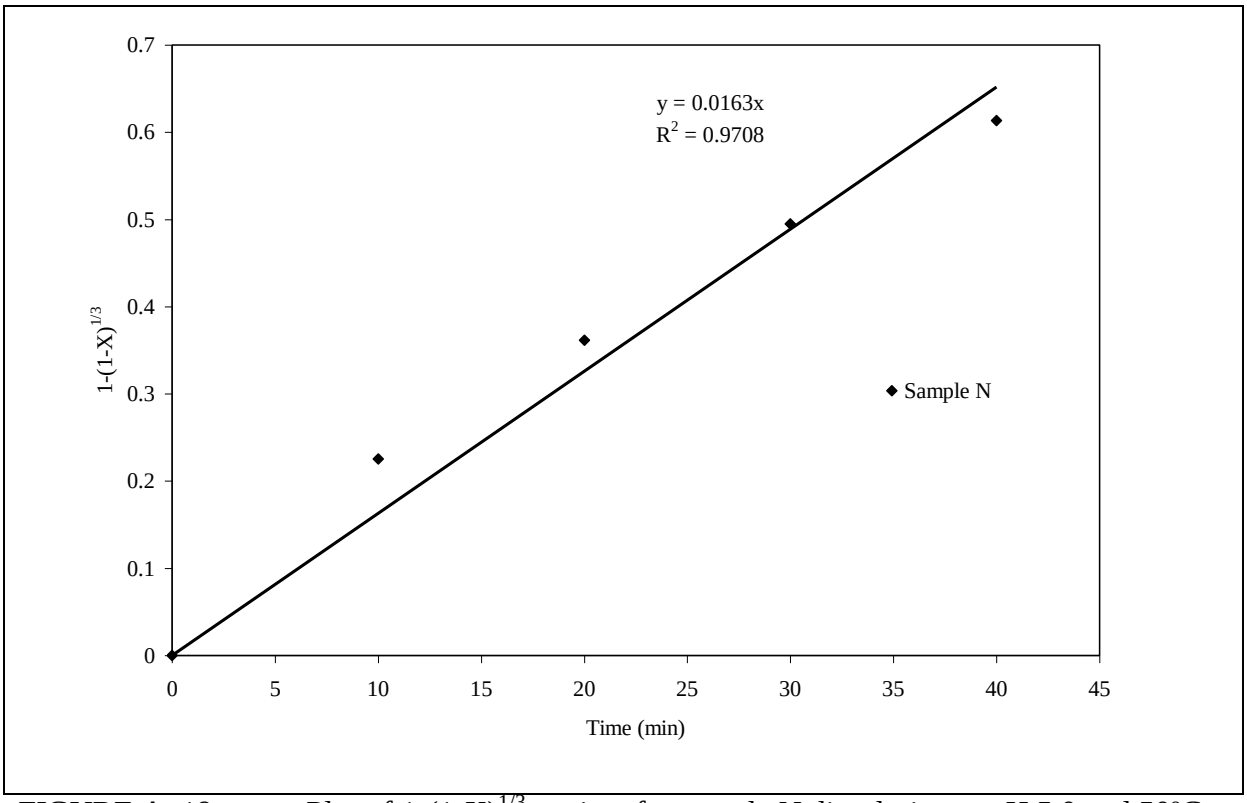

FIGURE A. 19: Plot of $1-(1-X)^{1/3}$ vs time for sample N dissolution at pH 5.0 and 50ºC

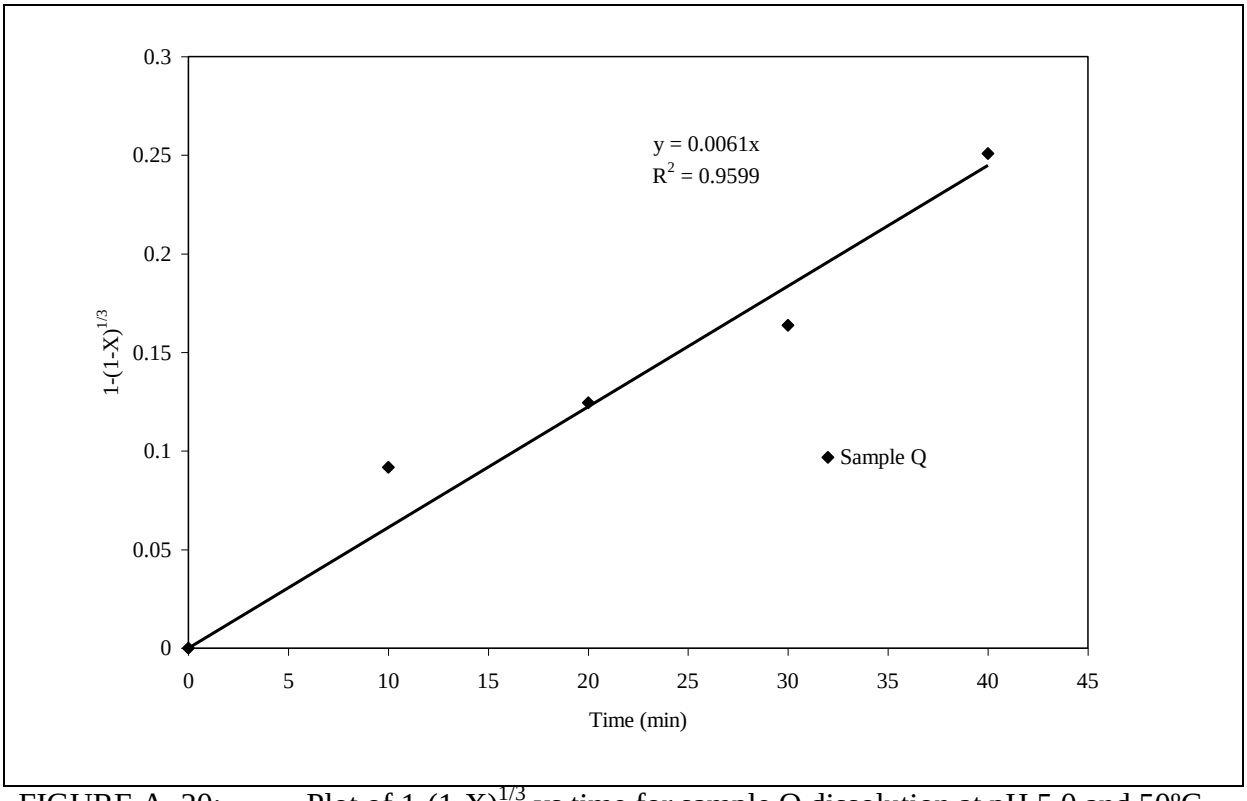

FIGURE A. 20: Plot of $1-(1-X)^{1/3}$ vs time for sample Q dissolution at pH 5.0 and 50ºC

GLOSSARY

Alkalinity The capacity of water to neutralize acids, a property imparted by the water's content of carbonates, bicarbonates, hydroxides and occasionally borates, silicates and phosphates.

Ash The incombustible inorganic matter in fuels such as coal.

Ash free basis The method of reporting fuel analysis whereby ash is deducted and other constituents are recalculated to 100%.

Baghouse A facility constructed at some coal-fired power plants to remove particulate matter (fly ash) from the flue gas by the use of fabric filter bags that mechanically trap particulate (fly ash) carried in the flue gases.

Beneficiation Improvement of the chemical or physical properties of a raw material or intermediate product by the removal or modification of undesirable components or impurities.

Bottom ash Agglomerated ash particles formed in pulverized coal furnaces that are too large to be carried in the flue gases and fall through open grates to an ash hopper at the bottom of the furnace.

Bulk density The mass of a material per unit volume including voids. Bulk density is usually reported on a dry basis.

Calcium sulfite ($CaSO_3$) The primary product (or byproduct) of a wet flue gas desulfurization system where there is no forced oxidation and lime or limestone is used as the reagent.

Carbon The principal combustible constituent of all fuels.

Clean coal combustion The burning of coal, coal culm, or coal fines in a furnace designed to operate to minimize emissions (that is a fluidized bed or aerated fluidized bed, etc.) or coal burned in the presence of alkaline materials, which combine to reduce emissions.

Coal A brown to black combustible sedimentary rock composed principally of consolidated and chemically altered plant remains. All coals are classified as anthracite, bituminous, sub-bituminous or lignite.

Coal combustion products (CCPs) Fly ash, bottom ash, boiler slag, fluidized-bed combustion (FBC) ash, or flue gas desulfurization (FGD) material produced primarily from the combustion of coal or the cleaning of the stack gases.

Co-firing The firing of two dissimilar fuels at the same time in the same boiler.

Economizer A heat recovery device designed to transfer heat from the products of combustion to a fluid, usually feedwater.

Fly ash A product of burning finely ground coal in a boiler to produce electricity. Physically, it is a very fine, powdery material, composed mostly of silica.

Electrostatic precipitator (ESP) A facility that removes fly ash from the flue gas by producing an electric charge on the fly ash and collecting it electrostatically.

Flue gas desulfurization (FGD) Removal of gaseous sulfur dioxide from boiler exhaust gas. Primary types of FGD processes are wet scrubbers, dry scrubbers, and sorbent injection. Sorbents include lime, limestone, sodium-based compounds, and high-calcium coal fly ash.

Forced oxidation A process employed to supply additional air in wet FGD systems, resulting in a predominantly calcium sulfate dihydrate (gypsum) byproduct.

Gypsum Name for calcium sulfate dihydrate ($CaSO_4 \cdot 2H_2O$); the common name for the mineral consisting primarily of fully hydrated calcium sulfate, $CaSO_4 \cdot 2H_2O$ or calcium sulfate dihydrate.

Heat of hydration Heat evolved by chemical reactions with water such as that evolved during the setting and hardening of Portland cement or quicklime.

Hygroscopic The term describing a compound that can absorb water vapor from the atmosphere.

in situ oxidation (wet FGD) A process in which both SO_2 absorption and oxidation are carried out within the scrubber.

Lime Calcium oxide (CaO).

Loss on Ignition (LOI) The weight change of a material when it is heated under prescribed conditions.

Low NO_x Burners (LNB) A combustion technology for reducing the emissions of nitrogen oxides (NO and NO_2, collectively referred to as NO_x) from coal fired power plants.

Organic Chemical compounds which contain carbon and hydrogen; chemicals associated with living entities.

Parts per million (PPM) 1×10^{-6} - a proportion by weight measurement equivalent to one unit weight of analyte per million unit weights of matrix.

Petrographic analysis The determination of the structural, mineralogical and chemical character of coal, ash or slag.

pH the logarithm of the reciprocal of the hydrogen ion activity in aqueous solutions.

Pulverized coal (PC) combustion refers to any combustion process that uses very finely ground (pulverized) coal in the process.

Reagent A substance used, because of its chemical activity, typically to reduce emissions or improve opacity from coal fired power plants. E.g. lime and limestone used for wet FGD.

Slurry A mixture of water and any finely divided insoluble material (fly ash, slaked lime, etc) in suspension.

Sorbent The term applied in some combustion systems, to the chemical compounds that are added to the gas side of the steam generator to reduce emissions. (Example: Limestone used in FGD systems).

Sulfur One of the elements present in varying quantities in coal that contributes to environmental degradation when coal is burned.

Trace element An element present in extremely small quantities. Metals are the predominant, naturally occurring trace elements in coal.

NOMENCLATURE AND ABBREVIATIONS

H^+	Hydrogen ion
$k^0_{H^+}$	The physical mass transfer coefficient for H^+ in Equation 5.7
D_{OH^-}	The diffusivity of OH^- ion in Equation 5.7
D_{H^+}	The diffusivity of H^+ ion in Equation 5.7
C_A	bulk concentration (mol cm^{-3})
E_a	activation energy (kJ mol^{-1})
k	reaction rate constant (s^{-1})
k_1	mass transfer coefficient (ms^{-1})
R	universal gas constant (kJ mol^{-1} K^{-1})
R_B	Initial sorbent particle radius (m)
t	reaction time (s)
T	temperature (K)
$X_B = X$	fraction of dissolved sorbent (-)
ρ_B	molar density of sorbent (kg mol m^{-3})
k_0	Pre-exponential factor
$a_{H^+,surf}$	hydrogen ion activity at the surface of the sorbent
$a_{H^+,bulk}$	hydrogen ion activity in the bulk solution.
pCO_2	CO_2 partial pressure
$\gamma_{H^+,s}$	Activity coefficient of hydrogen ion adjacent to surface (Eq. 3.18)
$c_{H^+,s}$	Concentration of the hydrogen ion adjacent to surface (Eq. 3.18)

$c_{H^+,b}$	Hydrogen ion concentration in the bulk solution
k_t	transport rate constant (Eq.3.19)
D_e	effective diffusion coefficient of gas in the ash layer (Eq.3.28)
k_g	mass transfer coefficient between gas and particle (Eq.3.28).
K_s	first order constant for surface reaction (Eq.3.28).
C_{SO_2}	SO_2 concentration (mol m^{-3}).
ε_{fb}	fixed bed porosity (Eq. 3.32).
$f_{v,s}$	volume fraction of sorbent in the bed (Eq. 3.32).
r_s	average reaction rate in the particle (mol $m^{-3}s^{-1}$) (Eq. 3.32).
M	molecular weight (g mol^{-1}).
S_e	specific surface area of the reagent (m^2 g^{-1})
ΔT_a	approach to saturation temperature
T_s	adiabatic saturation temperature.
ACF	activated carbon fibers
ASTM	American Society of Testing and Materials
BCF	billion cubic feet
BFBC	bubbling fluidized bed combustion
BJH	Barret, Joyner, & Halenda
CAAA	Clean Air Act Amendment of the USA
CCGT	Combined cycle gas turbine
CCT	Clean coal technology
CFBC	circulating fluidized bed combustion
DBA	dibasic acid

DESONOX	Degussa-SNOX
DOE	Department of energy
DSI	Duct Sorbent Injection Process
Dti	Department of Trade and Industry
EBA	Electron Beam Ammonia
EIA	Energy Information Administration
EPRI	Electric Power Research Institute
EPS	electric power stations
ESP	electrostatic precipitators
FBC	Fluidized bed combustion
FF	fabric filter
g/kWh	gram per kilowatt hour
GSA	gas suspension absorption
GW_e	Gegawatt electric
ID	induced draft
IGCC	Integrated gasification combined cycle
kWe	kilowatts electric
L/G	Liquid to gas ratio
LCPD	Large Combustion Plant Directive
MEL	Magnesium enhanced lime
MWe	megawatts electric
PBMR	Pebble-Bed Modular Reactor
PJBH	pulse jet baghouse

PPSB	powder particle sprouted bed
PWR	pressurized-water reactor
SCM	Shrinking core model
SCR	selective catalytic reduction
SNOX	combined SO_x/NO_x removal
SWW	sea-water washing
TCF	trillion cubic feet
WSA-SNOX	Wet-Gas Sulphuric Acid integrated with SNOX
XRD	x-ray diffraction.
RH	Relative humidity